



universität
wien

DISSERTATION

Titel der Dissertation

„MOLECULAR MODELING OF VOLTAGE-GATED CALCIUM CHANNELS“

Verfasserin

Chonticha Suwattanasophon

angestrebter akademischer Grad

Doktorin der Naturwissenschaften (Dr.rer.nat.)

Wien, 2012

Studienkennzahl lt. Studienblatt:

A 091 411

Dissertationsgebiet lt. Studienblatt:

Physik

Betreuer:

Ao- Univ.-Prof. Dr. Peter Wolschann

CONTENTS

| | |
|----------------------|-----------|
| ABSTRACT..... | II |
|----------------------|-----------|

| | |
|-------------------------------------|----------|
| CHAPTER 1- INTRODUCTION..... | 1 |
|-------------------------------------|----------|

| | |
|---|----|
| 1.1. Cellular Membranes..... | 1 |
| 1.2. Membrane proteins | 2 |
| 1.3 Ion channels | 2 |
| 1.4 Classification of the ion channels | 3 |
| 1.5 Voltage-gated calcium channels (Ca_v) | 3 |
| 1.6 Classification of voltage-gated calcium channels..... | 5 |
| 1.7 Mechanism of voltage-gated calcium channels | 7 |
| 1.8 Voltage-gated calcium channels molecular pharmacology | 8 |
| 1.9 L-type calcium channels | 9 |
| 1.10 Calcium channel blocker - Phenylalkylamines (PAAs)..... | 10 |
| 2.1 Lipid interaction of the channel. | 13 |
| 2.2 Lipid composition | 13 |
| 2.3 Cholesterol effect..... | 15 |

| | |
|---|-----------|
| CHAPTER 2-METHOD AND PROCEDURE | 16 |
|---|-----------|

| | |
|---|----|
| 2.1 Homology modeling | 17 |
| 2.2 <i>Ab Initio</i> method. | 18 |
| 2.3 Model evaluation. | 18 |
| 2.4. Molecular Docking | 19 |
| 2.4.1 Docking programs used in thesis | 20 |
| 2.4.2 Docking methodology..... | 22 |
| 2.5. Molecular dynamic simulations..... | 23 |
| 2.5.1 Molecular Dynamics simulation studies of the open conformation of Cav1.2 calcium channel with Verapamil, D619, T13 and qDiltiazem | 25 |
| 2.5.2 Molecular Dynamics simulation studied of closed and open conformation Cav1.2 calcium channel in pure POPC and content of cholesterol in the membrane..... | 26 |

CHAPTER 3-RESULTS AND DISCUSSION28

| | |
|--|----|
| 3.1 Sequence conservation of L-type calcium channel..... | 28 |
| 3.2 Sequence alignment of Ca _v 1.2 closed conformation | 30 |
| 3.3 Sequence alignment and inner pore domain prediction of Ca _v 3.1 T-type calcium channel | 32 |
| Paper 1. Cysteines in the loop between IS5 and the pore helix of Cav3.1 are essential for channel gating..... | 34 |
| 3.4 Docking studies of Phenylalkylamines (PAAs) verapamil and its derivatives to the open conformation of Ca _v 1.2..... | 56 |
| 3.4.1 Docking studies and molecular dynamic simulations of verapamil(s) in a open conformation of Ca _v 1.2..... | 58 |
| 3.4.2 Docking studies of three groups of verapamil derivatives with open conformation of Ca _v 1.2..... | 63 |
| 3.5 Stability of the pore region of Ca _v 1.2 in closed conformation and in improved open conformation..... | 68 |
| 3.6 Molecular Dynamics simulation studied of the improved open conformation of Cav1.2 calcium channel with verapamil and some of its derivatives. | 69 |
| 3.6.1 Molecular Dynamics simulations studies of the improved open conformation of Ca _v 1.2 calcium channel with verapamil..... | 69 |
| 3.6.2 Molecular Dynamics simulation studies of the improved open conformation of Ca _v 1.2 calcium channel with D619 and T13 | 72 |
| 3.7 Molecular Dynamics simulation studies of the improved open conformation of Cav1.2 calcium channel with quaternary (-) diltiazem | 79 |
| 3.8 Homology Modeling and model evaluation of pore region Ca _v 1.2 closed conformation .. | 80 |
| 3.9 Molecular Dynamics simulation studies of the pore region of Ca _v 1.2 in closed conformation and improved open conformation in dependence of the content of cholesterol in the membrane..... | 86 |
| Summary 1 | 80 |
| 3.10 Molecular Dynamics studies of the pore region of the newest model Ca _v 1.2 based on Voltage-gated sodium (NavAb) channel as a template..... | 86 |
| Manuscript | 80 |

CHAPTER 4-SUMMARY 131

REFERENCE..... 135

Appendix I – Parameter for molecular dynamics simulation using Gromacs

4.0.7..... 146

| | |
|---|------------|
| Appendix II - Multiply sequence alignment of pore domain I to II..... | 153 |
| Appendix III - Multiply sequence alignment of pore domain III to IV..... | 164 |
| Curriculum Vitae | 173 |

Acknowledgements

This research project would not have been possible without the support of many people. I would like to express my gratitude to my supervisor, Ao-Uni.-Prof Dr. Peter Wolschann for giving me a great opportunity to start my Ph.D study in our institute and acknowledge for your advice, guidance and suggestions.

I acknowledge the Ph.D program “Molecular Drug Targets” of University of Vienna for the financial support.

Deeply thank go to Dr. Anna Sary-Weinzinger for abundantly helpful and offered invaluable assistance, support and guidance. Without whose knowledge and assistance this study would not have been successful.

Many thanks also to my colleagues from Institute for Theoretical Chemistry, University of Vienna for the nice moments and good time together.

I would like to thank to my best friend here and my friend from Thailand who I met during my study here. Thank for sharing and joining a good time and make me feel as home all the time. Especially thank to Dr Andrea Schiesaro’s family for sharing the good dinner and happiness.

Lastly I also would like to special thank my beloved family member, especially my father, my uncle and my sister, for their understanding, supporting and encouraging me.

ABSTRACT

Ion channels are important molecular targets for the treatment of human diseases. They are responsible for the transport of ions (e.g. potassium and calcium) through cellular membranes. Calcium entry through voltage-gated calcium channels (Ca_v) initiates electrical impulses, sensory processes, muscle contraction, secretion of hormones and neurotransmitters, and other key cellular functions. Some specific organic compounds (drugs) can inhibit the ion flow, which consequently affects the cellular metabolism. Defective ion channels result in a variety of human diseases such as cardiovascular disease, night blindness and familial hemiplegic migraine, which are termed channelopathies.

Theoretical methods are used to obtain the detailed information about the structure and function of ion channels and the association complexes of ligands with the channels. Homology modeling based on the related potassium and sodium channel structures is used to create models for the diverse states of the channels. Subsequent docking studies allow the investigation of the interaction of drugs with the internal pore of the channels. Molecular Dynamics simulations and Molecular Docking procedures are methods which give insight into the molecular basis of the biological activities. Development of the model and subsequent refinement based on the theoretical considerations and mutation data resulted not only in a better understanding of the action mechanisms of ion channels but furthermore increases our knowledge about the voltage dependent opening and closing mechanism and allow a more detailed investigation of drug interaction mechanisms.

This thesis focuses on the mechanism and the structure of $\text{Ca}_v1.2$ calcium channel of closed and open pore region conformation. The $\text{Ca}_v1.2$ calcium channel belongs to the superfamily of voltage gated ion channels where crystal structures are not available. The closed model has been built based on the crystal structure of KcsA, MlotiK, Nak and a model of the bacterial sodium channel NaChBac. The structure of the open conformation was taken from Stary et al, 2009. At almost the end of the thesis in June 2011, a new voltage-gated sodium channel which shares the same highly conserved FxxxTxExW motif with calcium channel was published. Then, the newest homology model of $\text{Ca}_v1.2$ was built based on the new voltage-gated sodium channel crystal structure. Molecular docking of verapamil, its derivatives and qDiltiazem to the $\text{Ca}_v1.2$

open conformation using several Molecular Docking program packages (e.g. Glide and MOE) was performed to compare the best fitting results and to investigate the interaction of drugs with the internal pore of the channels. The results show that all drugs share similar results where the ligands are located in the same region between IIS6 and IVS6 and the positively charged nitrogen atom of all ligands binds between the glutamic acids E1145 and E1446. The best fitting of verapamil, D619, T13 and qDiltiazem in Cav1.2 open conformation was used to perform MD simulations.

A small variation in lipid composition can influence protein activity such as fluidity and lipid packing. Cholesterol is one of the main lipid components of the plasma membrane in mammalian cells, and is known to influence many ion channels. Here, we focus on how cholesterol interacts with Cav1.2 channels in open and closed conformation, applying molecular dynamics simulations. We used different lipid compositions, pure POPC and mixture POPC/CHOL bilayers to obtain information and to provide a first hint about the possible effects by which cholesterol influences Cav1.2 channels.

A mechanistic understanding of the molecular and structural details of ion channels in general and about the underlying principles of channelopathies raises hopes of improving and developing better targeted drugs in the future.

CHAPTER 1

INTRODUCTION

1.1. Cellular Membranes

Living cells are surrounded by membranes, which allow the cells to form units separated from the environment. These biological membranes are therefore important parts of the human cell and essential components of a living cell organization. They act as barriers and separate the organelles in interior of all cells (likes cytoplasm) from the surrounding outside of the cell. The basic unit of most biological membrane consists of phospholipid bilayers. An important function of the cellular membrane or plasma membrane is not only the separation of the cell but also to regulate the communication of the cell and the transport of various molecules as a selectively permeable membrane. Selected molecules or ions only are allowed to move through the membrane in a controlled way and also in both directions, in and out of a cell. Cellular membranes also play a crucial role in a variety of cellular processes, for example ion conductivity and cell signaling. The movement of molecules passing through the membrane can be either a passive or an active process. There are many mechanisms that allow the exchange of molecules in and out the cell as mentioned below.

The passive process: This movement occurs without input of cellular energy.

1. Diffusion. Some small molecules or ions are able to cross the cell membrane by diffusion.
2. Osmosis. The cell membrane behaves as a semipermeable barrier. If on both sides of the membrane different concentrations of solutes exist, then, the solvent molecules may move through the membrane into a region of higher solute concentration which leads to an equalization of the solute concentration at both sides.

The active process: This mechanism requires energy for transportation.

1. Mediated Transport. The movement of a solute such as sugar across a membrane occurs with the help of special proteins called transport proteins.

2. Endocytosis. It is a process where the cell absorbs the molecules from outside by engulfing and fusing.
3. Exocytosis. A process which releases the cellular substances contained in vesicles. The substances can pass into the cell by formation of a vesicle membrane with plasma membrane. After that, the substances release to the exterior of the cell.

Very important for the communication of the cell via the cellular membrane are membrane proteins.

1.2. Membrane proteins

Approximately 30% of the entire proteins are membrane proteins. Membrane proteins can be categorized into peripheral and integral membranes. Integral membrane proteins are permanently attached to the membrane (e.g. G-protein-coupled receptors and ion channel). Peripheral membrane proteins are temporary attached either to the lipid bilayer or the integral membrane by a combination of electrostatic or van der Waals interactions with the lipid head group (e.g Phospholipase C and Lipoxygenases). Membrane proteins are important in all cells. They play roles in all cellular processes and mediate a wide variety of important processes such as transport of nutrients, export of toxins and cell-cell interactions. Now a day, the majority of the drugs are targeted to membrane proteins [1, 2]. Due to the limited technology to express membrane proteins, the structure and function of membrane proteins are still not well understood. Right now there are 969 proteins in the protein database [3]. High quality crystal structures of membrane protein are required to extend the knowledge in this area. At the moment, there are new techniques applied to successfully crystallize a variety of membrane proteins the bicelle [4] and HILIDE [5] methods are introduced to obtain structure of membrane proteins Generally, there is continuous development to improve these methods.

1.3 Ion channels

Ion channels are pore-forming proteins and their function is to facilitate the diffusion of ions across the cellular membrane. Channels are usually ion selective. Ions are able to pass through in highly selective way the channel and they prevent the passage of others. Under physiology conditions, calcium channels allow only calcium ions to go through. [6]. The

pathway of selected ion flow through the channel by electrochemical gradients accounts for an ion's concentration gradient across a cell membrane. Channels are major components of the nervous system which play key roles in variety of biological processes such as cardiac, skeletal and smooth muscle contraction. Therefore, channels have been intensively studied and they are important molecular targets for the treatment of many human diseases.

There are now many techniques which have been applied to study the ion channels such as voltage clamp electrophysiology, immunohistochemistry, reverse transcriptase-polymerase chain reaction analysis (RT-PCR) and also large variety of computational methods.

1.4 Classification of the ion channels

There are several possible ways to classify ion channels into groups. For instance,

- (1) *By gating*: The conformational change between closed, open and inactivated of the channels is called gating.
 - (a) Voltage-gated ion channels are controlled by the voltage gradient across the membrane. (e.g. voltage-gated calcium channels, voltage-gated potassium channels and voltage-gated sodium channels etc.).
 - (b) Ligand-gated ion channels. These channels are regulated by conformation changes induced by ligands. (e.g. nicotinic acetylcholine receptor (nAChR) and neurotransmitter gamma-aminobutyric acid receptor (GABA) etc.)
- (2) *By ion*. Channels can be categorized by the species of ions passing through those gates. (e.g. chloride channel, sodium channel, potassium channel etc.)

1.5 Voltage-gated calcium channels (Ca_v)

Ca_v s play a major role to control calcium influx and respond to change in intracellular calcium concentrations that occur in such cellular system as cardiac muscle, neurotransmitter release and muscle contraction [7].

Crystal structures of the transmembrane domains of Ca_v s are not available. Therefore, the homology modeling method was used to build Ca_v structure models based on voltage-gated K^+ and Na^+ channels (K_v and Na_v). Even though, K_v and α_1 subunits of Ca_v are composed of four basic domains, each domain formed six transmembrane but there are still significant differences

at the atomic level. The K_v channel contains four identical repeats while Ca_v is non-identical formed by a single polypeptide [8]. Molecular dynamics simulations and experimental data are used to support that the four domain repeats of Ca_v are arranged in a clockwise manner [9]. Another difference between K_v and Ca_v are the P segments, especially selectivity filter region. For K_v , the main carbonyl oxygen atoms in the selectivity filter orient towards the lumen [10]. In case of Ca_v , the side-chains of four glutamates are predicted to face the pore [11-14].

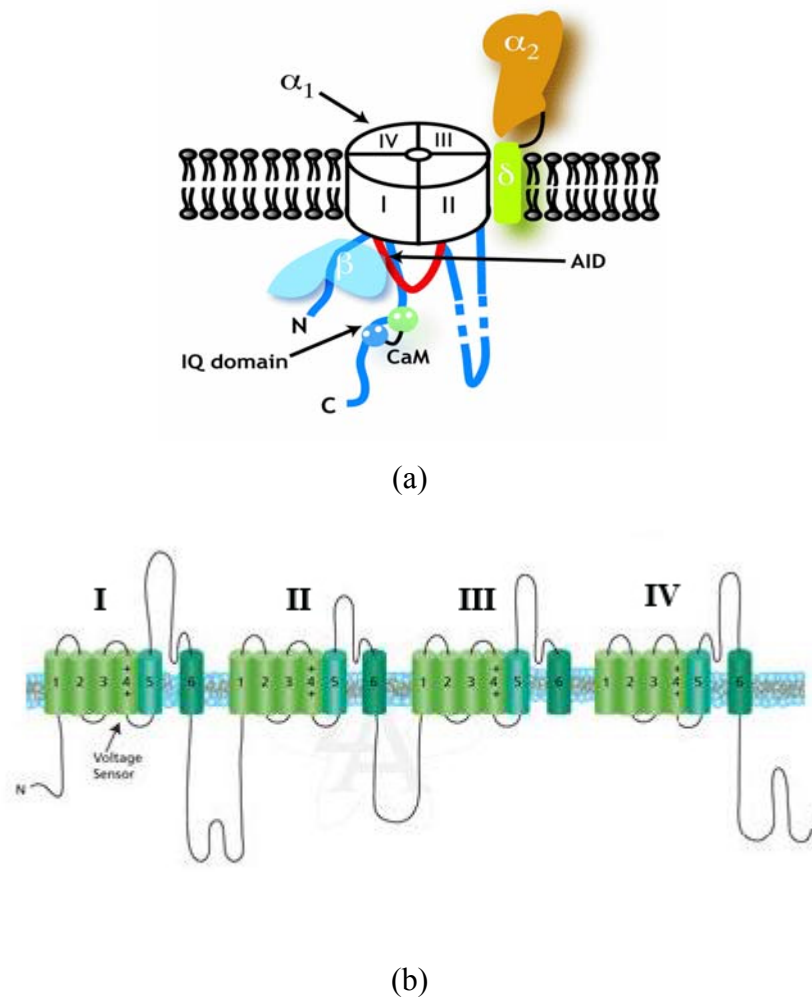


Fig 1.1 (a) Schematic cartoon of voltage-gated calcium channel (b) The α_1 subunit is comprised of four homologous domains, each of which contains six transmembrane helices.

The global architecture of Ca_v s is composed of four basic components. α_1 subunit is located in the cell membrane and calcium ions can pass through. The auxiliary β , CaM and $\alpha_2\delta$

subunits bind with high affinity to the loops of domain I and II. $\text{Ca}_v \alpha_2\delta$ is a single pass transmembrane subunit which is formed by two disulfide-linked proteins [15, 16]. Fig 1.1a shows also the transmembrane Ca_v which consists of four homologous repeats membrane-spanning domains (I–IV). Each repeat is formed by six segments (S1–S6) shown in Fig 1.1b.

The first 4 segments (S1–S4) are the voltage-segment domain and the last 2 segments (S5–S6) form the calcium-selective pore domain. The S4 segment contains positively charged residues and acts as a voltage sensors controlling Ca_v gating.

1.6 Classification of voltage-gated calcium channels

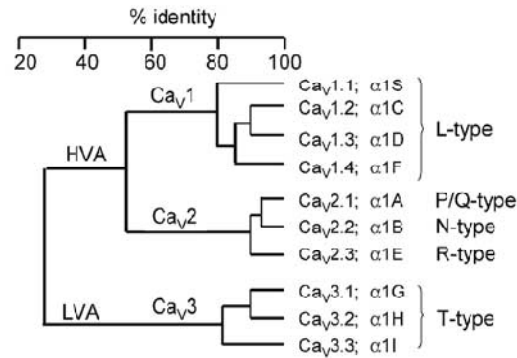


Fig 1.2 The percent identity of all voltage-gated calcium channels $\alpha 1$ subunits.

The Ca_v s can be divided into low-voltage-activated (LVA) and high-voltage-activated (HVA) calcium channels depending on the depolarization necessary to activate the channel [17]. HVA calcium channels are activated at the membrane rapidly and at more negative potentials than LVA. HVA channels are all members of $\text{Ca}_v 1$ and $\text{Ca}_v 2$ family. All members of the $\text{Ca}_v 1$ family ($\text{Ca}_v 1.1$ – 1.4) are of the L-type, $\text{Ca}_v 2.1$ is of the P/Q type, $\text{Ca}_v 2.2$ is of the N-type and $\text{Ca}_v 2.3$ is of the R-type. Furthermore, all members of the $\text{Ca}_v 3$ family ($\text{Ca}_v 3.1$ – 3.3) are in the HVA classification which is named T-type [18]. The amount of the similarity of the amino acid for

everal of voltage-gated calcium channel is given in Fig 1.2.

Table 1. Sizes of individual $\alpha 1$ subunits of voltage-gated calcium channels

| Subunit / origin | Molecular weight (kDa) | Number of amino acids | Reference |
|---------------------------------|------------------------|-----------------------|------------------------------|
| Cav1.1 / rabbit skeletal muscle | 212 | 1873 | Tanabe et al. 1987 [19] |
| Cav1.2 / rabbit heart | 242.8 | 2171 | Mikami et al. 1989 [20] |
| Cav1.2 / rabbit lung | 242.5 | 2166 | Biel et al. 1990 [21] |
| Cav1.2 / rat aorta | 243.6 | 2169 | Koch et al. 1990 [22] |
| Cav1.3 / human pancreas | 247.6 | 2181 | Seino et al. 1992 [23] |
| Cav1.3 / human brain | 245.2 | 2161 | Williams et al. 1992a [24] |
| Cav1.4 / human retina | | 1912 | Bech-Hansen et al. 1998 [25] |
| Cav1.4 / human retina | 219.5 | 1966 | Strom et al. 1998 [26] |
| Cav2.1 / rabbit brain | 257.3 | 2273 | |
| | 273.2 | 2424 | Mori et al. 1991 [27] |
| Cav2.2 / ray | 264.5 | 2326 | Horne et al. 1993 [28] |
| Cav2.2 / human brain | 262.5 | 2339 | |
| | 251.8 | 2237 | Williams et al. 1992b [29] |
| Cav2.3 / ray | 251.8 | 2223 | Horne et al. 1993 [28] |
| Cav2.3 / rat brain | 252 | 2222 | Soong et al. 1993 [30] |
| Cav3.1 / mouse brain | | 2295 | Klugbauer et al. 1999a [31] |
| Cav3.2 / human heart | | 2387 | Cribbs et al. 1998 [32] |
| Cav3.3 / rat brain | 205.2 | 1835 | Lee et al. 1999a [33] |

The length of the protein chain of almost all calcium channels ranges approximately from 1870 to 2420 amino acids. A summary over all calcium channels together with the number of amino acid of the $\alpha 1$ subunit and the related molecular weight is given in Table 1 [34]. As can be deduced from Fig 1.2, the similarity of LVA and HVA channels is less than 30 % of sequence

homology. Two subfamilies of HVA channels: L-type ($\text{Ca}_v 1$) and Neuronal types ($\text{Ca}_v 2$) have about 50% sequence homology. Individual members of each subfamilies share more than 80% of sequence homology.

1.7 Mechanism of voltage-gated calcium channels

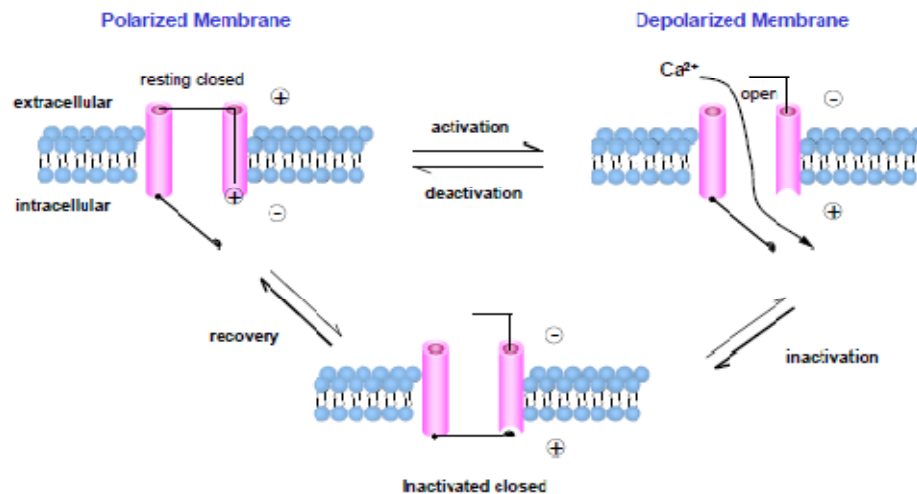


Fig 1.3 Activation and inactivation of voltage-gated calcium channel.

The voltage-gated calcium channels are opened and closed by voltage of calcium ion changes as shown in Fig 1.3. At resting closed state, the voltage-gated calcium channel is closed and ions cannot pass. Then, the membrane potential will be increased, which results that the channel can be activated to open state upon depolarization and allows ions to pass. During the depolarization, the open probability of the channel is remained briefly and then voltage-dependently reduced by channel inactivation leading to inactivated closed state. Instead, inactivated closed state cannot immediately be reactivated. It requires a brief period of time to repolarization of the membrane and recovery from inactivation. On the other hand, the membrane potential at the open state also can deactivate the channel leading to the resting closed state [35].

1.8 Voltage-gated calcium channels molecular pharmacology

The activity of voltage-gated calcium channels is essential to couple electrical signals on the cell surface to physiological events in cells. The pharmacology of the each family of calcium channels is individual e.g. the molecular targets of $\text{Ca}_v1.2$ channels are used widely in the therapy of cardiovascular diseases (Table 2). For more detail, the summarization of molecular, physiological, and pharmacological properties of all calcium channel family are reviewed by Catterall et al (2005) [8]. Detailed properties of L-type $\text{Ca}_v 1.2$ calcium channels are given in Table 2.

Table 2. Molecular properties of the L-type calcium channel $\text{Ca}_v 1.2$.

| | |
|------------------------------|---|
| <i>Channel name</i> | <i>$\text{Ca}_v1.2$</i> |
| <i>Description</i> | <i>voltage-gated calcium channel α_1 subunits</i> |
| <i>Other names</i> | <i>α_{1c}, cardiac or smooth muscle L-type Ca^{2+} channel, cardiac or smooth muscle dihydropyridine receptor</i> |
| <i>Molecular information</i> | <i>human: 2221aa, Q13936 (cardiac), L04569 (cardiac) chr. 12p13.3, CACNA1C rat: 2169aa, P22002 (cardiac) M59786 mouse : 2139aa, Q01815 (cardiac), L01776 (cardiac)</i> |
| <i>Associated subunits</i> | <i>$\alpha_2\delta$, β, γ</i> |
| <i>Functional assays</i> | <i>Patch clamp (whole cell, single channel),calcium imaging, cardiac or smooth muscle contraction hormone secretion.</i> |
| <i>Current</i> | <i>$I_{\text{Ca,L}}$</i> |
| <i>Conductance</i> | <i>Ba^{2+} (25pS) > Sr^{2+} = Ca^{2+} (9pS)³</i> |
| <i>Ion selectivity</i> | <i>Ca^{2+} > Sr^{2+} > Ba^{2+} >> Mg^{2+} from permeability ratios</i> |
| <i>Activation</i> | <i>V_a= -4mV (in 15 mM Ba^{2+}) to -17mV (in 2mM Ca^{2+}); τ_a = 1ms at +10mV</i> |
| <i>Inactivation</i> | <i>V_h = -50 to -60mV (in 2mM Ca^{2+}), -18 to -28mV (in 10-15mM Ba^{2+}); τ_{fast} = 150ms, τ_{slow} = 1100ms (at V_{max} in 15 mM Ba^{2+})</i> |
| <i>Activators</i> | <i>BayK8644, dihydropyridine agonists, FPL64176</i> |
| <i>Gating inhibitors</i> | <i>dihydropyridine antagonists (e.g. isradipine, IC_{50} = 7nM at -60mV; nimodipine, IC_{50} = 139nM at -80mV)</i> |

| | |
|--------------------------------------|---|
| <i>Blockers</i> | <i>selective: devapamil ($IC_{50} = 50\text{nM}$ in 10mM Ba^{2+} at -60mV) and other phenylalkylamines; diltiazem ($IC_{50} = 33\mu\text{M}$ in 10mM Ba^{2+} at -60mV and 0.05Hz); non-selective: Cd^{2+}</i> |
| <i>Radioligands</i> | <i>(+)-[^3H]-isradipine ($K_d < 0.1\text{nM}$) and other dihydropyridines; (-) - [H]-devapamil, ($K_d = 2.5\text{nM}$), (+)-cis-[H]-diltiazem ($K_d = 50\text{nM}$)</i> |
| <i>Channel distribution</i> | <i>cardiac muscle, smooth muscle (including blood vessels, intestine, lung, uterus); endocrine cells (including pancreatic β-cells, pituitary); neurons subcellular localisation: concentrated on granule containing side of pancreatic β-cells; on neurons preferentially located on proximal dendrites and cell bodies.</i> |
| <i>Physiological functions</i> | <i>excitation-contraction coupling in cardiac or smooth muscle, action potential propagation in sinoatrial and atrioventricular node, synaptic plasticity, hormone secretion.</i> |
| <i>Mutations and pathophysiology</i> | <i>required for normal embryonic development (mouse, zebrafish)</i> |
| <i>Pharmacological significance</i> | <i>mediates cardiovascular effects of clinically used Ca^{2+} antagonists</i> |
| <i>Comments</i> | <i>Tissue-specific splice variants exist; in addition to cardiac channels, smooth muscle (2169aa) and brain (2140-2144aa) channels have been cloned. The gene for $\text{Ca}_v1.2$ was first isolated and characterised in rabbit (2171aa, P15381, X15539)</i> |

1.9 L-type calcium channels

The four members of L-type calcium channels have specialized functions in skeletal muscle and cardiac muscle, and they are, therefore, therapeutic targets for cardiovascular disease treatment. The conformation changes of gating states (resting, open and inactivated) L-type calcium channels are accompanied by changes in drug binding affinity upon the change in membrane voltage (activation/depolarization). L-type calcium channels are sensitive to three major classes of drugs [34, 36] : dihydropyridines (DHPs) [37-39], phenylalkylamines (PAAs) [40-42], and benzothiazepines (BZPs) [43]. From experimental approaches [8, 34-43], it is known that these three classes of drugs bind to separate but overlapping regions in IIS5, IIS6, and IVS6 segments of the α_1 subunits. The binding residues of these drugs are shown in Fig 1.4.

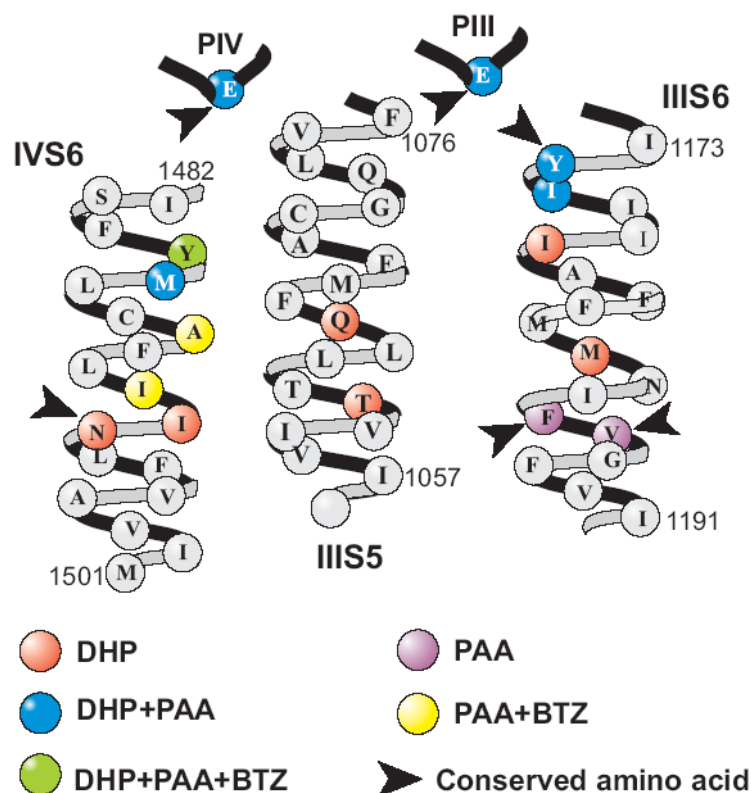


Fig 1.4 The amino acid residue interaction with dihydropyridines (DHPs), phenylalkylamines (PAAs), and benzothiazepines (BZPs).

As can be seen from the Fig 1.4 different drugs interact at different binding sites, leading there to different interaction mechanisms which have been investigated in more detail. However, there are still questions open which conformations (open or closed) are interacting with the drug.

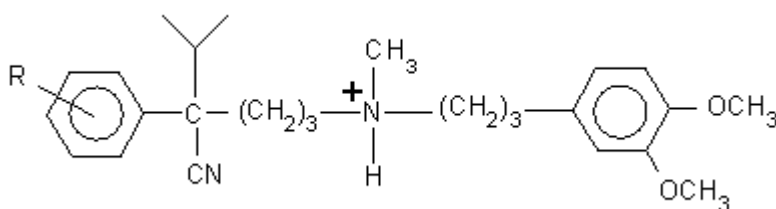
The intention of the present work is to focus on voltage gated L-type calcium channels $Ca_v1.2$ and to investigate the mechanism and the structure of closed and open pore region.

1.10 Calcium channel blocker - Phenylalkylamines (PAAs)

Phenylalkylamines (PAAs) such as verapamil, gallopamil or devapamil, belong to the class of calcium channel blockers of L-type [44]. The common structure of PAAs is the presence of two methoxylated aromatic rings. In this work, the structure-activity relationships of PAAs focus on verapamil and its derivative. Verapamil is a drug of this class within currently clinical

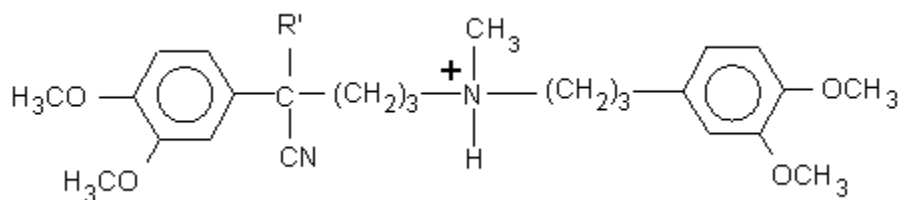
use in particular for the therapy of coronary heart disease. The qualitative and quantitative structure-activity relationship of various groups of verapamil was investigated based on an analysis of the frequency dependent negative inotropic action exerted in cat papillary muscles. The inotropic effect of verapamil which relate to muscular contractions is mainly caused by the S conformation [45]. The verapamil shows effects on the slow Ca^{2+} current and movement which affects cardiac excitation-contraction coupling. The quantitative results was obtained by comparing ED_{50} values [46].

The PAA verapamil and its derivatives can be divided into of 3 groups. Group A concerns derivatives differently substituted at the benzene ring near the asymmetric carbon atom (Fig 1.5). In Group B the isopropyl group is exchanged (Fig 1.6). The last group C contains derivatives with different substituents at the amino group nitrogen atom (Fig 1.7).



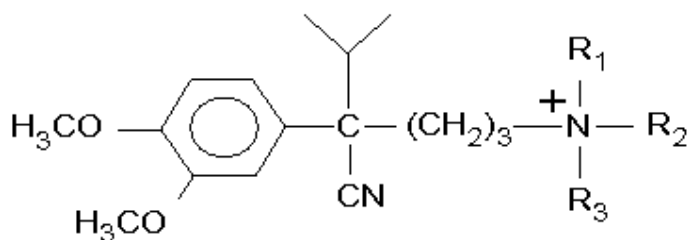
| | R = | Molecular name |
|---|---------------------------------------|-----------------------|
| \ | 3,4-(OCH_3) ₂ | Verapamil |
| | 3,4,5-(OCH_3) ₃ | D600 |
| | 4- OCH_3 | D557 |
| | 3,4- Cl_2 | D595 |
| | 3- CF_3 | T13 |
| | 3- OCH_3 -4-OH | PR23 |
| | 3,4- CH_3 | D559 |

Fig 1.5 Group A: Derivatives differently substituted at the benzene ring near the asymmetric carbon atom.



| R' = | Molecular name |
|---|-----------------------|
| C ₆ H ₅ CH ₂ - | D490 |
| n-C ₈ H ₁₇ - | D586 |
| CH ₃ CH ₂ - | D525 |

Fig 1.6 Group B: Exchange of isopropyl group by other substituent.



| R1 = | R2 = | R3 = | Molecular name |
|-------------------|-------------------|-------------------|-----------------------|
| Isopropyl- | homoveratryl- | H- | D594 |
| H- | CH ₃ - | H- | PR22 |
| CH ₃ - | CH ₃ - | H- | D619 |
| CH ₃ - | homoveratryl- | CH ₃ - | H1 |

Fig 1.7 Group C: Derivatives with different substituent at the amino group nitrogen atom.

In summary, for substituents of group A and B it was found that the character of the substituent strongly affects the potency of various compounds, but it is not affected by the inotropic effect. The tertiary amino nitrogen of group C and two benzene rings of group A are important for frequency dependent negative inotropic. Moreover, the molecular importance of the N-methyl group C is based on steric effects.

2.1 Lipid interaction of the channel.

The interaction of membrane lipids with integral membrane proteins is important and influences the membrane protein structure and function. However, the mechanisms between lipid composition and membranes are not well understood yet. The next part of the introduction gives an overview of various lipid compositions and how they modulate the membrane protein.

2.2 Lipid composition

The cell membrane or plasma membrane is a selectively permeable lipid bilayer. It separates the cytoplasm (intracellular fluid) from the extracellular moiety. It contains a variety of biological molecules such as phospholipids, glycolipids and cholesterol. Phospholipids are the most abundant compound in the cell membrane. The Mammalian cell membrane basically consists of thin layers of phospholipids which are arranged in such a way that the polar head groups point toward the intra- and extra- cellular areas. The phospholipids have a hydrophilic head which are exposed to water and two hydrophobic tails at the center of bilayer. Moreover, cholesterol is located inside the membrane (Fig 1.8) [47]. The cell membrane contains approximately 30-50 mol % of cholesterol.

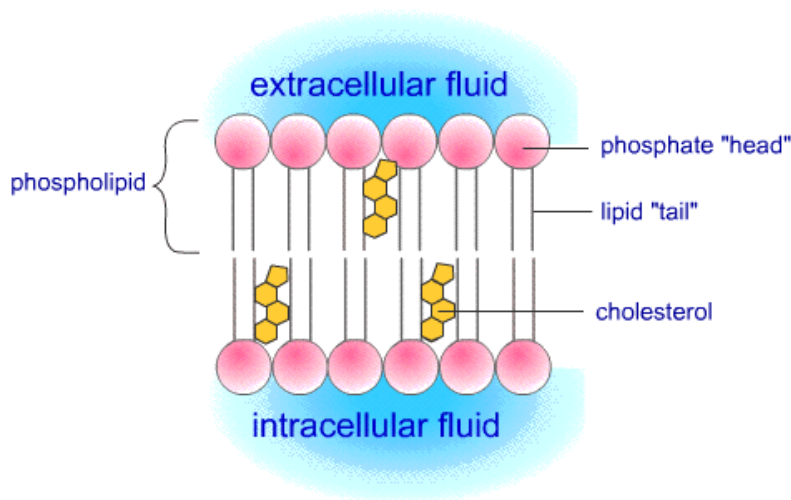


Fig 1.8 The primarily lipid bilayer consists of phospholipids and cholesterol.

The effects of lipid composition on the membrane protein and subsequent activity are very complex. Evidently, the molecular composition of lipids strongly affects the protein structure and function. Up to now, the molecular mechanisms of protein-lipid coupling are still

poorly understood. The changes of lipid characteristics, for example head group type, the length of the tail, additional presence of cholesterol are factors which modulate the protein functions. In case of ion channels, the molecular mechanisms of protein-lipid interactions can influence directly and indirectly the protein function [48] which may occur in different ways

1. Alteration of the protein structure and function. The membrane proteins folding are dictated by their primary structure and their environment. The residues in the interior membrane protein are less hydrophobic than the residues in contact with the tail of lipid bilayer. The hydrophobic and hydrophilic properties of the bilayer play a crucial role for protein folding and activity. However, not all domains of the channels are in contact with the bilayer, particularly the extracellular domains, mostly non-helical, which are located outside the membrane [49].
2. Alteration of membrane fluidity. The fluidity is a measurement of the packing efficiency of the lipid. The movement of a tightly packed membrane is more difficult than the movement in more fluid environment. Thus, membrane fluidity is affecting the dynamics of the membrane protein as observed in the nAChR studies [50].
3. Alteration of bilayer thickness. Normally, the hydrophobic region of transmembrane (TM) domains interacts with the acyl chain of bilayer while polar, aromatic and charged residues are in contact with the interface region on each side of bilayer. The short hydrophobic TM are usually expelled from the membrane, due to the fact that it is unfavorable for hydrophobic region of the TM and bilayer hydrophobic thickness to be mismatched. Furthermore, for the long hydrophobic TM in contact with the acyl chain of bilayer will tend to tilt to match with the membrane thickness. Then, this rearrangement may affect the protein function [51-53].

Lipid rafts are specialized regions that are enriched of cholesterol in membrane microdomains (Fig 1.9). These membrane regions influence the membrane fluidity, they are more tightly packed and form higher ordered ensembles than the surrounding bilayer.

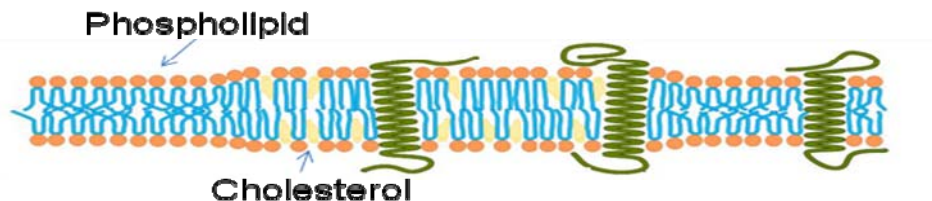


Fig 1.9 Lipid raft structure

2.3 Cholesterol effect

Cholesterol plays a crucial role in regulating the properties of membranes. As already mentioned it regulates the fluidity of the membrane and modulates the function of membrane protein [54]. In case of ion channels, it has been described that numerous ion channels are affected in different way by cholesterol. For example, the suppression of channel activity is affected by an increase in membrane cholesterol. This effect happens in several types of K^+ channel, voltage-gated Ca^{+2} and Na^+ channels etc. In contrast, there are several types of ion channels, such as transient receptor potential (Trp) channel which are inhibited by cholesterol depletion. Moreover, in some case changing in membrane cholesterol affects the biophysical properties such as the voltage dependence of active or inactive channels [55]. The mechanisms for cholesterol modulates of ion channel are not well understood. The regulation of ion channels by cholesterol have been proposed that cholesterol might interact directly or via indirectly with ion channel. Three different mechanisms of channel regulation have been suggested [56, 57]

1. Specific interactions of cholesterol with the channel protein.
2. Changes of the physical properties of the membrane bilayer (i.e. fluidity).
3. Importance of cholesterol for maintaining the scaffolds for protein-protein interactions (“lipid-rafts”).

CHAPTER 2

METHOD AND PROCEDURE

The access to experimental structural data of membrane proteins like G-protein coupled receptors (GPCRs) or ion channels by X-ray crystallography or NMR spectroscopy is still limited. For X-ray crystallography of these proteins it is rather difficult to obtain crystals, as the structure is dependent on the surrounding, the membrane. Separation of the proteins from the membrane can lead to irreversible structural changes, which inhibit ordered crystallization. Limitations for NMR spectroscopy are the size of the systems, as NMR-spectroscopy can be applied only to smaller protein systems.

Up to now, no transmembrane domains of calcium channels were crystallized. Many techniques such as patch clamp, fluorescence resonance energy transfer (FRET) used lead to significant new insights about the structure, function and drug interaction with the channels. Computational methods are also additional useful method to investigate these research areas. In general, the protein structure prediction using computational methods can be divided into three approaches

- 1) Homology modeling
- 2) Threading or fold recognition
- 3) *Ab Initio*.

For this work, homology modeling using multiple templates and modeling the loops using an *Ab Initio* method were applied. Homology modeling based on the crystal structure of potassium and sodium channels are used to create models for the diverse states of the voltage-gated calcium channel Cav1.2. Besides the model of L-type calcium channel Cav1.2, the T-type calcium channel Cav3.1 was investigated. Due to the lack of conserved residues at the loop region, the *Ab Initio* method was applied to predict the loop structure of calcium channel Cav 3.1 combined with the results of experimental investigations.

Subsequently, molecular docking studies were used to investigate ligands interacting with the internal pore of the Cav1.2 channel in the open state. Molecular dynamics simulations (MD) are important methods which give insight into the molecular basis of the biological activities. In this work, MD was also used to stabilize the model structures. Further, the MD of ligands with

Cav1.2 channel was investigated for better understanding of the action mechanism and to increase knowledge about drug interaction mechanisms.

2.1 Homology modeling

For unknown protein structures such as membrane proteins, homology modeling was introduced to construct the three-dimensional structure of a known atomic-resolution model of the protein (target) and related homologous protein (template). The procedure consists of three steps [58].

The first step: To select similar proteins (known 3D structures) as templates and to align between the target (unknown structure) and one or more templates:

The success of this method relies on the sequence alignment between target and suitable templates. In this work, sequence searches from Expasy [59] database using BLAST [60] were performed to identify related sequences. The quality of the models depends on the sequence identity of the sequence alignment. Unfortunately, voltage-gated calcium channel shares in general low sequence identity with K⁺ channel crystal structure templates. Thus, it is necessary to find possible homologs for a protein by comparing several sequences. In this work, the multiply sequence alignment was built from ClustalX [61] program combined with manual intervention based on sequence conservation information.

The second step: To build the model:

To construct the 3D model of Cav1.2 closed conformation, the software package MODELLER [62] was used to generate the model from the alignment of a sequence. This program builds a structure with an extended strand for target and fold by satisfaction of spatial restraints [63] from the alignment of the target and its templates. The hydrogen bonding features and main chain dihedral angles are preserved from the template structure. The model was manually adjusted according to the side-chains to optimize hydrophobic contacts, salt bridges, hydrogen bond formation and aromatic – aromatic interactions.

The third step: To evaluate the quality of the model:

It is important to check the model structure using the quality assessment tools. There are various quality assessment programs available to evaluate for correctness of the overall fold, errors over localized regions and stereochemical properties of the model e.g. Prosa2003 [64], Verify 3D [65], WHAT_CHECK [66], Procheck [67]. A simple preliminary check can also obtain by a Ramachandran plot.

The entire process of homology modeling may be necessary to repeat until a satisfactory model is obtained. In this work, molecular dynamic simulation of the satisfactory model in lipid bilayer environment is also used to evaluate the quality and to stabilize the model.

2.2 *Ab Initio* method.

Another approach for 3D structure prediction is the *Ab Initio* method. This method predicts the native state of a protein structure from the sequence information only. In general, *Ab Initio* methods consist of 3 steps:

- 1) Try to retrieve template proteins of similar folds from the database. In case that no appropriate template is identified in the database, the structure will be build by *Ab Initio* modeling.
- 2). Define the energy function compatible with the predicted structure.
- 3). Apply efficient and reliable algorithms to search the global predicted structure. The structure prediction ultimately is done through physical forces acting on all-atom of the model.

This method requires long computing time. Thus, we introduced the *Ab Initio* method to predict the loop structures of calcium channel Cav 3.1 using ROSETTA [68] program and I-Tasser server [69]. The ROSETTA method is a distributed-computing implementation based on Rosetta algorithm which tested, developed and succeed on globular proteins in Critical Assessment of Techniques for Protein Structure Prediction (CASP) [70]. For I-Tasser, the method is based on threading fragment structure reassembly [71].

2.3 Model Evaluation.

To evaluate the homology models, quality assessment method are necessary to check the quality of the constructed models. The quality check should be able to verify the reliability of the

model. It should be able to distinguish between properly versus improperly folded models, and evaluate steric and geometric properties of the models. There are numerous quality assessment programs which different criteria methods available. Most of the methods have been developed using empirical data from globular proteins of known structure. In our work, the models quality was assessed using Prosa2003, Verify3D, WHAT_CHECK Packing, Procheck, ProQresLG and ProQres MaxSub. Prosa2003 [64] is a program to check the potential error in 3D models of protein structures. It uses statistical potential of distance and surface-dependent statistical for C α atoms to obtain the model. Verify3D [65] is the method that analyzes the 3D atomic model with its own amino acid sequence 1D. It will provide with a statistical potentials from real proteins. WHAT_CHECK Packing [66] checks all possible atom types in all possible positions around the fixed fragments. Procheck [67] addresses the stereochemical parameter of a protein. The structure is classified into highly populated to forbidden regions by the Ramachandran plot. It shows the Φ/ψ torsion angles for all residues in the structure. ProQres [72] analyzes contact between atom-atom, residue-residue, solvent-accessible surfaces and secondary structure.

2.4. Molecular Docking [73].

Molecular docking is a method which gives insight into the molecular basis of the biological activities for better understanding of the action mechanism and increased knowledge about drug interaction mechanisms.

A basic component of every docking program is a search algorithm and an energy scoring function which can be based on

1. Force fields: molecular mechanics force fields for the estimation of binding affinity.
2. Empirical data: functions fitted to experimental data which based on the knowledge of known protein-ligand interaction.
3. Knowledge-based methods: capture the knowledge of receptor-ligand binding by statistical data alone.

The general docking procedure generates docked models by finding the binding region on macromolecules (proteins) where the ligand most likely interacts. Then, the results of docking for groups of ligands are clustered based on the location and examining energetic or ranking

score. Additionally, the experimental data are important in determining the probable binding sites. Then, the best models and experimental data should be compared to filter results. We can perform refinement docking where the ligand is restricted to a specified region based on these filtered results.

2.4.1 Docking programs used in thesis

Glide (Grid-based Ligand Docking with Energetics) [74] and MOE [75], which have a different approach are the docking programs used in this work. Glide program places ligands in the receptor by grid docking alignment. This program computes the grid in terms of position, orientation and conformation space available. Each ligand atom is matched with the grid point with the lowest energy within its neighborhood. The scoring function is reported in term of GlideScore (Fig. 2.1).

GlideScore (GScore) is given by

$$\text{GScore} = a * \text{vdW} + b * \text{Coul} + \text{Lipo} + \text{Hbond} + \text{Metal} + \text{Rewards} + \text{RotB} + \text{Site}$$

Where

| | | |
|---------|---|---|
| vdW | = | van der Waals interaction energy. |
| Coul | = | Coulomb interaction energy. |
| Lipo | = | Lipophilic-contact plus phobic-attractive term. |
| HBond | = | Hydrogen-bonding term. |
| Metal | = | Metal-binding term. |
| Rewards | = | Various reward or penalty terms. |
| RotB | = | Penalty for freezing rotatable bonds. |
| Site | = | Polar interactions in the active site. |
| a,b | = | the contribution from the Coulomb term is capped at -4 kcal/mol a= 0.050, b = 0.150 for Glide 5.0. |

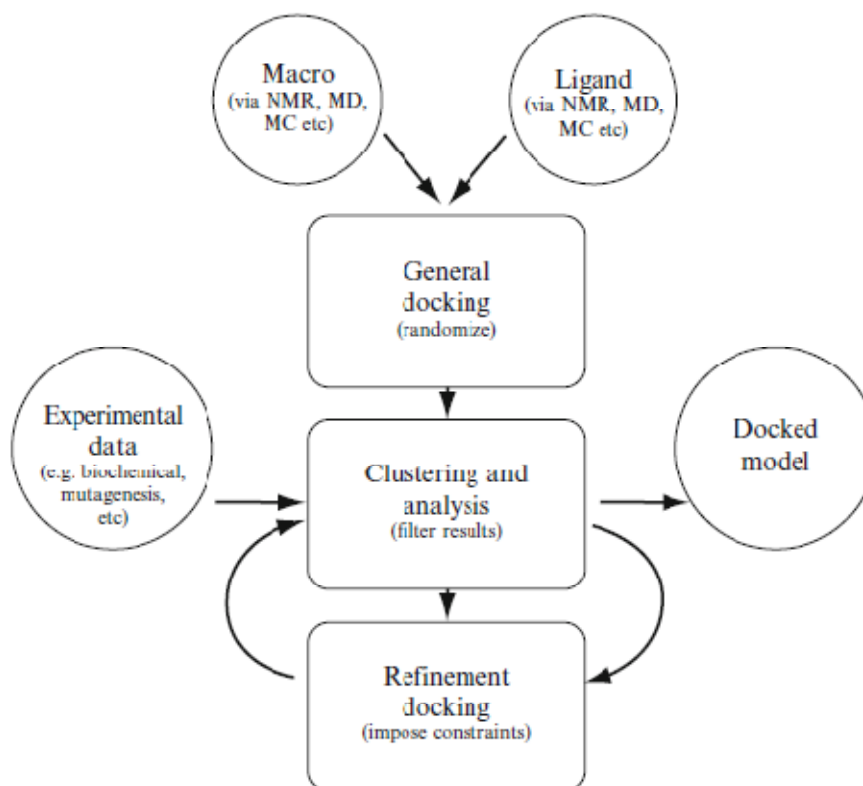


Fig 2.1. The standard docking protocol of GLIDE docking program.

The aim of MOE docking program is to search a favorable binding between ligand and receptor. Docking application in MOE program consists of several steps (Fig 2.2). Each ligand poses can be used to rescore and to refine poses. Additionally, the knowledge of pharmacophore was introduced to constrain the poses.

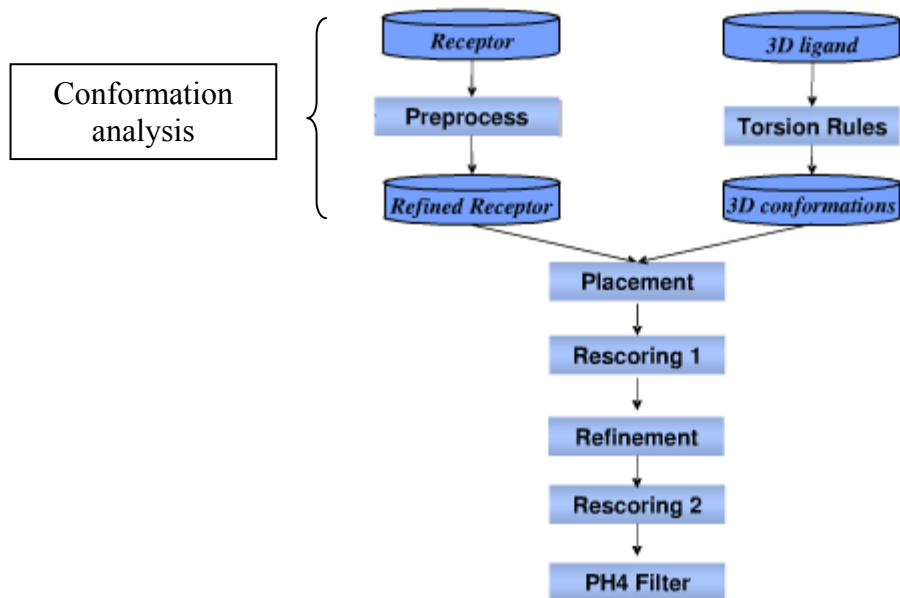


Fig 2.2. The work flow of the docking application of the program MOE

2.4.2 Docking methodology

From experiment it is known that ligands preferably to block the open conformation. Thus, the molecular docking of this work was focused on the open conformation (structure from Sary et al, 2009) of the ion-gated calcium channel and the improved open conformation with various ligands.

Ligand preparation:

Coordinates of ligands were generated with GaussView [76] and the geometry optimized with the Hartree-Fock method using 3-21G basis set implemented in Gaussian03 [77].

Glide Docking program:

Protein Preparation Wizard workflow implemented in Maestro 8.5 was used to prepare the protein using default settings. Both protein and ligands were parameterized with the OPLS force field. The Receptor Grid Generation panel performed the grid map generation of the receptor. The grid was generated overall binding residues known the experimentally. Docking

calculations performed in Standard Precision (SP) mode using the Ligand Docking panel. The Receptor Grid Generation and Ligand Docking panels are functions in the Glide module.

MOE Docking program:

The standard protocol of the procedure in MOE 2008 was applied in this work. The Alpha Triangle placement which derives poses by random superposition of ligand atom triplets alpha sphere dummies in the receptor site is to determine the poses. The London dG scoring function estimates the free energy of binding of the ligand from a given pose. The functional form is a sum of terms:

$$\Delta G = c + E_{flex} + \sum_{h-bonds} C_{HB} f_{HB} + \sum_{m-lig} C_M f_M + \sum_{atoms} \Delta P_i$$

Where

| | | |
|------------|---|---|
| c | = | the average gain/loss of rotational and translational motion. |
| E_{flex} | = | the energy due to loss of flexibility of the ligand. |
| C_{HB} | = | an hydrogen bond energy |
| f_{HB} | = | measures geometric imperfections of hydrogen bonds |
| C_M | = | a metal ligation energy |
| f_M | = | measures geometric imperfections of metal ligations |
| D_i | = | the desolvation energy of each atom i |

2.5. Molecular dynamic simulations

Molecular Dynamic Simulation (MD) is a theoretical and computational method based on solving the Newton's equation of motion. This method is used to mimic the behavior of the system as a function of time. MD provides a basis for a more complete understanding of biological systems and aids in the interpretation of experiments concerned with their properties.

In a molecular dynamics simulation, the trajectory of the molecules and atoms for choosing the potential function $U(r_1, \dots, r_N)$ of the position of the nuclei represent the potential energy of the system when the atoms are arranged in specific configuration. The potential energy is usually constructed from the relative positions of the atoms with respect to each other. Forces

are derived as the gradients of the potential with respect to atomic displacement as shown in below formula.

$$F_i = -\nabla_{r_i} U(r_1, \dots, r_N)$$

This form implies the presence of a conservation law of the total energy $E = K + V$, where K is the instantaneous kinetic energy.

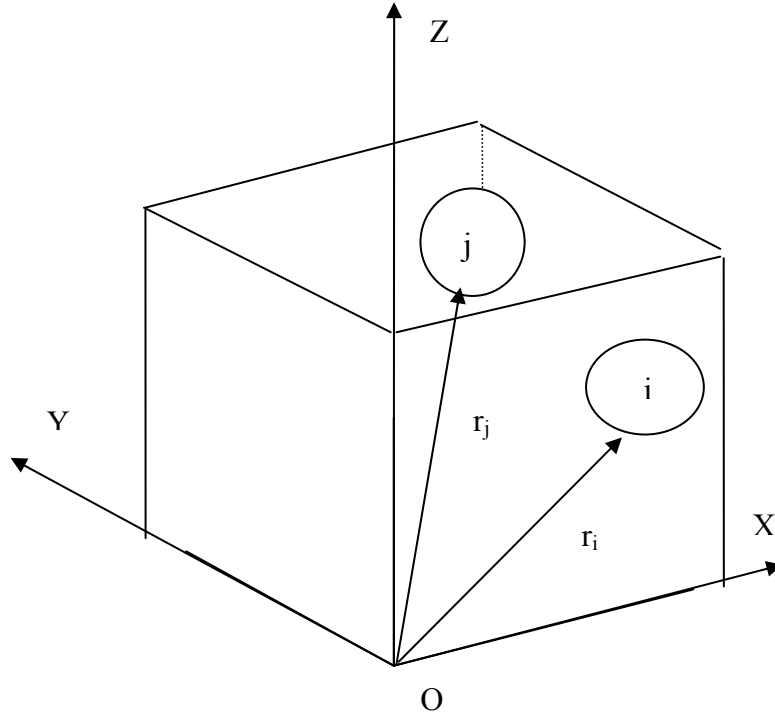


Fig 2.3. Cartesian coordinated laboratory-fixed reference frame used to define a position vector.

The translational motion of spherical molecules is caused by a force F_i exerted by some external agent. The motion and the applied force are explicitly interpreted by Newtonian. Newton's equation of motion of a N particle system is written in a set of N coupled second order differential equation in time. The functional form is a sum of terms:

$$m_i \frac{d^2 r_i}{dt^2} = -\nabla_i [U(r_1, r_2, \dots, r_N)] \quad i = 1, N$$

where m is the mass of the molecule, r_i is a vector that locates the atoms with respect to a set of coordinate axes as shown in Fig 2.3 [78]

The force fields describe atomic interactions with contributions from bonded (bond length, bond angle and bond torsion) and non-bonded (van der Waals and electrostatic) interactions. Several force fields have been developed such as AMBER [79], GROMOS [80], CHARMM [81] and OPLS [82].

2.5.1 Molecular Dynamics simulation studies of the open conformation of Cav1.2 calcium channel with Verapamil, D619, T13 and qDitiazem

The simulation setup of all ligands with open Cav1.2 is the same procedure as following. Molecular dynamics simulations have been carried out for the open conformation of Cav1.2 embedded in DOPC [83] lipid bilayer. These simulations were performed with the Gromacs software version 4.0.4 using the Amber-03 force-field. The topology of ligands was generated with antechamber [84]. The ligand charges were taken from the quantum chemical calculation (Gaussian 03) with the Hartree-Fock 3-21G basis set. The TIP3P water and 4 Ca^{2+} ions were placed along the z-axis. Cl^- ions were added randomly within the solvent to neutralize the system. Snapshots of the trajectory were written out every 20 ps. The system was energy minimized with the steepest descent algorithm, followed by positional restrained MD for 2 ns. Subsequently, 40 ns of unrestrained MD simulation were carried out using the NVT ensemble. The V-rescale thermostat and Parrinello-Rahman barostat algorithms were used. Electrostatic interactions were calculated explicitly at a distance smaller than 1 nm, and long-range electrostatic interactions were calculated at every step by particle-mesh Ewald summation. Lennard-Jones interactions were calculated with a cut-off of 1 nm. All bonds were constrained by using the LINCS algorithm, allowing for an integration time step of 2 fs. The simulation temperature was kept constant by weakly ($\tau = 0.1$ ps) coupling the lipids, protein, and solvent (water + counter ions) separately to a temperature bath of 300 K. The pressure was kept constant by weakly coupling the system to a pressure bath of 1 bar with semi-isotropic pressure coupling. More details of parameter files are shown in Appendix I.

2.5.2 Molecular Dynamics simulation studied of closed and open conformation Cav1.2 calcium channel in pure POPC and content of cholesterol in the membrane

Molecular dynamics simulations of Cav1.2 in a closed and an open conformation have been carried out in pure POPC and POPC/CHOL environment. The system was set up by the following steps:

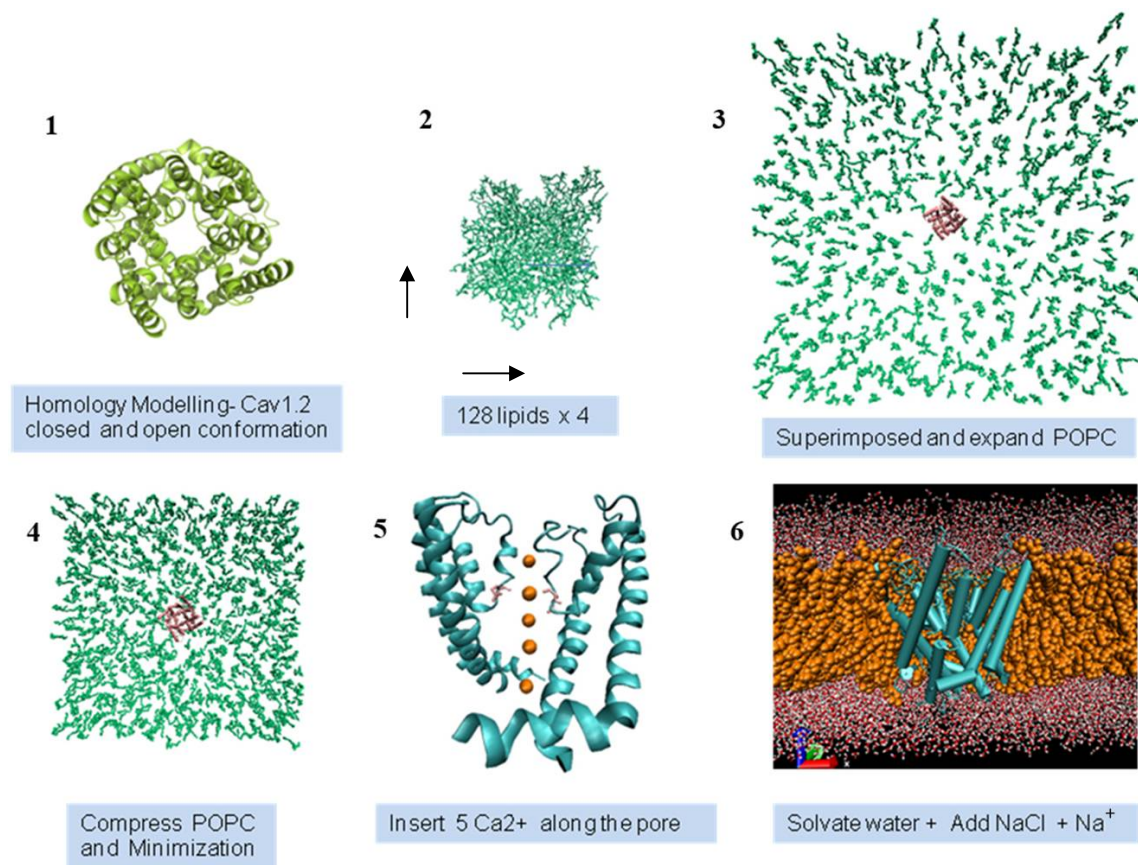


Fig 2.4. The setup of the molecular dynamics simulation of Cav1.2 channel in pure POPC.

1. Generate the topology file of Cav1.2 of closed and improved conformation obtained from homology modeling.
2. For POPC environment (Fig 2.4), replicate the starting configuration of a 128-lipid POPC bilayer in X and Y axis to create of a bilayer of 512 lipids. For POPC/CHOL environment (Fig 2.5), generate the mixture lipid bilayer POPC and 25% cholesterol from single POPC and cholesterol molecules. Randomly add cholesterol into the POPC bilayer.

3. Superimpose the Cav1.2 channel with POPC and POPC/CHOL bilayer and use INFLATEGRO tool to expand the POPC for POPC system. In case of the POPC/CHOL system, a minimal number of overlapping POPC and CHOL molecules was removed.
4. Slowly compress only the POPC using the INGLATEGRO tool and POPC/CHOL using the tool included in Gromacs. Locate the channel in the center of bilayer and minimize the whole system. Repeat the compress and minimize whole system step until the area per lipid of POPC is around 65 \AA^2 .
5. Insert the 5 Ca^{2+} along the pore.
6. Solvate water TIP3P, add NaCl. Neutralize system by adding Na^+ ion.

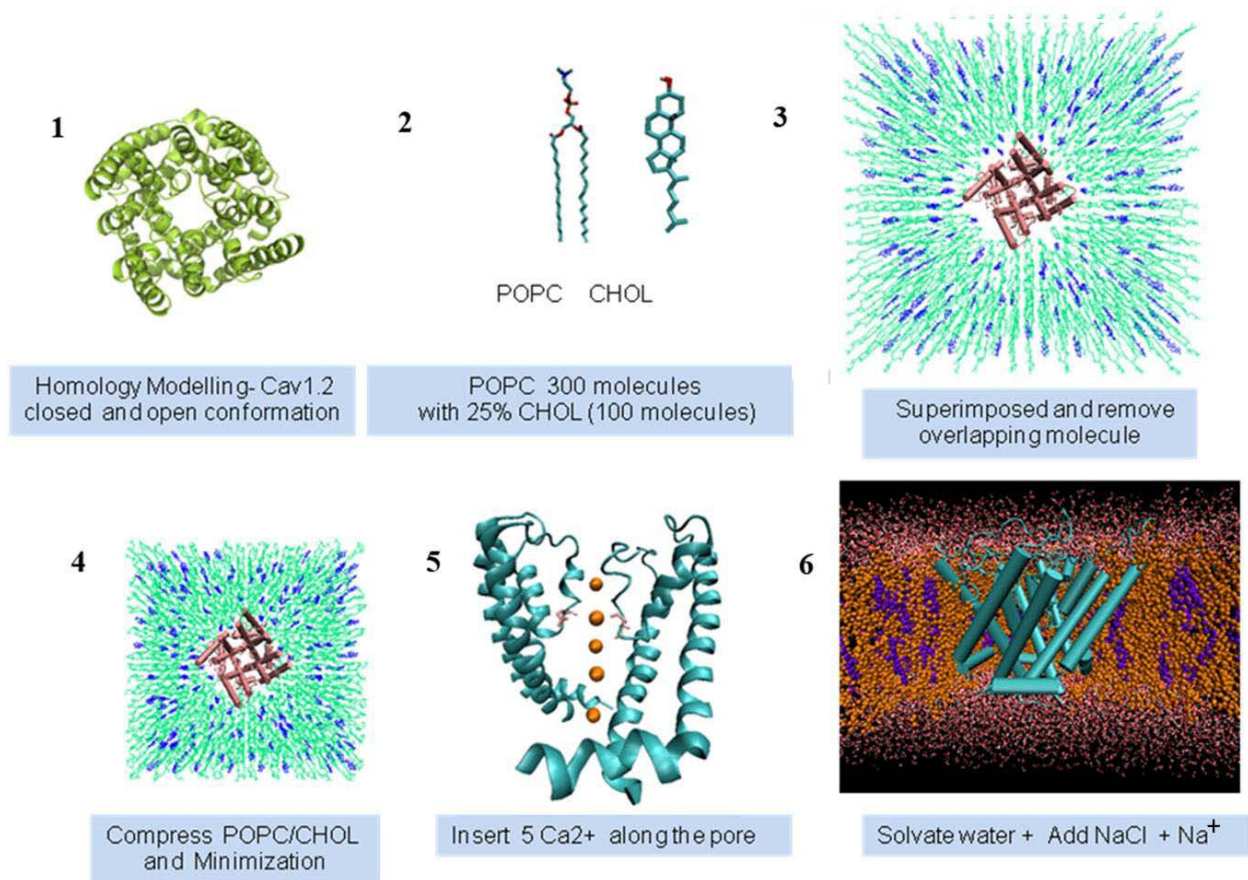


Fig 2.5. The setup of the molecular dynamics simulation of Cav1.2 channel in POPC/CHOL.

CHAPTER 3

RESULTS AND DISCUSSION

3.1 Sequence conservation of L-type calcium channel

The sequence between Ca_v1.2 from *Oryctolagus Cuniculus* rabbit (accession number: P15381) and other L-type calcium channels as performed to investigate the structure, functional and evaluation relationship of L-type calcium channels. All available sequences were downloaded from Expasy [85] and Blast database (Table 3.1).

Table 3.1 Species available of each isoforms of L-type calcium channel from Expasy and Blast database. The available sequences from Expasy and Blast database are highlighted in grey.

| Species | Ca _v 1.1 | Ca _v 1.2 | Ca _v 1.3 | Ca _v 1.4 |
|--|---------------------|---------------------|---------------------|---------------------|
| Oc = Rabbit = <i>Oryctolagus Cuniculus</i> | | | | |
| Hs = Homo sapiens | | | | |
| Ms = Mouse = <i>Mus musculus</i> | | | | |
| Rn = Rat = <i>Rattus Norvegicus</i> | | | | |
| Gg = Chicken = <i>Gallus gallus</i> | | | | |
| Cf = Dog = <i>Canis lupus</i> | | | | |
| Rc=Bull frog= <i>Rana catesbeiana</i> | | | | |
| Md= opossum = <i>Monodelphis domestica</i> | | | | |
| Cp=Chimpanzee= <i>Pan troglodytes</i> | | | | |
| Ma=MESAU= <i>Mesocricetus auratus</i> | | | | |
| Bt=Bovien= <i>Bos taurus</i> | | | | |
| ONCMY= <i>Oncorhynchus mykiss</i> | | | | |
| Mm = Monkey = <i>Macaca mulatta</i> | | | | |

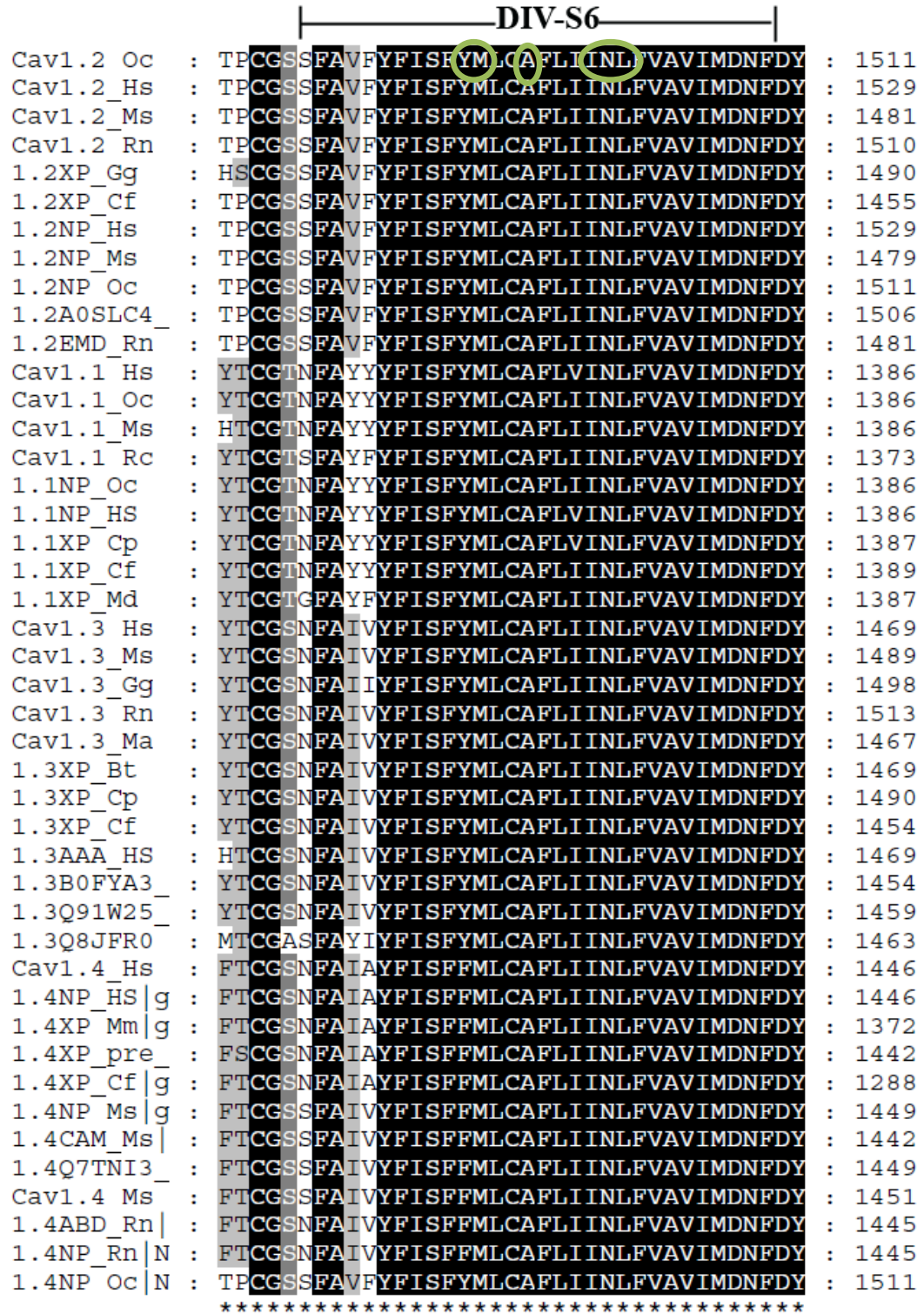
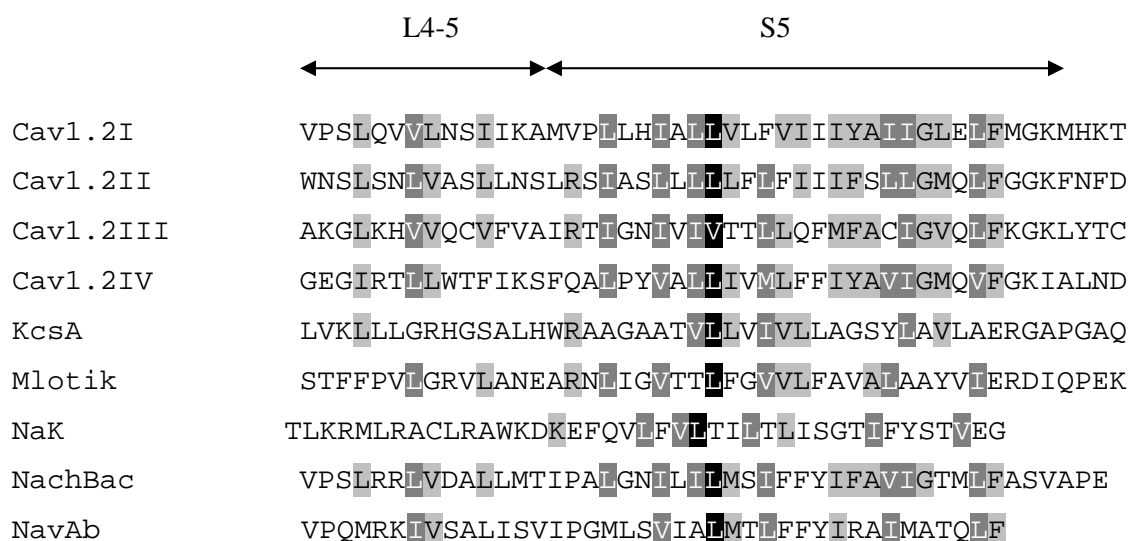


Fig 3.1. Multiple sequence alignment of the IVS6 of Ca_v1.2.

The multiple sequence alignment was constructed on all found of L-type channels to obtain the similarity among them. This family shares 80 % sequence identity. The multiple alignment of domains I to IV shown in Appendix II point out that the L45, S5, P-helix and S6 of every domain are conserved. All binding residues are located along IIIS5, IIIP, IIIS6, IVP and IVS6 [34] and are shown to be highly conserved. Our work focus on all binding residues of DHPs, PAAs and BTZs drug on L-type channel which are pointed by green circle. In Fig 3.1 only the IVS6 part is shown. For all binding residues see Appendix III.

3.2 Sequence alignment of Ca_v1.2 closed conformation



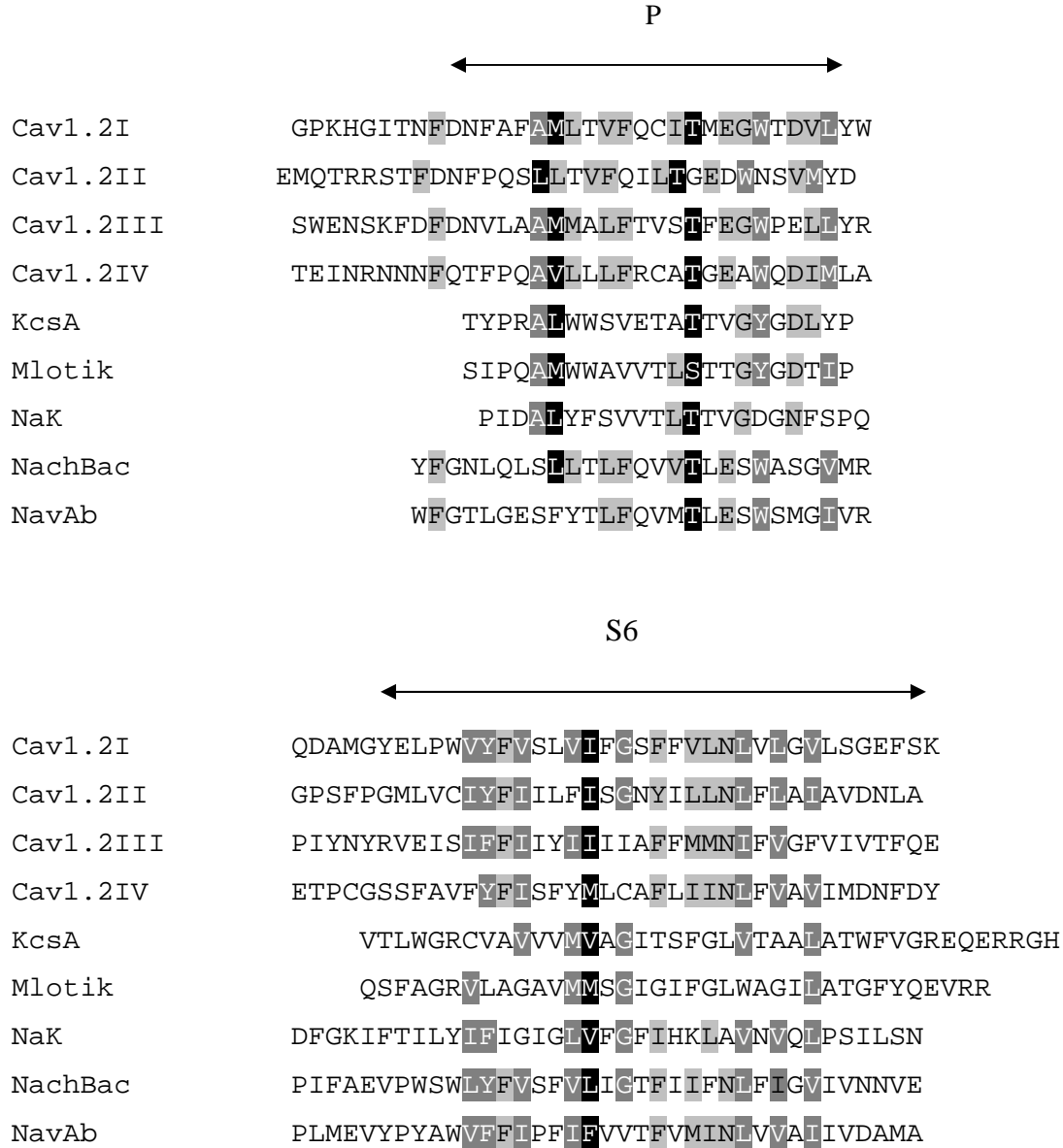


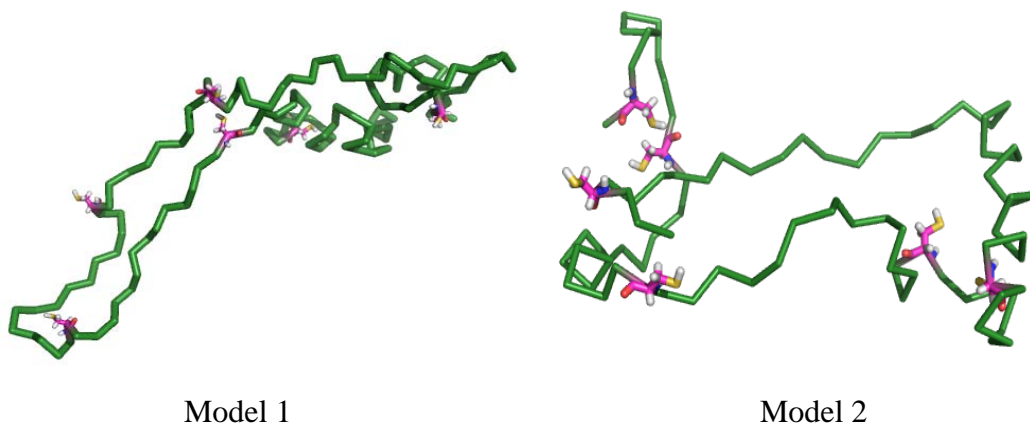
Fig 3.2. Multiple sequence alignment of the pore region of $\text{Ca}_v1.2$ closed conformation.

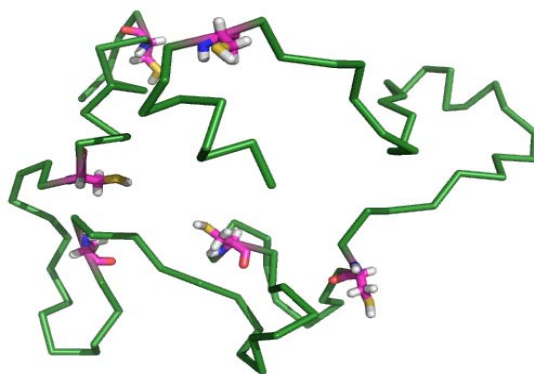
The alignment of the pore region of $\text{Ca}_v1.2$ closed channel based on multiple sequence alignment of potassium channel KcsA [86], Mlotik channel [87], the nonselective cation channel NaK [88] and homology model of the NaChBac sodium channel [89] (is shown in Fig 3.2). The overall sequence identity between calcium channels, potassium channels and the sodium channel NaK are quite low. An alignment between $\text{Ca}_v1.2$ and NaChBac are more closely related. Highly conserved residues are shaded black. Positions of mainly conserved changes are shaded grey.

3.3 Sequence alignment and inner pore domain prediction of Ca_v3.1 T-type calcium channel

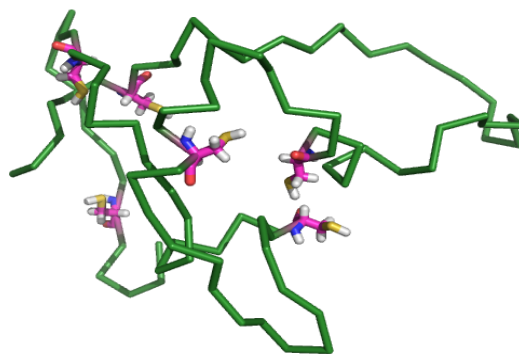
Due to the sequences similarity, the sequence of L-type channel Ca_v1.2, P/Q-type channel Ca_v2.1 and T-type channel Ca_v3.1, Ca_v3.2 and Ca_v3.3 were used for alignment on the inner pore domains (S5-P-S6) of Ca_v3.1 (Fig 1 in the following publication). The homology model of this region was built based on homology model of Ca_v1.2 as template [9]. The *Ab Initio* methods by using ROSETTA program and I-Tasser server were used to construct the structure and to compare the results with experimental data which focus on six cysteines residues located in the extracellular loop between segment IS5 and the pore helix. We hypothesize that forming of the disulfide bonds within the loop and/or neighboring segment of the cysteines in the extracellular loop influences gating.

The 10 structures obtained from ROSETTA program reveal that the position of six cysteine residues does not form disulfide bonds which is inconsistent with the hypothesis (Fig 3.3). For the I-Tasser server models, only 3 models from 10 models were in agreement with the experimental evidence which is demonstrated in Fig 3. on supplementary material of the publication. Therefore, *Ab Initio* methods are still not accurate enough to observe the various possible disulfide bonds in the model.

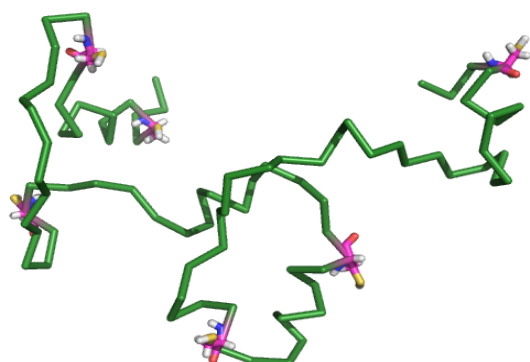




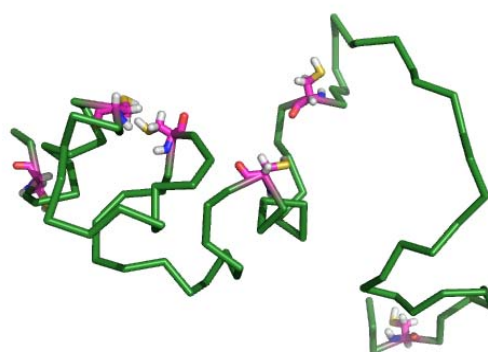
Model 3



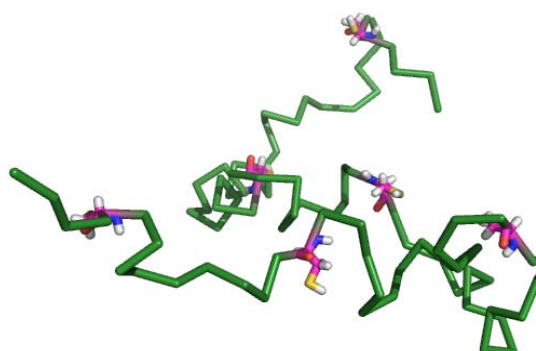
Model 4



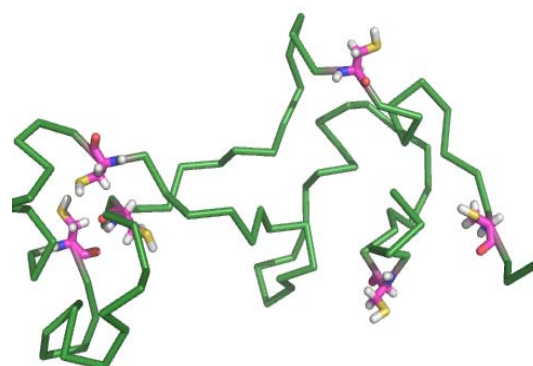
Model 5



Model 6



Model 7



Model 8

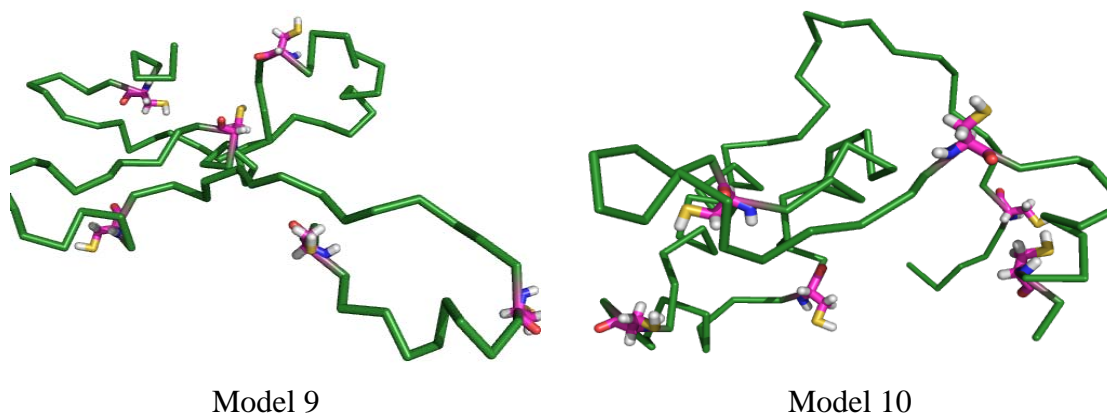


Fig 3.3. 10 different models from ROSETTA programs obtained by the *Ab Initio* method. The 6 cysteines are shown in purple sticks. The extracellular loop is presented in green ribbon.

Paper 1

Cysteines in the loop between IS5 and the pore helix of Ca_v3.1 are essential for channel gating.

Cysteines in the loop between IS5 and the pore helix of Ca_v3.1 are essential for channel gating

Maria Karmazinova · Stanislav Beyl ·
Anna Sary-Weinzinger · Chonticha Suwattanasophon ·
Norbert Klugbauer · Steffen Hering · Lubica Lacinova

Received: 3 June 2010 / Revised: 9 August 2010 / Accepted: 17 August 2010 / Published online: 9 September 2010
© Springer-Verlag 2010

Abstract The role of six cysteines of Ca_v3.1 in channel gating was investigated. C241, C271, C282, C298, C313, and C323, located in the extracellular loop between segment IS5 and the pore helix, were each mutated to alanine; the resultant channels were expressed and studied by patch clamping in HEK293 cells. C298A and C313A conducted calcium currents, while the other mutants were not functional. C298A and C313A as well as double mutation C298/313A significantly reduced the amplitude of the calcium currents, shifted the activation curve in the depolarizing direction and slowed down channel inactivation. Redox agents dithiothreitol (DTT) and 5,5'-dithiobis(2-nitrobenzoic acid) (DTNB) shifted the current activation curve of wild-type channels in the hyperpolarizing direction. Activation curve for all mutated channels was shifted in hyperpolarizing direction by DTT while DTNB caused a depolarizing shift. Our study reveals that the cysteines we studied have an essential role in Ca_v3.1

gating. We hypothesize that cysteines in the large extracellular loop of Ca_v3.1 form bridges within the loop and/or neighboring channel segments that are essential for channel gating.

Keywords T-type calcium channels · Voltage gating · Cysteine · Modulation · Modeling

Introduction

Low-voltage activated (LVA) calcium channels activate at more negative membrane voltages than high-voltage activated (HVA) channels [22]. By initiating so-called low-voltage calcium spikes, LVA channels specifically contribute to neuronal excitability [10]. The molecular basis of the gating peculiarities of LVA channels is largely unknown. All voltage-gated calcium channels are composed of four homologous domains, each containing six transmembrane segments S1–S6 and a pore loop (P) between segments S5 and S6. Four voltage-sensing domains each composed of the transmembrane segments S1–S4 are arranged around a central pore domain formed by four sets of S5-P-S6 [26]. First insights into a differential contribution of individual domains to channel gating were obtained by a domain swapping approach between the LVA Ca_v3.1 and the HVA Ca_v1.2 channel. These experiments demonstrated that domains I, III, and IV determine the midpoint for voltage-dependent activation [19]. Similarly, swapping parts of Ca_v3.1 and Ca_v3.3 channels pointed to a central role of domain IV and to a lesser impact of domain I [8]. Exchange of the basic uppermost arginines in each of the S4 segments by neutral cysteines substantiated the importance of the IIIS4 segment and a moderate role of the segments IS4 and IIS4 [17].

LVA calcium channels contain a unique conserved large external domain located between the IS5 region and the

Electronic supplementary material The online version of this article (doi:10.1007/s00424-010-0874-5) contains supplementary material, which is available to authorized users.

M. Karmazinova · L. Lacinova (✉)
Institute of Molecular Physiology and Genetics,
Slovak Academy of Sciences,
Bratislava, Slovakia
e-mail: lubica.lacinova@savba.sk

S. Beyl · A. Sary-Weinzinger · S. Hering
Institut für Pharmakologie und Toxikologie, University of Vienna,
Vienna, Austria

N. Klugbauer
Institut für Experimentelle und Klinische Pharmakologie
und Toxikologie, Albert-Ludwigs Universität,
Freiburg, Germany

C. Suwattanasophon
Institute of Theoretical Chemistry, University of Vienna,
Vienna, Austria

pore loop (P). In HVA calcium channels this loop is smaller and not well conserved. Six cysteines located within this region (Supplementary Figure 1) are conserved among all three Ca_v3 channels. Disulfide bonds between these cysteines may stabilize the conformation of this large extracellular region. Considering that this region is linked to the conducting pore, it might contribute to the modulation of the channel gating. Swapping the whole domain in the $\text{Ca}_v3.1$ channel had a much stronger effect on channel activation than the mutation in the voltage sensor itself [17, 19] suggesting a principal role of other structure(s) within domain I for channel gating. A possible role of this region for pore opening is underlined by the discovery of mutations within the $\text{Ca}_v3.2$ sequence related to epilepsy [15]. Several of these mutations resulted in a greater calcium current and some cause channel openings at more hyperpolarized potentials.

LVA channels were also found to be modulated by redox agents [14, 18, 21, 30]. Reducing agents were shown to interact specifically with $\text{Ca}_v3.2$ [14]. This effect was attributed to their ability to act as metal chelators rather than to reduction of channels' cysteines [21]. Thiol modulating agent lipoic acid interacts exclusively with four extracellular cysteines in the $\text{Ca}_v3.2$ channel sequence located in the extracellular loop between S1 and S2 segments of domain I and in the loop connecting S5 segment to the pore loop in domain II [18]. Traditional thiol oxidizing agent DTNB interact with these, but also with additional not yet identified sites.

Cysteines in the IS5-P connecting loop are on the extracellular side of the channel and could be the site of action of redox agents. Out of 16 extracellularly located cysteines in the $\text{Ca}_v3.1$ sequence, 13 are located in the pore regions of individual channel domains (Fig. 1). The length of some of these extracellular loops suggests that inter-domain disulfide bridges may be possible.

Here we investigated the contribution of each of the endogenous loop cysteines to channel gating and to redox modulation by substituting alanine for each of them in turn. Four of these mutants (C241A, C271A, C282A, and C323A) did not form functional channels, indicating a key role of these residues in channel gating. C298A and C313A conducted calcium currents, but with altered voltage dependencies of activation and kinetics of inactivation. These findings and the observed changes in redox regulation highlight the functional importance of these cysteine residues.

Materials and methods

Mutagenesis The mouse brain T-type $\text{Ca}_v3.1$ calcium channel cDNA (accession number AJ012569 [16]) was cloned into the plasmid pEGFP N-1 (Clontech, Mountain

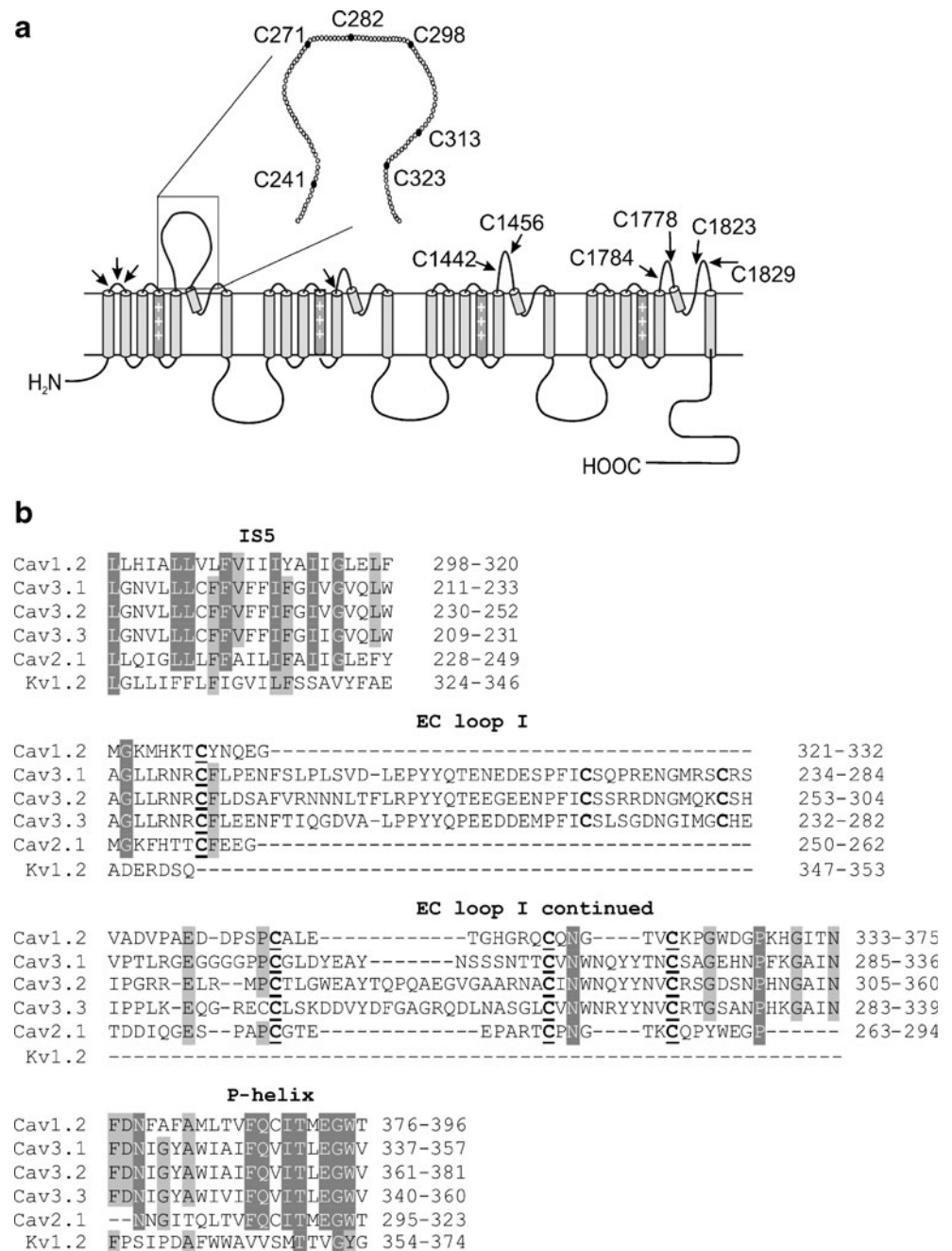
View, CA) after removing the stop codon, thereby creating a $\text{Ca}_v3.1$ -EGFP fusion protein. The mutations were introduced in wild-type (WT) $\text{Ca}_v3.1$ cDNA using a polymerase chain reaction based method. In general, PCR reactions were performed on partial cDNA fragments (cassettes) of $\text{Ca}_v3.1$. The mutant $\text{Ca}_v3.1$ channels were constructed by subcloning these mutant cassettes into the full-length $\text{Ca}_v3.1$ -EGFP fusion protein. All regions replaced by PCR fragments were sequenced and the presence of the desired mutation(s) was confirmed.

Cell culture and transfection All experiments were carried out on either HEK 293 cells (electrophysiological experiments) or tsA-201 cells (confocal imaging) transiently transfected by pEGFP N-1 plasmids containing either cDNA of wild-type or mutant $\text{Ca}_v3.1$ subunits. Cells were grown in MEM with Eagle's salts, containing 10% fetal calf serum, 100 U/ml penicillin–streptomycin in an atmosphere of 5% CO_2 , and 95% air at 37°C. Cells were harvested from their culture flasks by trypsinization and plated out onto 13-mm round glass coverslips (Slavus, Bratislava, Slovakia) coated with 0.01% poly-L-lysine. The cells were transiently transfected with the expression vector using LipofectAMINE 2000 according to the instructions of the manufacturer (Invitrogen, Carlsbad, CA). Cells were incubated for 2 to 3 days following transfection before electrophysiological experiments.

Confocal microscopy The confocal images were obtained ~30 h after transfection. The data illustrated are representative for 10–15 tsA-201 cells from three independent experiments. For confocal microscopy $\text{Ca}_v1.3$ were expressed in tsA-201 cells. $\text{Ca}_v1.3$ displayed similar kinetics in tsA-201 and HEK 293 cells. Confocal images were acquired with a Zeiss LSM-510 confocal laser scanning microscope, using a $\times 63$ (1.4 NA) oil immersion objective. The plasma membrane was stained with 1 μM FM4-64 (amphiphilic styryl dye, Molecular Probes). Images were acquired using an argon laser (excitation, 488 nm; emission BP505–530 nm emission filter) for the EGFP-tagged $\text{Ca}_v3.1$ α_1 -subunits and a He–Ne laser (excitation, 543 nm; emission filter, LP650 nm) for FM4-64.

Homology modeling The IS5 helix, the extracellular loop (EC loop I), and the IP segments of the L-type calcium channel $\text{Ca}_v1.2$ (accession number: P15381), the T-type channels $\text{Ca}_v3.1$ (accession number: Q9WUT2), $\text{Ca}_v3.2$ (accession number: Q95180), $\text{Ca}_v3.3$ (accession number: Q9P0X4), and the P/Q-type calcium channel $\text{Ca}_v2.1$ (accession number: P97445) were aligned using ClustalX [13]. Additionally, the sequence of the $\text{K}_v1.2$ crystal structure (pdb identifier: 2r9r) [20] was aligned with the Ca_v sequences, as suggested previously [24]. Supplemental Figure 1 shows the alignment of the full pore domain (S1–S6) of $\text{Ca}_v3.1$, $\text{Ca}_v3.2$, and NaChBac with that of $\text{K}_v1.2$.

Fig. 1 Schematic structure and alignment of the extracellular loop of $\text{Ca}_v \alpha_1$ subunits in domain I. **a** shows the loop connecting the IS5 segment and the putative pore helix. The loop region is enlarged in the *inset*. Each amino acid is represented by one *open circle*. Filled circles indicate the location of six cysteine residues in this loop. The approximate positions of other extracellularly located cysteines are indicated by *arrows*. *Barrels* represent putative α -helices in the channel structure. **b** illustrates an alignment of $\text{Ca}_v 1.2$ (accession number: P15381), $\text{Ca}_v 3.1$ (accession number: O43497), $\text{Ca}_v 3.2$ (accession number: O95180), $\text{Ca}_v 3.3$ (accession number: Q9P0X4), $\text{Ca}_v 2.1$ (accession number: P97445), and $\text{Kv} 1.2$ (pdb identifier: 2r9r). Identical residues in all five Ca_v channels are shaded *dark gray*; residues that are identical in four Ca_v channels are shaded *light gray*. Highly conserved cysteines in EC loop I are *bold* and *underlined*, whereas cysteines conserved only in the T-type family are shown in *bold*



The structure model of $\text{Ca}_v 3.1$ was generated with Modeller9v6 [6]. Ten ab initio models of the extracellular loop connecting IS5 and IP were constructed using the I-Tasser server [33].

The inner pore domain (S5-P-S6) of $\text{Ca}_v 3.1$ is based on the $\text{Ca}_v 1.2$ homology model. The validated homology model of $\text{Ca}_v 1.2$ was used as template, because it shares high sequence similarity with $\text{Ca}_v 3.1$ in these regions. The voltage-sensing domains (S1–S4) are based on the $\text{Kv} 1.2$ crystal structure (pdb: 2r9r, 3lut) [11, 20]. The accuracy of ab initio models is given by the TM-score [35], which measures the correctness of the global topology of such

models. The value for our best loop model is 0.46, which is slightly below the >0.5 threshold for correct topology models, but clearly above the ≤ 0.17 threshold indicating random prediction [34]. Therefore this model can be used to assess, if and which cysteines from other domains might be close enough for direct interactions within this loop.

Electrophysiology and data analysis The Ca^{2+} current through expressed WT and mutated channels was studied using the conventional whole cell configuration of the patch-clamp technique using the HEKA-10 patch-clamp amplifier (HEKA Electronic, Lambrecht, Germany). The

extracellular solution contained (in mM): NaCl, 155; CaCl₂, 2; MgCl₂, 1; CsCl, 5; HEPES, 10; pH 7.4 (NaOH). The intracellular solution contained (in mM): CsCl, 130; EGTA, 10; MgCl₂, 5; TEA-Cl, 10; Na₂-ATP, 5; and HEPES, 10; pH 7.4 (CsOH). The osmolarity of the internal solution was approximately 300 mOsm; the osmolarity of the external solution was adjusted by adding glucose to a final value 2–3 mOsm lower than the internal solution. Extracellular solutions were exchanged by a gravity-driven flow system with manually controlled valves. Patch pipettes were manufactured from borosilicate glass (Sutter Instrument, Novato, CA) with input resistance ranging from 1.6–2.0 MΩ. The cell capacitance had an average value of 15.5±0.4 pF (*n*=202). Average series resistance was 4.11±0.07 MΩ (*n*=202). Series resistance was compensated for up to 70%. The bath was grounded using an AgCl pellet connected to the experimental chamber through an agar bridge.

Data were recorded with HEKA Pulse 8.5 and analyzed offline using HEKA Pulsefit 8.5 and Origin 7.5 software. Data were sampled at 10 kHz and filtered at 3 kHz. Capacity transient and series resistance were compensated by built-in procedures of the EPC 10 amplifier. Residual linear leak current was subtracted by a built-in procedure of the EPC 10 amplifier. Only cells with a holding current smaller than 10% of peak current amplitude were used for experiments.

The holding potential (HP) in all experiments was −100 mV. Current–voltage (*I/V*) relationships were measured by stepping every 3 s from a HP to membrane potentials between −90 and +80 mV for 50 ms. Steady-state inactivation was measured by series of 5-s long prepulses to voltages between −150 and −10 mV, followed by a 5 ms return to a HP and a 40 ms test pulse to −30 mV.

Conductance was calculated according to the equation:

$$G(V) = \frac{I(V)}{V - V_{\text{rev}}} \quad (1)$$

where $G(V)$ is the conductance at test potential V , $I(V)$ is amplitude of the current measured at test potential V , V is the membrane voltage, and V_{rev} is the reversal potential. Voltage dependence of current activation was satisfactorily fitted by the Boltzmann equation:

$$\frac{G(V)}{G_{\text{max}}} = \frac{1}{1 + e^{\frac{-(V - V_{0.5\text{act}})}{dV_{\text{act}}}}} \quad (2)$$

where G_{max} is a maximal conductance, $V_{0.5\text{act}}$ is a half-maximal activation voltage, dV_{act} is a slope factor of activation curve, and other symbols have the same meaning as in previous equation. Steady-state inactivation curves were fitted by a Boltzmann equation in the form:

$$\frac{I(V)}{I_{\text{max}}} = \frac{1}{1 + e^{\frac{V - V_{0.5\text{inact}}}{dV_{\text{inact}}}}} \quad (3)$$

where I_{max} is the maximal current amplitude, $V_{0.5\text{inact}}$ is the voltage at which the current is half-inactivated, and dV_{inact} is the slope factor of the steady-state inactivation curves. To evaluate time constants of current activation and inactivation, individual current traces were fitted by the Hodgkin–Huxley equation, using the m^2h kinetics [17, 27].

The voltage dependence of τ_{inact} was fitted by a function:

$$\tau(V) = e^{\frac{-(V - V_{\tau})}{s_{\tau}}} + \tau(\infty) \quad (4)$$

where V_{τ} is the voltage at which τ is equal to $1 + \tau(\infty)$, s_{τ} represents the voltage sensitivity of inactivation, and $\tau(\infty)$ is the asymptotic value at positive potentials.

Data are given as mean ± SEM from *n* cells. Statistical significance between two groups was determined by unpaired Student's *t* test and considered significant when $p < 0.05$.

Drugs and reagents All drugs and chemicals were obtained from Sigma-Aldrich, St. Louis, MO, except where noted otherwise. Solutions of dithiothreitol (DTT) and 5,5'-dithiobis (2-nitrobenzoic acid) (DTNB) were prepared fresh prior to the experiment directly in the bath solution.

Results

Cysteine substitutions C241A, C271A, C282A, and C323A result in non-functional channels

Six cysteines located in the loop connecting the IS5 segment and the IP pore helix of the Ca_v3.1 channel (Fig. 1) were individually mutated to alanines. Further, the double-mutant C298/313A was constructed. C241A, C271A, C282A, and C323A resulted in non-functional channels when transiently expressed in HEK 293 cells, while mutants C298A and C313A conducted calcium channel currents (Fig. 2). To investigate whether the lack of current observed for mutants C241A, C271A, C282A, and C323A resulted from impaired plasma membrane targeting, we examined the subcellular distribution of EGFP-fused channel proteins by confocal microscopy. The localization of the channel proteins was visualized using the membrane-selective dye FM4-64 (Supplementary Figure 2). Similar overlap between green fluorescence of EGFP-fused channel proteins and red fluorescence of FM4-64 dye in functional and non-functional constructs suggests no differences in their membrane localization (exemplified in Supplementary Figure 2). These findings demonstrate that the lack of current observed for C241A, C271A, C282A, and C323A mutants is unlikely to be caused by a failure in membrane targeting of the mutant EGFP-fused Ca_v3.1 α₁-subunits.

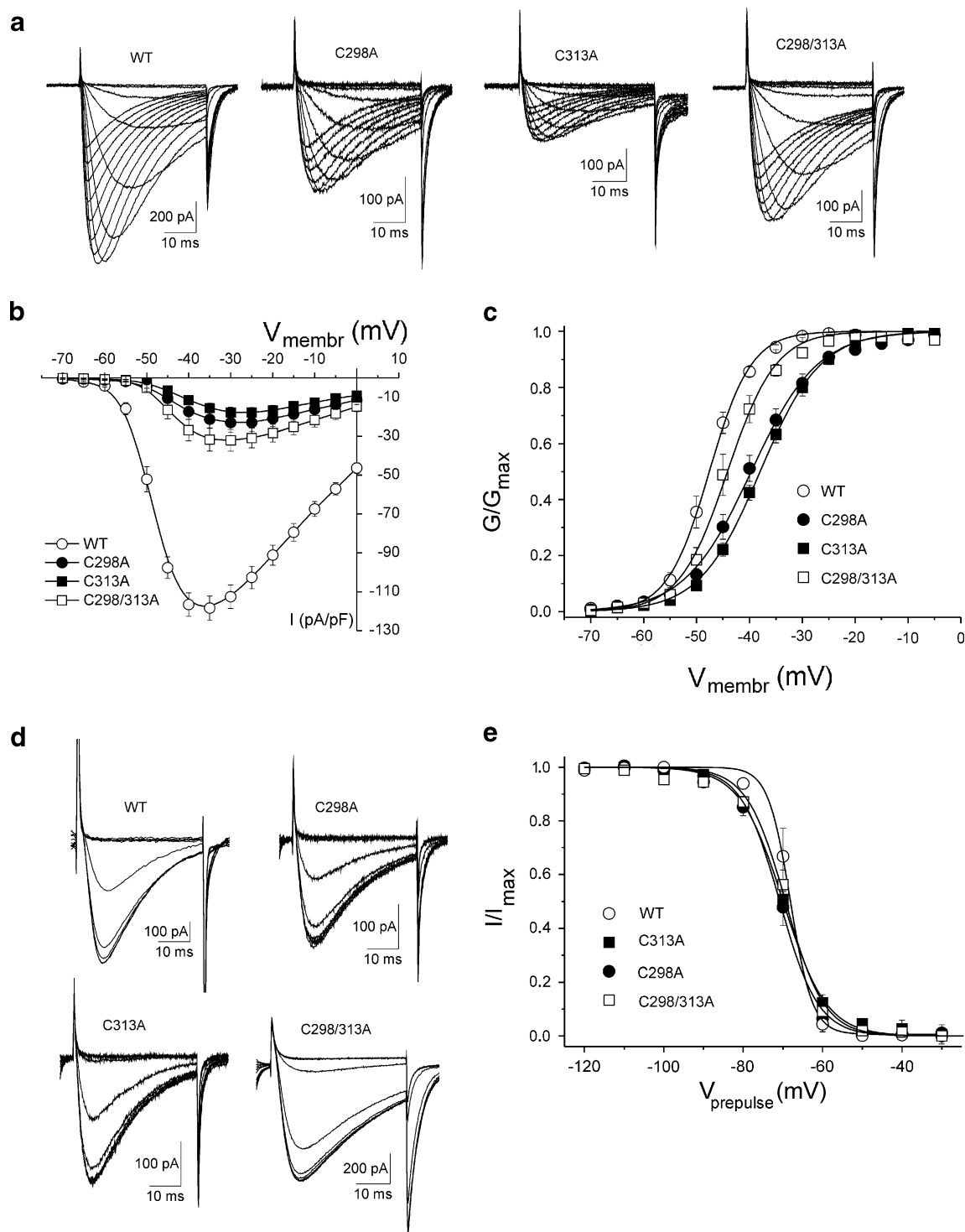


Fig. 2 Comparison of activation and inactivation of WT and mutant channels. Examples of current traces measured during a current-voltage protocol from the WT, C298A, C313A, and C298/313A channels are demonstrated in (a). Corresponding I/V relationships for inward current amplitudes are shown in (b). Solid lines are spline connectors of experimental data points. I/V relationships from (b) were

transformed into conductance-voltage relations using Eq. 1 in (c). Solid lines represent fits of experimental data by Eq. 2. Examples of current traces measured during a steady-state inactivation protocol from WT, C298A, C313A, and C298/313A channels are demonstrated in (d). Corresponding SSI relations are shown in (e). Solid lines represent fits of experimental data by Eq. 3

Cysteines C298 and C313 contribute to the voltage dependence of channel gating

A comparison of the voltage dependencies of activation and inactivation of WT channel, C298 and C313A channel mutants and C298/313A double-mutant channel is shown in Fig. 2. Examples of current traces are shown in Fig. 2a. Both single mutations as well as the double mutation reduced the current amplitude approximately fivefold (Fig. 2b), significantly shifted the voltage dependence of current activation in the depolarizing direction and significantly increased the slope factor of the activation curve (Fig. 2c, Table 2). However, the activation slope factor was not affected by the double mutation.

Examples of current traces measured from all three channels by a steady-state inactivation protocol are shown in Fig. 2d. The mutations did not affect the midpoint voltage of the inactivation curves (-69.4 ± 0.7 mV, $n=7$; -71.0 ± 1.2 mV, $n=10$; -70.0 ± 0.7 mV, $n=11$; and -69.0 ± 0.9 mV, $n=7$ for the WT, C298A, C313A, and C298/313A channels, respectively; Fig. 1e). The effects of both mutations on the slope factors of the voltage dependence of inactivation were less prominent than the effects on activation (3.6 ± 0.4 , 4.1 ± 0.2 , 4.9 ± 0.2 , and 4.3 ± 0.4 mV for the WT, C298A, C313A, and C298/313A channels, respectively) and only for C313A statistically significant ($p < 0.05$).

Functional cysteine mutants have altered channel kinetics

Next we investigated the kinetics of channel gating of the functional cysteine mutants. Activation and inactivation kinetics were determined by fitting the current recordings obtained with I/V protocol (Fig. 2a) by the Hodgkin–Huxley equation in the m^2h form [17, 27]. Both single mutations as well as a double mutation significantly accelerated current activation during depolarization to voltages between -40 and 0 mV (Fig. 3a and Supplementary Table 1). Inactivation was significantly accelerated by mutation C298A and by the double mutation C298/313A only (Fig. 3b and Supplementary Table 1).

Averaged inactivation time constants were fitted by the Eq. 4. Both mutations shifted voltage dependencies of time constants of macroscopic inactivation to more positive membrane voltages (Table 1). Mutation C298, but not C313 decreased the voltage sensitivity. This decrease was preserved in double mutant C298/313A. Plot of time constants of inactivation vs. time constants of activation revealed a moderate correlation ($R=0.94$) between both processes for the C313A mutant and the double-mutant C298/313A ($R=0.86$). No correlation was observed for mutant C298A suggesting a role of this residue in coupling the process of activation to inactivation (Fig. 3c).

Table 1 Mutations altered voltage dependence of inactivation time constants

| | V_τ (mV) | s_τ (mV) | $\tau(\infty)$ |
|-----------|-----------------|---------------|----------------|
| WT | -38.4 ± 2.2 | 5.1 ± 1.1 | 14.7 ± 0.1 |
| C298A | -12.1 ± 3.2 | 7.8 ± 1.0 | 17.8 ± 0.5 |
| C313A | -21.8 ± 1.7 | 4.9 ± 0.5 | 16.3 ± 0.2 |
| C298/313A | -10.1 ± 3.0 | 9.0 ± 0.9 | 24.2 ± 0.7 |

Averaged data presented in Fig. 3b were fitted by Eq. 4. V_τ represents the voltage at which τ is equal to $1 + \tau(\infty)$, s_τ is the voltage sensitivity of activation or inactivation and $\tau(\infty)$ is the asymptotic value at positive potentials. V_τ characterizes the position of voltage dependence of τ_{inact} along the voltage axis

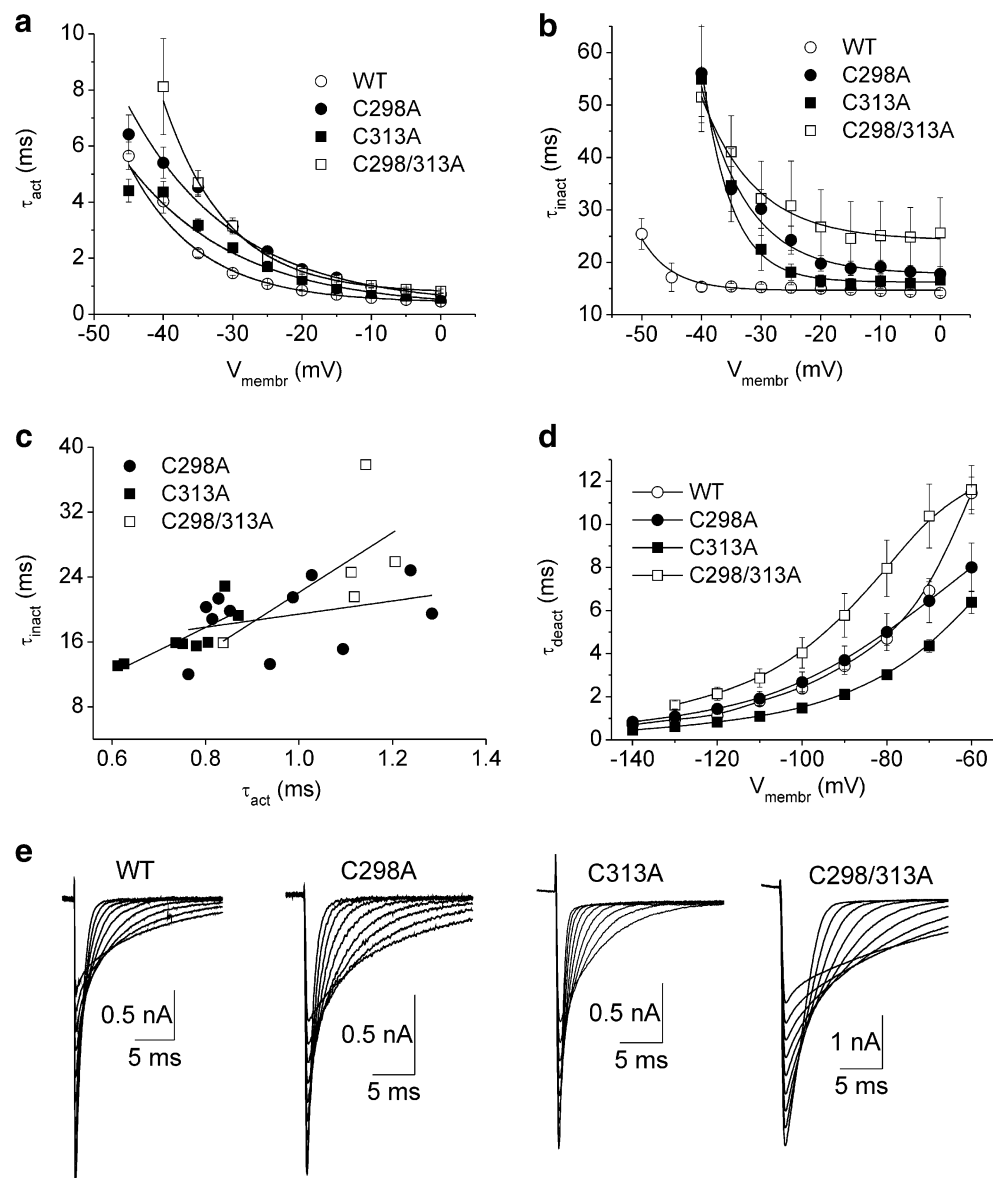
The kinetics of channel deactivation were evaluated at repolarization voltages between -140 and -50 mV (-60 mV for wild type and double mutant). Time constants of channel deactivation were calculated from monoexponential fits to tail currents (Fig. 3e). While deactivation was not affected by mutation C298A, it was statistically significantly accelerated by C313A. In contrast, the double mutation significantly slowed down deactivation (Fig. 3d and Supplementary Table 2).

Redox agents DTT and DTNB modulate WT and mutant $\text{Ca}_v3.1$ channels

It was previously shown [30] that the reducing agent dithiothreitol and the oxidizing agent 5,5'-dithiobis(2-nitrobenzoic acid) modulate T-type calcium channels. DTT is a highly selective redox agent for thiol groups in proteins. When applied to the bath solution one would expect an interaction with cysteines exposed on the extracellular side of $\text{Ca}_v3.1$. As shown in Fig. 4, DTT (10 mM) moderately inhibited WT channel. DTNB in 2.5 mM concentration completely blocked the current through the WT channel. Both mutations altered these redox regulations. In both single mutants as well as in double-mutant DTT slightly stimulated the calcium current. Removal of either cysteine at positions 298 and 313 reduced inhibition by DTNB by 50% and the double mutation further reduced this inhibition (Fig. 4 and Table 3).

Current enhancement by DTT may be due to a shift in the voltage dependence of current activation. Indeed, a small increase of the calcium current amplitudes was observed at voltages more negative than the peak of the I/V relationship. DTT had virtually no effect at voltages higher than the peak of the I/V relationship (Fig. 5, left column). The corresponding activation curves are shown in the right column of Fig. 5. Averaged $V_{0.5}$ and dV values are

Fig. 3 Comparison of activation–deactivation kinetics of the WT and mutant channels. **a** and **b** demonstrate voltage dependencies of activation (**a**) and inactivation (**b**) time constants for the WT, C298A, C313A, and C298/313A channels. Time constants of current activation were calculated by fitting current traces from Fig. 2a by the Hodgkin–Huxley equation in the m^2h form. *Solid lines in b* represent fits of averaged data by Eq. 4. Inactivation time constants for individual mutants are plotted versus activation time constants evaluated at a test potential of -10 mV in (**c**). *Solid lines* are fits of the data with a linear function with following correlation coefficients R and probability values P as follows: C298A $R=0.13$, $P<0.83$; C313A $R=0.94$, $P<0.006$; C298/313A $R=0.86$, $P<0.06$. The time constants of current deactivation depicted in (**d**) were obtained from monoexponential fits of current traces shown in (**e**). *Solid lines* represent fits by B-splines



summarized in Table 2. All three shifts of voltage dependencies of current activation were statistically significant. The slope factors were not significantly different from control (i.e., in the absence of DTT). Negative shifts caused by DTT application partly neutralized the positive shifts caused by the mutations, most prominently in the case of the double mutant. To illustrate both effects we have included the activation curve of WT $\text{Ca}_v3.1$ (dashed lines, Fig. 5d, f, h).

In parallel to the DTT effect on the I – V relation DTNB shifted the voltage dependence of current activation of the WT channel in the hyperpolarizing direction (Fig. 6). In contrast, the shift of channels activation was in the depolarizing direction in both single mutants and in the double mutant (Fig. 6 and Table 3). Activation slope factor was significantly increased in C298A mutant.

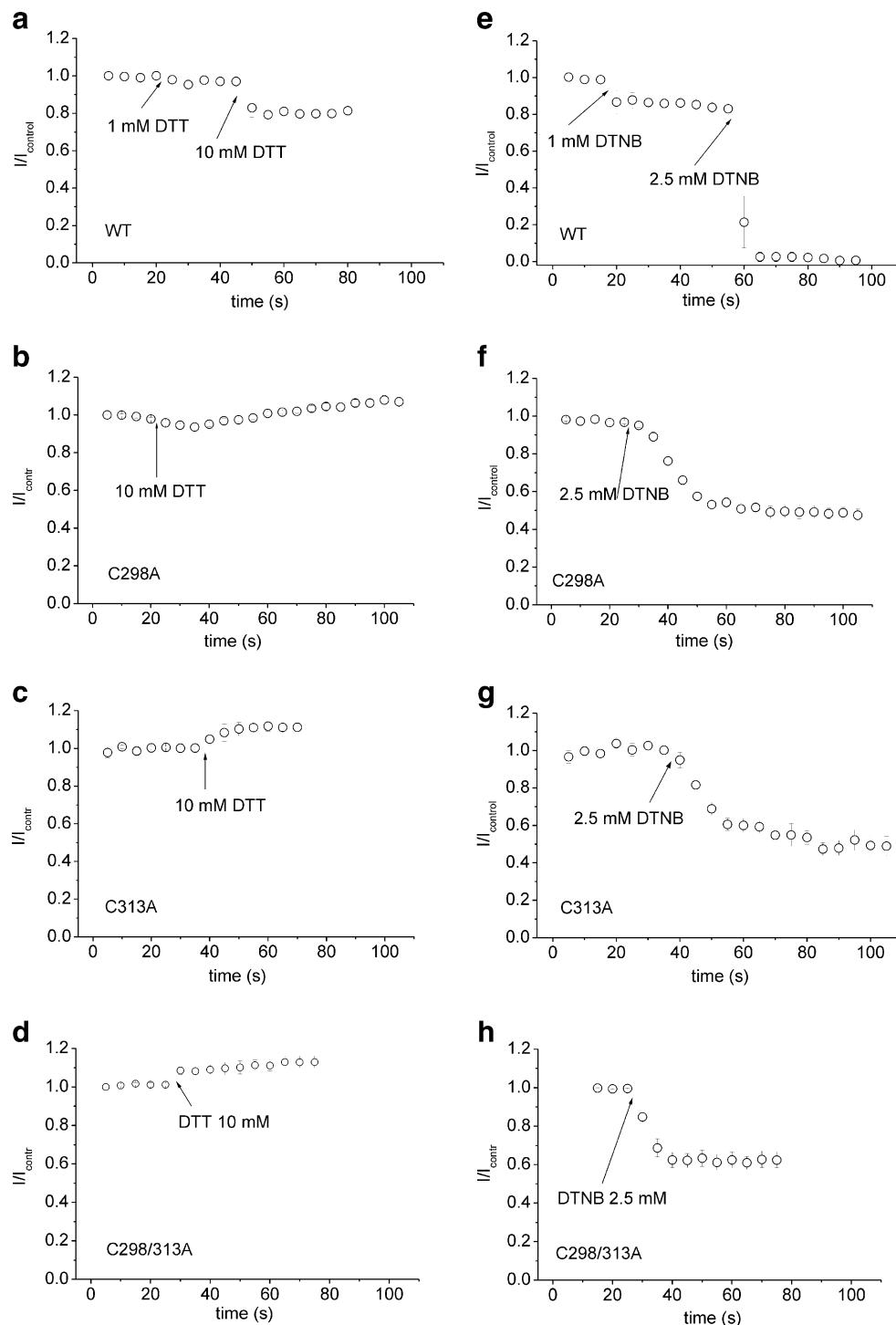
Significance of this increase was preserved in the double mutant.

Location and putative interactions of cysteines in a calculated model of $\text{Ca}_v3.1$

Next we generated a putative structural model of the membrane spanning S1–S6 segments with an attached extracellular pore loop built by ab initio methods. Out of the 55 cysteines in the $\text{Ca}_v3.1$ channel, 16 are located on the extracellular surface of the channel (see Fig. 1).

Domain I contains nine extracellular cysteines. Six are located in the long extracellular loop connecting IS5 and IP and three cysteine residues (C104, C109, and C114) are in the voltage-sensing domain, in the loop connecting

Fig. 4 Interaction of redox agents DTT and DTNB with WT and mutant channels. Averaged time courses of the amplitude of inward calcium currents measured during 40-ms long depolarizing pulses to -30 mV are shown for the WT Cav3.1 (**a** and **e**), C298A mutant (**b** and **f**), C313A mutant (**c** and **g**), and C298/313A mutant (**d** and **h**). *Left column* demonstrates effect of 10 mM DTT on inward current amplitudes. Inhibition of current amplitudes by 1 and 2.5 mM of DTNB is shown in the *right column*. The time of application of each agent is indicated by arrows



IS1 and IS2. These cysteines are in equivalent positions to the liponic acid interaction site described for Cav3.2. Domain II contains only one accessible cysteine residue, C889, which is also part of the liponic acid interaction site, as inferred from Cav3.2 studies. In domain III, two cysteines (C1441 and C1455) are found in the loop connecting helix IIIS5 and IIIP. Accessible cysteines in

domain IV are located in the loops connecting IVS5 and IVP (C1770 and C1776) and the loop connecting IVP and IVS6 (C1815 and C1821).

Extracellular located cysteines from domain III (C1441 and C1455) as well as loop cysteines from domain IV (C1770, C1776, C1815, and C1821) are in close proximity to EC loop I (see Fig. 7).

Fig. 5 DTT shifts channel activation in the hyperpolarizing direction. *I/V* relationships measured under control conditions and in the presence of 10 mM DTT are shown in (a). In b conductance–voltage relationships calculated from these *I/V* relationships are demonstrated. *Solid lines* are Boltzmann functions (Eq. 2). The same analysis for C298A channels is shown in (c) and (d). In e and f results from experiments on C313A channels are summarized. g and h show experimental data measured from double mutant C298/313A. *Dashed line* in d, f, and h represents the Boltzmann function calculated for WT $\text{Ca}_v3.1$ channel from the data demonstrated in (b)

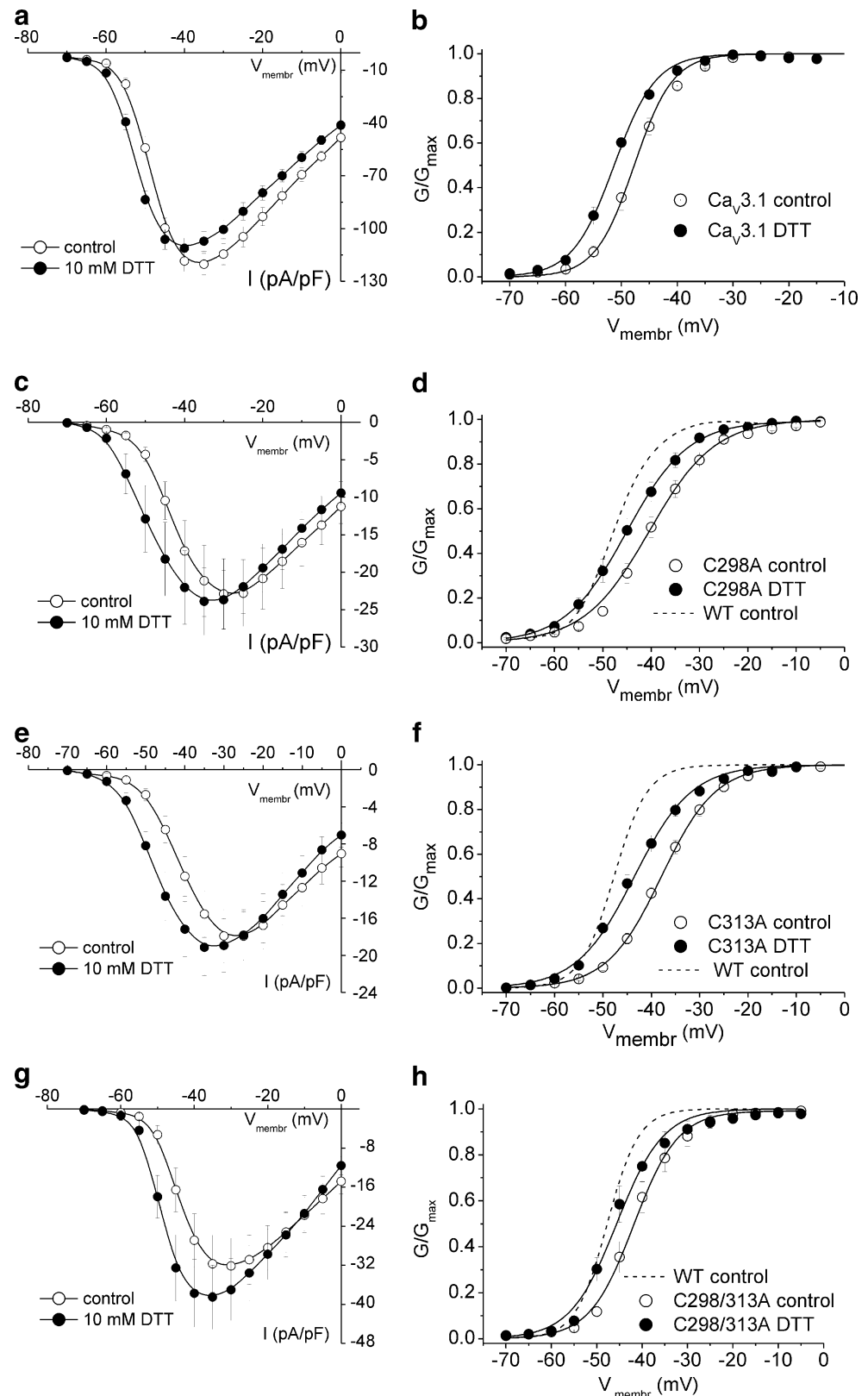


Table 2 Voltage dependence of activation and its alteration by DTT

| Channel construct | Control | | 10 mM DTT | |
|-------------------|----------------------------|---------------------|-----------------------|---------------|
| | $V_{0.5}$ (mV) | dV (mV) | $V_{0.5}$ (mV) | dV (mV) |
| WT | -47.7 ± 0.7 (12) | 3.5 ± 0.6 | $-51.3 \pm 0.5^{###}$ | 3.8 ± 0.2 |
| C298A | $-40.4 \pm 1.1^{***}$ (10) | $6.3 \pm 0.4^{***}$ | $-45.3 \pm 1.3^{###}$ | 6.4 ± 0.3 |
| C313A | $-37.9 \pm 0.7^{***}$ (8) | $5.6 \pm 0.3^{***}$ | $-43.5 \pm 0.9^{###}$ | 6.0 ± 0.3 |
| C298/313A | $-41.6 \pm 1.5^{**}$ (7) | 4.5 ± 0.5 | $-45.5 \pm 1.6^{\#}$ | 4.5 ± 0.8 |

Voltage dependencies of activation for WT, C298A, C313A, and C298/313A channels either under control conditions or in the presence of 10 mM DTT were fitted with Eq. 2. Resulting half-maximal voltages ($V_{0.5}$) and slope factors dV are listed together with the numbers of tested cells in brackets

*** $p < 0.001$; ** $p < 0.01$ (significantly different from the WT); ### $p < 0.001$, # $p < 0.05$ (significant differences between control and DTT)

Discussion

The extracellular loops connecting transmembrane segment IS5 and the pore loop IP of different members of the Ca_v family vary significantly in length and amino acid composition (Fig. 1). The large loops that are characteristic of $\text{Ca}_v3.1$ – $\text{Ca}_v3.3$ contain six cysteine residues. Their functional role in Ca_v3 gating is currently unknown. Four of the six cysteines in this loop region are conserved between LVA and HVA channels (Fig. 1) while cysteines at positions 271 and 282 (numbering of $\text{Ca}_v3.1$) are specific for Ca_v3 channels. Disulfide bonds formed between two cysteines are considered as stabilizing elements in proteins. We mutated these residues to alanines and analyzed the functional effects of the mutations by patch clamping. We provide evidence that cysteines C241, C271, C282, and C323 are essential for proper channel function. Replacing them by alanine resulted in non-functional channels. Membrane localization of functional and non-functional channel proteins was similar within resolution limits of confocal microscopy (Supplementary Figure 2) making a total failure of membrane trafficking caused by mutation in IS5-IP loop unlikely. Until now only intracellular motif—loop connecting domains I and II—was identified as determinant of trafficking Ca_v3 channels [2, 23, 31]. Nevertheless, we cannot exclude partial impairment of membrane localization of mutant channel proteins. Such impairment could also explain a decrease of average current densities through the mutant channels compared to the wild-type channel.

Altered gating properties of functional mutants demonstrate that cysteines C298 and C313 are likely to participate in conformational changes during activation, inactivation, and deactivation. A depolarizing shift of the activation curve with bigger slope factors was previously reported by Talavera and coauthors [27, 29] for aspartate-to-glutamate changes in the EEDD pore locus of the $\text{Ca}_v3.1$ channel. These authors hypothesized that the observed changes in

gating were caused by the change of the selectivity filter structure [27]. Since C298 and C313 are located outside the conducting pathway of the channel pore, the effects of their mutation are presumably due to a different molecular mechanism. We speculate that the IS5-P loop may contribute to the modulation of channel gating via its link to the pore helix and the pore forming segment IS6. The mutation of cysteines C241, C271, C282, and C323 may disable channel opening via a partial collapse of the structure of the IS5-P loop and/or a rearrangement of cysteine bridges within the loop.

Such profound structural change in tertiary structure of channel region directly linked to the pore could affect channel selectivity. This seems not to be the case for single mutants as reversal potentials extrapolated from experimental data in Fig. 2b resulted in similar values (22.3 ± 0.5 , 22.7 ± 1.4 , and 22.8 ± 1.2 for WT, C298a, and C313A channels, respectively). We cannot exclude that the double mutation C298/313A may affect selectivity as evident from the extrapolated average reversal potential of 25.8 ± 1.5 (significantly different from wt, $p < 0.05$).

Mutations of C298 and C313 slowed down activation, inactivation, and deactivation gating. This effect was more prominent when these cysteines were mutated simultaneously. Cysteines C298 and C313 probably do not interact with each other because in this case removal of each single cysteine should have a similar effect as removal of both of them. Alterations of inactivation time constants correlated with alterations of activation time constants in mutant C313A. No correlation was observed for mutant C298A. A correlation between activation and inactivation parameters is observed for many but not for all mutations [28].

Todorovic and coauthors [30] demonstrated that redox agents modulate the current through T-type calcium channels both in vivo and in vitro. Reducing agents DTT and L-cysteine selectively enhanced current through the $\text{Ca}_v3.2$ channel by relieving zinc inhibition mediated by H191 in the IS3–IS4 loop [21]. H191 is specific for the

Fig. 6 DTNB causes depolarizing shift of channel activation in mutant channels. **a**, **c**, **d**, and **e** show I - V relations measured under control conditions (*open circles*) and in the presence of 2.5 mM DTNB (*filled circles*). Experimental points are connected by spline lines. In **b**, **d**, **f**, and **h**, data from these I - V relations are converted into conductance-voltage relations. *Solid lines* are Boltzmann functions (Eq. 2). First row demonstrates results from the WT $\text{Ca}_v3.1$ channels, the second one from the C298A channels, third one from the C313A channels, and the last one from the double-mutant channel C298/313A

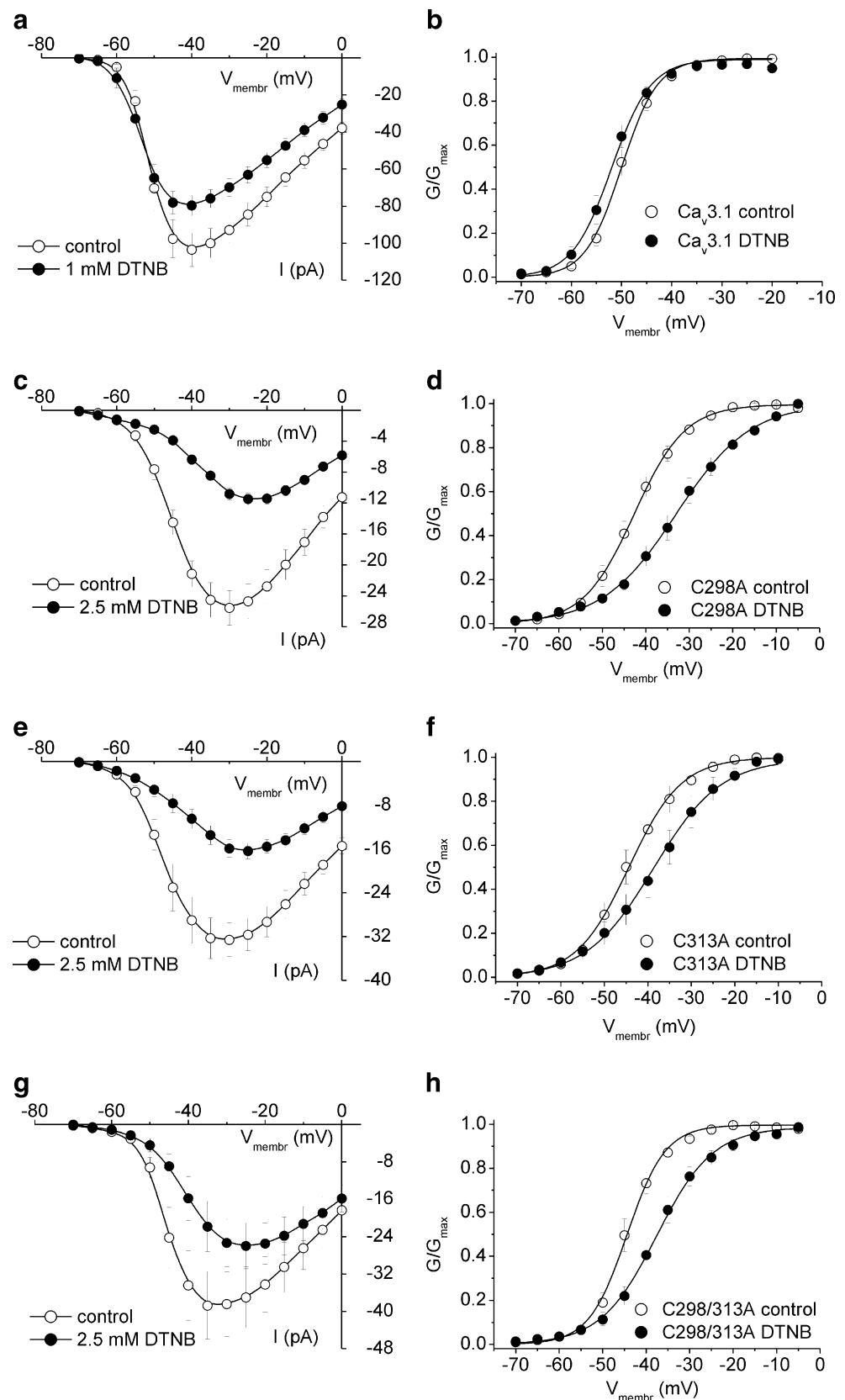


Table 3 Effects of DTNB on current amplitude and voltage dependence of current activation

| Channel construct | Control | | 2.5 mM DTNB | | I _{Ca} inhibition(%) |
|-------------------|----------------|---------|----------------|------------|-------------------------------|
| | $V_{0.5}$ (mV) | dV (mV) | $V_{0.5}$ (mV) | dV (mV) | |
| WT | -49.9±0.8 (12) | 3.3±0.2 | -52.4±1.0** | 3.4±0.3 | 99±1 (6) |
| C298A | -42.8±1.3 (6) | 6.2±0.3 | -33.6±1.6*** | 8.6±0.3** | 50±3 (6) |
| C313A | -43.4±1.8 (10) | 5.8±0.7 | -38.2±2.6** | 6.8±0.5 | 52±4 (6) |
| C298/313A | -44.9±1.1 (5) | 4.2±0.5 | -37.9±1.5** | 6.4±0.5*** | 38±3 (10) |

Voltage dependences of activation for WT, C298A, C313A, and C298/313A channels either under control conditions or in the presence of DTNB were fitted with Eq. 2. Resulting half-maximal voltages ($V_{0.5}$) and slope factors dV are listed together with the numbers of tested cells in brackets. In case of WT channel concentration of DTNB was 1 mM. The inhibition of the amplitude of calcium currents evoked by 50 ms depolarization from -100 mV to -30 mV by 2.5 mM DTNB is listed in the last column. The number of cells tested is indicated in brackets. Inhibition of the double mutant C298/313A was significantly different from inhibition of both C298A and C313A ($p<0.05$)

*** $p<0.001$; ** $p<0.01$ (significant differences between control and DTNB)

Ca_v3.2 channel and in a previous report [14] reducing agents did not affect Ca_v3.1 and Ca_v3.3 channels. In accord with this finding DTT did not enhance current through the Ca_v3.1 channel, instead, it caused a minor

inhibition of the inward current. Nevertheless, DTT did enhance current at membrane voltages below -30 mV when C298 and/or C313 were replaced by alanine. This enhancement was caused mostly by a hyperpolarizing shift of current activation. Shift of activation curve towards more negative membrane voltages caused by DTT partly compensated the depolarizing shift of activation caused by the mutations (Fig. 5b, d, f, and h).

Oxidizing agents like DTNB or lipoic acid inhibit the current through all Ca_v3 channels [14, 18]. While the interaction site for lipoic acid was identified [18] and consists of three cysteine residues in the IS1–IS2 linker plus one cysteine at the top of IIS5 segment, the interaction site for DTNB is more complex. Here we present the first evidence that C298 and C313 are likely to participate in the DTNB site. Removal of each single cysteine reduced current inhibition by DTNB. Removal of both cysteines simultaneously further diminished this inhibition, but did not eliminate it completely. Hence, DTNB interacts with multiple sites on the Ca_v3.1 channel. In accord with this assumption the roughly estimated Hill coefficient for the WT channel is 1.8 suggesting positive cooperativity between multiple binding sites. The Hill coefficient provides only a minimum estimate of interaction sites involved [32]. Cysteines C298 and C313 are part of these interaction sites, however, our data do not allow to distinguish if each of them is part of separate sites or both are part of the same site.

The importance of domain I in Ca_v3 gating is underlined by mutations related to childhood epilepsy. A gain-of-function point mutation was discovered in the proximal I–II loop of the Ca_v3.2 channel [12]. This mutation destabilizes the closed state of Ca_v3.2. Such a scenario is supported by the recent discovery of a “gating brake” in the I–II loop of Ca_v3.2 [1, 31], which is conserved in all three Ca_v3 channels [2] and prevents Ca_v3 channels from opening at membrane voltages close to cell resting potential. These

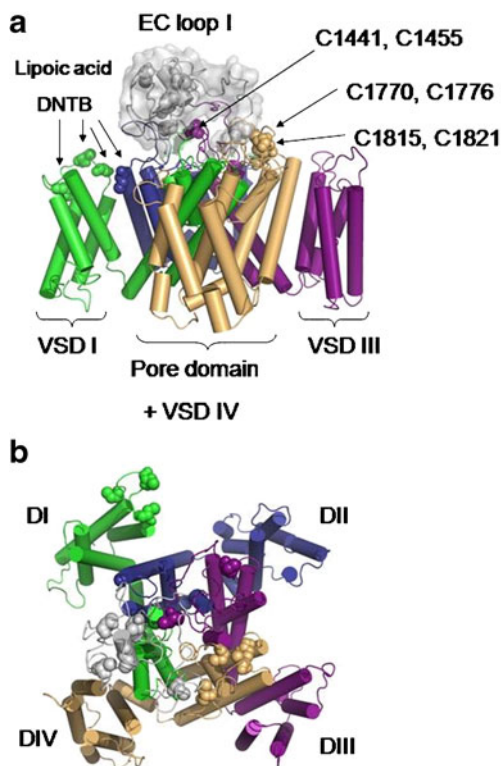


Fig. 7 Homology model of Ca_v3.1 with ab initio EC loop I. **a** Ribbon representation (side view) of the Ca_v3.1 structure model with the extracellular loop connecting IS5–IP, generated with I-Tasser shown on top (gray, surface representation). Domain I (S1–S6) is colored green, domain II is shown in blue, the color of domain III is purple, and domain IV is shown in orange. Extracellular cysteines are shown as spheres. Due to the lack of modeling constraints, both segments are not connected. The lipoic acid and DTNB interaction site as inferred from studies on Ca_v3.2 [9] is indicated with arrows. **b** Ribbon representation (top view) of the Ca_v3.1 model with EC loop I colored gray. The color scheme is identical as in (a)

studies suggest that pore region of the domain I is an important determinant of Ca_v3 channels activation and inactivation. Loop connecting domains I and II have previously been shown to play a key role in inactivation of high-voltage-activated calcium channels $\text{Ca}_v2.3$ [3, 25], $\text{Ca}_v1.2$ [3, 9], and $\text{Ca}_v2.1$ [4, 5, 9]. Further, self-reliant molecular determinants of channel activation were discovered in a region responsible for association with the beta subunit in the I–II loop of $\text{Ca}_v1.2$ and $\text{Ca}_v2.3$ channels [7]. However, the I–II linker of Ca_v3 channels has a low degree of homology with the corresponding linker in high-voltage-activated channels making an extrapolation of mutational studies in this region difficult.

Our results point to essential role of all cysteines in the IS5-P loop in channel gating. The question whether they form disulfide bonds within this loop or with cysteines in other channel domains remains open. To evaluate this possibility we have designed a homology model of the $\text{Ca}_v3.1$ pore domain and included the extracellular loop connecting IS5 and P segments, by means of ab initio modeling. Ab initio methods are not yet accurate enough to distinguish between various possible disulfide bonds, since different cysteine bridges were observed in seven out of the ten generated models. However, three of the generated models support a scenario, where replacement of one cysteine involved in disulfide bridge formation by alanine would lead to the formation of an alternative cysteine bridge (see Supplementary Figure 3).

The homology model of the pore domain (I–IV S1–S6) shows which of the many cysteines are located on the extracellular side of the protein and thereby possibly accessible for interactions with the extracellular loop I (Fig. 7). The $\text{Ca}_v3.1$ model suggests that cysteines located in the loop connecting helix IIIS5 and IIIP, and cysteines in the loops connecting IVS5 and IVP and the loop connecting IVP and IVS6 might be possible interaction candidates for cysteines from the EC loop I. Such possible disulfide bonds can be tested in future experiments and might improve the quality of the models considerably.

The reducing agent DTT acts either by breaking existing disulfide bonds and/or by scavenging metal ions thus relieving current inhibition. The observed shift of the activation curve and moderate enhancement of calcium current at voltages negative to the peak of the $I-V$ curve in mutant channels is consistent with a model in which cysteines C298 and C313 form bridges with some other cysteines. Their replacement either individually or simultaneously frees their interaction partner, which then can be involved in inhibition by an unknown ion. Such inhibition is consistent with observed changes in channel gating observed in mutant channels. DTT application relieves this inhibition by its scavenger effect. This suggestion is supported by observed restoration of channels activation gating.

Reduced current inhibition by DTNB seems to be in contradiction with the hypothesis that cysteines C298 and C313 form disulfide bonds. Both participate in the interaction with DTNB, which is a specific thiol oxidizing agent. Nevertheless, disulfide bonds formed by oxidizing thiol groups are relatively stable. Rapid reversibility of current inhibition by DTNB suggests that other mechanism than direct binding to –SH group underlies this effect.

The present study is, to our knowledge, the first to analyze the role of individual cysteine residues in the IS5-P loop of the $\text{Ca}_v3.1$ channel. Our data suggest that all mutated cysteines are essential for proper channel gating. Additionally, we have identified new residues involved in redox regulation of the $\text{Ca}_v3.1$ channel.

Acknowledgment Supported by grants from VEGA 2/0195, VVCE-0064-07, Center of Excellence for Cardiovascular Research SAS (LL) and the DFG (NK). The authors thank Emilia Kocurova and Ute Christoph for skillful technical assistance and Martina Kurejova for help with construction of C241A and C298A mutants and Eugen Timin for helpful comments on the manuscript.

Ethical standards No specific ethical issues are related to reported experiments.

Conflict of interest The authors declare that they have no conflict of interest.

References

1. Arias O II, Vitko I, Fortuna M, Baumgart JP, Sokolova S, Shumilin IA, Van Deusen A, Soriano-Garcia M, Gomora JC, Perez-Reyes E (2008) Characterization of the gating brake in the I-II loop of $\text{Ca}_v3.2$ T-type Ca^{2+} channels. *J Biol Chem* 283:8136–8144
2. Baumgart JP, Vitko I, Bidaud I, Kondratskiy A, Lory P, Perez-Reyes E (2008) I-II loop structural determinants in the gating and surface expression of low voltage-activated calcium channels. *PLoS ONE* 3: e2976
3. Berrou L, Bernatchez G, Parent L (2001) Molecular determinants of inactivation within the I-II linker of $\alpha 1E$ ($\text{Ca}_v2.3$) calcium channels. *Biophys J* 80:215–228
4. Bourinet E, Soong TW, Sutton K, Slaymaker S, Mathews E, Monteil A, Zamponi GW, Nargeot J, Snutch TP (1999) Splicing of $\alpha 1A$ subunit gene generates phenotypic variants of P- and Q-type calcium channels. *Nat Neurosci* 2:407–415
5. Ellinor PT, Zhang JF, Randall AD, Zhou M, Schwarz TL, Tsien RW, Horne WA (1993) Functional expression of a rapidly inactivating neuronal calcium channel. *Nature* 363:455–458
6. Fiser A, Do RK, Sali A (2000) Modeling of loops in protein structures. *Protein Sci* 9:1753–1773
7. Gonzalez-Gutierrez G, Miranda-Laferte E, Contreras G, Neely A, Hidalgo P (2010) Swapping the I-II intracellular linker between L-type $\text{Ca}_v1.2$ and R-type $\text{Ca}_v2.3$ high-voltage gated calcium channels exchanges activation attributes. *Channels (Austin)* 4:42–50
8. Hamid J, Peloquin JB, Monteil A, Zamponi GW (2006) Determinants of the differential gating properties of $\text{Ca}_v3.1$ and $\text{Ca}_v3.3$ T-type channels: a role of domain IV? *Neuroscience* 143:717–728

9. Herlitze S, Hockerman GH, Scheuer T, Catterall WA (1997) Molecular determinants of inactivation and G protein modulation in the intracellular loop connecting domains I and II of the calcium channel $\alpha 1A$ subunit. *Proc Natl Acad Sci U S A* 94:1512–1516
10. Huguenard JR (1998) Low-voltage-activated (T-type) calcium-channel genes identified. *Trends Neurosci* 21:451–452
11. Chen X, Wang Q, Ni F, Ma J (2010) Structure of the full-length Shaker potassium channel Kv1.2 by normal-mode-based X-ray crystallographic refinement. *Proc Natl Acad Sci U S A* 107:11352–11357
12. Chen Y, Lu J, Pan H, Zhang Y, Wu H, Xu K, Liu X, Jiang Y, Bao X, Yao Z, Ding K, Lo WH, Qiang B, Chan P, Shen Y, Wu X (2003) Association between genetic variation of CACNA1H and childhood absence epilepsy. *Ann Neurol* 54:239–243
13. Jeanmougin F, Thompson JD, Gouy M, Higgins DG, Gibson TJ (1998) Multiple sequence alignment with Clustal X. *Trends Biochem Sci* 23:403–405
14. Jokovic PM, Nelson MT, Jevtovic-Todorovic V, Patel MK, Perez-Reyes E, Campbell KP, Chen CC, Todorovic SM (2006) $Ca_v3.2$ is the major molecular substrate for redox regulation of T-type Ca^{2+} channels in the rat and mouse thalamus. *J Physiol (Lond)* 574:415–430
15. Khosravani H, Altier C, Simms B, Hamming KS, Snutch TP, Mezeyova J, McRory JE, Zamponi GW (2004) Gating effects of mutations in the $Ca_v3.2$ T-type calcium channel associated with childhood absence epilepsy. *J Biol Chem* 279:9681–9684
16. Klugbauer N, Marais E, Lacinova L, Hofmann F (1999) A T-type calcium channel from mouse brain. *Pflugers Arch* 437:710–715
17. Kurejova M, Lacinova L, Pavlovicova M, Eschbach M, Klugbauer N (2007) The effect of the outermost basic residues in the S4 segments of the $Ca_v3.1$ T-type calcium channel on channel gating. *Pflugers Arch* 455:527–539
18. Lee WY, Orestes P, Latham J, Naik AK, Nelson MT, Vitko I, Perez-Reyes E, Jevtovic-Todorovic V, Todorovic SM (2009) Molecular mechanisms of lipoic acid modulation of T-type calcium channels in pain pathway. *J Neurosci* 29:9500–9509
19. Li J, Stevens L, Klugbauer N, Wray D (2004) Roles of molecular regions in determining differences between voltage dependence of activation of $Ca_v3.1$ and $Ca_v1.2$ calcium channels. *J Biol Chem* 279:26858–26867
20. Long SB, Tao X, Campbell EB, MacKinnon R (2007) Atomic structure of a voltage-dependent K^+ channel in a lipid membrane-like environment. *Nature* 450:376–382
21. Nelson MT, Woo J, Kang HW, Vitko I, Barrett PQ, Perez-Reyes E, Lee JH, Shin HS, Todorovic SM (2007) Reducing agents sensitize C-type nociceptors by relieving high-affinity zinc inhibition of T-type calcium channels. *J Neurosci* 27:8250–8260
22. Perez-Reyes E (2003) Molecular physiology of low-voltage-activated T-type calcium channels. *Physiol Rev* 83:117–161
23. Shcheglovitov A, Vitko I, Bidaud I, Baumgart JP, Navarro-Gonzalez MF, Grayson TH, Lory P, Hill CE, Perez-Reyes E (2008) Alternative splicing within the I-II loop controls surface expression of T-type $Ca_v3.1$ calcium channels. *FEBS Lett* 582:3765–3770
24. Stary A, Shafir Y, Hering S, Wolschann P, Guy HR (2008) Structural model of the $Ca_v1.2$ pore. *Channels (Austin)* 2:210–215
25. Stotz SC, Barr W, McRory JE, Chen L, Jarvis SE, Zamponi GW (2004) Several structural domains contribute to the regulation of N-type calcium channel inactivation by the $\beta 3$ subunit. *J Biol Chem* 279:3793–3800
26. Swartz KJ (2008) Sensing voltage across lipid membranes. *Nature* 456:891–897
27. Talavera K, Janssens A, Klugbauer N, Droogmans G, Nilius B (2003) Pore structure influences gating properties of the T-type Ca^{2+} channel α_{1G} . *J Gen Physiol* 121:529–540
28. Talavera K, Nilius B (2006) Evidence for common structural determinants of activation and inactivation in T-type Ca^{2+} channels. *Pflugers Arch* 453:189–201
29. Talavera K, Staes M, Janssens A, Klugbauer N, Droogmans G, Hofmann F, Nilius B (2001) Aspartate residues of the Glu-Glu-Asp-Asp (EEDD) pore locus control selectivity and permeation of the T-type Ca^{2+} channel α_{1G} . *J Biol Chem* 276:45628–45635
30. Todorovic SM, Jevtovic-Todorovic V, Meyenburg A, Mennerick S, Perez-Reyes E, Romano C, Olney JW, Zorumski CF (2001) Redox modulation of T-type calcium channels in rat peripheral nociceptors. *Neuron* 31:75–85
31. Vitko I, Bidaud I, Arias JM, Mezghrani A, Lory P, Perez-Reyes E (2007) The I-II loop controls plasma membrane expression and gating of $Ca_v3.2$ T-type Ca^{2+} channels: a paradigm for childhood absence epilepsy mutations. *J Neurosci* 27:322–330
32. Weiss JN (1997) The Hill equation revisited: uses and misuses. *FASEB J* 11:835–841
33. Zhang Y (2008) I-TASSER server for protein 3D structure prediction. *BMC Bioinform* 9:40
34. Zhang Y (2009) Protein structure prediction: when is it useful? *Curr Opin Struct Biol* 19:145–155
35. Zhang Y, Skolnick J (2004) Scoring function for automated assessment of protein structure template quality. *Proteins* 57:702–710

Supplementary material.

Cysteines in the loop between IS5 and the pore helix of Cav3.1 are essential for channel gating.

Pflügers Archive – European Journal of Physiology

Maria Karmazinova¹, Stanislav Beyl², Anna Stry-Weinzinger², Chonticha Suwattanasophon⁴,
Norbert Klugbauer³, Steffen Hering², Lubica Lacinova¹

¹Institute of Molecular Physiology and Genetics, Slovak Academy of Sciences, Bratislava,
Slovakia

²Institut für Pharmakologie und Toxikologie, University of Vienna, Vienna, Austria

³Institut für Experimentelle und Klinische Pharmakologie und Toxikologie, Albert-Ludwigs
Universität, Freiburg, Germany

⁴Institute of Theoretical Chemistry, University of Vienna, Vienna, Austria

corresponding author e-mail: lubica.lacinova@savba.sk

Supplementary Table 1.

Significance of differences in time constants of channel's activation and inactivation. WT and mutants were compared by unpaired t-test. n.s. – not significant; * - $p < 0.05$; ** - $p < 0.01$; *** - $p < 0.001$.

| V (mV) | τ_{act} | | | τ_{inact} | | |
|--------|--------------|-------|-----------|----------------|-------|-----------|
| | C298A | C313A | C298/313A | C298A | C313A | C298/313A |
| -45 | n.s. | n.s. | n.s. | - | - | - |
| -40 | n.s. | n.s. | n.s. | *** | *** | *** |
| -35 | *** | *** | ** | *** | ** | *** |
| -30 | *** | *** | ** | ** | n.s. | ** |
| -25 | *** | *** | *** | ** | n.s. | * |
| -20 | *** | *** | *** | ** | n.s. | * |
| -15 | *** | *** | *** | * | n.s. | * |
| -10 | *** | *** | *** | ** | n.s. | * |
| -5 | *** | ** | *** | * | n.s. | * |
| 0 | *** | * | - | * | n.s. | * |

Supplementary Table 2.

Significance of differences in deactivation time constants. WT and mutants were compared by unpaired t-test. n.s. – not significant; * - $p < 0.05$; ** - $p < 0.01$; *** - $p < 0.001$.

| V (mV) | τ_{deact} | | |
|--------|-----------------------|-------|-----------|
| | C298A | C313A | C298/313A |
| -140 | n.s. | ** | - |
| -130 | n.s. | ** | ** |
| -120 | n.s. | * | ** |
| -110 | n.s. | *** | ** |
| -100 | n.s. | *** | ** |
| -90 | n.s. | *** | ** |
| -80 | n.s. | *** | ** |
| -70 | n.s. | *** | ** |
| -60 | * | *** | *** |

Supplementary Figure 1. Sequence alignment of Cav3.1, Cav3.2, NaChBac and Kv1.2.

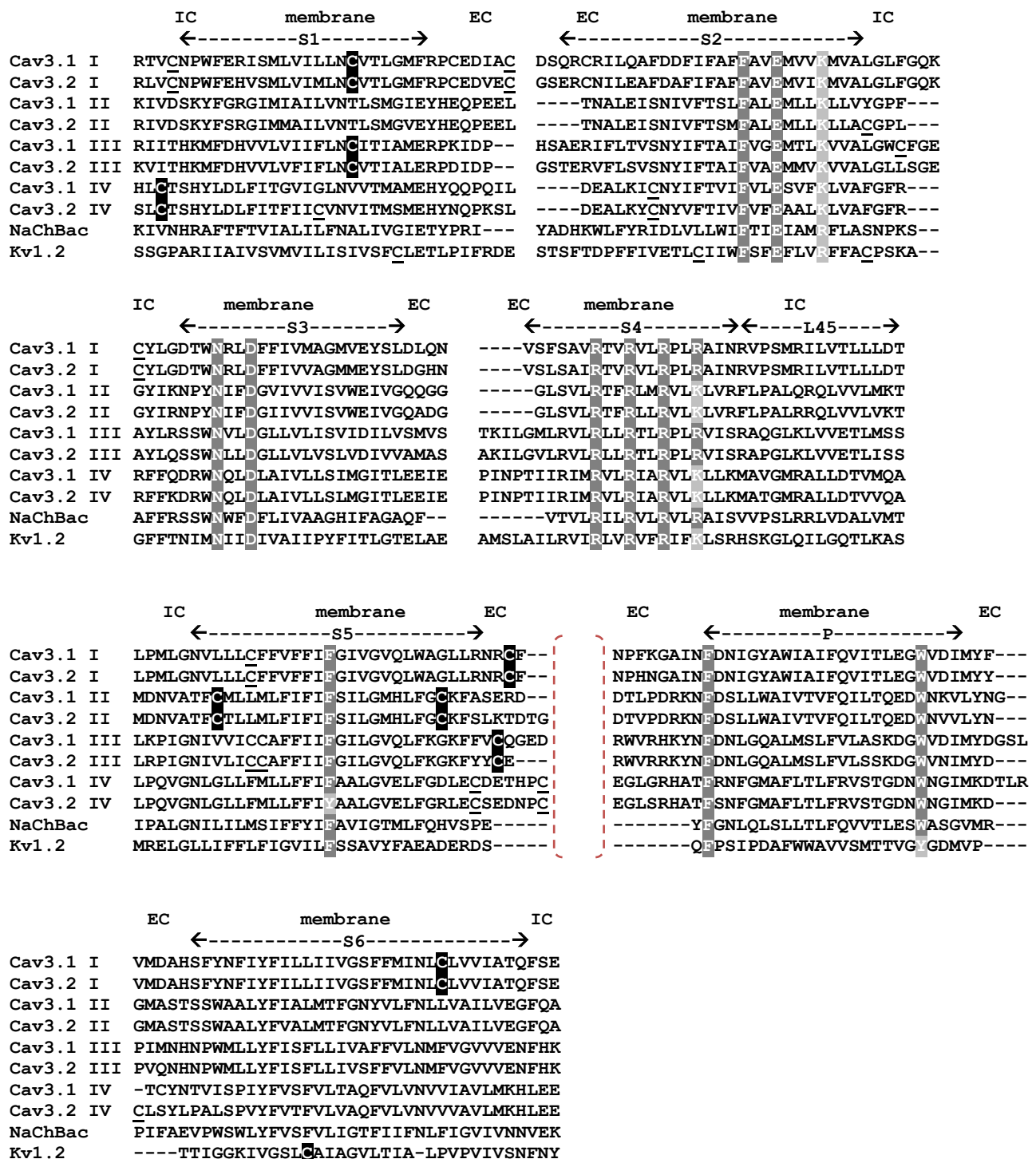
The alignment of the full pore domain (S1- S6) of Cav3.1 (Accession number: O43497), Cav3.2 (Accession number: O95180), Cav3.3 (Accession number: Q9P0X4), NaChBac (Accession number: Q9KCR8) and Kv1.2 (PDB IDs: 2r9r, 3lut) is shown. Residues conserved in all channels are shaded dark gray, similar residues in all sequences are shaded light gray and highly conserved cysteines are shaded black. All other cysteine residues are underlined. The approximate membrane boundaries, as well as extra- (EC) and intracellular (IC) location of residues are indicated above the alignment.

Supplementary Figure 2. Membrane localization of expressed channel proteins.

The first column demonstrates the subcellular distribution of the wild type (WT) Cav3.1 channel as well as C271A, C298A and C313A mutant constructs visualized by EGFP fused to their carboxy-terminus. The second column shows the membrane staining by the FM4-64 protein. The third column represents an overlap of the two previous columns. Colocalization of EGFP fusion and FM4-64 proteins is visualized in yellow.

Supplementary Figure 3. Hypothetical cysteine bridge formations in *ab initio* loop model

Detailed view of hypothetical cysteine bridge formations based on a Tasser *ab initio* loop model. In this model 3 cysteines (shown as sticks) are in close proximity and mutation of one cysteine to an alanine could possibly promote the switch between cysteine bridges. SH-groups of cysteine residues are coloured yellow, nitrogen atoms are shown in blue and carbon atoms are coloured grey.



Colour Code :

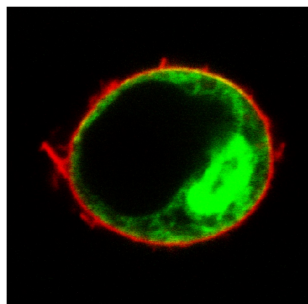
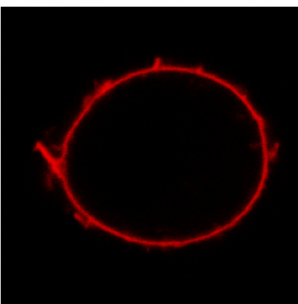
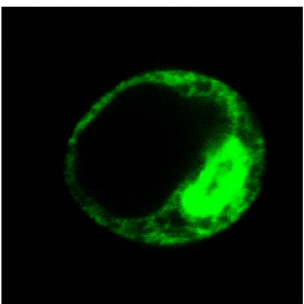
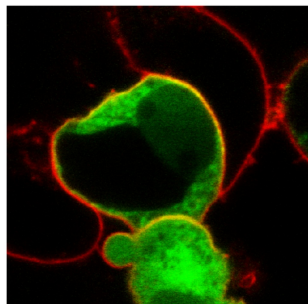
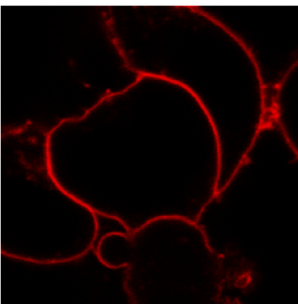
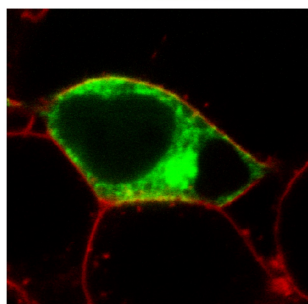
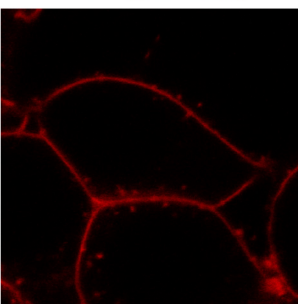
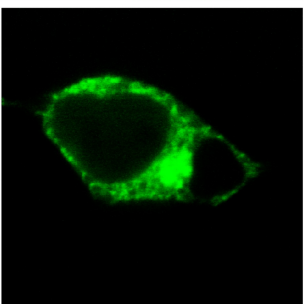
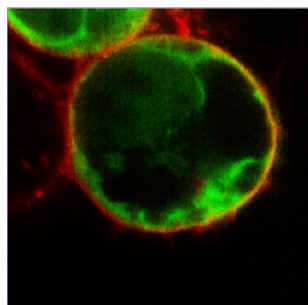
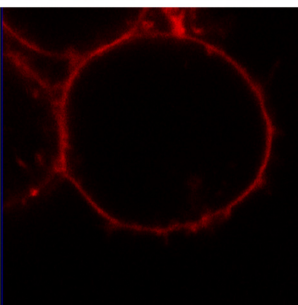
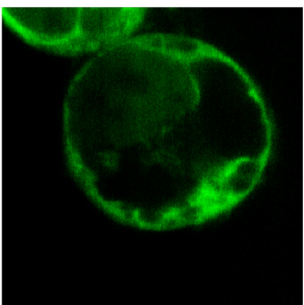
Highly-conserved cysteines in T-type Cav

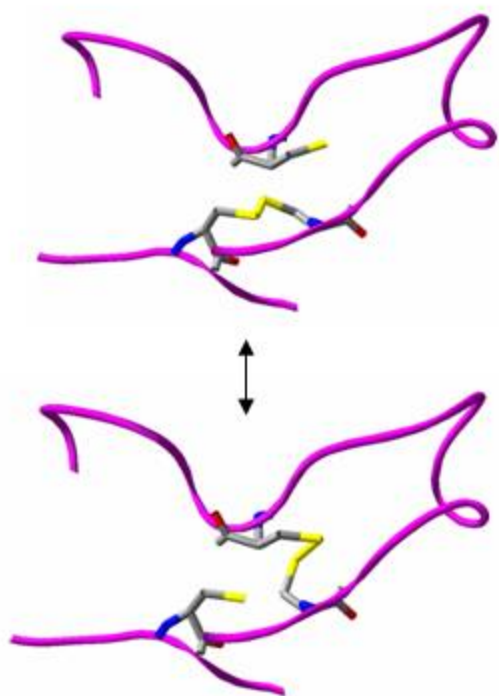
Identical amino acids in Cav, NaChBac and Kv1.2

Similar amino acids in Cav, NaChBac and Kv1.2

() EC loop I shown in Fig. 1 (main manuscript)

Sequence alignment of Cav3.1 (hs), Cav3.2 (hs), NaChBac and Kv1.2.

GFP**FM4-64****Merge****WT****C271A****C298A****C313A**



3.4 Docking studies of Phenylalkylamines (PAAs) verapamil and its derivatives to the open conformation of Ca_v1.2.

Molecular docking of PAA verapamil and its derivatives was performed to the Cav1.2 open conformation taken from Stary et al, 2009. The binding site of PAA verapamil are in particular located in transmembrane helices IIIS6, IVS6 and P-loops of repeats III and IV. The following amino acids Y1180, I1181, F1191 and V1192 in IIIS6, Y1490, M1491, A1494 and I1491 in IVS6 and E1145 and E1446 in the selectivity filter of domains III and IV were considered in this docking [40, 42, 90].

The PAA verapamil and its derivatives (see chapter 1.9) were built with Gauss View program in protonated states of both, R and S chirality and optimized with the Hartree-Fock 3-21G basis set implemented in Gaussian03. Due to the flexible conformation of the ligands, the concrete interaction with the channel is uncertain. Then, each of the ligands was generated in different conformations using the conformation search option in MOE program. The first 10 conformations were selected using energy criteria.

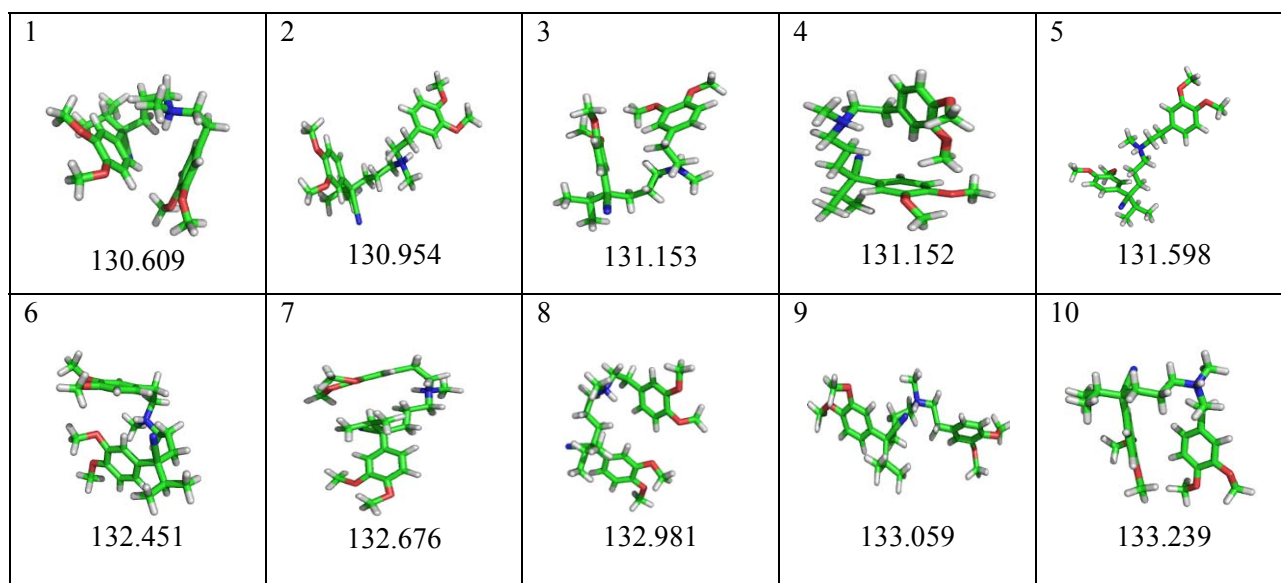


Fig 3.4. The 10 different conformations of S chirality verapamil which were selected using energy criteria.

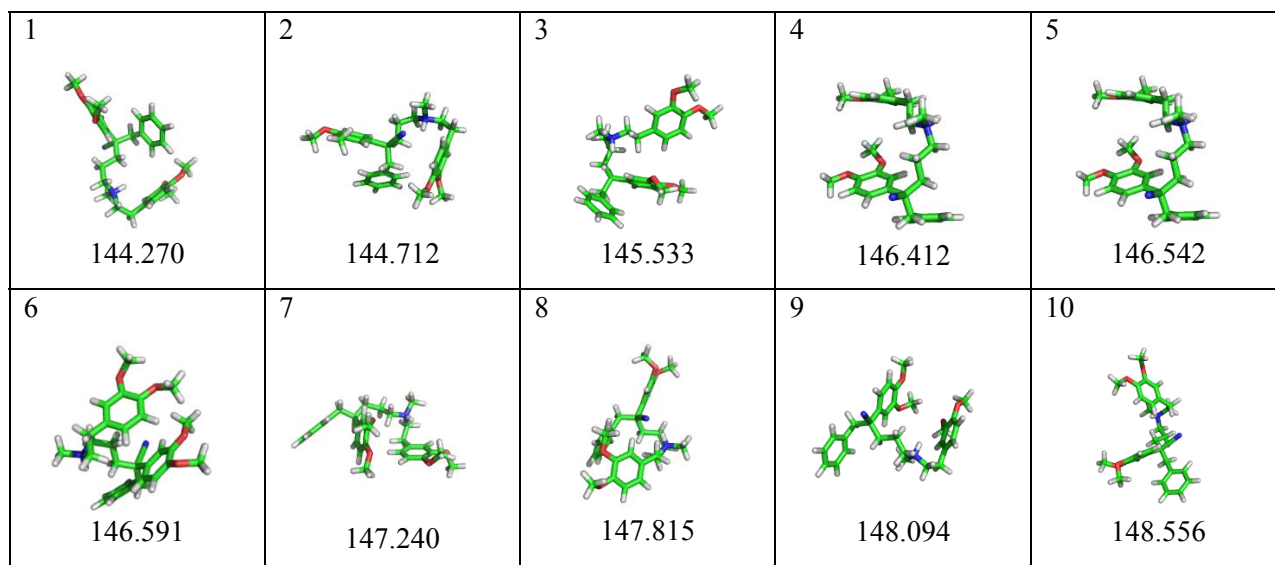


Fig 3.5. The 10 different conformations of S chirality D490 which were selected using energy criteria.

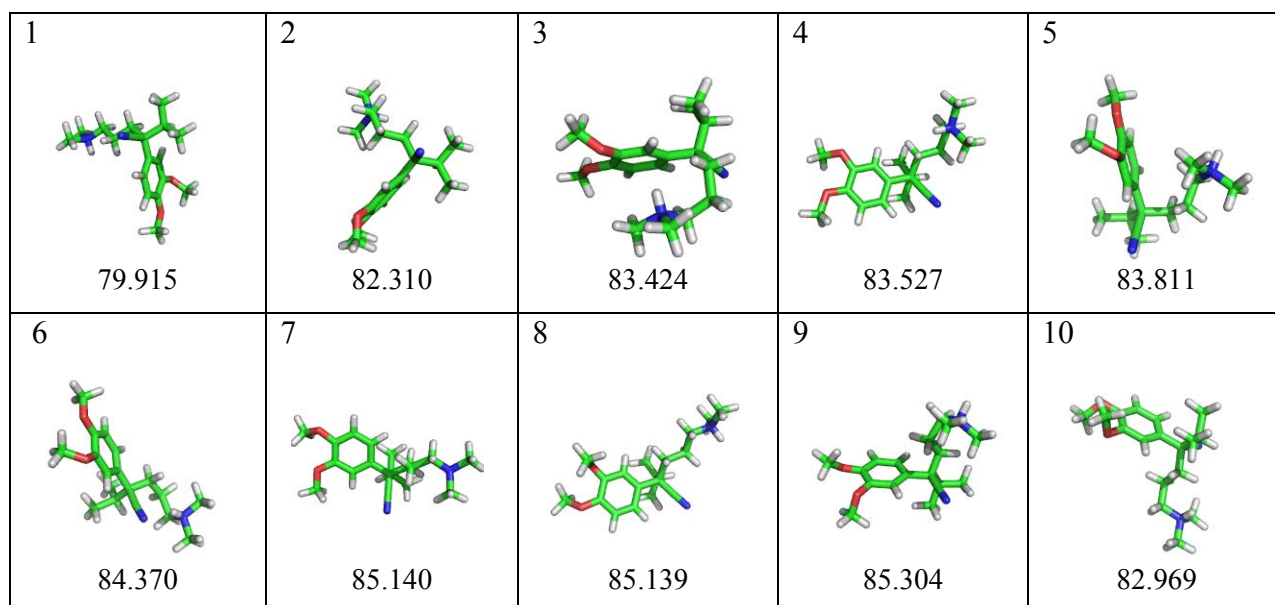


Fig 3.6. The 10 different conformations of S chirality D619 which were selected using energy criteria.

The examples of 10 ranked conformations of each group of PAA verapamil are shown: Group A verapamil-S chirality (shown in Fig 3.4), Group B D490-S chirality (shown in Fig 3.5) and Group C D619-S chirality (shown in Fig 3.6).

3.4.1 Docking studies and molecular dynamic simulations of verapamil(S) in a open conformation of Ca_v1.2.

Table 3.2 illustrates a summary of the best scorings from 10 different starting conformations of verapamil(S). For each conformation 100 poses were analysed. Lipkind et al, 2003 [91] proposed that the PAA drugs occupy and occlude the interface of III/IV crevice by adopting the half-folded conformation shapes. The superimposition of the first ranking of each conformation of verapamil(S) demonstrated that verapamil(S) is located between domains III and IV (Fig 3.7). The docking results as shown in Fig 3.8 revealed that almost all the best poses from each different starting conformation form the half-folded shapes with the channel except the 6th and the 7th conformation which form the extended shape.

Table 3.2 Glide scoring functions of 10 different S chirality verapamil conformations.

| Conformation | GScore | Lipo | HBond | vdW | Coul |
|--------------|--------|-------|-------|--------|--------|
| 1 | -5.23 | -2.10 | -0.1 | -35.1 | -10.9 |
| 2 | -5.40 | -1.90 | 0 | -39.01 | -12.89 |
| 3 | -5.29 | -2.00 | 0 | -38.3 | -11.2 |
| 4 | -5.60 | -2.30 | -0.3 | -34.9 | -10.2 |
| 5 | -5.10 | -1.30 | -0.2 | -36.0 | -13.9 |
| 6 | -5.45 | -2.30 | 0 | -40.5 | -8.4 |
| 7 | -5.28 | -1.60 | -0.4 | -32.5 | -13.5 |
| 8 | -5.59 | -1.90 | -0.3 | -42.2 | -11.3 |
| 9 | -5.51 | -2.30 | -0.1 | -36.1 | -9.60 |
| 10 | -5.05 | -1.90 | -0.1 | -33.0 | -10.9 |

Note: The protocol explanation in Chapter 2.3.1.

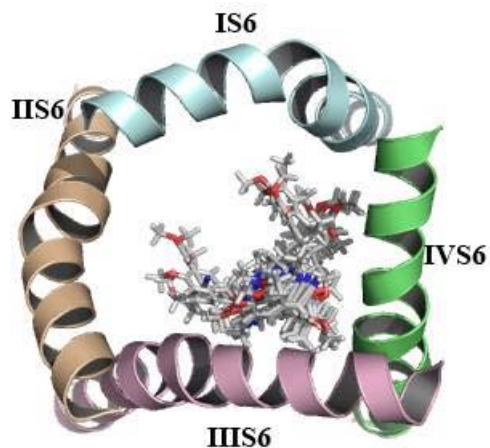
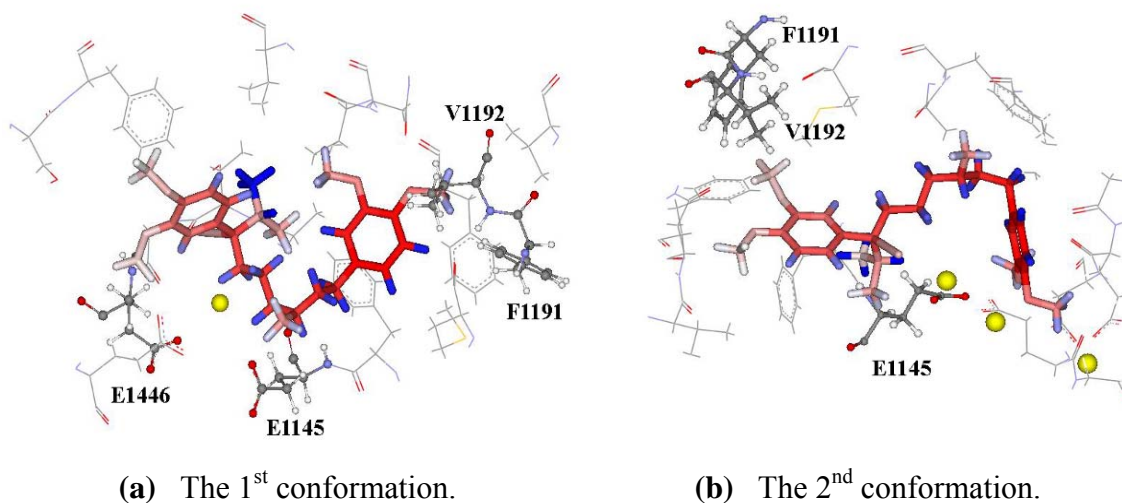
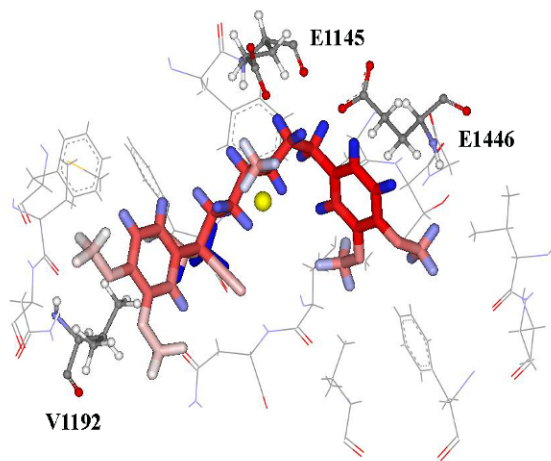


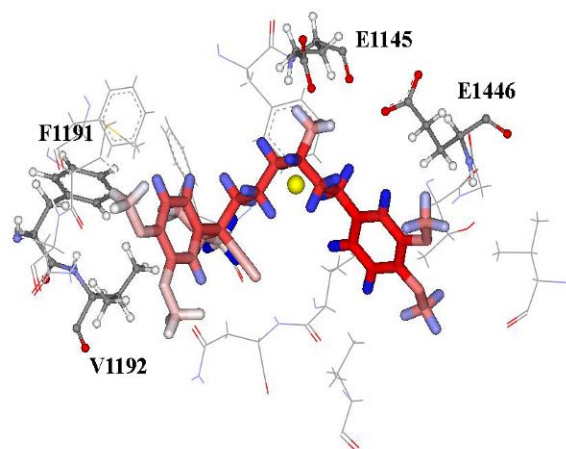
Fig 3.7. Superimposition of first rankings of each conformation of verapamil(S). Each verapamil show in grey stick. Each domain of S6 is colored: blue (IS6), brown (IIS6), purple (IIIS6) and green (IVS6).

A molecular dynamic simulation of the pore region of Cav1.2 in open conformation with verapamil complexed was generated and the system was simulated for 40 ns. The first docking pose of verapamil conformation 4th which is the best ranking of all 10 different conformations was selected to start the simulation.

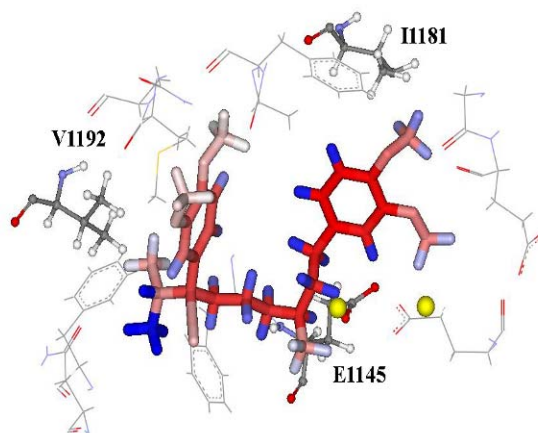




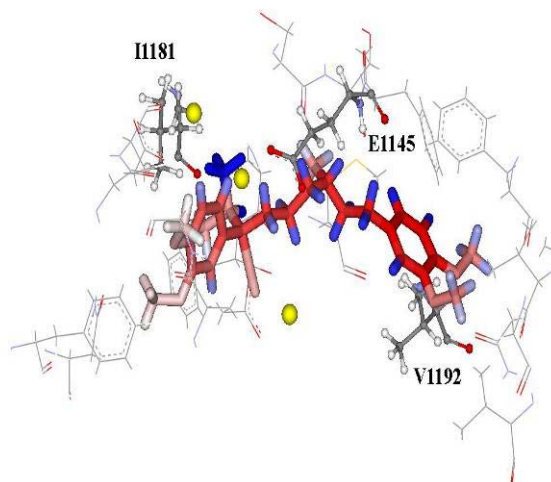
(c) The 3rd conformation.



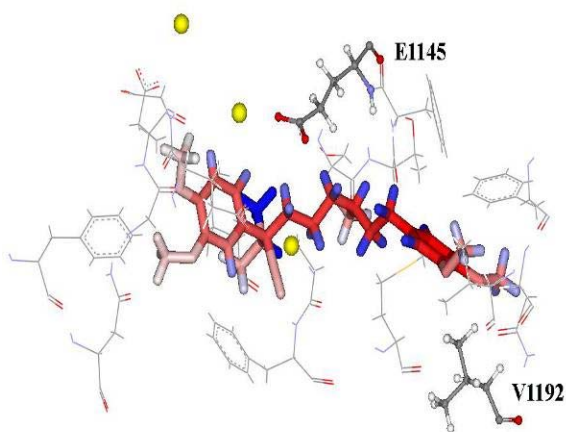
(d) The 4th conformation.



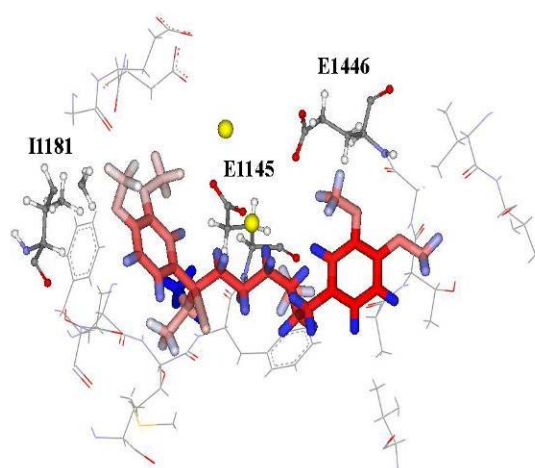
(e) The 5th conformation.



(f) The 6th conformation.



(i) The 7th conformation.



(g) The 8th conformation.

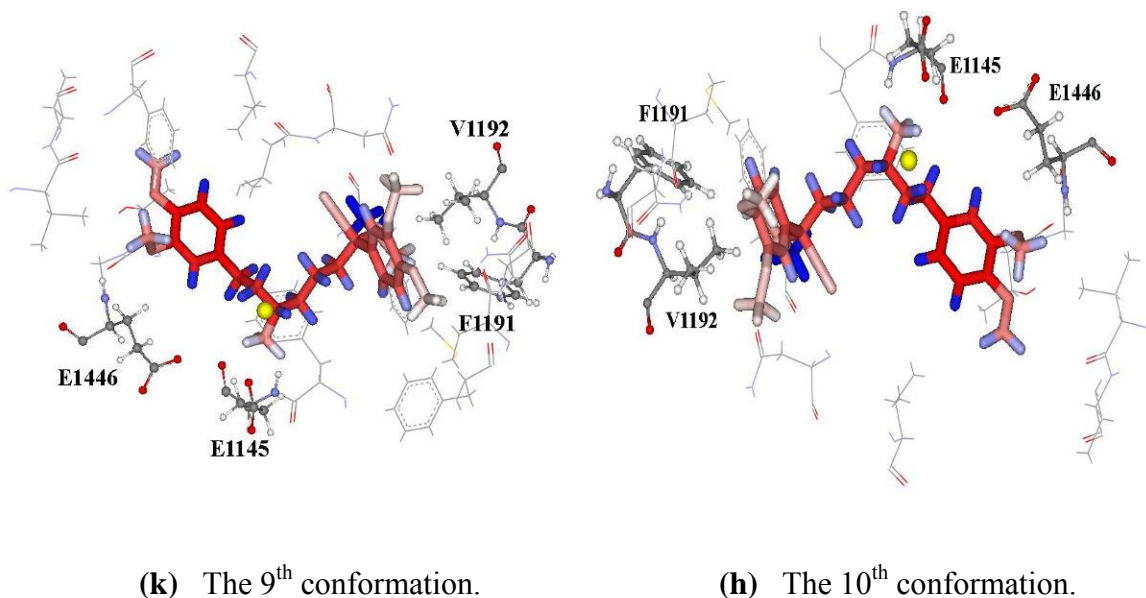
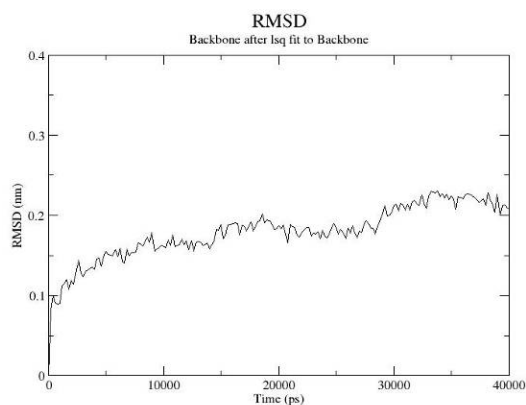
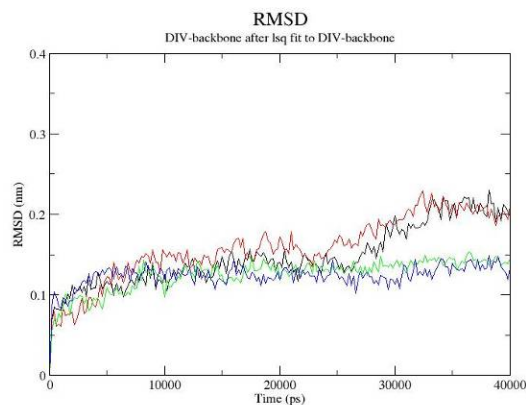


Fig 3.8. The 3D diagrams showing the interaction between verapamil(S) and surrounding residues. The verapamil(S) are presented in red stick. The surrounding residues are shown in gray stick and ball. Binding residues are shown in gray line. The yellow ball is representing the Ca^{2+} .

The stability of the verapamil complex was analyzed using the root-mean-square displacement (RMSD). The conformational change of the protein during the simulation can be indirectly described by RMSD values. The backbone RMSD value of the pore region of the open conformation of $\text{Ca}_v1.2$ steadily increases over 40ns (Fig 3.9 a). The RMSD value of each domain was calculated as shown in Fig 3.9 b. For domain I and II, the RMSD values still increase. The RMSD value of domain III and IV steadily increases for the first ns and then stably remains at 0.15 nm. It is implied that domains I and II are responsible for instability of the pore region.



(a)



(b)

Fig 3.9. RMSD values of (a) the pore region backbone of Ca_v1.2 in open conformation (b) each domain backbone. Domains I, II, III and IV are shown in black, red, green and blue, respectively.

The RMSD of verapamil was obtained. Fig 3.10 shows that the RMSD value of verapamil in complex has a fluctuation during the whole simulation. These plots indicate that the pore region complex with verapamil shows some instability which might be because of the model or the binding residues are not sufficient and good enough.

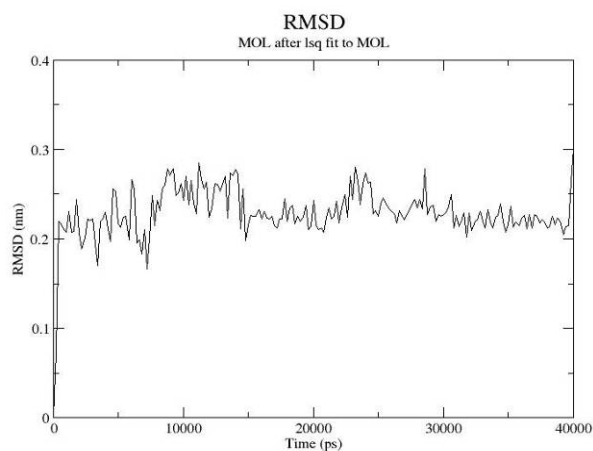


Fig 3.10. RMSD values of Verapamil over 40 ns simulation.

3.4.2 Docking studies of three groups of verapamil derivatives with open conformation of Ca_v1.2.

These docking studies focus on details of the interaction between drug and the pore region of the open channel. In particular, molecular docking for verapamil's derivatives to the open channel have been performed and the results have been compared with the experimental data and hypotheses of other groups. The summary of the best docking poses of group A, B and C in S and R conformation with open conformation of Ca_v1.2 are demonstrated in Table 3.3.

Table 3.3 The Glide scoring function of the docking of each protonated ligand in R and S conformation to the open conformation of Ca_v1.2.

Group A

| Title | GScore | Lipo | HBond | vdW | Coul |
|-----------------------|--------|-------|-------|-------|-------|
| S conformation | | | | | |
| Verapamil | -5.60 | -2.30 | -0.3 | -34.9 | -10.2 |
| D600 | -5.41 | -1.10 | -0.5 | -38.6 | -15.4 |
| D557 | -5.98 | -1.30 | -0.4 | -37.7 | -17.2 |
| D595 | -5.76 | -2.70 | 0.0 | -36.3 | -8.2 |
| T13 | -5.86 | -1.50 | -0.3 | -34.0 | -14.6 |
| PR23 | -6.77 | -2.90 | 0.0 | -31.8 | -17.8 |
| D559 | -6.24 | -3.91 | 0.0 | -31.5 | -6.8 |
| R conformation | | | | | |
| Verapamil | -5.84 | -1.1 | -0.8 | -32.6 | -32.6 |
| D600 | -5.41 | -2.4 | -0.3 | -28.0 | -10.5 |
| D557 | -6.46 | -1.1 | -0.6 | -35.0 | -20.0 |
| D595 | -6.10 | -2.0 | -0.6 | -36.8 | -11.8 |
| T13 | -5.97 | -1.4 | -0.2 | -34.0 | -16.7 |
| PR23 | -6.40 | -2.09 | 0.0 | -31.8 | -19.4 |
| D559 | -6.37 | -2.96 | -0.3 | -39.8 | -7.3 |

Group B

| Title | GScore | Lipo | HBond | vdW | Coul |
|-----------------------|--------|------|-------|-------|-------|
| S conformation | | | | | |
| D490PS | -7.41 | -4.2 | 0.0 | -47.2 | -9.4 |
| D586PS | -6.99 | -3.4 | -0.4 | -44.3 | -12.0 |
| D525PS | -6.57 | -2.9 | -0.2 | -38.3 | -12.1 |
| R conformation | | | | | |
| D490PR | -6.48 | -3.9 | 0.0 | -50.3 | -4.6 |
| D586PR | -7.32 | -4.1 | 0.0 | -47.5 | -9.6 |
| D525PR | -6.19 | -3.0 | -0.2 | -37.8 | -9.3 |

Group C

| Title | GScore | Lipo | HBond | vdW | Coul |
|-----------------------|--------|------|-------|--------|--------|
| S conformation | | | | | |
| D594PS | -6.57 | -3.1 | 0.0 | -43.17 | -12.37 |
| PR22PS | -6.59 | -3.4 | 0.0 | -37.0 | -10.7 |
| D619PS | -6.00 | -1.8 | 0.0 | -27.8 | -14.0 |
| H1PS | -6.36 | -2.5 | -0.5 | -37.6 | -12.4 |
| R conformation | | | | | |
| D594PR | -6.81 | -3.3 | -0.3 | -40.4 | -11.32 |
| PR22PR | -6.34 | -2.7 | -0.2 | -36.9 | -12.5 |
| D619PR | -5.35 | -2.6 | 0.0 | -27.8 | -5.0 |
| H1PR | -6.82 | -3.0 | -0.6 | -37.3 | -12.0 |

Note GScore = Glide Score (kcal/mol)
 Lipo = Lipophilic-contact plus phobic-attractive term
 HBond = Hydrogen-bonding term
 vdW = van der Waals interaction energy
 Coul = Coulomb interaction energy

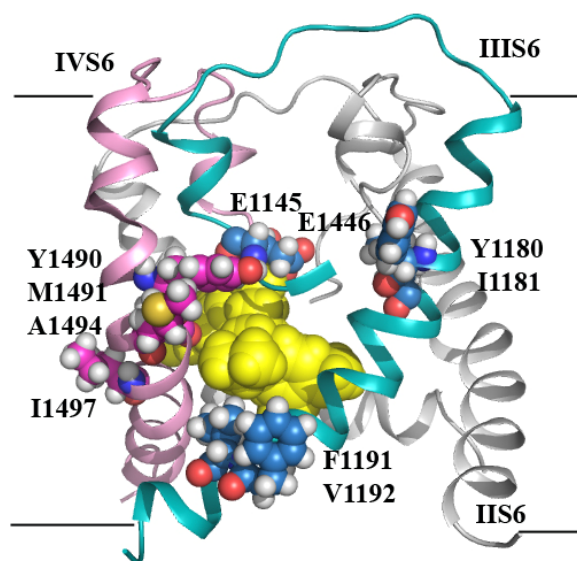


Fig 3.11. Side view of the PAA drug binding in open conformation of $\text{Ca}_v1.2$ homology model.

Cheng et al 2009 [92] suggested a geometry of the PAA – L-type calcium channel complexes, where the *meta*-methoxy group in the benzene ring near the ammonium group accepts the H-bond from Y1180, and the *meta*-methoxy group of another benzene ring accepts the H-bond from Y1490. From the results, it is shown that all drugs share similar orientation and position where the ligands are located between IIS6 and IVS6 as shown in Fig 3.11 [91]. The positively charged nitrogen atoms of all ligands bind to the glutamic acids E1145 and E1446 due to the electrostatic interactions (Fig 3.12).

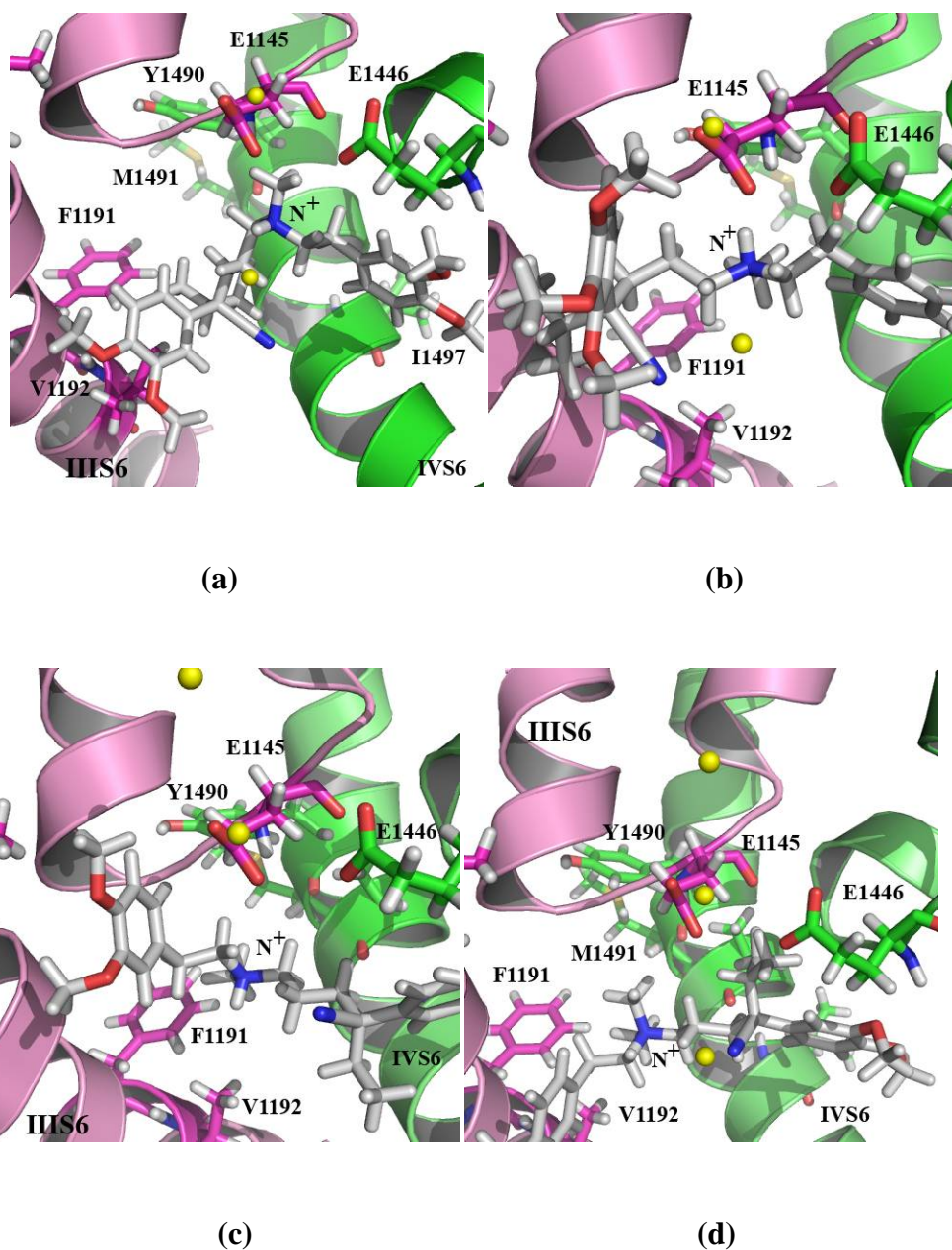
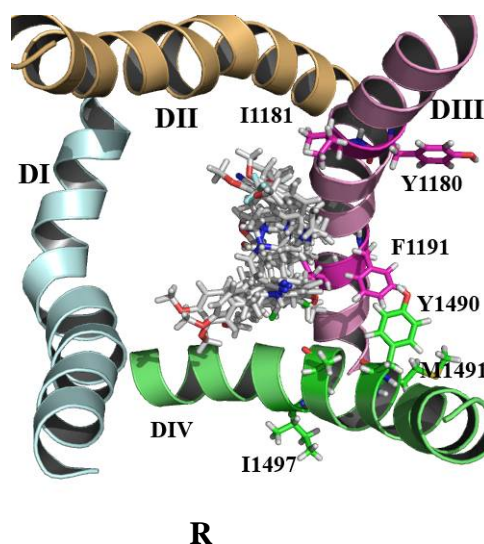
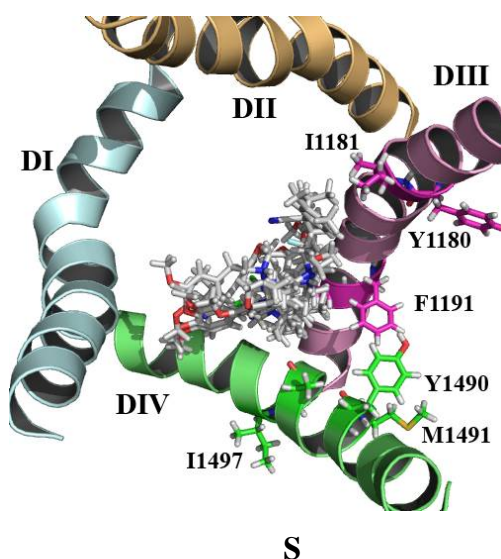


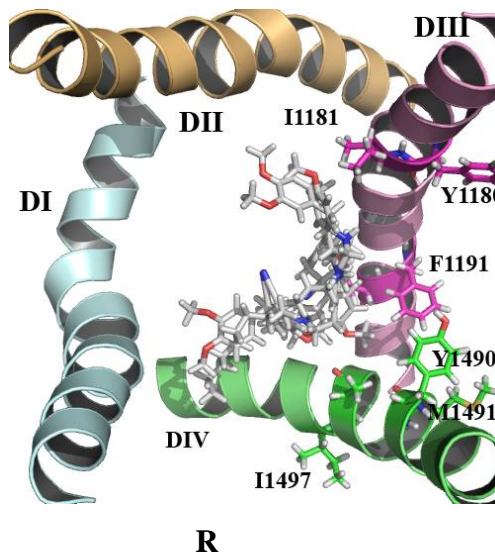
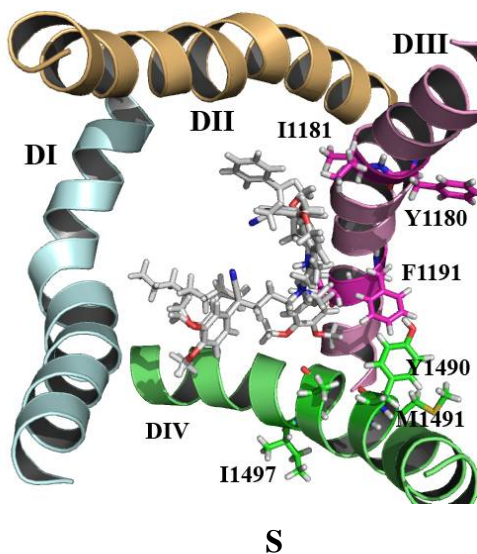
Fig 3.12. The best docking poses of (a) Group A- verapamil (b) Group A- D600 (c) Group B- D525 (d) Group C- H1. Each ligand are shown in grey sticks. IIIS6 is colored in purple and binding residue along the IIIS6 is shown as stick in purple. IVS6 is colored in green and binding residue along the IVS6 is shown as stick in green. The yellow ball is representing Ca^{2+} .

However, almost all binding residues are in some cases not facing into the pore. Especially, Y1152 and Y1463 do not interact with the drug (Fig. 3.13). It might be due to the template is still not good enough. Therefore the results of Cav1.2 open conformation model with verapamil and its derivatives obtained from molecular docking is in disagreement with experimental data. Also the molecular dynamic simulation of the open conformation of the channel with verapamil is not stable. Further studies are needed with an improved refinement of the homology model based on drug interaction data.

Group A



Group B



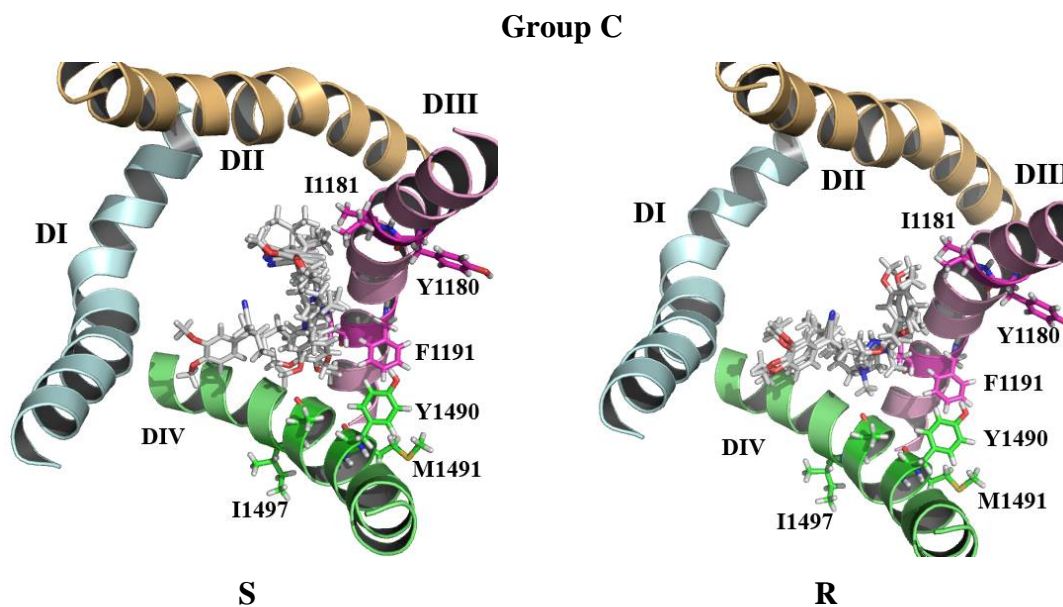


Fig 3.13. The superimposition of the best poses from docking. The PAA are presented in grey sticks. The binding residues at domain III and IV are shown in purple and green sticks.

3.5 Stability of the pore region of Ca_v1.2 in closed conformation and in improved open conformation.

Consequently, because of the inconsistency of docking results of the MD results and in particular the experimental data for open conformation of Ca_v1.2, the homology model of this channel was modified and improved [9] by H.R. Guy. The improvement of the open structure was mainly at III-P helix by shifting it slightly outward (Fig. 3.14a). From the improved model, it is shown that the binding residue Y1490 slightly moves facing into the pore, Y1180 and F1191 are slightly shifted too, which should improve the interaction between drug and the new model (Fig. 3.14b).

To refine the structures of the closed and the improved open models, 2 ns of restrained position and the 50 ns of unrestrained molecular dynamics simulations was performed. The stability of both systems are analyzed by RMSD (root mean square deviation). The RMSD of closed and improved open channels in POPC are around 0.3 nm as show in Fig 3 of Summary 1.

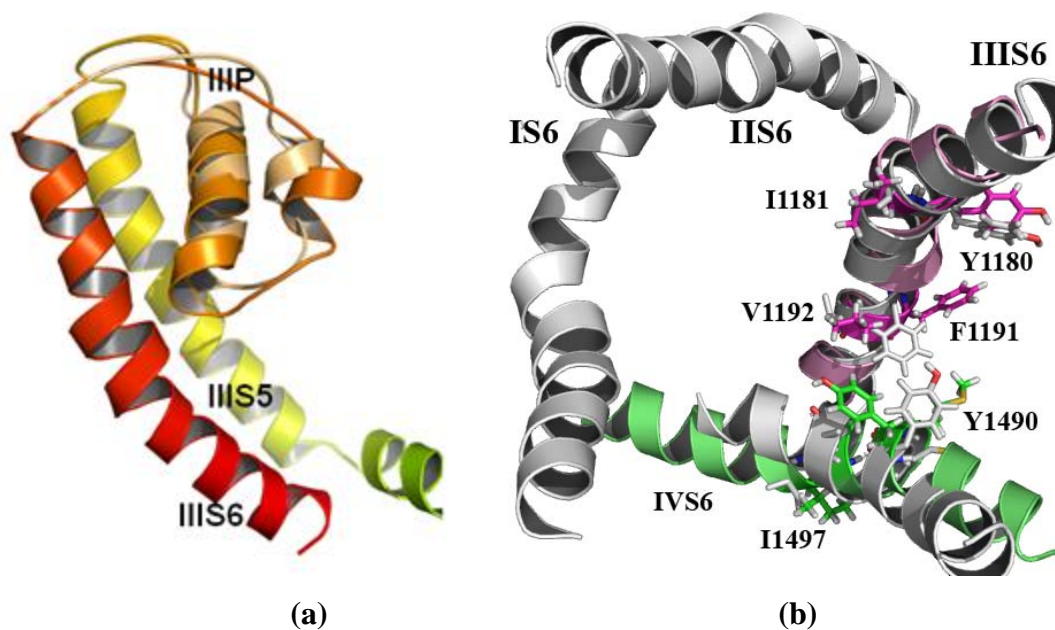


Fig. 3.14. Superimposition of the published homology model of the open conformation of the channel and the improved homology model. (a) Domain III-P helix (b) Domain IIIS6 and IVS6 are presented in purple and green, respectively. The binding residues of published model are shown in grey sticks. The binding residues of improved model on domain IIIS6 and IVS6 are shown in purple and green sticks.

3.6 Molecular Dynamics simulation studied of the improved open conformation of Cav1.2 calcium channel with verapamil and some of its derivatives.

MD simulation of verapamil and some of its derivatives were carried out to check the stability of the complex and examine conformational variations of verapamil and some of its derivatives. The starting structure of verapamil and the derivatives were taken from the good pose docking structures which were obtained by the program GLIDE.

3.6.1 Molecular Dynamics simulations studies of the improved open conformation of Cav1.2 calcium channel with verapamil

The stability of the system was investigated using RMSD of C_{α} atoms of the protein (Fig 3.15a) and the C_{α} atoms of each domain (Fig 3.15b) as a function of the simulation time. The RMSD values of protein rose to 0.27 nm and were relatively stable after 7 ns. During the first 7

ns the RMSD values are increased to 0.2 nm for domain I and II, 0.25 nm for domain II and IV and remain stable. This simulations show that the pore region of the improved open conformation is well behaved and rather stable after 7 ns.

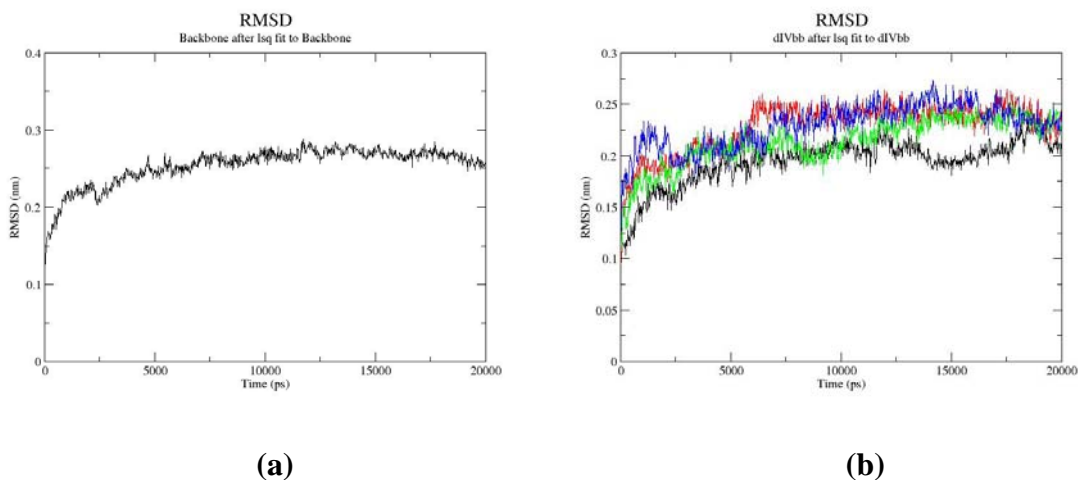


Fig 3.15. RMSD values of (a) backbone of the pore region of the open conformation (b) backbone of each domain. Domain I, II, III and IV are shown in black, red, green and blue, respectively.

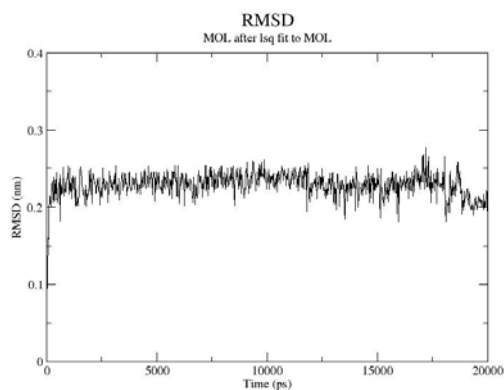
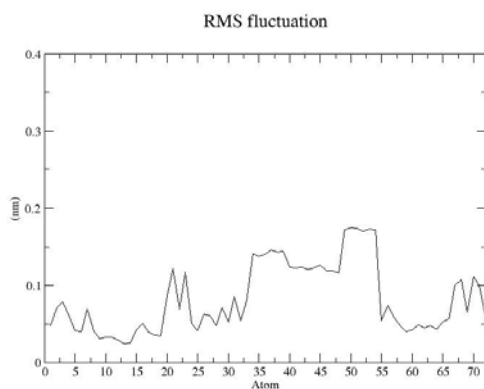


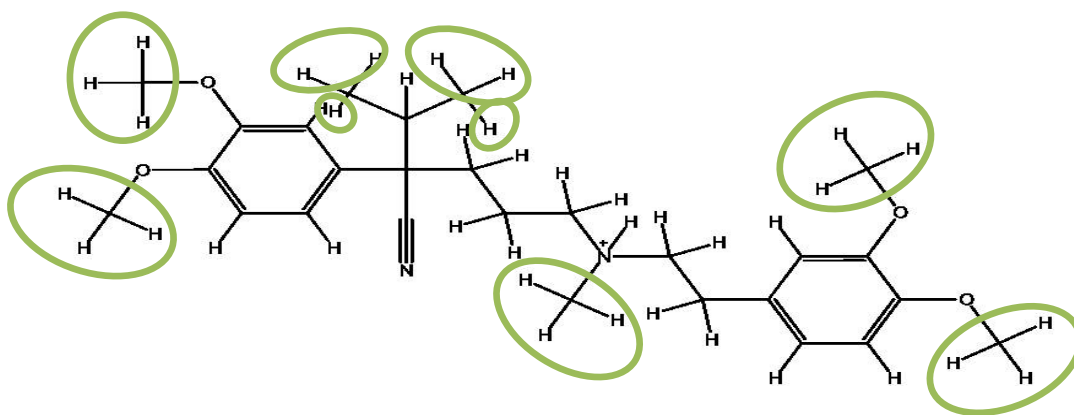
Fig 3.16. RMSD values of Verapamil in the pore region of the open conformation.

To insight the information on the ligand, the RMSD and RMSF values of verapamil were calculated. Fig 3.16 shows that the RMSD of verapamil remains stable at 0.25 nm after 2 ns. The fluctuation of each verapamil atom during 2 – 20 ns was investigated in terms of root mean

square fluctuation (RMSF). From Fig 3.17a, it can be seen that the fluctuation of the benzene ring, the ammonium group and the nitrile group of verapamil are small. The highest flexibility was exhibited at the hydrogen atoms that are surrounded by green circle as shown in Fig 3.17b. They belong to methyl groups, which have in general a larger mobility because of the rotation of the single bond. The RMSD and RMSF profile characterized that, after an initial increase in the magnitude of verapamil atoms fluctuation, the verapamil reached an equilibrium state.



(a)



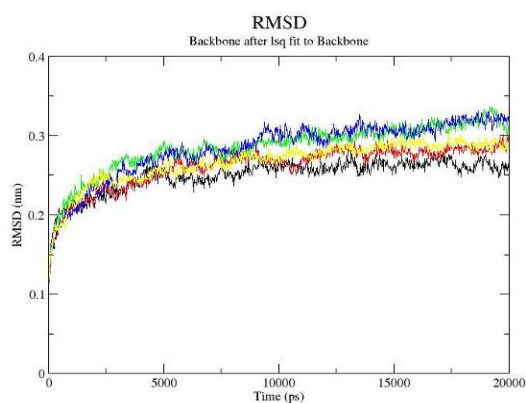
(b)

Fig 3.17. (a) RMSF values of Verapamil in pore region or the open conformation. (b) 2D structure of Verapamil. Green circle indicate the hydrogen atoms of highest flexibility.

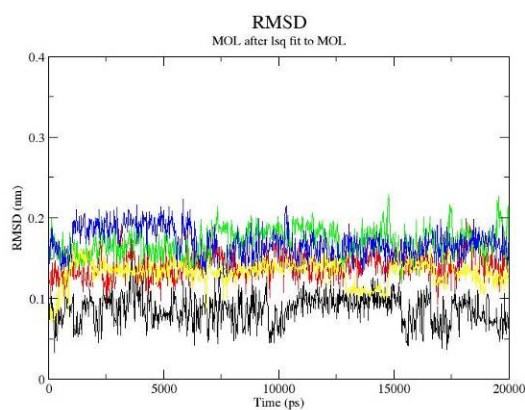
The results from MD simulation suggest that the structure of the improved open conformation of $\text{Ca}_v1.2$ is more stable and suitable for the description of the PAA verapamil complex than the previous open conformation. Thus, this improved structure was used for further studies of verapamil derivatives.

3.6.2 Molecular Dynamics simulation studies of the improved open conformation of $\text{Ca}_v1.2$ calcium channel with D619 and T13

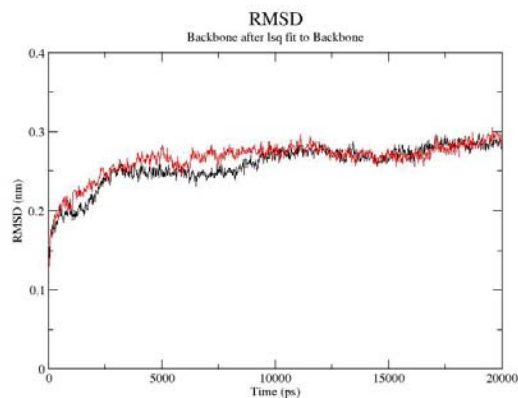
The verapamil derivative D619 of group C and T13 of group A was selected to gain insight into the structural and dynamic features of this ligand-receptor interaction. MD simulations of D619 and T13 were carried out from 5 (D619) and 2 (T13) initial orientations of the ligands. Analysis of the RMSD of the C_α atoms showed that all simulations reached an equilibrium after 15 ns (Fig. 3.18 a and c). Additionally, the RMSD of D619 and T13 remained at small fluctuations after 15 ns of the simulation giving further confirmation of the stability of the simulation (Fig. 3.18 b and d).



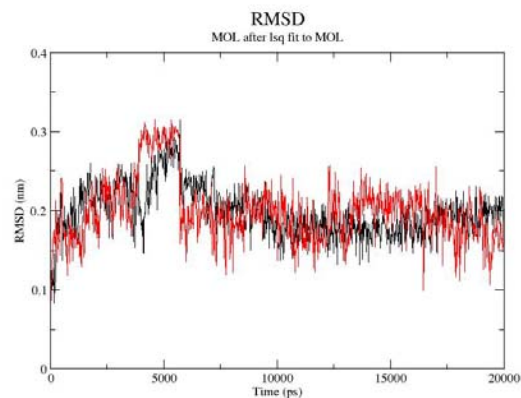
(a)



(b)



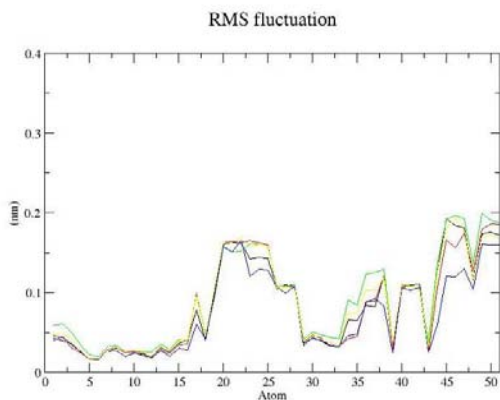
(c)



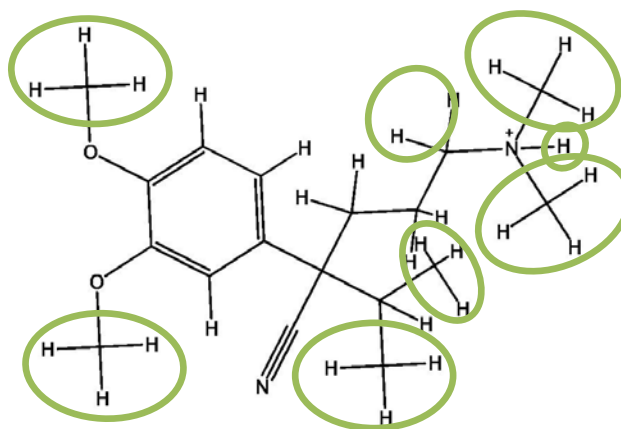
(d)

Fig 3.18. RMSD values of (a) backbone of the improved pore region of the open conformation of D619 complex. (b) D619 in the pore region of the open conformation. Each 5 different starting positions of D619 are shown in black, red, green, blue and yellow, respectively. (c) backbone of the improved pore region of the open conformation of T13 complex. (d) T13 in the pore region of the open conformation. Each of the two different starting positions of T13 are shown in black and red.

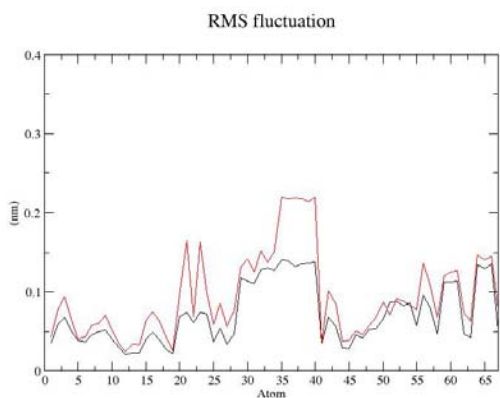
RMSF analyses of the ligands between 15 to 20 ns were also performed. Most of the flexible parts of D619 and T13 can be seen as peaks in the Fig 3.19 a and c. The hydrogen and fluorine atoms are circled in green as shown in Fig 3.19 b and d show that the hydrogen atoms which belong to methyl group are higher fluctuation than the other atoms. It is also indicated that the benzene ring, the ammonium group and the nitrile group are rather rigid.



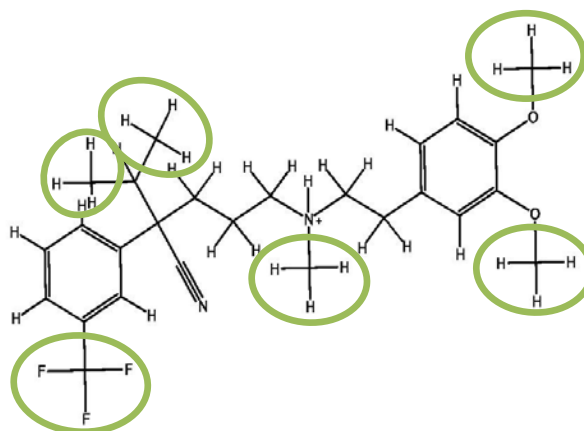
(a)



(b)



(c)



(d)

Fig 3.19. (a) RMSF values of D619 in open conformation of $\text{Ca}_v1.2$. (b) 2D structure of D619. (c) RMSF values of T13 in open conformation. (d) 2D structure of T13. Green circle indicate hydrogen atoms of the highest flexibility.

The superimposition of the average structures of D619 and T13 complex of the last 5ns of MD simulation with initial models does show ligand conformation changes in each different run (Fig 3.20 and 3.22). The initial structure was randomly started from 5 different positions for D619 and 2 different positions for T13 in the cavity. The information obtained from these simulations found that D619 and T13 are located between the domains III/IVS6. For D619, the

benzene ring faces to IIIS6 or either to IVS6. In the T13 complex system, each benzene ring binds to each domain IIIS6 and IVS6. The average structure from MD simulation supports the hypothesis that the benzene ring as a part of the ligand should interact with IIIS6 and/or IVS6.

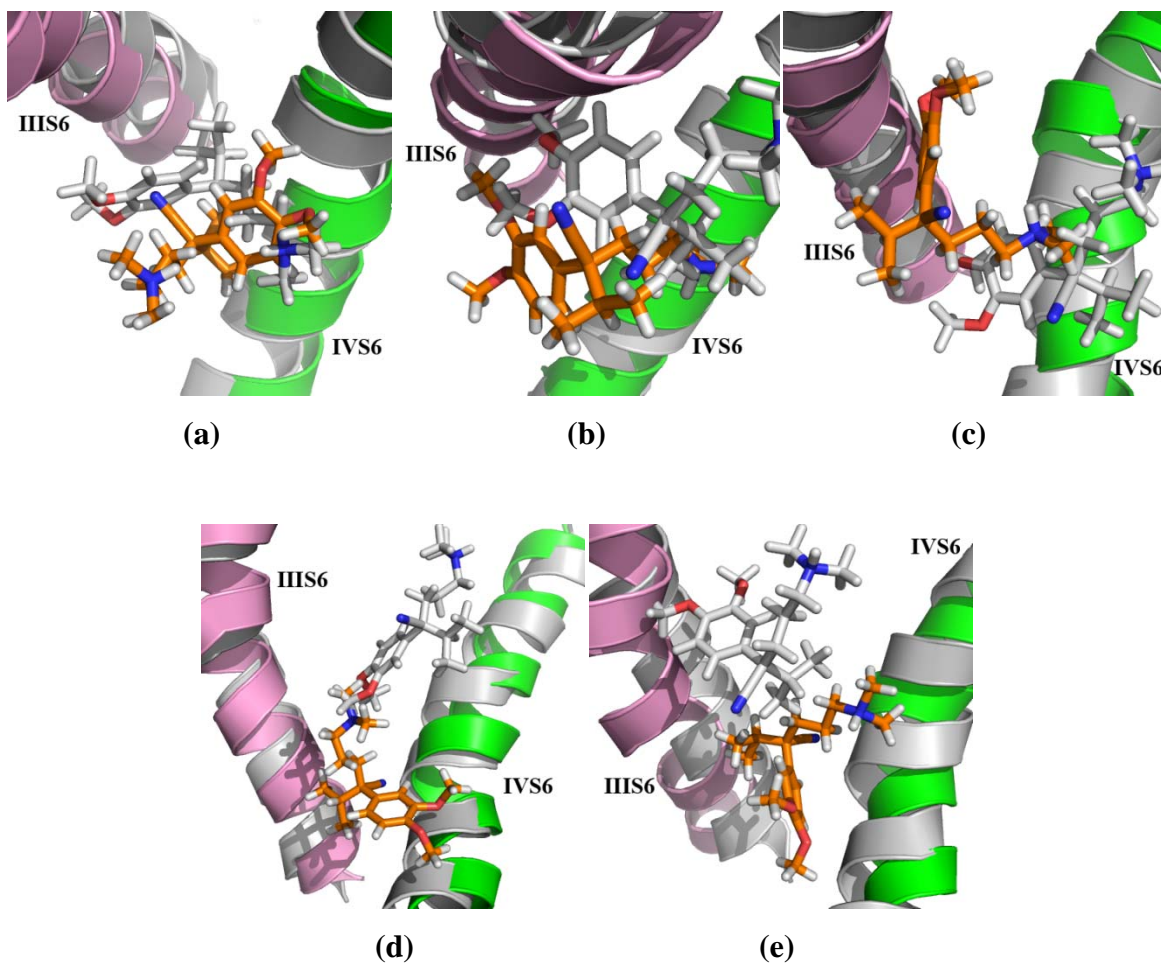
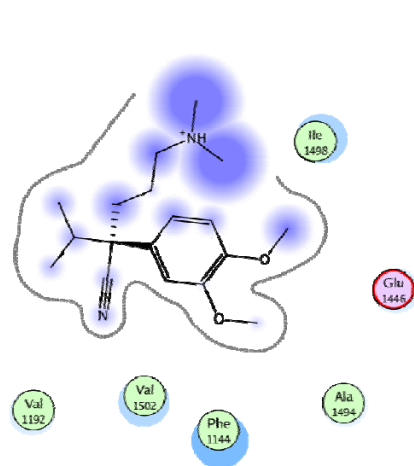
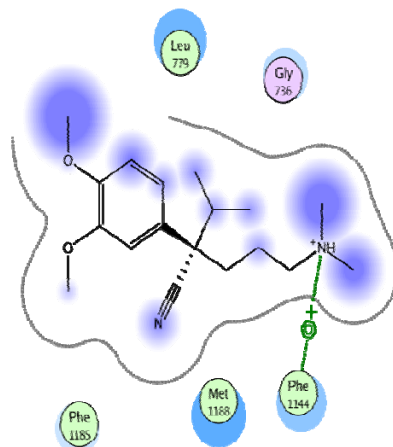


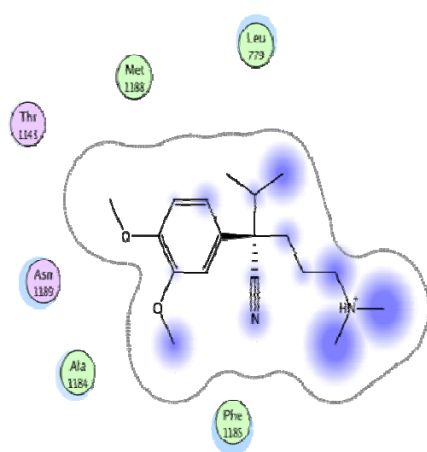
Fig 3.20. Superposition of the initial D619 complex structure (gray) and the averaged structures of the last 5ns of MD simulation complexes. The domain IIIS6 (pink) and IVS6 (green) are also given. The position of the ligand D619 after docking and the average structure from MD simulation are shown in gray and orange sticks. (a) 1st run. (b) 2nd run (c) 3rd run (d) 4th run (e) 5th run.



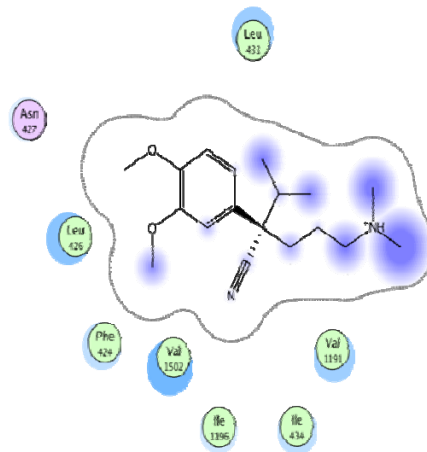
(a)



(b)



(c)



(d)

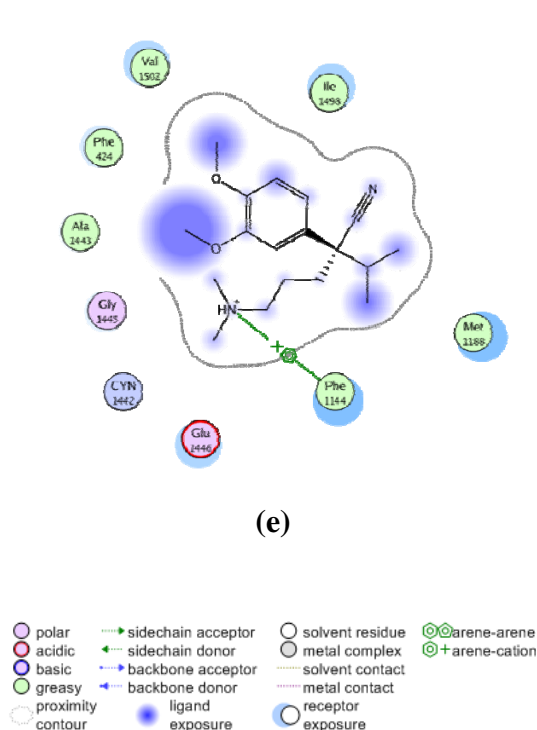


Fig 3.21. The interaction between D619 and receptor from averaged structures of the last 5ns of MD simulation using MOE program. (a) 1st run (b) 2nd run (c) 3rd run (d) 4th run (e) 5th run. In (b) and (c) are shown an arene-cation interaction with Phe1144.

Each simulation of D619 in the complex results in a binding pattern by using MOE program as shown in Fig 3.21. The interaction between protein and ligand mainly involves hydrophobic interactions which hydrophobic residues shown by green circles. It can be seen from the Fig 3.21 b and e that the positively charged nitrogen atom of D619 interacts with the aromatic ring of Phe 1144, which is the residue before the selectivity filter residue on domain III (TFE). The annotation also shows a high degree of reduction of solvent-exposed surface area (a halolike disc around the residue) on Phe1144 which indicates a favorable stabilizing interaction. In most simulation runs of the D619 complex the positively charged nitrogen points outwards from the binding pocket, this is indicated by a blue surface. Only in the 5th run, there is an interaction of this group with one amino acid of the pocket (Phe1144) (Fig 3.21 e).

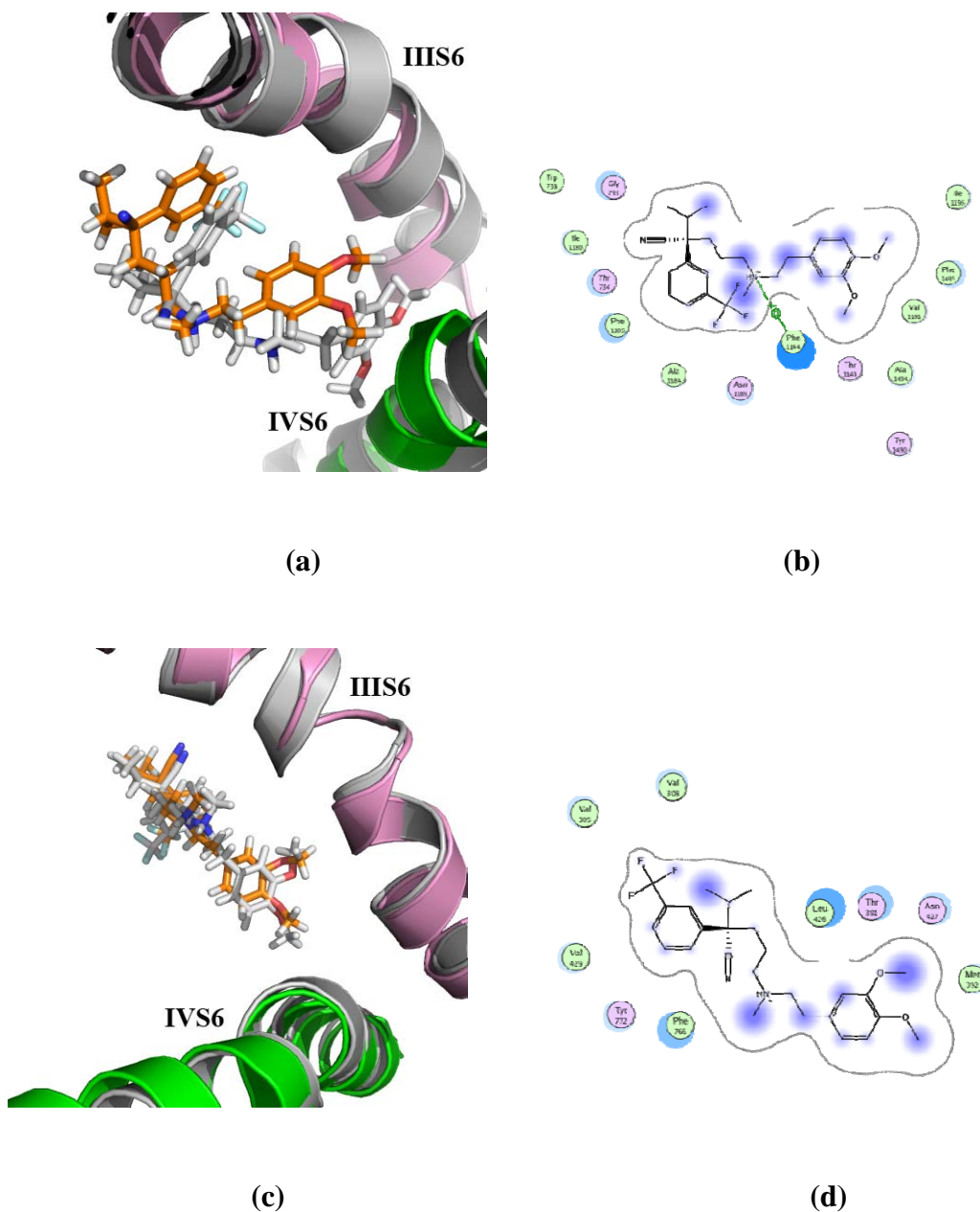


Fig 3.22. (a) Superpositions of the 1st run. The initial T13 complex structure (gray) and the averaged structures of the last 5ns of MD simulation complexes in contact with IIS6 (pink) and IVS6 (green) are shown. The T13 ligand from docking and from averaged structure of MD simulation is shown in sticks in gray and orange. (b) 2nd run. The 2D diagram of the interactions between T13 and receptor results from averaged structures of the last 5ns of MD simulation.

The ligand T13 is fitting to binding pocket, which is shown by the contour line (Fig 3.22). Fig 3.22b shows that the π -cation interaction between the positively charged nitrogen atom of T13 and Phe1144 is present. Additionally, it is also interesting to note that all of the receptor residues located on one side of the T13 point out of the binding residues. In the 2nd run as shown in Fig 3.18, the starting position of T13 was at the middle of the pore. The ligand T13 from averaged structure of the last 5 ns of simulation were still located around the center of the pore.

From these five and two different starting positions of D619 and T13 ligand, it can be seen that the difference of the starting positions of the ligand is important. Different geometries are obtained from these simulations which appear to be stable throughout the whole simulation time. This implies that MD is not suitable to distinguish between different starting poses probably because simulation times are not long enough and or the model is not good enough. This remarkable result needs some further investigation. Particular supporting experimental data are needed.

3.7 Molecular Dynamics simulation studies of the improved open conformation of Cav1.2 calcium channel with quaternary (-) diltiazem

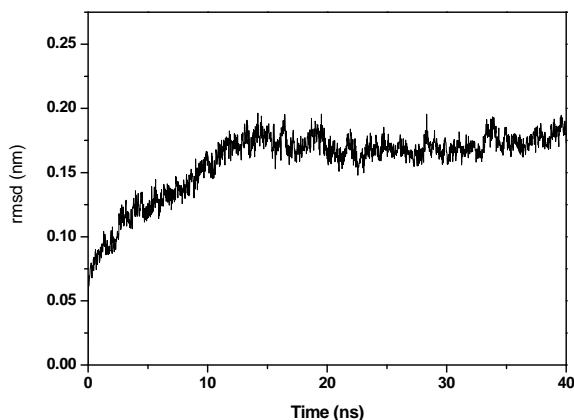


Fig. 3.23. Stability of refined Cav1.2 homology model in MD

The quaternary (-) diltiazem (qDil) chemically belongs to the benzothiazepines BTZ which is also inhibiting L-type calcium channels in a state dependent manner [93]. The simulation was set to compare the result and to test the quality of the improved model with the experimental data from group of Prof. Hering [94]. The stability of the drug-refined model was tested in a 40 ns MD simulation. Simulation parameters are similar as previously published by Stary et al, 2008. The RMSD (root mean square deviation) of the backbone atoms as a function of time is shown in Fig 3.23. During the first 15 ns the RMSD continually rises to approximately 0.2 nm and remains stable at this level for the next 25 ns. This value is in good agreement with published values for low sequence identity homology models.

3.8 Homology Modeling and model evaluation of pore region $\text{Ca}_v1.2$ closed conformation

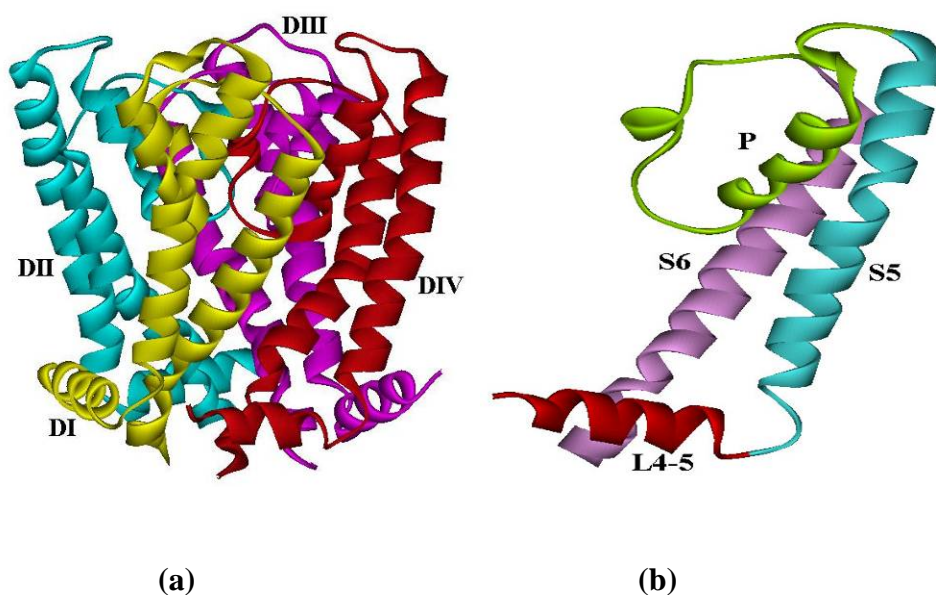


Fig 3.24. Homology models of $\text{Ca}_v1.2$ closed conformation. (a) Side view detail of pore domain. Each domain is colored: yellow (Domain I), blue (Domain II), pink (Domain III) and red (Domain IV). (b) Pore forming subunits. L4-5, S5, P and S6 are colored red, blue, green and purple, respectively.

The pore domains are formed by 4 homologous subunits and are arranged clockwise. Each subunit consists of linker helices L4-5, helices S5, a selectivity filter P segment and S6 helices as show in Fig 3.24. Starting from the initial homology model of pore region Ca_v1.2 closed conformation done by A. Stary [95] built from KcsA, MlotiK crystal structures and homology model of NaChBac, we used a new higher resolution crystal structure of NaK sodium channel [88] to improve the initial homology model of pore region Ca_v1.2 closed conformation. The Ca_v1.2 model in closed conformation was built because in the next step of our work weare interested in the channel interaction with cholesterol.

To increase the precision and accuracy of the models, we applied multiple templates approaches. Eight models based on KcsA, Mlotik , NaK and the homology model of NaChBac as a template were built. For each model, ten different structures were performed. Due to the lack of conserved residues between potassium and cation NaK channel with Ca_v1.2 channel at selectivity filter P region, the P-helices and the selectivity filter were modeled based on homology model of NaChBac which contain the same highly conserved sequence FxxxTxExW motif, whereas the S5 and S6 segments were based on all templates.

The protein quality accuracy of a model related to the accuracy of the model. The homology model needs to assess the quality of a model. This implies that the reliability of the model obtained from various assessment methods is important for structure determination, reasonable for MD simulations and suitable to study drug interaction. Various quality assessment methods (Prosa2003, Verify 3D, WHAT_CHECK Packing, Procheck, ProQresLG and ProQres MaxSub) were applied to evaluate, validate and screen the quality of all models. The result outputs from the checking programs are summarized in Table 3.4. The best values of entire structures are highlighted in black. The scores of structure number 2 of model 1 are favorable and ranked as a first ranking from Verify 3D, ProQresLG and ProQres MaxSub with acceptance of Prosa2003, WHAT_CHECK Packing and Procheck method. Consequently, this structure is chosen for the further work.

Prosa2003 calculated the z-score of protein which based on known structure from all available protein of different sources (X-ray and NMR). It can be used to check that the z-score of the input structure is within the range of scores typically found for native protein of similar size. The good structure protein supposes to be inside this range and small deviation from the statistical average over the known structure. In our structure, the range of all known structure of

similar size is between 10 to -15. Thus, the good structure is indicated the score which is close to -2.5. Verify3D analyzes the compatibility of an atomic model with its own amino acid sequence. The scores of Verify3D are shown in percentage term of the satisfactory structure. The high percentage implies to be the good structure. WHAT_CHECK packing judges the quality of the structure based on z-score. The good structure reports the positive value. Procheck illustrates the percentage in most favored region of Ramachandran plot. Therefore, the higher value is the better one. ProQres LG score and MaxSub determine the range of quality in different ranges as follow:

For LGscore

LGscore > 1.5 fairly good model
 LGscore > 2.5 very good model
 LGscore > 4 extremely good model

For MaxSub

MaxSub > 0.1 fairly good model
 MaxSub > 0.5 very good model
 MaxSub > 0.8 extremely good model

Table 3.4 Static quality of Ca_v1.2 closed conformation.

Model 1: KcsA, MlotiK, NaK and homology model of NaChBac as a template.

| Structure no. | Prosa2003 | Verify 3D | WHAT_CHECK Packing | Procheck | ProQres LG score | ProQres MaxSub |
|---------------|-----------|-----------|--------------------|----------|------------------|----------------|
| 1 | -0.49 | 53.88 | -0.131 | 82.5 | 2.962 | 0.307 |
| 2 | -1.08 | 72.54 | -0.676 | 84.8 | 4.312 | 0.430 |
| 3 | -0.84 | 64.99 | -0.075 | 83.0 | 3.452 | 0.355 |
| 4 | -0.73 | 58.7 | -0.035 | 84.8 | 3.118 | 0.311 |
| 5 | -0.97 | 57.44 | -0.031 | 83.9 | 3.063 | 0.330 |
| 6 | -0.14 | 62.26 | -0.049 | 81.4 | 2.772 | 0.292 |
| 7 | -0.82 | 58.49 | 0.030 | 82.1 | 3.249 | 0.35 |
| 8 | -0.05 | 54.09 | -0.106 | 83.7 | 3.172 | 0.355 |
| 9 | 0.14 | 66.88 | 0.229 | 83.7 | 3.032 | 0.335 |
| 10 | -0.33 | 65.41 | -0.095 | 84.4 | 2.984 | 0.310 |

Model 2: KcsA, MlotiK, NaK and only P region of homology model of NaChBac as a template.

| Structure no. | Prosa2003 | Verify3D | WHAT_CHECK Packing | Procheck | ProQres LG score | ProQres MaxSub |
|---------------|-----------|----------|--------------------|----------|------------------|----------------|
| 1 | -1.81 | 53.04 | -0.497 | 80.9 | 2.777 | 0.25 |
| 2 | -1.53 | 54.51 | -0.502 | 82.3 | 2.374 | 0.214 |
| 3 | -1.21 | 62.47 | 0.715 | 82.8 | 2.804 | 0.249 |
| 4 | -1.47 | 50.52 | -0.217 | 82.8 | 2.81 | 0.261 |
| 5 | -1.36 | 60.38 | -0.715 | 80.7 | 2.735 | 0.265 |
| 6 | -1.67 | 59.12 | -0.588 | 82.1 | 3.173 | 0.279 |
| 7 | -0.98 | 55.77 | -0.627 | 80.4 | 3.314 | 0.302 |
| 8 | -0.99 | 55.35 | -0.731 | 84.6 | 2.887 | 0.276 |
| 9 | -0.96 | 57.44 | 0.270 | 80.7 | 2.639 | 0.250 |
| 10 | 0.19 | 52.41 | 0.185 | 80.7 | 2.438 | 0.232 |

Model 3: KcsA and homology model of NaChBac as a template.

| Structure no. | Prosa2003 | Verify3D | WHAT_CHECK Packing | Procheck | ProQres LG score | ProQres MaxSub |
|---------------|-----------|----------|--------------------|----------|------------------|----------------|
| 1 | -1.03 | 64.99 | 0.502 | 83.9 | 3.82 | 0.381 |
| 2 | -1.37 | 55.56 | 0.134 | 84.6 | 3.692 | 0.377 |
| 3 | -0.96 | 69.18 | 0.779 | 83.7 | 3.83 | 0.388 |
| 4 | -1.44 | 63.1 | 0.369 | 83.7 | 3.396 | 0.337 |
| 5 | -1.73 | 69.18 | 0.280 | 83.4 | 3.263 | 0.365 |
| 6 | -1.44 | 59.54 | 0.977 | 83.2 | 3.579 | 0.372 |
| 7 | -1.02 | 62.47 | 0.704 | 84.8 | 3.918 | 0.398 |
| 8 | -1.34 | 59.54 | 0.128 | 83.7 | 3.29 | 0.361 |
| 9 | -1.53 | 66.67 | 1.125 | 84.8 | 3.221 | 0.327 |
| 10 | -1.62 | 55.77 | 0.080 | 84.6 | 3.521 | 0.366 |

Model 4: KcsA and only P region of homology model of NaChBac as a template.

| Structure no. | Prosa2003 | Verify3D | WHAT_CHECK Packing | Procheck | ProQres LG score | ProQres MaxSub |
|---------------|-----------|----------|--------------------|----------|------------------|----------------|
| 1 | 0.36 | 29.35 | 0.606 | 88.1 | 2.042 | 0.170 |
| 2 | 0.40 | 47.17 | 0.113 | 87.9 | 2.950 | 0.279 |
| 3 | -0.56 | 46.12 | 0.169 | 87.6 | 2.659 | 0.229 |
| 4 | 0.37 | 32.91 | 0.302 | 84.1 | 2.349 | 0.198 |
| 5 | 0.06 | 42.35 | 0.464 | 87.4 | 2.222 | 0.201 |
| 6 | -0.16 | 41.93 | 0.113 | 89.0 | 2.311 | 0.209 |
| 7 | 0.09 | 48.22 | 0.314 | 87.4 | 2.007 | 0.186 |
| 8 | 0.17 | 50.31 | 0.305 | 88.1 | 2.381 | 0.209 |
| 9 | 0.52 | 47.38 | 0.272 | 86.7 | 2.497 | 0.234 |
| 10 | 0.00 | 39.2 | 0.778 | 85.5 | 1.896 | 0.189 |

Model 5: MlotiK and homology model of NaChBac as a template.

| Structure no. | Prosa2003 | Verify3D | WHAT_CHECK Packing | Procheck | ProQres LG score | ProQres MaxSub |
|---------------|-----------|----------|--------------------|----------|------------------|----------------|
| 1 | -1.79 | 59.96 | 0.194 | 83.2 | 2.840 | 0.303 |
| 2 | -0.71 | 55.77 | -0.148 | 85.1 | 2.775 | 0.284 |
| 3 | -1.34 | 54.93 | -0.113 | 85.5 | 3.105 | 0.313 |
| 4 | -1.26 | 62.68 | -0.124 | 84.1 | 3.102 | 0.311 |
| 5 | -1.30 | 56.39 | -0.146 | 86.2 | 2.837 | 0.295 |
| 6 | -0.69 | 55.97 | -0.110 | 83.7 | 2.723 | 0.268 |
| 7 | -1.33 | 61.84 | 0.129 | 85.1 | 3.166 | 0.322 |
| 8 | -1.38 | 59.54 | -0.005 | 83.9 | 2.935 | 0.308 |
| 9 | -1.12 | 59.12 | 0.264 | 85.3 | 3.071 | 0.327 |
| 10 | -0.39 | 54.93 | 0.080 | 83.7 | 2.975 | 0.293 |

Model 6: Mlotik and only P region of homology model of NaChBac as a template.

| Structure no. | Prosa2003 | Verify3D | WHAT_CHECK Packing | Procheck | ProQres LG score | ProQres MaxSub |
|---------------|-----------|----------|--------------------|----------|------------------|----------------|
| 1 | -0.16 | 63.73 | -0.385 | 90 | 2.479 | 0.238 |
| 2 | -0.19 | 50.73 | -0.043 | 90.4 | 3.352 | 0.287 |
| 3 | -0.06 | 49.06 | -0.083 | 88.6 | 3.064 | 0.291 |
| 4 | 0.51 | 54.30 | 0.143 | 89.7 | 2.947 | 0.307 |
| 5 | 0.33 | 48.64 | -0.388 | 86.9 | 2.742 | 0.269 |
| 6 | 0.27 | 48.22 | -0.232 | 87.6 | 2.548 | 0.253 |
| 7 | -0.16 | 58.70 | -0.365 | 86.9 | 2.890 | 0.269 |
| 8 | 0.10 | 55.14 | -0.177 | 89 | 3.022 | 0.280 |
| 9 | 0.11 | 60.17 | -0.485 | 88.8 | 2.842 | 0.288 |
| 10 | 0.17 | 51.15 | -0.057 | 89.5 | 3.323 | 0.334 |

Model 7: NaK and homology model of NaChBac as a template.

| Structure no. | Prosa2003 | Verify 3D | WHAT_CHECK Packing | Procheck | ProQres LG score | ProQres MaxSub |
|---------------|-----------|-----------|--------------------|----------|------------------|----------------|
| 1 | -1.19 | 61.22 | 0.564 | 84.6 | 2.853 | 0.297 |
| 2 | -1.45 | 55.35 | 0.391 | 82.5 | 2.734 | 0.286 |
| 3 | -1.41 | 54.93 | -0.113 | 85.5 | 2.701 | 0.286 |
| 4 | -1.69 | 63.94 | 0.842 | 82.5 | 2.992 | 0.310 |
| 5 | -1.29 | 60.59 | 0.804 | 84.1 | 2.834 | 0.295 |
| 6 | -2.25 | 54.30 | 0.185 | 83.7 | 2.464 | 0.277 |
| 7 | -1.61 | 55.77 | 0.709 | 84.1 | 3.011 | 0.304 |
| 8 | -1.34 | 59.12 | 0.432 | 84.4 | 3.171 | 0.307 |
| 9 | -0.75 | 58.28 | 0.367 | 86.7 | 2.626 | 0.257 |
| 10 | -2.15 | 61.84 | 0.686 | 84.1 | 3.183 | 0.308 |

Model 8: NaK and only P region of homology model of NaChBac as a template.

| Structure no. | Prosa2003 | Verify 3D | WHAT_CHECK Packing | Procheck | ProQres LG score | ProQres MaxSub |
|---------------|-----------|-----------|--------------------|----------|------------------|----------------|
| 1 | -1.81 | 53.04 | -0.497 | 80.9 | 2.777 | 0.250 |
| 2 | -1.53 | 54.51 | -0.502 | 82.3 | 2.374 | 0.214 |
| 3 | -1.21 | 62.47 | 0.715 | 82.8 | 2.804 | 0.249 |
| 4 | -1.47 | 50.52 | -0.217 | 82.8 | 2.810 | 0.261 |
| 5 | -1.36 | 60.38 | -0.715 | 80.7 | 2.735 | 0.265 |
| 6 | -1.67 | 59.12 | -0.588 | 82.1 | 3.173 | 0.279 |
| 7 | -0.98 | 55.77 | -0.627 | 80.4 | 3.314 | 0.302 |
| 8 | -0.99 | 55.35 | -0.731 | 84.6 | 2.887 | 0.276 |
| 9 | -0.96 | 57.44 | 0.270 | 80.7 | 2.639 | 0.250 |
| 10 | 0.19 | 52.41 | 0.185 | 80.7 | 2.438 | 0.232 |

Note: The best scores from each model are highlighted in gray. The overall best scoring structure is highlighted in black.

3.9 Molecular Dynamics simulation studies of the pore region of Ca_v1.2 in closed conformation and improved open conformation in dependence of the content of cholesterol in the membrane

In this section, we focus on the effect of both models by addition of cholesterol into the lipid bilayer. Some part of this work presented and published in European Biophysics Journal with Biophysics Letters 40:118-118, 2011 [96]. The possible effects by which cholesterol influences Cav1.2 channels see Summary 1.

Summary 1

Molecular Dynamics Simulations on the Function of the Transmembrane Cav1.2 Channel in Dependence of the Content of Cholesterol in the Membrane

Cholesterol is known to influence voltage-gated calcium channel currents. It has been previously shown that increased membrane free cholesterol levels decrease calcium channel currents in coronary arterial smooth muscle cells [97]. The underlying mechanisms of cholesterol regulation of Cav1.2 channels are, however, poorly understood. To investigate possible effects by which cholesterol influences Cav1.2 channels we use MD simulations with different lipid compositions.

Methods.

All simulations were performed with Gromacs software version 4.0.7 [98] using the 43a1 force-field [99]. Both closed and open channels were embedded in a 1-palmitoyl-2-oleoyl phosphatidylcholine (POPC) and POPC/CHOL lipid bilayer (Fig. 1). The structure model of the closed channel was generated using Modeller 9v7 [63]. The crystal structures of the potassium channels KcsA (PDB:1K4C) [86], MlotiK channel (PDB:3BEH) [100], the nonselective cation channel NaK (PDB:2AHZ) [88] and a homology model of the NaChBac sodium channel [101] served as templates. The closed model was developed using similar procedures as described previously [95]. The P-helices and selectivity filter are based on the NaChBac homology model only, while the L4-5, S5 and S6 segments are based on all templates.

The structure of the open conformation was taken from Stary et al. [102]. The P-helix of domain III was slightly modified to increase hydrogen bonding between polar side chains. The starting configuration of a 128-lipid POPC bilayer was obtained from the end of a 1.6 ns simulation performed by Kandt et al. (<http://www.moose.bio.ucalgary.ca>) and replicated four

times to create a bilayer of 512 lipids. The INFLATEGRO [103] tool was used to embed the channels in a POPC lipid bilayer. The POPC/CHOL lipid bilayer was generated by the following procedure: A cylindrical hole was introduced to implant the protein by removing a minimal number of overlapping POPC/CHOL lipids and compressing the bilayer using Gromacs tools. The system was solvated with around 25,339 SPC waters and included 0.1 mol/liter concentration of sodium chloride (NaCl). 5 Ca^{2+} ions were placed along the pore.

The final POPC systems contained 502 POPC and 147 NaCl molecules. There were 537 POPC, 176 CHOL and 135 NaCl molecules in the closed channel POPC/CHOL system. The open channel POPC/CHOL system contained 525 POPC, 176 CHOL and 115 NaCl molecules. Na^+ ions were added randomly within the solvent to neutralize the systems. Thus, there were 11 and 7 Na^+ ion in the closed and open channels, respectively.

Snapshots of the trajectory were written out every 20 ps. The system was energy minimized with the steepest descent algorithm, followed by positional restrained MD for 2 ns. Subsequently, 10 ns of unrestrained MD simulation were carried out using the NPT ensemble. All simulations were repeated 5 times. The Nose-Hoover thermostat [104] with a coupling constant of 0.1 ps to a temperature bath of 300 K was used. Pressure was held constant using a semi-isotropic Parrinello-Rahman barostat algorithm [105] with a coupling constant of 1 ps. Electrostatic interactions were calculated explicitly at a distance smaller than 1 nm, and long-range electrostatic interactions were calculated at every step by particle-mesh Ewald summation [106]. Lennard-Jones interactions were calculated with a cutoff of 1 nm. Bond lengths were constrained using the LINCS algorithm Lennard-Jones interactions were calculated with a cutoff of 1 nm. Bond lengths were constrained using the LINCS algorithm [107]. Subsequent analyses of the MD simulation data were performed using tools available within GROMACS.

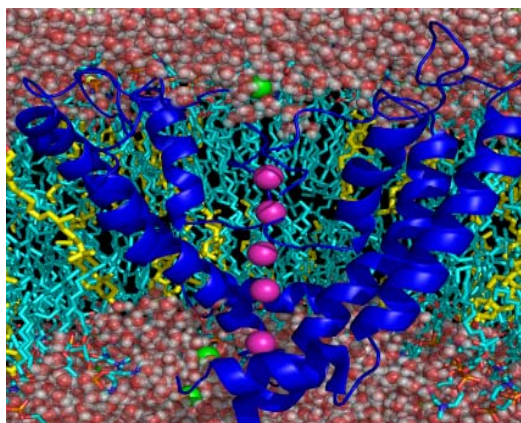


Fig. 1. A snapshot of the channel in the POPC/CHOL bilayer. The helices from domain I and III are represented as blue ribbons. POPC and CHOL are shown in gray and yellow. The oxygen atoms and hydrogen atoms of the water molecules are shown in white and red, respectively. Calcium and NaCl ions are shown as pink and green spheres.

Results

Stability of system

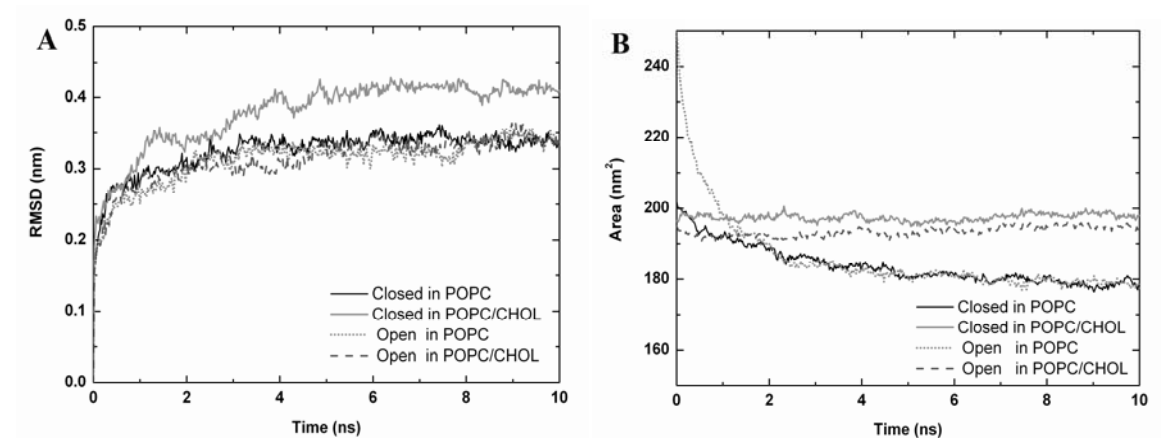


Fig. 2. (a) Average RMSD values of the backbone and (b) lateral area in closed and open channels in POPC and POPC/CHOL systems.

The stability of each simulation system is analysed by the root-mean-square displacement (RMSD) of the protein backbone atoms. The backbone RMSD of both closed and open channels in POPC and POPC/CHOL systems over 10 ns is shown in Fig. 3A. For the first 3 ns, the RMSD value steadily increases and then reaches a plateau. After 3 ns, the RMSD of the closed channel in the POPC/CHOL system stabilizes at approximately 0.4 Å. The RMSD of closed and open channels in POPC and the open channel in the POPC/CHOL bilayer are around 0.3 Å. The RMSD value of the closed channel in POPC/CHOL is relatively high compared to the other systems suggesting a conformational change. To investigate this in more details, decomposition of the backbone RMSD values into contributions from different helices is performed as shown in Fig 3. It turned out that the loop connecting helix S5 with the P-helix is mainly responsible for the increased RMSD values.

To further analyse the stability of the system we examined the lateral area of the whole system as a function of time (Fig. 2B). In the pure POPC systems with closed and open channels, the lateral area value decreased to around 180 nm² and stabilized within 8 ns. Upon addition of cholesterol to the POPC bilayer, the area remains stable during the whole simulation at around 200 and 195 nm² for closed and open channels. RMSD and the lateral area values confirm that 10 ns simulation is sufficient for stabilizing the system.

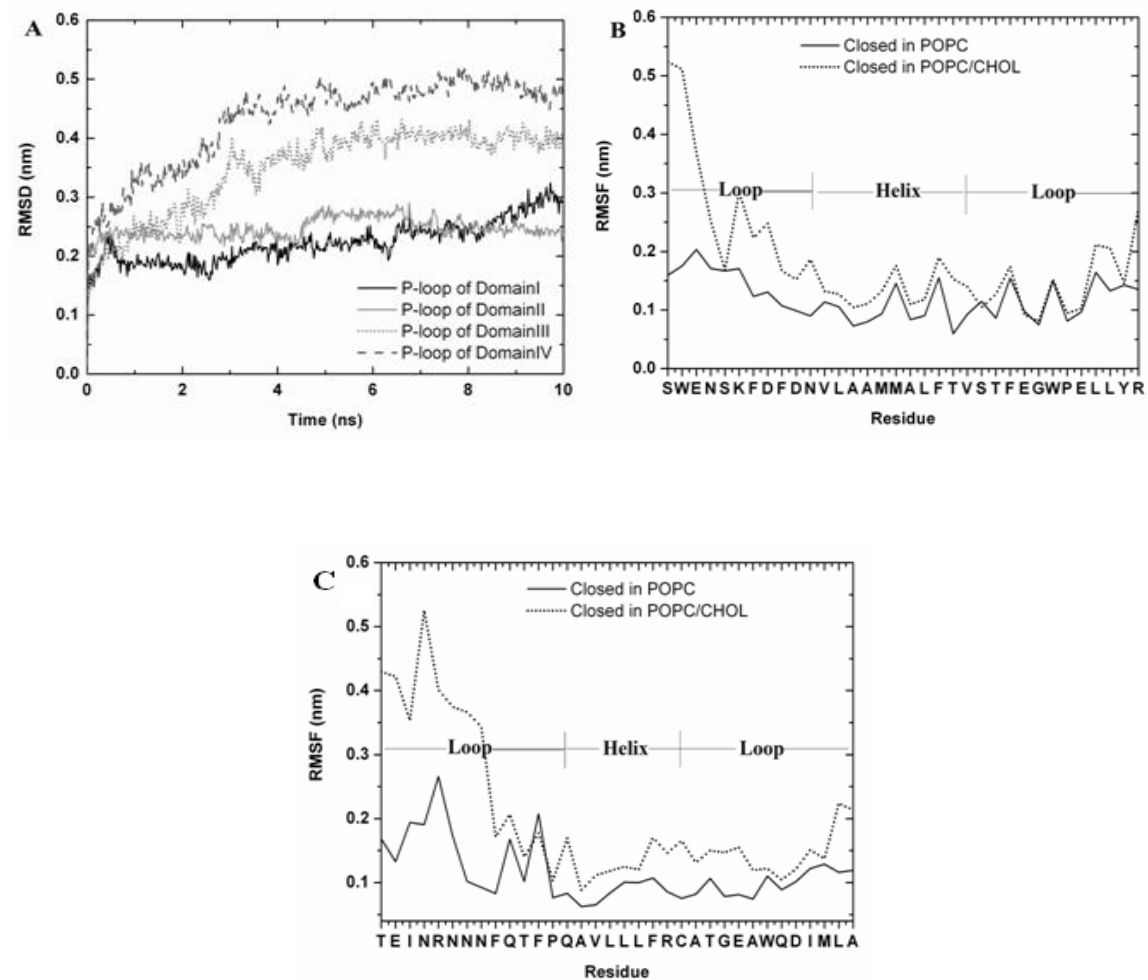


Fig. 3. (a) The RMSD from each P helices backbone in closed channel in POPC/CHOL systems (b) The RMSF for the P-helix domain III of closed in POPC and POPC/CHOL system (c) The RMSF for the P-helix domain IV of closed in POPC and POPC/CHOL system.

Dynamics of Ca^{2+} in different lipid compositions

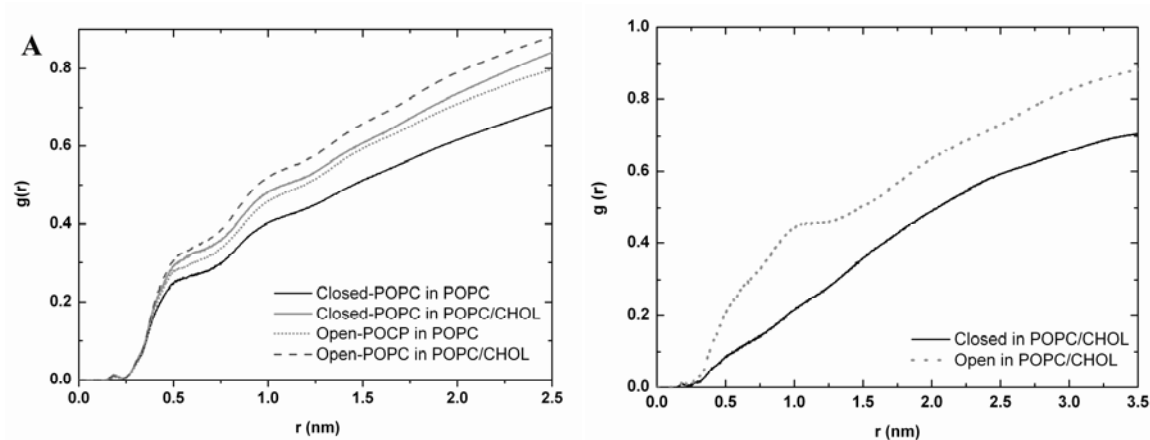


Fig. 4. Radial distribution functions between (a) whole protein atoms and POPC. (b) whole protein atoms and CHOL.

The selectivity filter in calcium channels is formed by side chains of highly conserved glutamates in homologous positions in all four domains, also referred to as EEEE locus [107] (Fig. 5).

The Ca^{2+} ion movements from the center of the selectivity filter are analysed using mean square displacements (MSD). Ca^{2+} ions along the pore separate into 2 dynamical groups – fast and slow. Simulations show that the Ca^{2+} ions in the slow group remain at the EEEE locus during the whole simulation, while the fast group moves around in the water layer (Fig. 6).

The slow group MSDs in both closed and open channels in pure POPC have larger values compared to simulations containing CHOL. The Ca^{2+} ions of the slow POPC group are in the range of 0 to 5 nm^2 for closed and open channels. In the POPC/CHOL system, the MSD values were reduced to 0 to 0.2 nm^2 for the closed channel and to 0 to 1.6 nm^2 for the open channel. Fig. 6 shows that the Ca^{2+} ion movement is decreased in both POPC/CHOL systems. This clearly shows that cholesterol modulates Ca^{2+} movement within the channel.

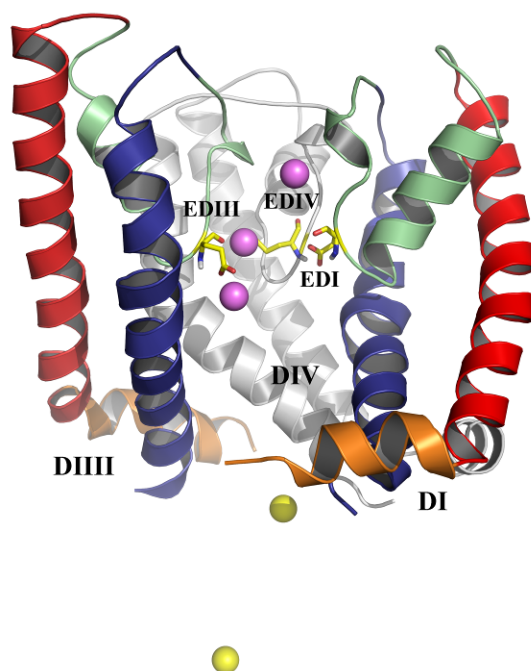


Fig. 5. Location of the calcium ions around the selectivity filter. P-helices and S6 domains I and III are shown as blue and green ribbons, respectively. Domain IV is colored gray. Glutamates of domains I, III and IV are shown as sticks. Domain II is removed for clarity. Slow and fast moving Ca^{2+} ions around the selectivity filter are shown as pink and yellow spheres.

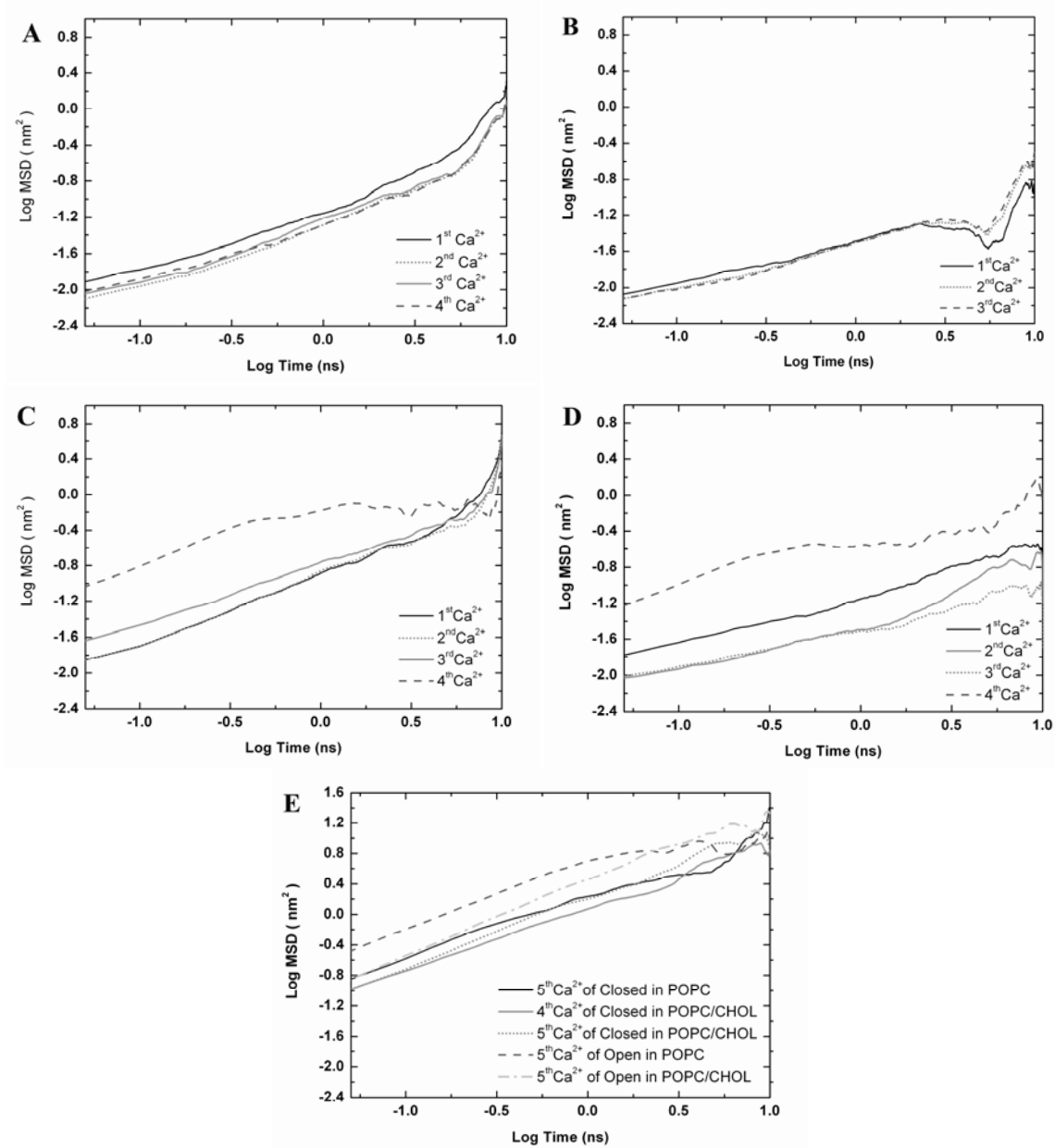


Fig. 6. The MSD of Ca²⁺ ions from the center of mass of the selectivity filter consists of 2 groups. slow group (a) closed in POPC system (b) closed in POPC/CHOL system (c) open in POPC system (d) open in POPC/CHOL system. For fast group of (e) closed and open in POPC and POPC/CHOL systems.

Bilayer Fluidity

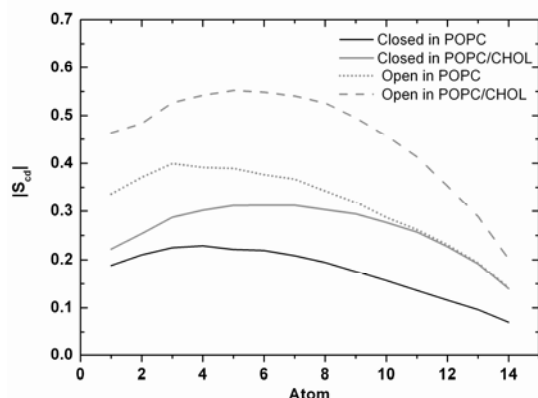


Fig. 7. The order parameter profile of hydrocarbon tails for the POPC system.

The order parameter (S_{cd}) as a function of carbon atom number along the hydrocarbon tails is shown in Fig. 7. The order parameter values for POPC lipids within 1 nm around the closed and open channels are calculated. The values decrease in the order from open channel in POPC/CHOL > open channel in POPC > closed channel in POPC/CHOL > closed channel in POPC. It is interesting to note that the POPC lipid tail in the open channel shows higher S_{cd} values than the closed channel in both systems indicating that the protein has an influence on lipid conformation in its neighborhood. This has been seen in other simulations of lipid protein interaction as well [108]. Fig. 7 gives a comparison of the order parameter of each system. It is obvious that the lipids in the POPC/CHOL system are more ordered than the lipids of the pure POPC system. Hence, addition of cholesterol increases lipid packing. This has been found experimentally [109] as well as in simulation [110].

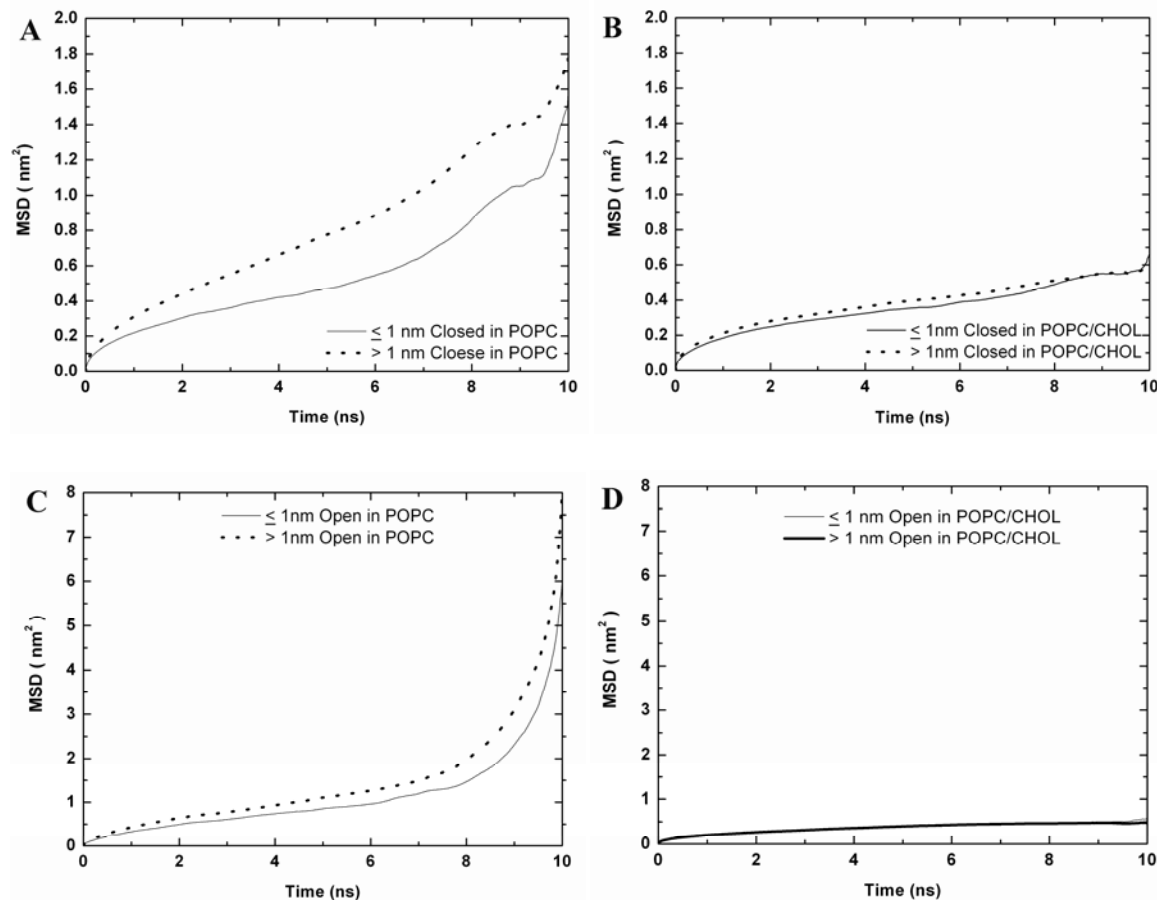


Fig. 8. MSD of POPC surrounding the protein \leq and $>$ than 1 nm (a) closed in POPC system (b) closed in POPC/CHOL system (c) open in POPC system (d) open in POPC/CHOL system.

The mobility of the lipids as a function of distance from the protein, i.e. lipids with \leq 1 nm (inner shell) and $>$ 1 nm (outer shell) of the protein are displayed in Fig. 8. The MSD values reveal details about the movement of POPC. Significant differences are observed between the inner and outer shell in the POPC systems but not in the POPC/CHOL systems. There the MSD values indicate that POPC movement is homogeneous in the whole bilayer. Fig. 8, A and B show that lipids in pure POPC systems which are more than 1 nm away from the protein are faster than lipids within 1 nm. This clearly indicates a binding or at least dynamic coupling between the protein and the surrounding lipids. On the other hand, for the POPC/CHOL system such a

dynamical difference is not found. This implies that cholesterol plays a crucial rule in restricting the lipid movement around 1 nm of POPC.

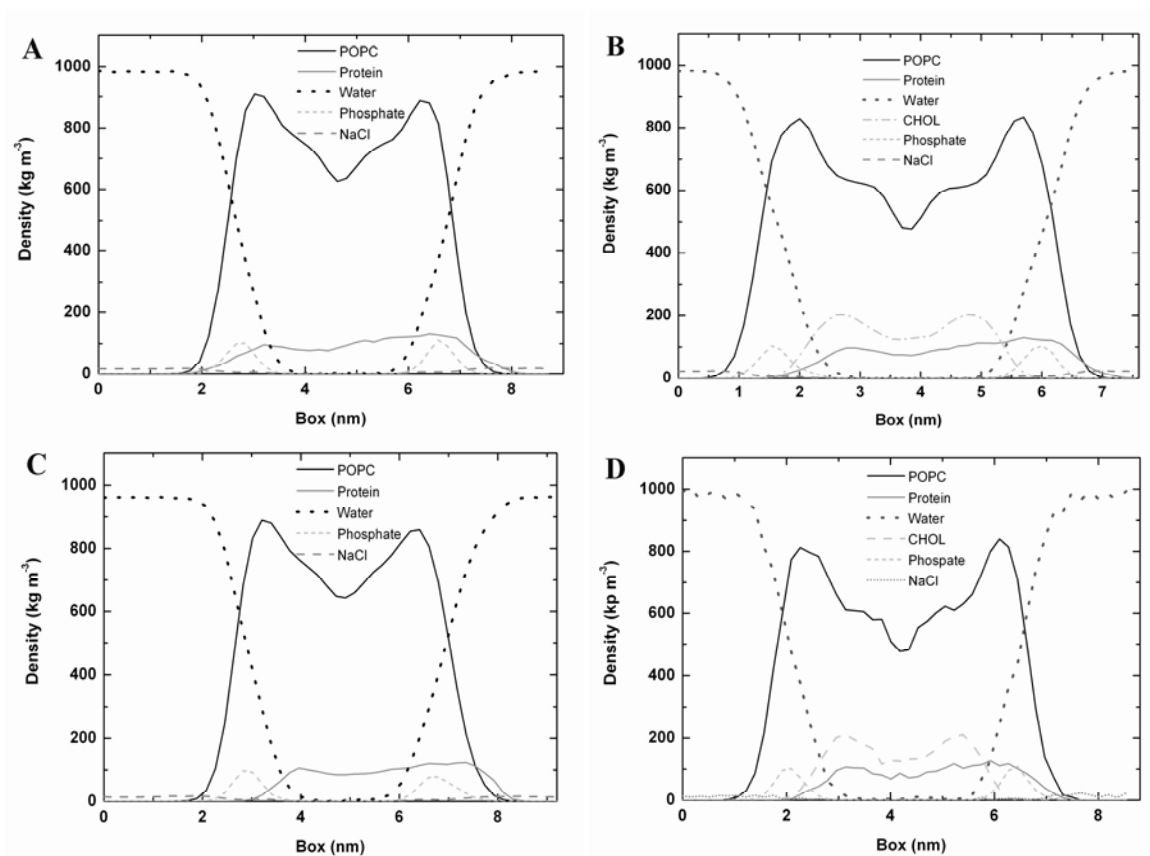


Fig. 9. Density profiles for the (a) closed channel in POPC system (b) closed channel in POPC/CHOL system (c) open channel in POPC system (d) open channel in POPC/CHOL system.

The density profiles of POPC and POPC/CHOL systems with the protein are plotted in Fig. 9 which shows that most of the protein resides within the hydrophobic region of the bilayer. Its density is asymmetric between the two leaflets. The salt ions Na^+ and Cl^- are mainly located in the water and some ions in the head group of POPC. The thickness of the bilayer can be

defined as the distance between the phosphorus atom density profile peaks of the two leaflets. Fig. 9 shows that the bilayer thickness is 3.8 nm for closed and open channels in pure POPC and 4.4 nm for closed and open channels in the POPC/CHOL system. It is also noticed that the addition of CHOL increases the thickness of the bilayer in agreement with earlier studies [111] in POPC whereas the channel protein has no such effect.

Conclusions

In this study, we examined the effects of different lipid compositions (POPC vs. POPC/CHOL) on open and closed Cav1.2 channel structure models.

The interactions between Cav1.2 open and closed conformations with pure POPC and POPC cholesterol mixtures are shown in Fig. 4. It can be seen that cholesterol is not preferentially interacting with the closed channel and only a slight interaction with the open channel can be observed.

To determine the dynamics of calcium ions when cholesterol is added to the lipid composition, we calculated the average distance of each calcium along the pore from the center of mass of selectivity filter travel during the simulation time. It appears that cholesterol decreased Ca^{2+} ion mobility in POPC/CHOL systems in both closed and open Cav1.2 channels. This indicates that cholesterol modulates the Ca^{2+} ion movement.

The lipid order parameters demonstrate the bilayer fluidity. The open channels in POPC and POPC/CHOL have order parameter values higher than the closed channels with both lipid compositions. Furthermore, POPC lipids around 1 nm in POPC/CHOL systems (closed and open conformation) are more ordered than the lipids in the POPC system. These results show that cholesterol has an ordering effect on the POPC lipid tail. Additionally, we investigated the

mobility of POPC calculating the MSD values of POPC, where the POPC lipids were classified into 2 groups, for lipids whose distance ≤ 1 nm and > 1 nm from the protein. Fig. 8 shows different lipid behavior for POPC systems vs. POPC/CHOL systems.

Cholesterol plays a crucial role in restricting the lipid around 1 nm of protein. Thus, our simulation demonstrates effects of cholesterol addition to POPC bilayers. It decreases the bilayer fluidity and increases the thickness of the bilayer.

3.10 Molecular Dynamics studies of the pore region of the newest model Cav1.2 based on Voltage-gated sodium (NavAb) channels as a template

The weak point of the Cav1.2 homology modeling is the lack of the conserved residues at the selectivity filter P region between potassium and calcium channel. On June 2011, a new voltage-gated sodium channel was published [112] which shares the same highly conserved motif with the calcium channel. Based on these studies, a new homology model of Cav1.2 was built. The newest homology model was set in the POPC and POPC/CHOL system to focus on the effect of the cholesterol of interaction influence with Cav1.2 channel (see manuscript 1). The results show in this manuscript is the preliminary data. The part of cholesterol access to the channel is in progress.

Manuscript 1

Molecular Dynamics studies of the pore region of the newest model Cav1.2 based on Voltage-gated sodium (NavAb) channels as a template

**Molecular Dynamics Simulations on the Function of the Transmembrane Cav1.2 Channel
in Dependence of the Content of Cholesterol in the Membrane**

**Chonticha Suwattanasophon[#], Roland Faller^{†*}, Peter Wolschann[#], Song Ke[‡], Anna Sary-
Weinzinger[‡]**

[#]Institute for Theoretical Chemistry, University of Vienna, Vienna, Austria

[†]Department of Chemical Engineering and Materials Science, University of California, Davis,
California, USA

[‡]Department of Pharmacology and Toxicology, University of Vienna, Vienna, Austria

* Corresponding author

Roland Faller

Department of Chemical Engineering and Materials Science

University of California Davis

One Shields Ave

Davis, CA 95616

E-mail: rfaller@ucdavis.edu

Keywords

Cav1.2, Cholesterol, Membrane composition.

Abstract

Increased cholesterol levels are associated with multiple pathological conditions. Here, Molecular Dynamics simulations are applied to explain the influence of membrane cholesterol levels on voltage-gated calcium channels. We used different lipid compositions to obtain information about the possible effects by which cholesterol influences Cav1.2 channels. Cholesterol is directly interacting with the protein in the open or the closed conformation. Cholesterol is preferentially interacting and penetrates to both channels conformation. Cholesterol increases lipid packing implying that it plays a crucial role in restricting lipid movement in the region around 1 nm of POPC. This leads to a direct modulation of Cav1.2 channel function.

Introduction

Cholesterol, a major lipid component of the plasma membrane in mammalian cells, is essential for normal cell function and growth. Normal cholesterol levels are in the range of 10 – 45 mol% with respect to other lipids. High cholesterol levels in humans, termed hypercholesterolemia, are associated with multiple pathological conditions [1], including cardiovascular disease such as stroke and coronary heart disease. Cholesterol blood levels are influenced by genetic factors and nutrition. Long term hypercholesterolemia can result in disorders such as diabetes mellitus and underactive thyroid. Diet induced hypercholesterolemia has been shown to alter the activity of several ion channels and pumps, including voltage-gated potassium and calcium channels. For example, Bowles et al, 2004 [2] demonstrated a direct link between increased membrane free cholesterol levels and voltage-gated calcium current decrease in coronary arterial smooth muscle cells.

Over the years members of all major ion channel families have been shown to be regulated by the level of membrane cholesterol [3]. These include different types of K⁺ channels [4-9], Ca²⁺ channels [2, 10-13], Na⁺ channels [14, 15], and Cl⁻ channels [16, 17]. Cholesterol effects include suppression of channel activity an effect that was seen in inwardly-rectifying K⁺ channels, voltage gated K⁺ channels as well as voltage gated Na⁺ and Ca²⁺ channels. Other channels such as epithelial amiloride-sensitive Na⁺ channels or TRP (transient receptor potential) channels are inhibited by cholesterol depletion.

The specific mechanisms by which cholesterol modulates ion channel activity are not well understood. The regulation of ion channels by cholesterol might occur either via direct interaction or via indirect mechanisms. Three different mechanisms of channel regulation have been suggested [18, 19]: specific interactions of cholesterol with the channel protein, changes of the physical properties of the membrane bilayer (i.e. fluidity) and importance of cholesterol for maintaining the scaffolds for protein-protein interactions (“lipid-rafts”).

Studies by Singh et al [20] suggest that elevated membrane cholesterol levels might directly inhibit KirBac1.1 currents. This hypothesis is supported by the fact that these channels are sensitive to the chiral nature of cholesterol. In contrast, volume-regulated anion channels (VRAC) have been shown to be insensitive to the chirality of cholesterol, suggesting an indirect effect, possibly via changes of physical membrane properties such as fluidity and lipid packing [16].

A growing number of studies on different ion channels indicate that the influence of cholesterol is highly heterogeneous [3, 21, 22]. With the recent successes in X-ray crystallization of a number of K⁺ and Na⁺-channels, a detailed structural analysis investigating the mechanism of cholesterol channel interaction becomes possible.

Even though, calcium channel crystal structures are not yet available, the recently solved X-ray structure of NavAb [23] provides a good template for structure modelling. In analogy to voltage-gated potassium and sodium channels, it is assumed that helices L4-5, S5 and S6, the P-helices and the loops connecting them, form a selective pore for ion conduction (Fig. 1). Numerous homology models of Cav channels based on K^+ channel templates have been successfully used to explain experimental data and suggest new experiments (Zhorov, Lipkind, Fozzard, Stary etc) [24-28]. However, to our knowledge this is the first study reporting on a Cav1.2 model based on the more closely related NavAb sodium channel structure. This template is especially advantageous for modelling the selectivity filter region and P-helices, since there is high sequence similarity in these regions and for both channel type side chains in the selectivity filter are assumed to participate in conductance.

In the present study, we focus on how cholesterol interacts with a closed Cav1.2 channels model, by applying Molecular Dynamics simulations. Our results provide strong evidence for a direct modulation of Cav1.2 channels by membrane cholesterol.

Methods

Simulation Setup

All simulations were performed with Gromacs software version 4.0.7 [29] using the 43a1 force-field [30]. The pore region of Cav1.2 channel was embedded in a 1-palmitoyl-2-oleoyl phosphatidylcholine (POPC) and POPC/CHOL lipid bilayer (Fig. 2). The structure model of Cav1.2 pore region channel was generated using Modeller 9v7 [31]. The crystal structures of the NavAb voltage-gated sodium channel (PDB: 3RVY) [23] served as templates.

The starting configuration of a 128-lipid POPC bilayer was obtained from the end of a 1.6 ns simulation performed by Kandt et al. (<http://www.moose.bio.ucalgary.ca>) and replicated four times to create a bilayer of 512 lipids. The POPC/CHOL lipid bilayer was generated by the starting configuration of 260-single POPC bilayer and 65-single CHOL to create a monolayer and replicated 2 times to create a 520 POPC and 130 CHOL bilayer. The Gromacs tools were used to embed and compressing the channels in a POPC and POPC/CHOL lipid bilayer. The systems were solvated with around 25,339 SPC waters and included 0.1 mol/liter concentration of sodium chloride (NaCl). 9 Ca^{2+} ions were placed randomly along the pore.

The three systems of the Cav1.2 pore region in POPC and POPC/CHOL environment were performed by vary the starting position of Ca^{2+} along the pore. As same as, three systems of the Cav1.2 pore region in POPC/CHOL environment were generated by add the starting position of Ca^{2+} along the pore and CHOL randomly. The final POPC system contains 502 POPC and 147 NaCl molecules. For POPC/CHOL system, there were 501 POPC and 130 CHOL in the first system, 490 POPC and 130 CHOL in the second system and 498 POPC and 129 CHOL in the third system. Cl^- ions were added randomly within the solvent to neutralize the systems. Thus, there were 9 Cl^- ions in the channels.

Snapshots of the trajectory were written out every 20 ps. The system was energy minimized with the steepest descent algorithm, followed by positional restrained MD for 2 ns. Subsequently, 50 ns of unrestrained MD simulation were carried out using the NPT ensemble. The Nose-Hoover thermostat [32] with a coupling constant of 0.1 ps to a temperature bath of 300 K was used. Pressure was held constant using a semi-isotropic Parrinello-Rahman barostat algorithm [33] with a coupling constant of 1 ps. Electrostatic interactions were calculated explicitly at a distance smaller than 1 nm, and long-range electrostatic interactions were

calculated at every step by particle-mesh Ewald summation [34]. Lennard-Jones interactions were calculated with a cutoff of 1 nm. Bond lengths were constrained using the LINCS algorithm [35]. Subsequent analyses of the MD simulation data were performed using tools available within GROMACS.

Umbrella Sampling Simulations.

Starting structure of the umbrella simulation of cholesterol pulling through the Cav1.2 pore region channel was taken from the snapshots of equilibration simulation for Cav1.2 in POPC/CHOL system. Potential of mean force (PMF) was performed by one dimensional umbrella sampling. The 32 positions were selected in range 3.5 – 5.0 nm. Adjacent umbrella windows were separated by 0.25 nm. Each window was simulated for 5 ns. The reaction coordinate for cholesterol permeation is the y-axis along the distance of the center of mass of pulling cholesterol and reference cholesterol molecule at a pull rate of 0.2 Å/ps. During simulation, the probing cholesterol was restrained harmonically with a 1000 kJ/mol/nm² force constant in the y-axis.

Results

Cholesterol is known to influence different type of ion channel. The underlying mechanisms of cholesterol regulation of Cav1.2 channels are, however, poorly understood. To investigate possible effects by which cholesterol influences Cav1.2 channels we use MD simulations with different lipid compositions.

Stability of system

Fig 3

The stability of each simulation system is analysed by the root-mean-square displacement (RMSD) of the protein backbone atoms. The backbone RMSD of channels in POPC and POPC/CHOL systems over 50 ns is shown in Fig. 3A and 3B. For the first 30 ns, the RMSD value steadily increases and then reaches a plateau. After 30 ns, the RMSD of each simulation of the Cav1.2 channel in the POPC system stabilizes at approximately 0.350, 0.30 and 0.325 Å. The RMSD of each simulation of the Cav1.2 channels in POPC/CHOL bilayer are around 0.3 Å.

To further analyse the stability of the system we examined the lateral area of the whole system as a function of time (Fig. 4A and 4B). In the pure POPC systems of Cav1.2 channels, the lateral area value decreased to around 170 nm² and stabilized within 30 ns. Upon addition of cholesterol to the POPC bilayer, the area remains stable during the whole simulation at around 175 nm². RMSD and the lateral area values confirm that 50 ns simulation is sufficient for stabilizing the system.

Fig 4

Bilayer Fluidity

Fig 5

The order parameter (S_{cd}) as a function of carbon atom number along the hydrocarbon tails is shown in Fig. 5. The order parameter values for POPC lipids within 1 nm around the channels are calculated. It is interesting to note that the POPC/CHOL lipid tail in the channel shows higher S_{cd} values than the channel in POPC indicating that the protein has an influence on lipid conformation in its neighborhood. This has been seen in other simulations of lipid protein interaction as well [36]. Fig. 5 gives a comparison of the order parameter of each system. It is obvious that the lipids in the POPC/CHOL system are more ordered than the lipids of the pure POPC system. Hence, addition of cholesterol increases lipid packing. This has been found experimentally [37] as well as in simulation [38].

Fig 6,7

The mobility of the lipids as a function of distance from the protein, i.e. lipids with ≤ 1 nm (inner shell) and > 1 nm (outer shell) of the protein are displayed in Fig. 6 and 7. The MSD values reveal details about the movement of POPC. Significant differences are observed between the inner and outer shell in the POPC systems but not in the POPC/CHOL systems. There the MSD values indicate that POPC movement is homogeneous in the whole bilayer. Fig. 6, A to C shows that lipids in pure POPC systems which are more than 1 nm away from the protein are faster than lipids within 1 nm. This clearly indicates a binding or at least dynamic coupling

between the protein and the surrounding lipids. On the other hand, for the POPC/CHOL system such a dynamical difference is not found. This implies that cholesterol plays a crucial role in restricting the lipid movement around 1 nm of POPC.

Fig 8

The density profiles of POPC and POPC/CHOL systems with the protein are plotted in Fig. 8 which shows that most of the protein resides within the hydrophobic region of the bilayer. Its density is asymmetric between the two leaflets. The salt ions Na^+ and Cl^- are mainly located in the water and some ions in the head group of POPC. The thickness of the bilayer can be defined as the distance between the phosphorus atom density profile peaks of the two leaflets. Fig. 8A to C shows that the bilayer thickness is 4.0 nm for channels in pure POPC and 4.2 nm for channels in the POPC/CHOL system. It is also noticed that the addition of CHOL increases the thickness of the bilayer in agreement with earlier studies [39] in POPC whereas the channel protein has no such effect.

Dynamics of cholesterol

Fig 9

To determine the interaction between protein and POPC or cholesterol (CHOL) radial distribution functions (RDF) were calculated. The radial distribution function of POPC around the center of mass of protein of all 3 simulations reveals three peaks (Fig. 9A). The first peak occurs at around 3.0 nm. The following peaks are approximately at 3.5 and 4.0 nm. This

indicates increased probability to find POPC molecules in the direct neighborhood of the entire region around the protein, which is around 3.0 nm (first solvation shell), 3.5 nm and 4.0 nm. Fig. 9B to 9C shows the RDF between the center of mass of the protein with POPC and CHOL of each run in POPC/CHOL system. All 3 simulations of channel in POPC/CHOL demonstrate that the first peak of POPC is around 3.0 nm while there are several peaks of CHOL occur between 0.4 to 3.0 nm. These imply that cholesterol is preferentially interacting and penetrate to the channel as shown in Fig 10b.

Direction of cholesterol access to Cav1.2 pore channel.

From our 3 runs of free MD, we found from 2 of 3 simulations that the head of cholesterol enter predominantly between these S6 of domain I and IV helices. Then, our PMFs are focused on this region only.

Fig10, 11

The potentials of mean force (PMFs) are used to characterize the energies of the pulling cholesterol. The pulling cholesterol was pulled in between domain I and IV to the cavity of Cav1.2 (Fig 10). The PMFs for pulling cholesterol across the y-axis is displayed in Fig 11. The PMFs value between 3.5 – 4.0 nm which is the interface of S6 domain I and IV region decrease. After 4.0 nm which is the cavity of Cav1.2 region, the barrier values are steadily increases. It is implied that cholesterol prefer to locate at the interface region of S6 domain I and IV, due to the hydrophobic residue (Phe, Ile, Val, Leu) at the interface interact with cholesterol. The most

favorable position of cholesterol is at 4 nm which is the lowest PMFs value. At the cavity of Cav1.2 which is hydrophilic region, cholesterol is less prefers to locate in this area.

Conclusions

In this study, we examined the effects of different lipid compositions (POPC vs. POPC/CHOL) on Cav1.2 channel structure models.

The lipid order parameters demonstrate the bilayer fluidity. The channels in POPC/CHOL have order parameter values higher than channels in pure POPC compositions. Furthermore, POPC lipids around 1 nm in POPC/CHOL systems are more ordered than the lipids in the POPC system. These results show that cholesterol has an ordering effect on the POPC lipid tail. Additionally, we investigated the mobility of POPC calculating the MSD values of POPC, where the POPC lipids were classified into 2 groups, for lipids whose distance ≤ 1 nm and > 1 nm from the protein. Fig. 6 and 7 shows different lipid behavior for POPC systems vs. POPC/CHOL systems.

Cholesterol plays a crucial role in restricting the lipid around 1 nm of protein. Thus, our simulation demonstrates effects of cholesterol addition to POPC bilayers. It decreases the bilayer fluidity and increases the thickness of the bilayer. The interactions between Cav1.2 with pure POPC and POPC cholesterol mixtures are shown in Fig. 8.

A remarkable feature, only seen in a handful of ion channels (including TWIK, TRAAK and NavAb) are lateral pore openings below the selectivity filter, leading from the lumen of the pore to the membrane. It can be seen that cholesterol is directly interacting and penetrating to the side open of channel (Fig. 9). The predomination enter of head of cholesterol access to Cav1.2 is the region between domain I and IV (Fig 10).

Acknowledgments

We thank Juan Vanegas for help with the setup of some simulations. Financial support by the Molecular Drug Target program and Kurzfristige Auslandsstipendien Grant from the University of Vienna is gratefully acknowledged. CS thanks the Department of Chemical Engineering & Materials Science of UC Davis for the hospitality during her stay.

References

1. Kellner-Weibel, G., Y.J. Geng, and G.H. Rothblat, *Cytotoxic cholesterol is generated by the hydrolysis of cytoplasmic cholesteryl ester and transported to the plasma membrane*. *Atherosclerosis*, 1999. **146**(2): p. 309-19.
2. Bowles, D.K., et al., *Hypercholesterolemia inhibits L-type calcium current in coronary macro-, not microcirculation*. *J Appl Physiol*, 2004. **96**(6): p. 2240-8.
3. Levitan, I., et al., *Cholesterol and ion channels*. *Subcell Biochem*, 2010. **51**: p. 509-49.
4. Rosenhouse-Dantsker, A., D.E. Logothetis, and I. Levitan, *Cholesterol sensitivity of KIR2.1 is controlled by a belt of residues around the cytosolic pore*. *Biophys J*, 2011. **100**(2): p. 381-9.
5. Romanenko, V.G., et al., *Cholesterol sensitivity and lipid raft targeting of Kir2.1 channels*. *Biophys J*, 2004. **87**(6): p. 3850-61.
6. Bolotina, V., et al., *Variations of membrane cholesterol alter the kinetics of Ca²⁺-dependent K⁺ channels and membrane fluidity in vascular smooth muscle cells*. *Pflugers Arch*, 1989. **415**(3): p. 262-8.
7. Heaps, C.L., D.L. Tharp, and D.K. Bowles, *Hypercholesterolemia abolishes voltage-dependent K⁺ channel contribution to adenosine-mediated relaxation in porcine coronary arterioles*. *Am J Physiol Heart Circ Physiol*, 2005. **288**(2): p. H568-76.
8. Martens, J.R., et al., *Differential targeting of Shaker-like potassium channels to lipid rafts*. *J Biol Chem*, 2000. **275**(11): p. 7443-6.
9. Martens, J.R., et al., *Isoform-specific localization of voltage-gated K⁺ channels to distinct lipid raft populations. Targeting of Kv1.5 to caveolae*. *J Biol Chem*, 2001. **276**(11): p. 8409-14.
10. Ambudkar, I.S., *Cellular domains that contribute to Ca²⁺ entry events*. *Sci STKE*, 2004. **2004**(243): p. pe32.
11. Lockwich, T.P., et al., *Assembly of Trp1 in a signaling complex associated with caveolin-scaffolding lipid raft domains*. *J Biol Chem*, 2000. **275**(16): p. 11934-42.
12. Lundbaek, J.A., et al., *Membrane stiffness and channel function*. *Biochemistry*, 1996. **35**(12): p. 3825-30.
13. Toselli, M., et al., *Caveolin-1 expression and membrane cholesterol content modulate N-type calcium channel activity in NG108-15 cells*. *Biophys J*, 2005. **89**(4): p. 2443-57.
14. Lundbaek, J.A., et al., *Regulation of sodium channel function by bilayer elasticity: the importance of hydrophobic coupling. Effects of Micelle-forming amphiphiles and cholesterol*. *J Gen Physiol*, 2004. **123**(5): p. 599-621.
15. Wu, C.C., et al., *The effect of hypercholesterolemia on the sodium inward currents in cardiac myocyte*. *J Mol Cell Cardiol*, 1995. **27**(6): p. 1263-9.
16. Levitan, I., et al., *Membrane cholesterol content modulates activation of volume-regulated anion current in bovine endothelial cells*. *J Gen Physiol*, 2000. **115**(4): p. 405-16.
17. Romanenko, V.G., G.H. Rothblat, and I. Levitan, *Sensitivity of volume-regulated anion current to cholesterol structural analogues*. *J Gen Physiol*, 2004. **123**(1): p. 77-87.
18. Barrantes, F.J., *Structural basis for lipid modulation of nicotinic acetylcholine receptor function*. *Brain Res Brain Res Rev*, 2004. **47**(1-3): p. 71-95.
19. Lundbaek, J.A. and O.S. Andersen, *Spring constants for channel-induced lipid bilayer deformations. Estimates using gramicidin channels*. *Biophys J*, 1999. **76**(2): p. 889-95.

20. Singh, D.K., et al., *Direct regulation of prokaryotic Kir channel by cholesterol*. J Biol Chem, 2009. **284**(44): p. 30727-36.
21. Maguy, A., T.E. Hebert, and S. Nattel, *Involvement of lipid rafts and caveolae in cardiac ion channel function*. Cardiovasc Res, 2006. **69**(4): p. 798-807.
22. Martens, J.R., K. O'Connell, and M. Tamkun, *Targeting of ion channels to membrane microdomains: localization of KV channels to lipid rafts*. Trends Pharmacol Sci, 2004. **25**(1): p. 16-21.
23. Payandeh, J., et al., *The crystal structure of a voltage-gated sodium channel*. Nature, 2011. **475**(7356): p. 353-8.
24. Cheng, R.C., D.B. Tikhonov, and B.S. Zhorov, *Structural modeling of calcium binding in the selectivity filter of the L-type calcium channel*. Eur Biophys J, 2010. **39**(5): p. 839-53.
25. Cheng, M.H., Y. Xu, and P. Tang, *Anionic lipid and cholesterol interactions with alpha4beta2 nAChR: insights from MD simulations*. J Phys Chem B, 2009. **113**(19): p. 6964-70.
26. Stary, A., et al., *Molecular dynamics and mutational analysis of a channelopathy mutation in the IIS6 helix of Ca V 1.2*. Channels (Austin), 2008. **2**(3): p. 216-23.
27. Lipkind, G.M. and H.A. Fozzard, *Molecular modeling of interactions of dihydropyridines and phenylalkylamines with the inner pore of the L-type Ca²⁺ channel*. Mol Pharmacol, 2003. **63**(3): p. 499-511.
28. Huber, I., et al., *Conserved Ca²⁺-antagonist-binding properties and putative folding structure of a recombinant high-affinity dihydropyridine-binding domain*. Biochem J, 2000. **347 Pt 3**: p. 829-36.
29. Hess, B., et al., *GROMACS 4: Algorithms for Highly Efficient, Load-Balanced, and Scalable Molecular Simulation*. Journal of Chemical Theory and Computation, 2008. **4**(3): p. 435-447.
30. Chiu, S.W., et al., *An improved united atom force field for simulation of mixed lipid bilayers*. J Phys Chem B, 2009. **113**(9): p. 2748-63.
31. Sali, A. and T.L. Blundell, *Comparative protein modelling by satisfaction of spatial restraints*. J Mol Biol, 1993. **234**(3): p. 779-815.
32. Nose, S., *A unified formulation of the constant temperature molecular dynamics methods*. The Journal of Chemical Physics, 1984. **81**(1): p. 511-519.
33. Parrinello, M. and A. Rahman, *Polymorphic transitions in single crystals: A new molecular dynamics method*. Journal of Applied Physics, 1981. **52**(12): p. 7182-7190.
34. Essmann, U., et al., *A smooth particle mesh Ewald method*. The Journal of Chemical Physics, 1995. **103**(19): p. 8577-8593.
35. Hess, B., et al., *LINCS: A linear constraint solver for molecular simulations*. Journal of Computational Chemistry, 1997. **18**(12): p. 1463-1472.
36. Dickey, A. and R. Faller, *Examining the contributions of lipid shape and headgroup charge on bilayer behavior*. Biophysical journal, 2008. **95**(6): p. 2636-46.
37. Brown, D.A. and E. London, *Functions of lipid rafts in biological membranes*. Annual review of cell and developmental biology, 1998. **14**: p. 111-36.
38. de Meyer, F. and B. Smit, *Effect of cholesterol on the structure of a phospholipid bilayer*. Proceedings of the National Academy of Sciences of the United States of America, 2009. **106**(10): p. 3654-8.
39. Pike, L.J., *The challenge of lipid rafts*. Journal of lipid research, 2009. **50 Suppl**: p. S323-8.

Figure legends

Fig. 1. Structure details of the Ca_v1.2 pore region, which is composed of linker L45, helices S5 and S6 from four domains. The helices from domains I and III are shown in gray. The helices of domains II and IV are colored: orange (L45), red (S5), green (P) and blue (S6).

Fig. 2. A snapshot of the channel in the POPC/CHOL bilayer. The helices from domain I to III are represented as orange, white and violet surface. POPC and CHOL are shown in blue and yellow. The oxygen atoms and hydrogen atoms of the water molecules are shown in white and red, respectively. Calcium and NaCl ions are shown as red and green spheres.

Fig. 3. (a) Average RMSD values of the backbone of channel in POPC system (b) Average RMSD values of the backbone of channel in POPC/CHOL systems.

Fig. 4. (a) Lateral area of channels in POPC and (b) POPC/CHOL systems.

Fig. 5. The order parameter profile of hydrocarbon tails for the POPC and POPC/CHOL system.

Fig. 6. MSD of POPC surrounding the protein \leq and $>$ than 1 nm in POPC (a) 1st run (b) 2nd run (c) 3rd run.

Fig. 7. MSD of POPC surrounding the protein \leq and $>$ than 1 nm in POPC/CHOL (a) 1st run (b) 2nd run (c) 3rd run.

Fig. 8. Density profiles for the (a) 1st run in POPC (b) 2nd run in POPC (c) 3rd run in POPC (d) 1st run in POPC/CHOL (e) 2nd run in POPC/CHOL (f) 3rd run in POPC.

Fig. 9. Radial distribution functions between (a) 3 different run of center of mass of protein atoms and POPC in POPC system. (b) center of mass of protein atoms with POPC and CHOL of 1st run in POPC/CHOL (c) center of mass of protein atoms with POPC and CHOL of 2nd run in POPC/CHOL (d) b) center of mass of protein atoms with POPC and CHOL of 3rd run in POPC/CHOL.

Fig. 10. Direction of cholesterol access to Cav1.2. Domain I and IV of Cav1.2 are represented as orange and pink ribbon. Domain II and II are shown in grey. (a) top view show cholesterol before access to the Cav1.2 (b) top view show cholesterol locate at the interface of domain I and IV of Cav1.2 . (c) side view show cholesterol before access to the Cav1.2 (d) side view show cholesterol when access into the interface of domain I and IV of Cav1.2.

Fig. 11. A. the PMFs of pulling cholesterol permeation across the Cav1.2 pore region B. a snapshot of cholesterol which penetrates to the channel. The Cav1.2 pore region is represented as grey ribbon. The pulling cholesterol is shown in green. The oxygen atoms and hydrogen atoms of the water molecules are shown in white and red, respectively. The POPC and cholesterol in POPC are shown as blue and yellow, respectively.

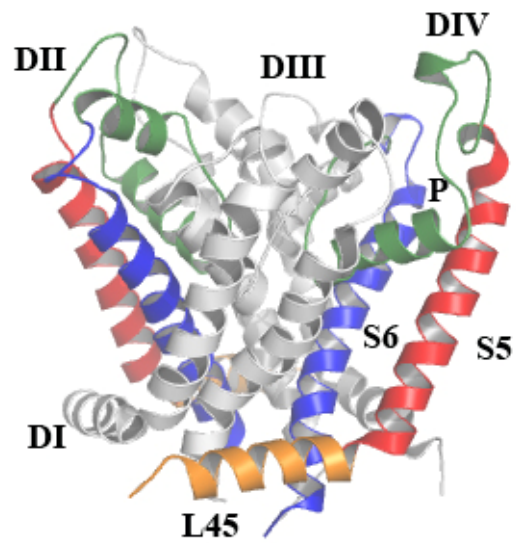


Fig. 1.

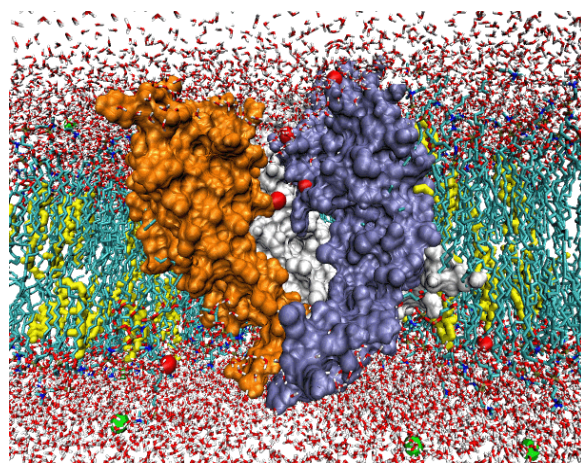


Fig. 2.

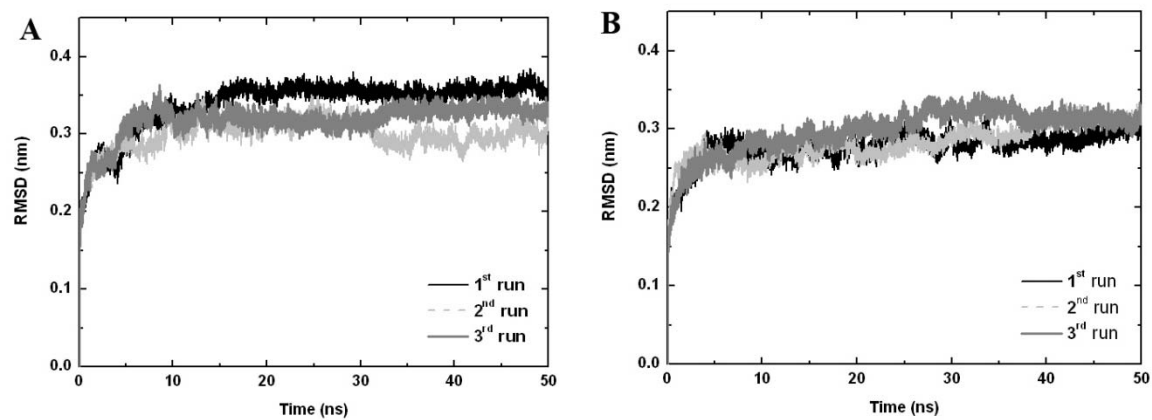


Fig. 3.

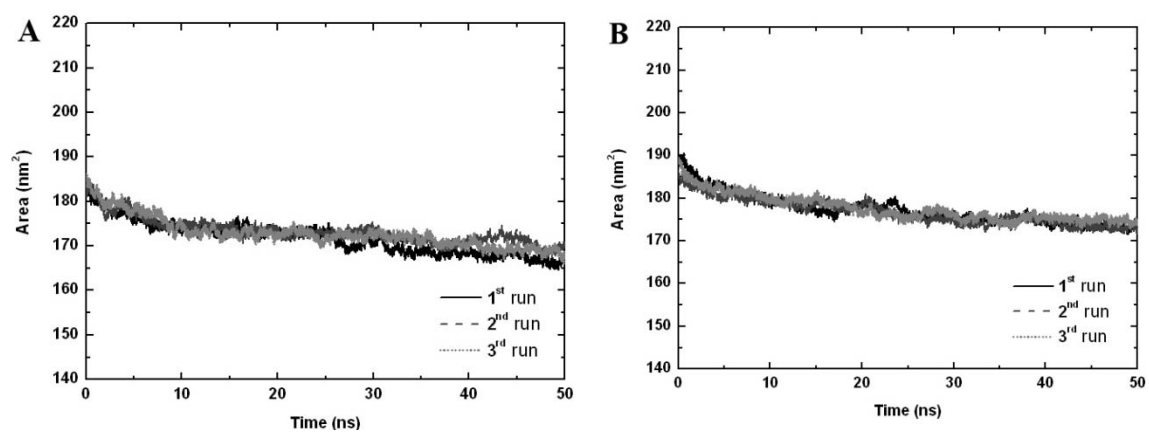


Fig. 4.

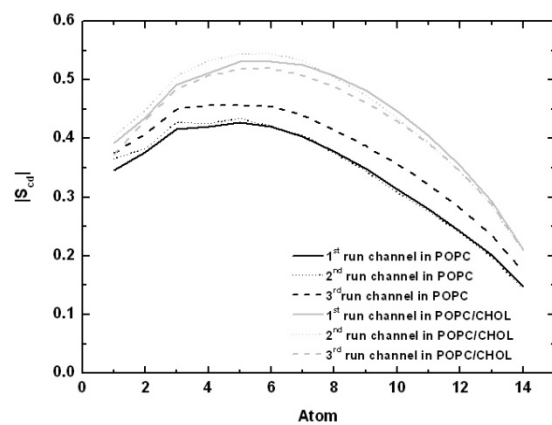


Fig. 5.

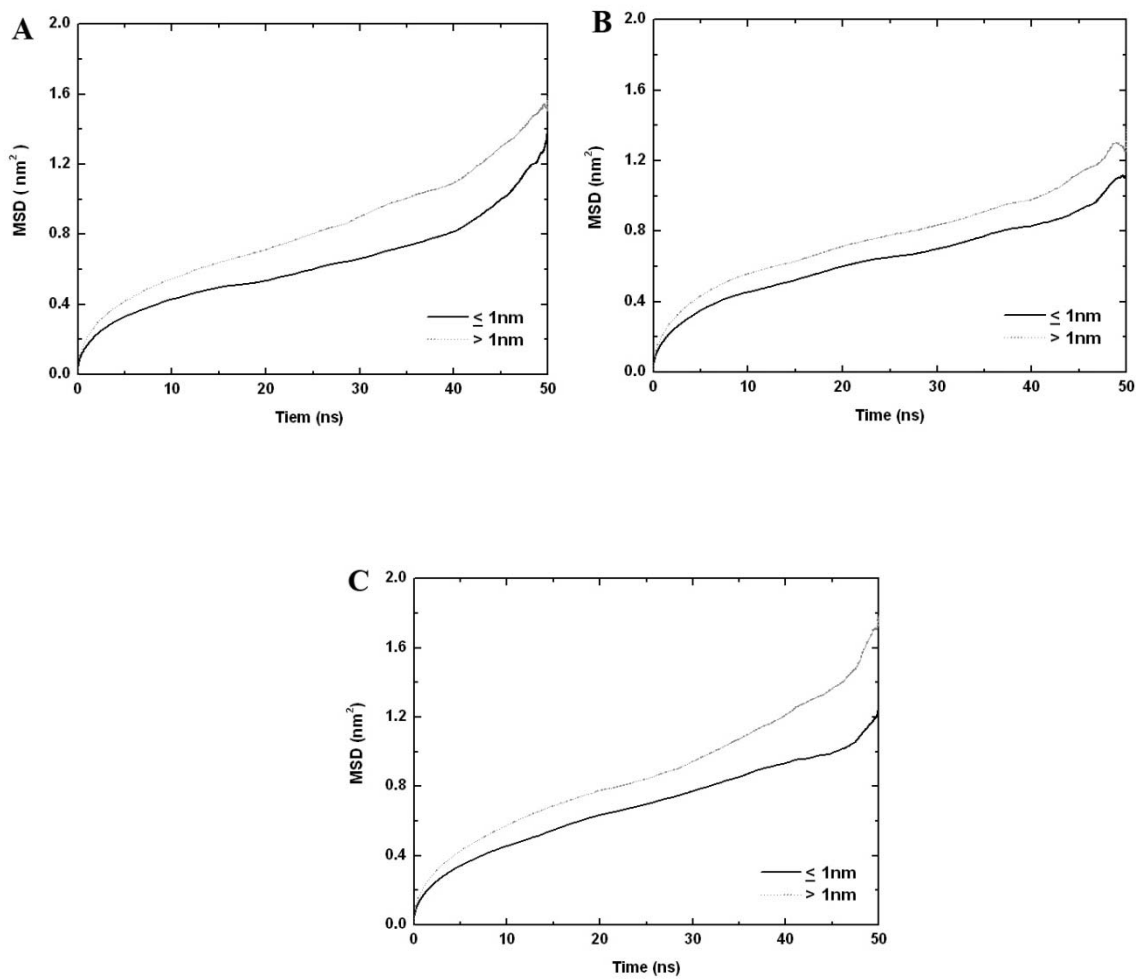


Fig. 6.

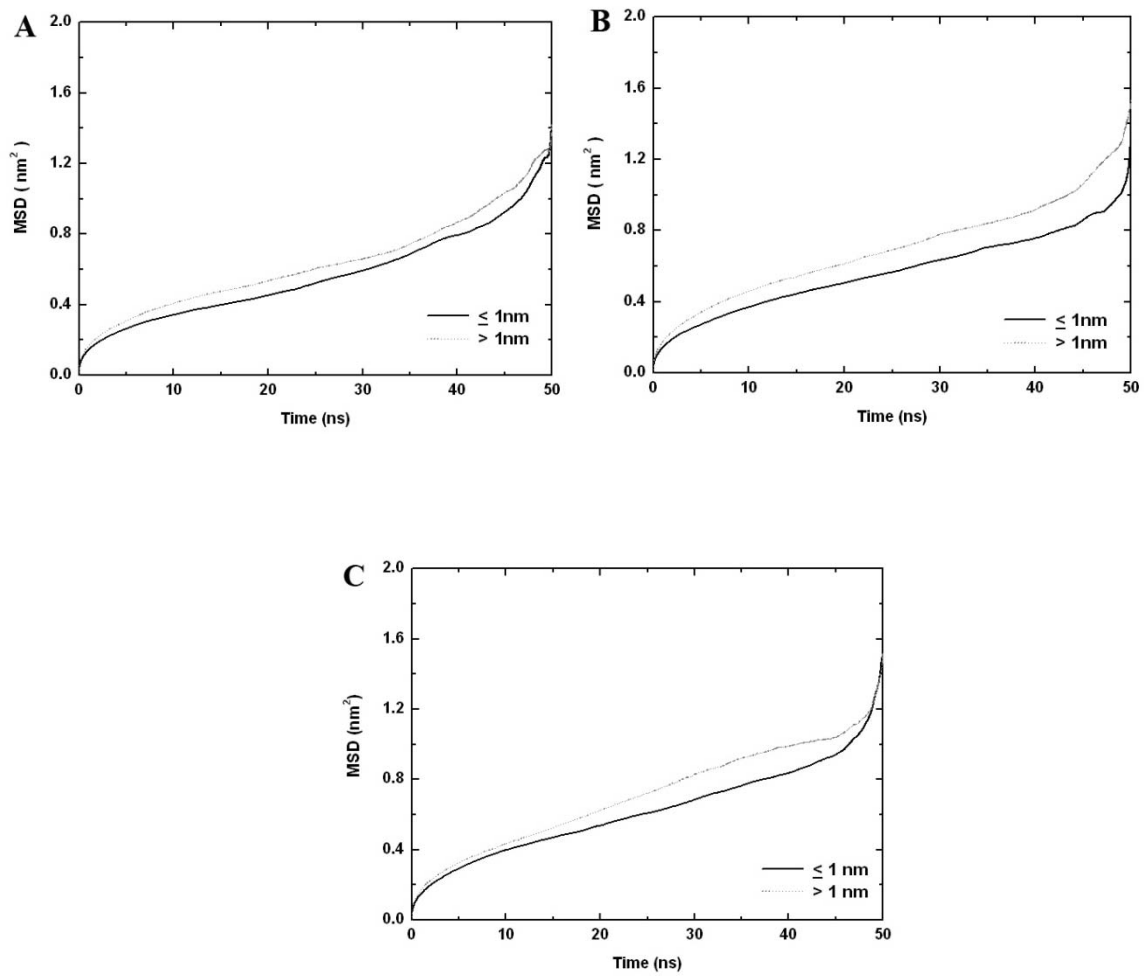


Fig. 7.

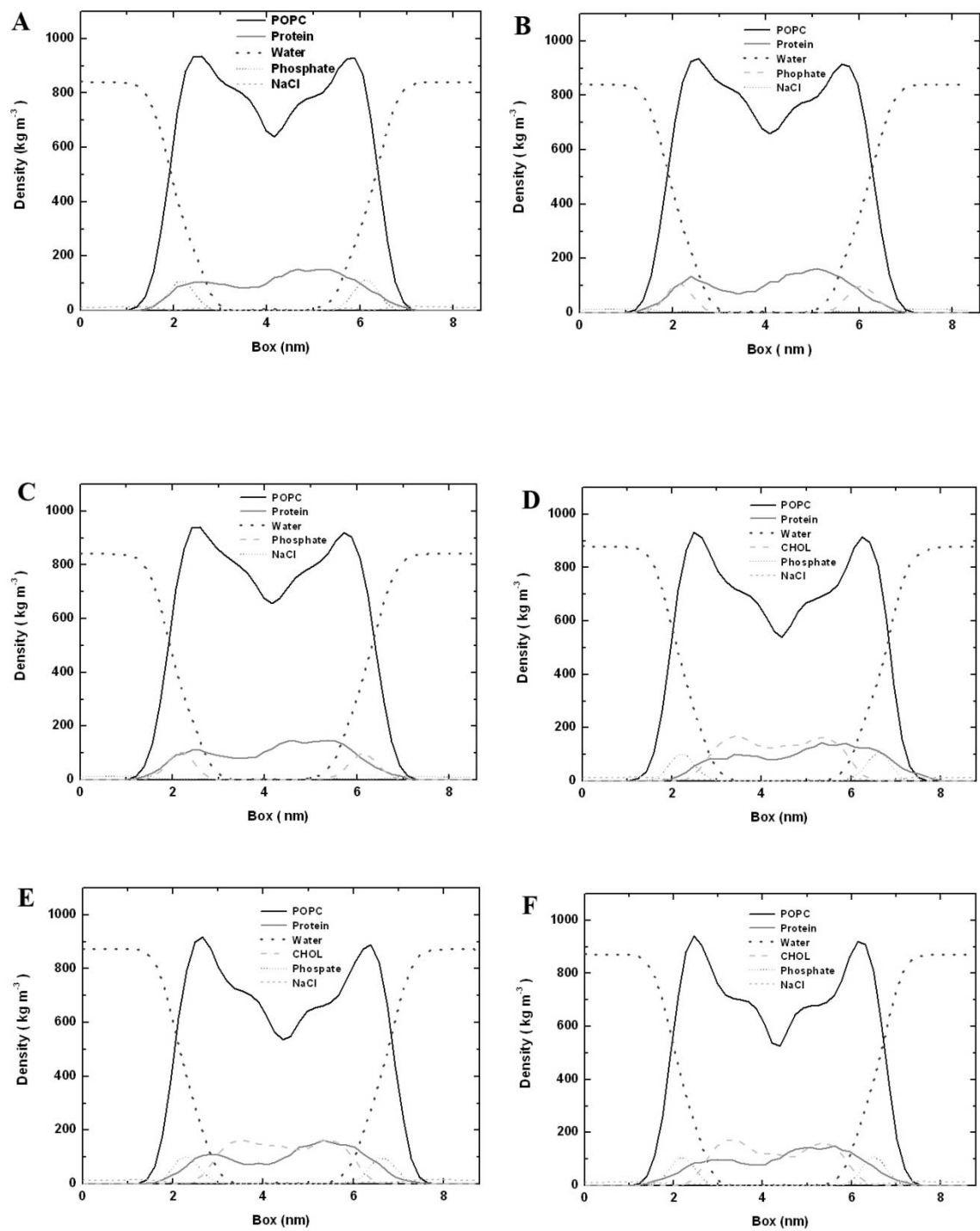


Fig. 8

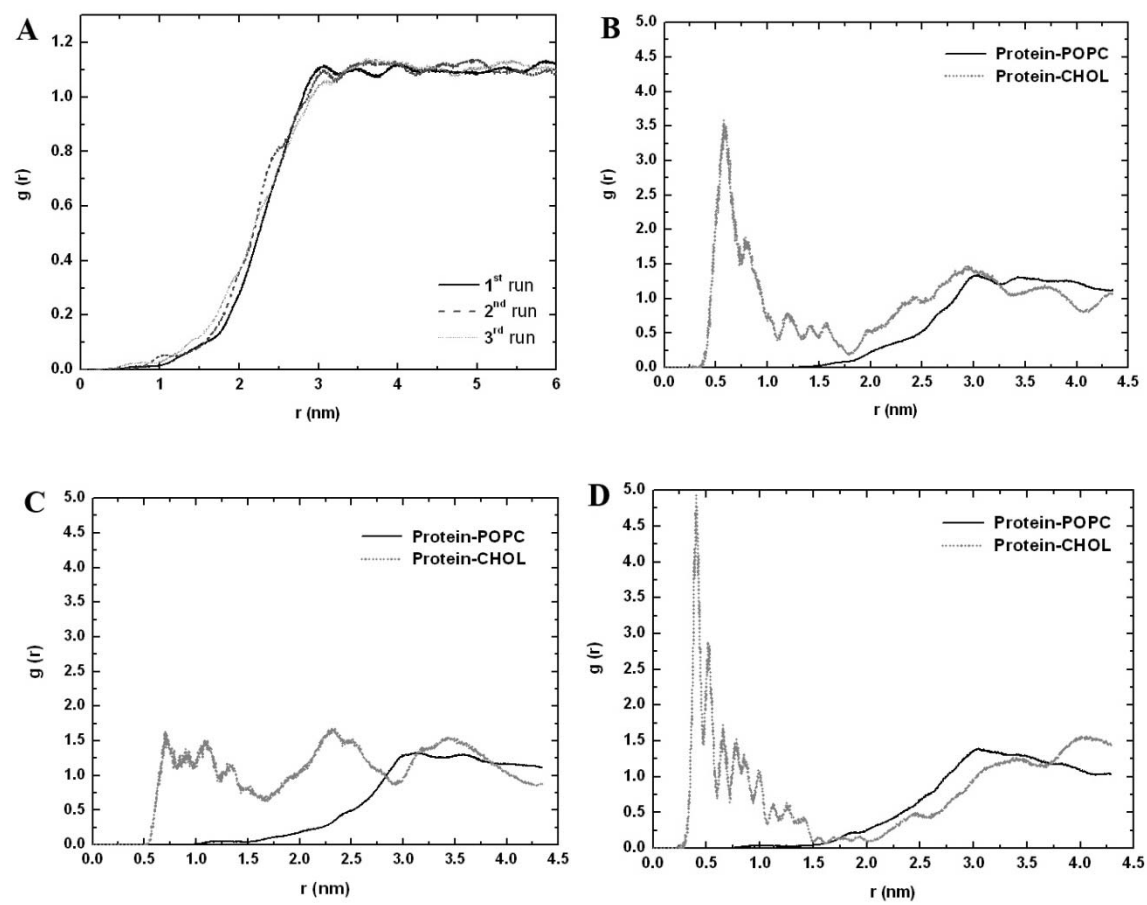


Fig. 9

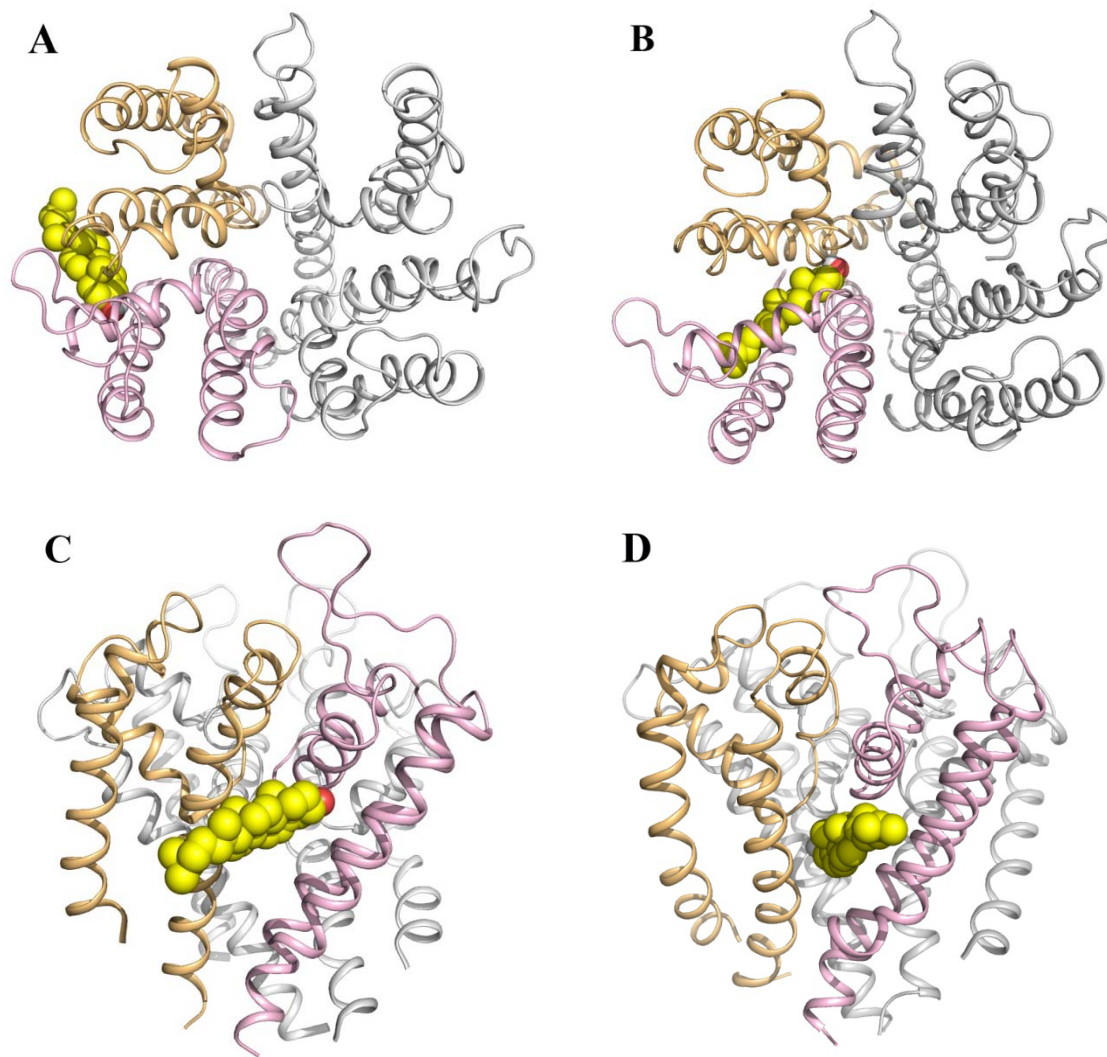


Fig. 10

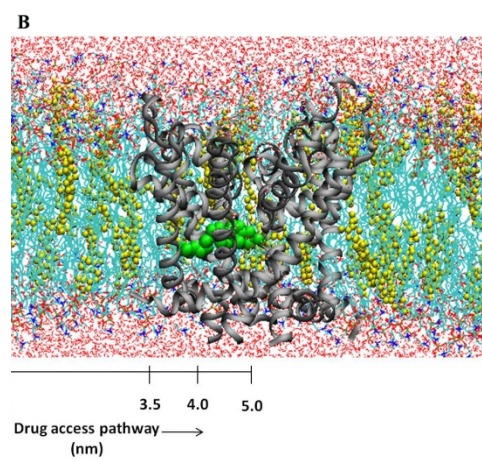
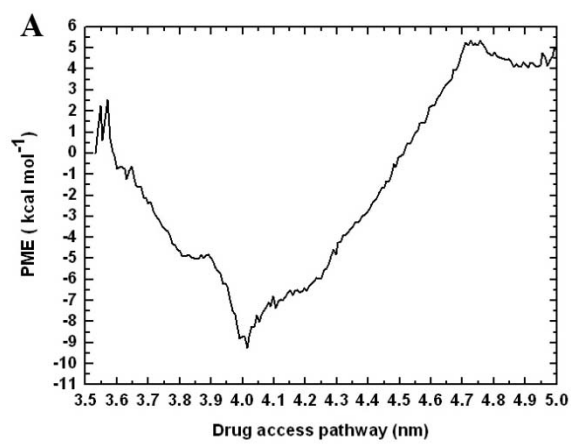


Fig. 11

3.11 Comparison between the closed conformation models of Ca_v1.2 based on Voltage-gated potassium (KcsA) and Voltage-gated sodium (NavAb) channel

In our work, two closed conformations of Ca_v1.2 were built and used to investigate the structure and dynamics. The first model was built based on the voltage-gated potassium (KcsA) and the second model build based on the new Voltage-gated sodium (NavAb) channel structure. The global architecture of these two models is almost similar as seen from the top (Fig 3.25 a) and side (Fig 3.25 b) view, respectively. The root mean square displacement (RMSD) of the backbone atoms of these two models is 1.9 Å which is remarkable similar.

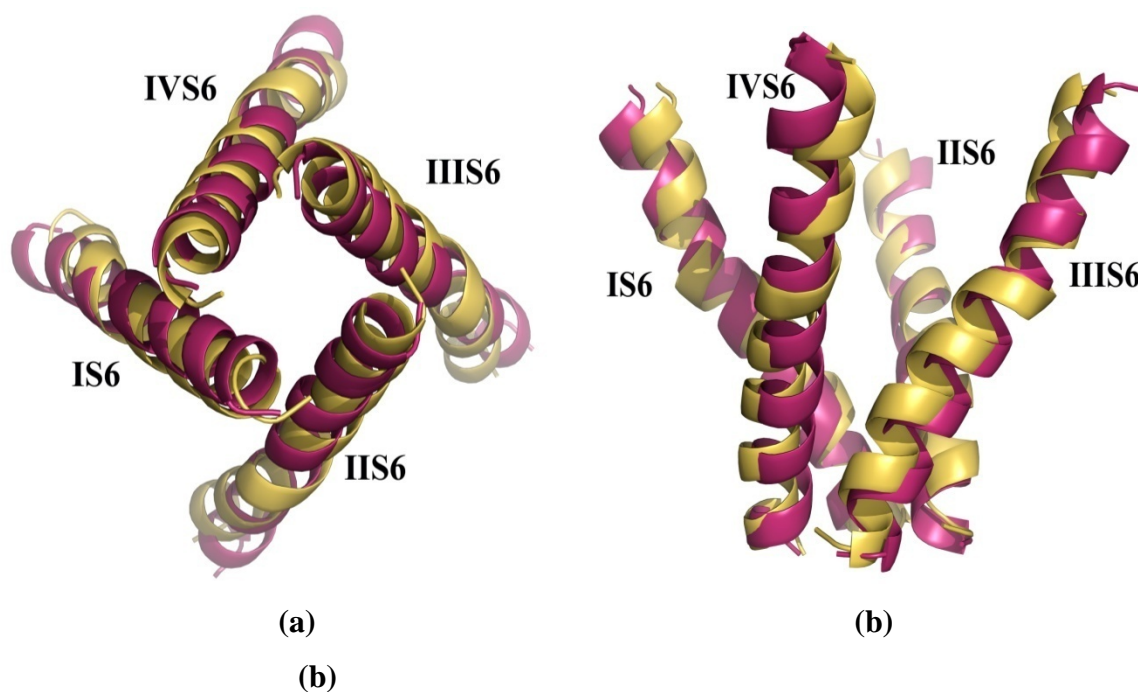


Fig 3.25. The superposition of the Ca_v1.2 based on Voltage-gated potassium (KcsA) and Voltage-gated sodium (NavAb) are colored in yellow and pink, respectively. (a) Top view detail of pore domain (b) Side view detail of pore domain.

The main difference of these two models is at the P-linker. As shown in Fig 3.26 a, the tilt of these two models at selectivity filter is different. Fig 3.26 b show that P-helix in the Ca_v1.2 model based on Voltage-gated potassium (KcsA) are tilt closed to binding residue Y1490 which prevents optimal interactions.

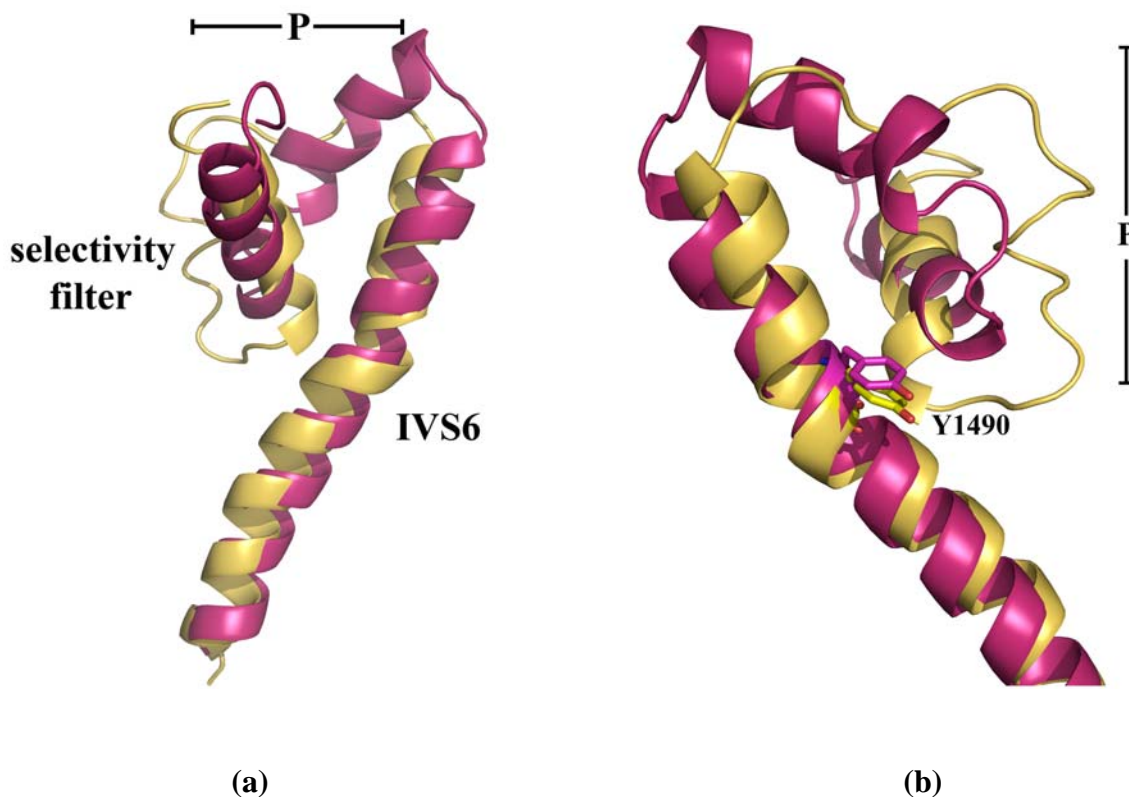


Fig 3.26. The superimposition of the Ca_v1.2 pore forming subunits based on Voltage-gated potassium (KcsA) and Voltage-gated sodium (NavAb) are colored in yellow and pink, respectively: shows IVP and IVS6. (b) Details of P-helix and binding residue Y1490.

Fig 3.27 demonstrate the selectivity filter of both models in more detail showing hydrogen bonds between selected residues. As can be seen in Fig. 3.27a and b the selectivity filter region, which in the old model (a) was not based on any template is significantly different compared to the new model. This is not unexpected, since ab initio homology modeling is still rather challenging and the accuracies can vary significantly. The most remarkable difference is in the positioning of the highly conserved tryptophan residues, which was assumed to be pore facing in the old model. A direct contribution of this residue to ion selectivity has also been wrongly proposed by the Zhorov group [113].

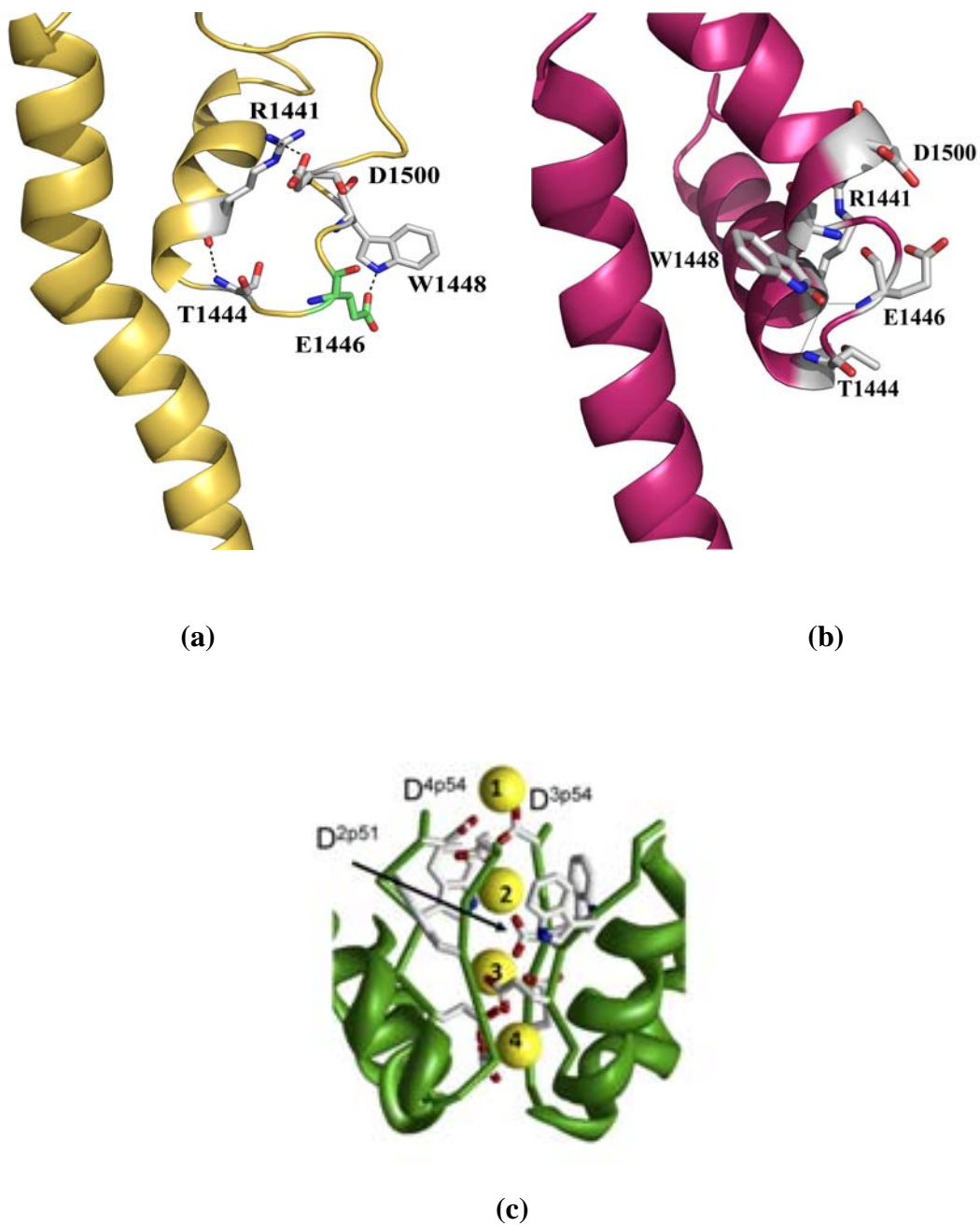


Fig 3.27. The selectivity filter of (a) Ca_v1.2 model based on Voltage-gated potassium (KcsA) (b) Ca_v1.2 model based on Voltage-gated sodium (NavAb). The dashed-lines indicate the hydrogen bonding (c) The prediction pattern of calcium atom binding in the Ca_v1.2 proposed by the Zhorov Group

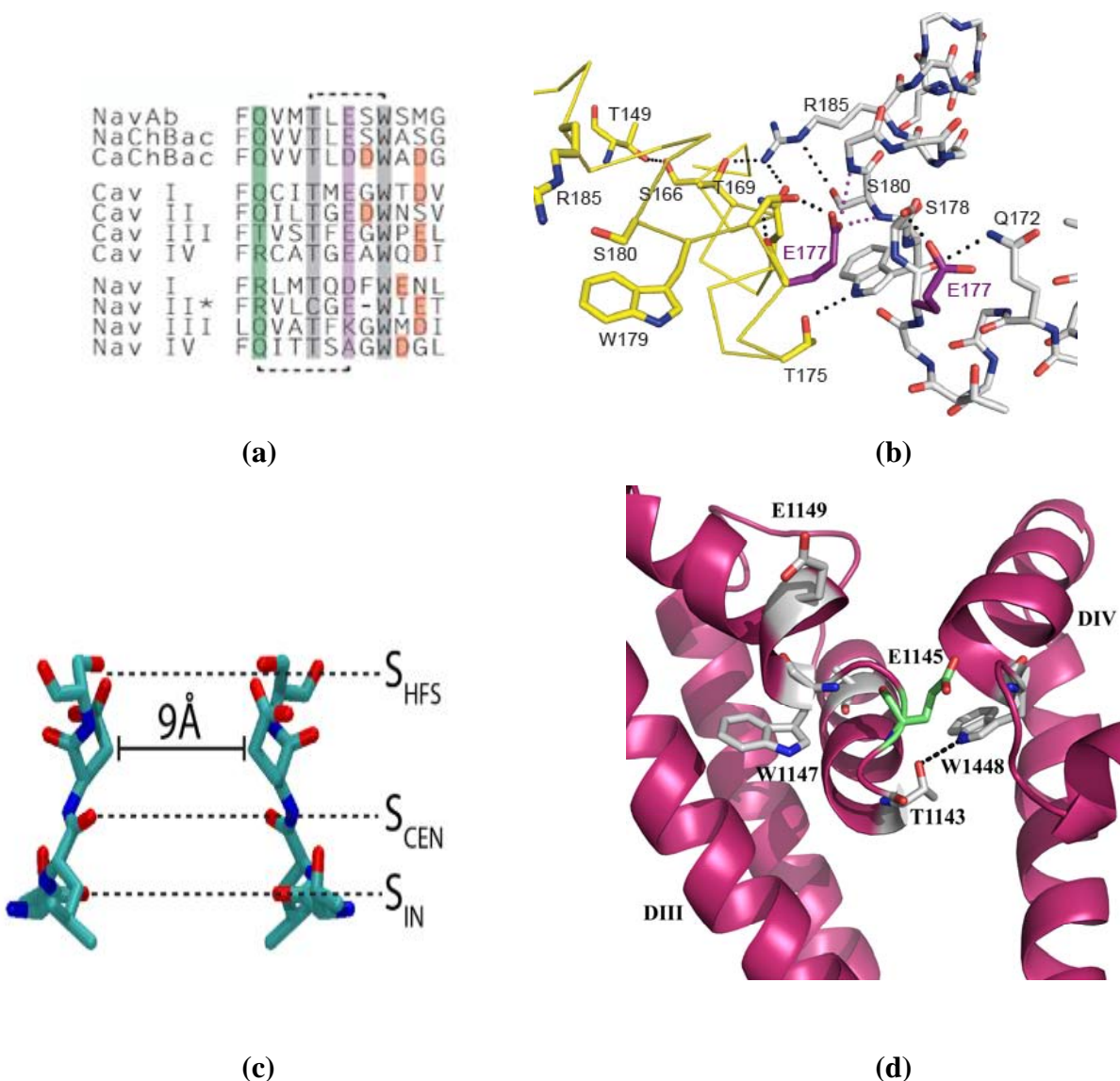


Fig 3.28. (a) Selectivity filter sequence alignment. Glutamic acids homologues in selectivity filter are shaded purple; outer ring of negatively charged residues is shaded orange (b) Conserved interaction network within the NavAb pore (c) the selectivity filter of backbone and side chain of NavAb (d) the Ca_v1.2 based on Voltage-gated sodium (NavAb). The dashed-lines indicate the hydrogen bonding.

Based on the high sequence similarity (see Fig 3.28 a) Payandeh et al, 2011 strongly suggests that the architecture of the calcium channel pore might be highly similar to the structure observed in NavAb [112]. The NavAb pore architecture (can be seen in Fig 3.28 b), which shows important interactions in the selectivity filter region. Interactions within one P-helix and between

P-helices are shown. These interaction networks probably play an important role determines the stability of the pore and the selectivity filter. Probably the most unexpected feature is the fact that not only glutamate side chains line the wall of the selectivity filter, but that backbone residues including a highly conserved threonine residue participate in filter formation (Fig 3.28 c). These hydrogen bond networks are also see in our new Cav1.2 model based on NavAb. Fig 3.28 d shows that Thr 1143 of DIII interacts with the TRP1448 of DIV. Similar hydrogen bonds are also formed between threonine and tryptophane residues from the other domains (not shown).

These new models also provide a good explanation, why docking studies (see chapters 3.4) and MD simulations on blockers were only partially successful based on the old models.

CHAPTER 4

SUMMARY

The voltage gated L-type calcium channels $\text{Ca}_v1.2$ are membrane proteins which are important components of living cells. The majority of drugs are targeted to membrane proteins. The structure and function of closed and open conformations of voltage gated L-type calcium channels $\text{Ca}_v1.2$ were studied in the thesis. The molecular targets of $\text{Ca}_v1.2$ channels are used widely in the therapy of cardiovascular diseases. Due to absence of three dimensional structures, the function of these membrane proteins are still not well understood for this channel, therefore theoretical methods including sequence alignment, homology modeling, molecular docking and molecular dynamic simulation were performed to investigate this channel in detail.

The pore region of the closed and the open conformation of $\text{Ca}_v1.2$ channel models were used to address the key questions of the structure and function of this channel. For the closed conformation model, eight different models were built based on multiple templates of KcsA, MlotiK, nonselective cation channel NaK sodium channel crystal structure and homology model of the NaChBac sodium channel. The various quality assessment methods (Prosa2003, Verify 3D, WHAT_CHECK Packing, Procheck, ProQresLG and ProQres MaxSub) were applied to evaluate the quality of the model. The best ranked structure from the agreement of all programs was selected for further work. For the open conformation model, there are 2 models. 1) The $\text{Ca}_v1.2$ open conformation model is taken from Stary et al, 2009. 2) The $\text{Ca}_v1.2$ open conformation improved model was built by H.R Guy, it was modified and improved from the experimental and computational data. Moreover, *Ab Initio* method was applied to predict the loop structure of calcium channel $\text{Ca}_v3.1$ combined with the results of experimental

investigation. We found that for our work the *Ab Initio* methods are still not accurate enough to observe the various possible disulfide bonds in the model.

The molecular docking method was used to investigate the ligand interaction with Cav1.2. The open conformation model is taken from Strydom et al, 2008. As ligands were used on PAA verapamil and its derivatives in protonated states of both R and S chirality. The results showed that all ligands share similar orientation and position where the ligands are located between IIS6 and IVS6. The positively charged nitrogen atoms of all ligands bind to the glutamic acids E1145 and E1446 due to the electrostatic interactions. We found that Cav1.2 in the open conformation model with verapamil and its derivatives obtained from molecular docking is somehow in disagreement with experimental data. Then, the Cav1.2 open conformation improved model was introduced to be used for further investigation.

The Molecular dynamics simulations were performed over 50 ns to refine the closed and improved open conformation model. These simulations show that the closed and improved open conformations are stable. Consequently, the molecular docking of improved open model with various ligand were performed again. The good pose docking structures of each ligand were selected to set the MD simulation.

The MD simulation of the improved open conformation with verapamil, and quaternary (-) diltiazem were carried out for 20 and 40 ns to check the stability of the complex and examine conformational variations of ligands. The results from MD simulation of verapamil and quaternary (-) diltiazem complex demonstrate that the complexes are stable and in good agreement with published values for low sequence identity homology models. In addition, five different starting orientations of the D619 and two different starting orientations of the T13 were performed for simulation. Simulations show that those complexes remain stable after 15 ns. The

benzene ring, the ammonium group and the nitrile group are rather rigid, the hydrogen and fluorine atoms are fluctuation to some extent. For D619, the benzene ring faces to one of IIS6 or IVS6. In case of T13, benzene ring of the hydrogen binds to each domain IIS6 and IVS6. However, these simulations of D619 and T13 complexes are a preliminary study. Thus, more experimental data are needed for further studies.

Another focus of this thesis concerned the effect of cholesterol influencing Cav1.2 channels in both closed and open conformation. Both closed and improved open channels were taken and embedded into POPC and POPC/CHOL lipid bilayer. MD simulation methods are applied in this work. In the POPC system of both models, the movement of the outer shell ($> 1\text{nm}$) is faster than that of the inner shell ($\leq 1\text{ nm}$). For POPC/CHOL system of both models there no movement difference could be observed. In term of bilayer fluidity, the lipid order parameters demonstrate that order parameter values of both models in POPC/CHOL system are higher than in the POPC system. The density profiles notice that the bilayer thickness of both models in POPC/CHOL system is higher than in the POPC system. It implies that the addition of CHOL decreases the bilayer fluidity and increases the thickness of the bilayer.

Due to the weak point of the first homology modeling of Cav1.2 based on potassium channel as a template. On June 2011, a new voltage-gated sodium channel (NavAb) was published. NavAb channel shares the same highly sequence identity at the selectivity filter P region with Cav1.2. Then, a new homology modeling of Cav1.2 was built and uses to investigate the effect of cholesterol influence with Cav1.2 channel. The global architecture of these two models is almost similar which the RMSD of the backbone of these two models is only 1.9 \AA . These two difference models are mainly different at the P-linker. Moreover, MD simulation method is used to investigate the effect of cholesterol with new Cav1.2 homology model. New

homology model channels were taken and embedded into POPC and POPC/CHOL lipid bilayer. The results show that cholesterol plays a crucial role to increase lipid packing and increase the thickness of the bilayer. From the RDF of cholesterol and channel, it shows that there are several peaks of cholesterol occur inside the $\text{Ca}_v1.2$. These imply that cholesterol is preferentially interacting and penetrate to the $\text{Ca}_v1.2$. The umbrella sampling method was used in this work which focuses in more detail about the access pathway of cholesterol into channel. The potentials of mean force demonstrate that the most favorable region of cholesterol interact with $\text{Ca}_v1.2$ locate at the interface region of S6 domain I and IV due to the hydrophobic residue on this region. At the cavity of $\text{Ca}_v1.2$ which is hydrophilic region, cholesterol is less prefers to locate in this area.

REFERENCE

1. Hedin, L.E., K. Illergard, and A. Elofsson, *An introduction to membrane proteins*. J Proteome Res, 2011. **10**(8): p. 3324-31.
2. Kleinschmidt, J.H., *Membrane Proteins – Introduction*. Cellular and Molecular Life Sciences, 2003. **60**(8): p. 1527-1528.
3. <http://www.blanco.biomol.uci.edu/mpstruc/listAll/list>.
4. Ujwal, R. and J.U. Bowie, *Crystallizing membrane proteins using lipidic bicelles*. Methods. **55**(4): p. 337-41.
5. Gourdon, P., et al., *HiLiDe-Systematic Approach to Membrane Protein Crystallization in Lipid and Detergent*. Crystal Growth & Design. **11**(6): p. 2098-2106.
6. Hille, B., *Ion Channels of Excitable Membranes*, ed. rd. 2001: Sinauer Associates
7. Bidaud, I., et al., *Voltage-gated calcium channels in genetic diseases*. Biochim Biophys Acta, 2006. **1763**(11): p. 1169-74.
8. Catterall, W.A., et al., *International Union of Pharmacology. XLVIII. Nomenclature and structure-function relationships of voltage-gated calcium channels*. Pharmacol Rev, 2005. **57**(4): p. 411-25.
9. Stary, A., et al., *Structural model of the Ca V 1.2 pore*. Channels (Austin), 2008. **2**(3): p. 210-5.
10. Doyle, D.A., et al., *The structure of the potassium channel: molecular basis of K⁺ conduction and selectivity*. Science, 1998. **280**(5360): p. 69-77.
11. Kim, M.S., et al., *Structural determinants of ion selectivity in brain calcium channel*. FEBS Lett, 1993. **318**(2): p. 145-8.

12. Tang, S., et al., *Molecular localization of ion selectivity sites within the pore of a human L-type cardiac calcium channel*. J Biol Chem, 1993. **268**(18): p. 13026-9.
13. Yang, J., et al., *Molecular determinants of Ca²⁺ selectivity and ion permeation in L-type Ca²⁺ channels*. Nature, 1993. **366**(6451): p. 158-61.
14. Ellinor, P.T., et al., *Ca²⁺ channel selectivity at a single locus for high-affinity Ca²⁺ interactions*. Neuron, 1995. **15**(5): p. 1121-32.
15. Van Petegem, F. and D.L. Minor, Jr., *The structural biology of voltage-gated calcium channel function and regulation*. Biochem Soc Trans, 2006. **34**(Pt 5): p. 887-93.
16. Daniel L. Minor, J., *An overview of ion channel structure*. Handbook of Cell Signaling, Three-Volum Set 2 ed., 2010.
17. Hagiwara, S., S. Ozawa, and O. Sand, *Voltage clamp analysis of two inward current mechanisms in the egg cell membrane of a starfish*. J Gen Physiol, 1975. **65**(5): p. 617-44.
18. Dolphin, A.C., *A short history of voltage-gated calcium channels*. Br J Pharmacol, 2006. **147 Suppl 1**: p. S56-62.
19. Tanabe, T., et al., *Primary structure of the receptor for calcium channel blockers from skeletal muscle*. Nature, 1987. **328**(6128): p. 313-8.
20. Mikami, A., et al., *Primary structure and functional expression of the cardiac dihydropyridine-sensitive calcium channel*. Nature, 1989. **340**(6230): p. 230-3.
21. Biel, M., et al., *Primary structure and functional expression of a high voltage activated calcium channel from rabbit lung*. FEBS Lett, 1990. **269**(2): p. 409-12.

22. Koch, W.J., P.T. Ellinor, and A. Schwartz, *cDNA cloning of a dihydropyridine-sensitive calcium channel from rat aorta. Evidence for the existence of alternatively spliced forms.* J Biol Chem, 1990. **265**(29): p. 17786-91.
23. Seino, S., et al., *Cloning of the alpha 1 subunit of a voltage-dependent calcium channel expressed in pancreatic beta cells.* Proc Natl Acad Sci U S A, 1992. **89**(2): p. 584-8.
24. Williams, M.E., et al., *Structure and functional expression of alpha 1, alpha 2, and beta subunits of a novel human neuronal calcium channel subtype.* Neuron, 1992. **8**(1): p. 71-84.
25. Bech-Hansen, N.T., et al., *Loss-of-function mutations in a calcium-channel alpha1-subunit gene in Xp11.23 cause incomplete X-linked congenital stationary night blindness.* Nat Genet, 1998. **19**(3): p. 264-7.
26. Strom, T.M., et al., *An L-type calcium-channel gene mutated in incomplete X-linked congenital stationary night blindness.* Nat Genet, 1998. **19**(3): p. 260-3.
27. Mori, Y., et al., *Primary structure and functional expression from complementary DNA of a brain calcium channel.* Nature, 1991. **350**(6317): p. 398-402.
28. Horne, W.A., et al., *Molecular diversity of Ca²⁺ channel alpha 1 subunits from the marine ray *Discopyge ommata*.* Proc Natl Acad Sci U S A, 1993. **90**(9): p. 3787-91.
29. Williams, M.E., et al., *Structure and functional expression of an omega-conotoxin-sensitive human N-type calcium channel.* Science, 1992. **257**(5068): p. 389-95.
30. Soong, T.W., et al., *Structure and functional expression of a member of the low voltage-activated calcium channel family.* Science, 1993. **260**(5111): p. 1133-6.
31. Klugbauer, N., et al., *A T-type calcium channel from mouse brain.* Pflugers Arch, 1999. **437**(5): p. 710-5.

32. Cribbs, L.L., et al., *Cloning and characterization of $\alpha 1H$ from human heart, a member of the T-type Ca^{2+} channel gene family*. Circ Res, 1998. **83**(1): p. 103-9.
33. Lee, A., et al., *Ca^{2+} /calmodulin binds to and modulates P/Q-type calcium channels*. Nature, 1999. **399**(6732): p. 155-9.
34. Lacinova, L., *Voltage-dependent calcium channels*. Gen Physiol Biophys, 2005. **24 Suppl 1**: p. 1-78.
35. Lehmann-Horn, F. and K. Jurkat-Rott, *Voltage-gated ion channels and hereditary disease*. Physiol Rev, 1999. **79**(4): p. 1317-72.
36. Hockerman, G.H., et al., *Molecular determinants of drug binding and action on L-type calcium channels*. Annu Rev Pharmacol Toxicol, 1997. **37**: p. 361-96.
37. Benitah, J.P., et al., *Voltage-gated Ca^{2+} currents in the human pathophysiologic heart: a review*. Basic Res Cardiol, 2002. **97 Suppl 1**: p. I11-8.
38. Hering, S., et al., *Ca^{2+} channel block and inactivation: common molecular determinants*. Trends Pharmacol Sci, 1998. **19**(11): p. 439-43.
39. Motoike, H.K., et al., *A region in IVS5 of the human cardiac L-type calcium channel is required for the use-dependent block by phenylalkylamines and benzothiazepines*. J Biol Chem, 1999. **274**(14): p. 9409-20.
40. Hering, S., et al., *Molecular mechanism of use-dependent calcium channel block by phenylalkylamines: role of inactivation*. Proc Natl Acad Sci U S A, 1997. **94**(24): p. 13323-8.
41. Hockerman, G.H., et al., *Molecular determinants of high affinity phenylalkylamine block of L-type calcium channels in transmembrane segment IIIS6 and the pore region of the $\alpha 1$ subunit*. J Biol Chem, 1997. **272**(30): p. 18759-65.

42. Hockerman, G.H., et al., *Molecular determinants of high affinity phenylalkylamine block of L-type calcium channels*. J Biol Chem, 1995. **270**(38): p. 22119-22.
43. Hockerman, G.H., et al., *Molecular determinants of diltiazem block in domains IIIS6 and IVS6 of L-type Ca(2+) channels*. Mol Pharmacol, 2000. **58**(6): p. 1264-70.
44. Hescheler, J., et al., *Does the organic calcium channel blocker D600 act from inside or outside on the cardiac cell membrane?* Pflugers Arch, 1982. **393**(4): p. 287-91.
45. Bayer, R., R. Kaufmann, and R. Mannhold, *Inotropic and electrophysiological actions of verapamil and D 600 in mammalian myocardium. II. Pattern of inotropic effects of the optical isomers*. Naunyn Schmiedebergs Arch Pharmacol, 1975. **290**(1): p. 69-80.
46. Mannhold, R., et al., *Investigations on the structure-activity relationships of verapamil*. Naunyn Schmiedebergs Arch Pharmacol, 1978. **302**(2): p. 217-26.
47. Spector, A.A. and M.A. Yorek, *Membrane lipid composition and cellular function*. J Lipid Res, 1985. **26**(9): p. 1015-35.
48. Tillman, T.S. and M. Cascio, *Effects of membrane lipids on ion channel structure and function*. Cell Biochem Biophys, 2003. **38**(2): p. 161-90.
49. Rees, D.C., L. DeAntonio, and D. Eisenberg, *Hydrophobic organization of membrane proteins*. Science, 1989. **245**(4917): p. 510-3.
50. Baenziger, J.E., T.E. Darsaut, and M.L. Morris, *Internal dynamics of the nicotinic acetylcholine receptor in reconstituted membranes*. Biochemistry, 1999. **38**(16): p. 4905-11.
51. Ren, J., et al., *Control of the transmembrane orientation and interhelical interactions within membranes by hydrophobic helix length*. Biochemistry, 1999. **38**(18): p. 5905-12.

52. Ren, J., et al., *Transmembrane orientation of hydrophobic alpha-helices is regulated both by the relationship of helix length to bilayer thickness and by the cholesterol concentration*. Biochemistry, 1997. **36**(33): p. 10213-20.
53. Mall, S., et al., *Effects of aromatic residues at the ends of transmembrane alpha-helices on helix interactions with lipid bilayers*. Biochemistry, 2000. **39**(8): p. 2071-8.
54. de Meyer, F. and B. Smit, *Effect of cholesterol on the structure of a phospholipid bilayer*. Proc Natl Acad Sci U S A, 2009. **106**(10): p. 3654-8.
55. Levitan, I., et al., *Cholesterol and ion channels*. Subcell Biochem, 2010. **51**: p. 509-49.
56. Barrantes, F.J., *Structural basis for lipid modulation of nicotinic acetylcholine receptor function*. Brain Res Brain Res Rev, 2004. **47**(1-3): p. 71-95.
57. Lundbaek, J.A. and O.S. Andersen, *Spring constants for channel-induced lipid bilayer deformations. Estimates using gramicidin channels*. Biophys J, 1999. **76**(2): p. 889-95.
58. Xu, D., Y. Xu, and E.C. Uberbacher, *Computational tools for protein modeling*. Curr Protein Pept Sci, 2000. **1**(1): p. 1-21.
59. Boeckmann, B., et al., *The SWISS-PROT protein knowledgebase and its supplement TrEMBL in 2003*. Nucleic Acids Res, 2003. **31**(1): p. 365-70.
60. Altschul, S.F., et al., *Gapped BLAST and PSI-BLAST: a new generation of protein database search programs*. Nucleic Acids Res, 1997. **25**(17): p. 3389-402.
61. Chenna, R., et al., *Multiple sequence alignment with the Clustal series of programs*. Nucleic Acids Res, 2003. **31**(13): p. 3497-500.
62. Eswar, N., et al., *Comparative protein structure modeling using Modeller*. Curr Protoc Bioinformatics, 2006. **Chapter 5**: p. Unit 5 6.

63. Sali, A. and T.L. Blundell, *Comparative protein modelling by satisfaction of spatial restraints*. J Mol Biol, 1993. **234**(3): p. 779-815.
64. Wiederstein, M. and M.J. Sippl, *ProSA-web: interactive web service for the recognition of errors in three-dimensional structures of proteins*. Nucleic Acids Res, 2007. **35**(Web Server issue): p. W407-10.
65. Bowie, J.U., R. Luthy, and D. Eisenberg, *A method to identify protein sequences that fold into a known three-dimensional structure*. Science, 1991. **253**(5016): p. 164-70.
66. Hooft, R.W., et al., *Errors in protein structures*. Nature, 1996. **381**(6580): p. 272.
67. Laskowski, R.A., et al., *PROCHECK: a program to check the stereochemical quality of protein structures*. Journal of Applied Crystallography, 1993. **26**(2): p. 283-291.
68. Kim, D.E., D. Chivian, and D. Baker, *Protein structure prediction and analysis using the Robetta server*. Nucleic Acids Research, 2004. **32**(suppl 2): p. W526-W531.
69. Zhang, Y., *I-TASSER server for protein 3D structure prediction*. BMC Bioinformatics, 2008. **9**: p. 40.
70. Moult, J., et al., *A large-scale experiment to assess protein structure prediction methods*. Proteins, 1995. **23**(3): p. ii-v.
71. <http://zhanglab.ccmb.med.umich.edu/I-TASSER/>.
72. Larsson, P., et al., *Using multiple templates to improve quality of homology models in automated homology modeling*. Protein Sci, 2008. **17**(6): p. 990-1002.
73. Saxena, A., et al., *The basic concepts of molecular modeling*. Methods Enzymol, 2009. **467**: p. 307-34.
74. Glide. 2008: New york.
75. MOE, Chemical Computing Group, Inc.: Montreal, Quebec, Canada.

76. GaussView. 2009., Roy Dennington, Todd Keith and John Millam, Semichem Inc, Shawnee Mission KS.
77. GAUSSIAN, e.a. M.J. Frisch, Editor. 2004, Gaussian, Inc.: Wallingford CT.
78. Charles, L.B., Martin , K. and Montgomery. P, ed. *Proteins :A Theoretical perspective of Dynamics, Structure and Thermodynamics.* . 1988, John Wiley & Sons: USA.
79. Weiner, S.J., et al., *A new force field for molecular mechanical simulation of nucleic acids and proteins.* Journal of the American Chemical Society, 1984. **106**(3): p. 765-784.
80. Daura, X., A.E. Mark, and W.F. Van Gunsteren, *Parametrization of aliphatic CH_n united atoms of GROMOS96 force field.*
81. Brooks, B.R., et al., *CHARMM: The biomolecular simulation program.* Journal of Computational Chemistry, 2009. **30**(10): p. 1545-1614.
82. Jorgensen, W.L. and J. Tirado-Rives, *The OPLS [optimized potentials for liquid simulations] potential functions for proteins, energy minimizations for crystals of cyclic peptides and crambin.* Journal of the American Chemical Society, 1988. **110**(6): p. 1657-1666.
83. Siu, S.W., et al., *Biomolecular simulations of membranes: physical properties from different force fields.* J Chem Phys, 2008. **128**(12): p. 125103.
84. Sousa Da Silva, A.W., W.F. Vranken, and E.D. Laue, *ACPYPE - AnteChamber PYthon Parser interfacE., in Manuscript to be submitted.:*
<http://acpype.googlecode.com/svn/trunk/acpype.py>.
85. Gasteiger, E., et al., *ExPASy: The proteomics server for in-depth protein knowledge and analysis.* Nucleic Acids Res, 2003. **31**(13): p. 3784-8.

86. Zhou, Y., et al., *Chemistry of ion coordination and hydration revealed by a K⁺ channel-Fab complex at 2.0 Å resolution*. Nature, 2001. **414**(6859): p. 43-8.
87. Clayton, G.M., et al., *Structure of the transmembrane regions of a bacterial cyclic nucleotide-regulated channel*. Proc Natl Acad Sci U S A, 2008. **105**(5): p. 1511-5.
88. Shi, N., et al., *Atomic structure of a Na⁺- and K⁺-conducting channel*. Nature, 2006. **440**(7083): p. 570-4.
89. Shafrir, Y., S.R. Durell, and H.R. Guy, *Models of voltage-dependent conformational changes in NaChBac channels*. Biophys J, 2008. **95**(8): p. 3663-76.
90. Beyl, S., et al., *Probing the architecture of an L-type calcium channel with a charged phenylalkylamine: evidence for a widely open pore and drug trapping*. The Journal of biological chemistry, 2007. **282**(6): p. 3864-70.
91. Lipkind, G.M. and H.A. Fozzard, *Molecular modeling of interactions of dihydropyridines and phenylalkylamines with the inner pore of the L-type Ca²⁺ channel*. Molecular pharmacology, 2003. **63**(3): p. 499-511.
92. Cheng, R.C., D.B. Tikhonov, and B.S. Zhorov, *Structural model for phenylalkylamine binding to L-type calcium channels*. The Journal of biological chemistry, 2009. **284**(41): p. 28332-42.
93. Lee, K.S. and R.W. Tsien, *Mechanism of calcium channel blockade by verapamil, D600, diltiazem and nitrendipine in single dialysed heart cells*. Nature, 1983. **302**(5911): p. 790-4.
94. Shabbir, W., et al., *Interaction of diltiazem with an intracellularly accessible binding site on Ca(V)1.2*. British Journal of Pharmacology. **162**(5): p. 1074-1082.

95. Kudrnac, M., et al., *Coupled and independent contributions of residues in IS6 and IIS6 to activation gating of CaV1.2*. The Journal of biological chemistry, 2009. **284**(18): p. 12276-84.
96. Suwattanasophon, C., et al., *Molecular dynamics simulations on the function of the transmembrane Cav1.2 channel in dependence of the content of cholesterol in the membrane*. European Biophysics Journal with Biophysics Letters. **40**: p. 118-118.
97. Bowles, D.K., et al., *Hypercholesterolemia inhibits L-type calcium current in coronary macro-, not microcirculation*. J Appl Physiol, 2004. **96**(6): p. 2240-8.
98. Hess, B., et al., *GROMACS 4: Algorithms for Highly Efficient, Load-Balanced, and Scalable Molecular Simulation*. Journal of Chemical Theory and Computation, 2008. **4**(3): p. 435-447.
99. Chiu, S.W., et al., *An improved united atom force field for simulation of mixed lipid bilayers*. J Phys Chem B, 2009. **113**(9): p. 2748-63.
100. Clayton, G.M., et al., *Structure of the transmembrane regions of a bacterial cyclic nucleotide-regulated channel*. Proceedings of the National Academy of Sciences of the United States of America, 2008. **105**(5): p. 1511-5.
101. Shafrir, Y., S.R. Durell, and H.R. Guy, *Models of voltage-dependent conformational changes in NaChBac channels*. Biophysical journal, 2008. **95**(8): p. 3663-76.
102. Stary, A., et al., *Molecular dynamics and mutational analysis of a channelopathy mutation in the IIS6 helix of Ca V 1.2*. Channels (Austin), 2008. **2**(3): p. 216-23.
103. Kandt, C., W.L. Ash, and D.P. Tieleman, *Setting up and running molecular dynamics simulations of membrane proteins*. Methods, 2007. **41**(4): p. 475-88.

104. Nose, S., *A unified formulation of the constant temperature molecular dynamics methods*. The Journal of Chemical Physics, 1984. **81**(1): p. 511-519.
105. Parrinello, M. and A. Rahman, *Polymorphic transitions in single crystals: A new molecular dynamics method*. Journal of Applied Physics, 1981. **52**(12): p. 7182-7190.
106. Essmann, U., et al., *A smooth particle mesh Ewald method*. The Journal of Chemical Physics, 1995. **103**(19): p. 8577-8593.
107. Yang, J., et al., *Molecular determinants of Ca²⁺ selectivity and ion permeation in L-type Ca²⁺ channels*. Nature, 1993. **366**(6451): p. 158-161.
108. Dickey, A. and R. Faller, *Examining the contributions of lipid shape and headgroup charge on bilayer behavior*. Biophysical journal, 2008. **95**(6): p. 2636-46.
109. Brown, D.A. and E. London, *Functions of lipid rafts in biological membranes*. Annual review of cell and developmental biology, 1998. **14**: p. 111-36.
110. de Meyer, F. and B. Smit, *Effect of cholesterol on the structure of a phospholipid bilayer*. Proceedings of the National Academy of Sciences of the United States of America, 2009. **106**(10): p. 3654-8.
111. Pike, L.J., *The challenge of lipid rafts*. Journal of lipid research, 2009. **50 Suppl**: p. S323-8.
112. Payandeh, J., et al., *The crystal structure of a voltage-gated sodium channel*. Nature, 2011. **475**(7356): p. 353-8.
113. Tikhonov, D.B. and B.S. Zhorov, *Possible roles of exceptionally conserved residues around the selectivity filters of sodium and calcium channels*. J Biol Chem, 2011. **286**(4): p. 2998-3006.

Appendix I – Parameter for molecular dynamics simulation using Gromacs

4.0.7

; VARIOUS PREPROCESSING OPTIONS

title =
cpp = /lib/cpp -traditional
include =

; RUN CONTROL PARAMETERS

integrator = md
; Start time and timestep in ps
tinit = 0
dt = 0.002
nstps = 5000000
; For exact run continuation or redoing part of a run
init_step = 0
; mode for center of mass motion removal
comm-mode = Linear
; number of steps for center of mass motion removal
nstcomm = 1

; LANGEVIN DYNAMICS OPTIONS

; Temperature, friction coefficient (amu/ps) and random seed
bd-fric = 0
ld-seed = 1993

; ENERGY MINIMIZATION OPTIONS

; Force tolerance and initial step-size
emtol = 10
emstep = 0.01
; Max number of iterations in relax_shells

```

niter                                = 20
; Step size (1/ps^2) for minimization of flexible constraints
fcstep                               = 0
; Frequency of steepest descents steps when doing CG
nstcgsteep                           = 1000
nbgscorr                             = 10

; OUTPUT CONTROL OPTIONS
; Output frequency for coords (x), velocities (v) and forces (f)
nstxout                              = 10000
nstvout                              = 10000
nstfout                              = 0
; Checkpointing helps you continue after crashes
nstcheckpoint                        = 10000
; Output frequency for energies to log file and energy file
nstlog                              = 10000
nstenergy                            = 10000
; Output frequency and precision for xtc file
nstxtcout                            = 10000
xtc-precision                        = 10000
; This selects the subset of atoms for the xtc file. You can
; Selection of energy groups
energygrps                           = Protein MOL Ca

; NEIGHBORSEARCHING PARAMETERS
; nblist update frequency
nstlist                              = 10
; ns algorithm (simple or grid)
ns-type                              = Grid
; Periodic boundary conditions: xyz (default), no (vacuum)
; or full (infinite systems only)

```

```

pbc                      = xyz
; nblast cut-off

rlist                    = 1
domain-decomposition     = no

; OPTIONS FOR ELECTROSTATICS AND VDW
; Method for doing electrostatics
coulombtype              = PME
rcoulomb-switch          = 0
rcoulomb                  = 1
; Dielectric constant (DC) for cut-off or DC of reaction field
epsilon-r                = 1
; Method for doing Van der Waals
vdw-type                  = Cut-off
; cut-off lengths
rvdw-switch              = 0
rvdw                      = 1
; Apply long range dispersion corrections for Energy and Pressure
DispCorr                  = No
; Extension of the potential lookup tables beyond the cut-off
table-extension          = 1
; Spacing for the PME/PPPM FFT grid
fourierspacing            = 0.12
; FFT grid size, when a value is 0 fourierspacing will be used
fourier_nx                = 0
fourier_ny                = 0
fourier_nz                = 0
; EWALD/PME/PPPM parameters
pme_order                 = 4
ewald_rtol                = 1e-05
ewald_geometry            = 3d

```

epsilon_surface = 0
optimize_fft = no

; GENERALIZED BORN ELECTROSTATICS

; Algorithm for calculating Born radii

gb_algorithm = Still

; Frequency of calculating the Born radii inside rlist

nstgbradii = 1

; Cutoff for Born radii calculation; the contribution from atoms

; between rlist and rgradii is updated every nstlist steps

rgradii = 2

; Salt concentration in M for Generalized Born models

gb_saltconc = 0

; IMPLICIT SOLVENT (for use with Generalized Born electrostatics)

implicit_solvent = No

; OPTIONS FOR WEAK COUPLING ALGORITHMS

; Temperature coupling

tcoupl = V-rescale

; Groups to couple separately

tc-grps = Protein DOP SOL MOL Ca Cl

; Time constant (ps) and reference temperature (K)

tau-t = 0.1 0.1 0.1 0.1 0.1 0.1

ref-t = 300 300 300 300 300 300

; Pressure coupling

Pcoupl = Parrinello-Rahman

Pcoupltype = semiisotropic

; Time constant (ps), compressibility (1/bar) and reference P (bar)

tau-p = 1

compressibility = 4.5e-5 4.5e-5

```

ref-p                      = 1.0 1.0
; Random seed for Andersen thermostat
andersen_seed              = 815131

; SIMULATED ANNEALING
; Type of annealing for each temperature group (no/single/periodic)
annealing                  = no no no no no no

; GENERATE VELOCITIES FOR STARTUP RUN
gen-vel                    = no
gen-temp                   = 300
gen-seed                   = 173529

; OPTIONS FOR BONDS
constraints                 = all-bonds
; Type of constraint algorithm
constraint-algorithm        = Lincs
; Do not constrain the start configuration
unconstrained-start        = no
; Use successive overrelaxation to reduce the number of shake iterations
Shake-SOR                  = no
; Relative tolerance of shake
shake-tol                  = 1e-04
; Highest order in the expansion of the constraint coupling matrix
lincs-order                 = 4
; Number of iterations in the final step of LINCS. 1 is fine for
; normal simulations, but use 2 to conserve energy in NVE runs.
; For energy minimization with constraints it should be 4 to 8.
lincs-iter                 = 1
; Lincs will write a warning to the stderr if in one step a bond
; rotates over more degrees than

```



```

lincs-warnangle          = 30
; Convert harmonic bonds to morse potentials
morse                    = no

; ENERGY GROUP EXCLUSIONS

; NMR refinement stuff
; Distance restraints type: No, Simple or Ensemble
disre                    = No
; Force weighting of pairs in one distance restraint: Conservative or Equal
disre-weighting          = Conservative
; Use sqrt of the time averaged times the instantaneous violation
disre-mixed              = no
disre-fc                  = 1000
disre-tau                = 0
; Output frequency for pair distances to energy file
nstdisreout              = 100
; Orientation restraints: No or Yes
orire                    = no
; Orientation restraints force constant and tau for time averaging
orire-fc                  = 0
orire-tau                = 0
; Output frequency for trace(SD) to energy file
nstorireout              = 100
; Dihedral angle restraints: No, Simple or Ensemble
dihre                    = No
dihre-fc                  = 1000
dihre-tau                = 0
; Output frequency for dihedral values to energy file
nstdihreout              = 100

```

; Free energy control stuff

free-energy = no

init-lambda = 0

delta-lambda = 0

sc-alpha = 0

sc-sigma = 0.3

Appendix II - Multiply sequence alignment of pore domain I to II.

| | | DI-L45 | DI-S5 | |
|------------|---|--|-------|-----|
| Cav1.2_Oc | : | GVPSLQVVLNSIIKAMVPLLHIALLVLFVIIIIYAIIG | : | 316 |
| Cav1.2_Hs | : | GVPSLQVVLNSIIKAMVPLLHIALLVLFVIIIIYAIIG | : | 286 |
| Cav1.2_Ms | : | GVPSLQVVLNSIIKAMVPLLHIALLVLFVIIIIYAIIG | : | 286 |
| Cav1.2_Rn | : | GVPSLQVVLNSIIKAMVPLLHIALLVLFVIIIIYAIIG | : | 316 |
| 1.2XP_Gg | : | GVPSLQVVLNSIIKAMVPLLHIALLVLFVIIIIYAIIG | : | 294 |
| 1.2XP_Cf | : | GVPSLQVVLNSIIKAMVPLLHIALLVLFVIIIIYAIIG | : | 260 |
| 1.2NP_Hs | : | GVPSLQVVLNSIIKAMVPLLHIALLVLFVIIIIYAIIG | : | 286 |
| 1.2NP_Ms | : | GVPSLQVVLNSIIKAMVPLLHIALLVLFVIIIIYAIIG | : | 286 |
| 1.2NP_Oc | : | GVPSLQVVLNSIIKAMVPLLHIALLVLFVIIIIYAIIG | : | 316 |
| 1.2A0SLC4_ | : | GVPSLQVVLNSIIKAMVPLLHIALLVLFVIIIIYAIIG | : | 286 |
| 1.2EMD_Rn | : | GVPSLQVVLNSIIKAMVPLLHIALLVLFVIIIIYAIIG | : | 286 |
| Cav1.1_Hs | : | GVPSLQVVLNSIEKAMLPLFHIALLVLFMVIIYAIIG | : | 214 |
| Cav1.1_Oc | : | GVPSLQVVLNSIEKAMLPLFHIALLVLFMVIIYAIIG | : | 214 |
| Cav1.1_Ms | : | GVPSLQVVLNSIEKAMLPLFHIALLVLFMVIIYAIIG | : | 214 |
| Cav1.1_Rc | : | GVPSLQVVLNSIIKAMIPLFHIALLVLFMIIIIYAIVG | : | 212 |
| 1.1NP_Oc | : | GVPSLQVVLNSIEKAMLPLFHIALLVLFMVIIYAIIG | : | 214 |
| 1.1NP_HS | : | GVPSLQVVLNSIEKAMLPLFHIALLVLFMVIIYAIIG | : | 214 |
| 1.1XP_Cp | : | GVPSLQVVLNSIEKAMLPLFHIALLVLFMVIIYAIIG | : | 214 |
| 1.1XP_Cf | : | GVPSLQVVLNSIEKAMLPLFHIALLVLFMVIIYAIIG | : | 214 |
| 1.1XP_Md | : | GVPSLQVVLNSIIKAMIPLFHIALLVLFMVIIYAIIG | : | 215 |
| Cav1.3_Hs | : | GVPSLQVVLNSIIKAMVPLLHIALLVLFVIIIIYAIIG | : | 289 |
| Cav1.3_Ms | : | GVPSLQVVLNSIIKAMVPLLHIALLVLFVIIIIYAIIG | : | 289 |
| Cav1.3_Gg | : | GVPSLQVVLNSIIKAMVPLLHIALLVLFVIIIIYAIIG | : | 284 |
| Cav1.3_Rn | : | GVPSLQVVLNSIIKAMVPLLHIALLVLFVIIIIYAIIG | : | 289 |
| Cav1.3_Ma | : | GVPSLQVVLNSIIKAMVPLLHIALLVLFVIIIIYAIIG | : | 288 |
| 1.3XP_Bt | : | GVPSLQVVLNSIIKAMVPLLHIALLVLFVIIIIYAIIG | : | 289 |
| 1.3XP_Cp | : | GVPSLQVVLNSIIKAMVPLLHIALLVLFVIIIIYAIIG | : | 290 |
| 1.3XP_Cf | : | GVPSLQVVLNSIIKAMVPLLHIALLVLFVIIIIYAIIG | : | 289 |
| 1.3AAA_HS | : | GVPSLQVVLNSIIKAMVPLLHIALLVLFVIIIIYAIIG | : | 289 |
| 1.3B0FYA3_ | : | GVPSLQVVLNSIIKAMVPLLHIALLVLFVIIIIYAIIG | : | 289 |
| 1.3Q91W25_ | : | GVPSLQVVLNSIIKAMVPLLHIALLVLFVIIIIYAIIG | : | 280 |
| 1.3Q8JFR0 | : | GVPSLQVVLNSIIKAMVPLLHIALLVLFVIIIIYAIIG | : | 292 |
| Cav1.4_Hs | : | GVPSLHIVLNSIMKALVPLLHIALLVLFVIIIIYAIIG | : | 255 |
| 1.4NP_HS g | : | GVPSLHIVLNSIMKALVPLLHIALLVLFVIIIIYAIIG | : | 255 |
| 1.4XP_Mm g | : | GVPSLHIVLNSIMKALVPLLHIALLVLFVIIIIYAIIG | : | 255 |
| 1.4XP_pre_ | : | GVPSLHIVLNSIMKALVPLLHIALLVLFVIIIIYAIIG | : | 255 |
| 1.4XP_Cf g | : | GVPSLHIVLNSIMKALVPLLHIALLVLFVIIIIYAIIG | : | 223 |
| 1.4NP_Ms g | : | GVPSLHIVLNSIMKALVPLLHIALLVLFVIIIIYAIIG | : | 255 |
| 1.4CAM_Ms | : | GVPSLHIVLNSIMKALVPLLHIALLVLFVIIIIYAIIG | : | 255 |
| 1.4Q7TNI3_ | : | GVPSLHIVLNSIMKALVPLLHIALLVLFVIIIIYAIIG | : | 255 |
| Cav1.4_Ms | : | GVPSLHIVVNSIMKALVPLLHIALLVLFVIIIIYAIIG | : | 255 |
| 1.4ABD_Rn | : | GVPSLHIVLNSIMKALVPLLHIALLVLFVIIIIYAIIG | : | 255 |
| 1.4NP_Rn N | : | GVPSLHIVLNSIMKALVPLLHIALLVLFVIIIIYAIIG | : | 255 |
| 1.4NP_Oc N | : | GVPSLQVVLNSIIKAMVPLLHIALLVLFVIIIIYAIIG | : | 316 |
| ***** | | | | |

| | | | | |
|------------|---|--|---|-----|
| Cav1.2_Oc | : | LELFMGKMHKTCYNQ---EG-VADVPAEDDPSPCALE | : | 349 |
| Cav1.2_Hs | : | LELFMGKMHKTCYNQ---EG-IADVPAEDDPSPCALE | : | 319 |
| Cav1.2_Ms | : | LELFMGKMHKTCYNQ---EG-IIDVPAEDDPSPCALE | : | 319 |
| Cav1.2_Rn | : | LELFMGKMHKTCYNQ---EG-IIDVPAEDDPSPCALE | : | 349 |
| 1.2XP_Gg | : | LELFMGKMHKTCYHV---QGG-LIDTPAEDDPSPCAPQ | : | 328 |
| 1.2XP_Cf | : | LELFMGKMHKTCYNQ---EG-IADVPAEDDPSPCALE | : | 293 |
| 1.2NP_Hs | : | LELFMGKMHKTCYNQ---EG-IADVPAEDDPSPCALE | : | 319 |
| 1.2NP_Ms | : | LELFMGKMHKTCYNQ---EG-IIDVPAEDDPSPCALE | : | 319 |
| 1.2NP_Oc | : | LELFMGKMHKTCYNQ---EG-VADVPAEDDPSPCALE | : | 349 |
| 1.2A0SLC4 | : | LELFMGKMHKTCYNQ---EG-IIDVPAEDDPSPCALE | : | 319 |
| 1.2EMD_Rn | : | LELFMGKMHKTCYNQ---EG-IIDVPAEDDPSPCALE | : | 319 |
| Cav1.1_Hs | : | LELFKGKMHKTCYFIG--TD-IVATVENEKPSPCART | : | 248 |
| Cav1.1_Oc | : | LELFKGKMHKTCYFIG--TD-IVATVENEKPSPCART | : | 248 |
| Cav1.1_Ms | : | LELFKGKMHKTCYFIG--TD-IVATVENEKPSPCART | : | 248 |
| Cav1.1_Rc | : | LELPSGKMHKTCYFKD--TD-ITATVDNEKPAPCSST | : | 246 |
| 1.1NP_Oc | : | LELFKGKMHKTCYFIG--TD-IVATVENEKPSPCART | : | 248 |
| 1.1NP_HS | : | LELFKGKMHKTCYFIG--TD-IVATVENEKPSPCART | : | 248 |
| 1.1XP_Cp | : | LELFKGKMHKTCYFTG--TD-IVATVENEKPSPCART | : | 248 |
| 1.1XP_Cf | : | LELFKGKMHKTCYFIG--TD-IVATVENEKPSPCART | : | 248 |
| 1.1XP_Md | : | LELFKGKMHKTCYFIG--TD-IVATVDMKPSPCART | : | 249 |
| Cav1.3_Hs | : | LELFIGKMHKTCFFAD--SD-IVAE---EDPAPCAFS | : | 320 |
| Cav1.3_Ms | : | LELFIGKMHKTCFFAD--SD-IVAE---EDPAPCAFS | : | 320 |
| Cav1.3_Gg | : | LELFIGKMHKSCFLID--SD-ILVE---EDPAPCAFS | : | 315 |
| Cav1.3_Rn | : | LELFIGKMHKTCFFAD--SD-IVAE---EDPAPCAFS | : | 320 |
| Cav1.3_Ma | : | LELFIGKMHKTCFFAD--SD-IVAE---EDPAPCAFS | : | 319 |
| 1.3XP_Bt | : | LELFIGKMHKTCFFAD--SD-MVAE---EDPAPCAFS | : | 320 |
| 1.3XP_Cp | : | LELFIGKMHKTCFFAD--SD-IVAE---EDPAPCAFS | : | 321 |
| 1.3XP_Cf | : | LELFIGKMHKTCFFAD--SD-IIAE---EDPAPCAFS | : | 320 |
| 1.3AAA_HS | : | LELFIGKMHKTCFFAD--SD-IVAE---EDPAPCAFS | : | 320 |
| 1.3B0FYA3 | : | LELFIGKMHKTCFFAD--SD-IVAE---EDPAPCAFS | : | 320 |
| 1.3Q91W25 | : | LELFIGKMHKTCFFAD--SD-IVAE---EDPAPCAFS | : | 311 |
| 1.3Q8JFR0 | : | LELFIGKMHKTCFFPS--TG-MIAE---DDPAPCAIS | : | 323 |
| Cav1.4_Hs | : | LELFLGRMHKTCYFLG--SD-MEAE---EDSPCASS | : | 286 |
| 1.4NP_HS g | : | LELFLGRMHKTCYFLG--SD-MEAE---EDSPCASS | : | 286 |
| 1.4XP_Mm g | : | LELFLGRMHKTCYFLG--SD-LEAE---EDSPCASS | : | 286 |
| 1.4XP_pre | : | LELFLGRMHKTCYFLG--SD-VEAE---EDSPCASS | : | 286 |
| 1.4XP_Cf g | : | LELFLGRMHKTCYFLG--SG-HGG----GPVALCVF | : | 252 |
| 1.4NP_Ms g | : | LELFLGRMHKTCYFLG--SD-MEAE---EDSPCASS | : | 286 |
| 1.4CAM_Ms | : | LELFLGRMHKTCYFLG--SD-MEAE---EDSPCASS | : | 286 |
| 1.4Q7TNI3 | : | LELFLGRMHKTCYFLG--SD-MEAE---EDSPCASS | : | 286 |
| Cav1.4_Ms | : | LELFLGRMHKTCYFLG--SD-MEAE---EDSPCASS | : | 286 |
| 1.4ABD_Rn | : | LELFLGRMHKTCYFLG--SD-MEAE---EDSPCASS | : | 286 |
| 1.4NP_Rn N | : | LELFLGRMHKTCYFLG--SD-MEAE---EDSPCASS | : | 286 |
| 1.4NP_Oc N | : | LELFMGKMHKTCYNQEGVAD-VP AE---DDPSPCALE | : | 349 |

—DI-P—

| | | | | |
|------------|---|--|---|-----|
| Cav1.2_Oc | : | TGHGRQCQNGTVCKPGWDGPKHGITNFDNFAFAMLTV | : | 386 |
| Cav1.2_Hs | : | TGHGRQCQNGTVCKPGWDGPKHGITNFDNFAFAMLTV | : | 356 |
| Cav1.2_Ms | : | TGHGRQCQNGTVCKPGWDGPKHGITNFDNFAFAMLTV | : | 356 |
| Cav1.2_Rn | : | TGHGRQCQNGTVCKPGWDGPKHGITNFDNFAFAMLTV | : | 386 |
| 1.2XP_Gg | : | SAHGRQCQNGTECKAGWEGPKHGITNFDNFAFAMLTV | : | 365 |
| 1.2XP_Cf | : | TGHGRQCQNGTVCKPGWDGPKHGITNFDNFAFAMLTV | : | 330 |
| 1.2NP_Hs | : | TGHGRQCQNGTVCKPGWDGPKHGITNFDNFAFAMLTV | : | 356 |
| 1.2NP_Ms | : | TGHGRQCQNGTVCKPGWDGPKHGITNFDNFAFAMLTV | : | 356 |
| 1.2NP_Oc | : | TGHGRQCQNGTVCKPGWDGPKHGITNFDNFAFAMLTV | : | 386 |
| 1.2A0SLC4 | : | TGHGRQCQNGTVCKPGWDGPKHGITNFDNFAFAMLTV | : | 356 |
| 1.2EMD_Rn | : | TGHGRQCQNGTVCKPGWDGPKHGITNFDNFAFAMLTV | : | 356 |
| Cav1.1_Hs | : | GSGRRCTINGSECRGGWFGPNHGITHFDNFGFSMLTV | : | 285 |
| Cav1.1_Oc | : | GSGRPCTINGSECRGGWFGPNHGITHFDNFGFSMLTV | : | 285 |
| Cav1.1_Ms | : | GSGRPCTINGSECRGGWFGPNHGITHFDNFGFSMLTV | : | 285 |
| Cav1.1_Rc | : | GQGRQCSINGSECRGGWFGPNNGITHFDNFGFAMLTV | : | 283 |
| 1.1NP_Oc | : | GSGRPCTINGSECRGGWFGPNHGITHFDNFGFSMLTV | : | 285 |
| 1.1NP_HS | : | GSGRRCTINGSECRGGWFGPNHGITHFDNFGFSMLTV | : | 285 |
| 1.1XP_Cp | : | GSGRRCTINGSECRGGWFGPNHGITHFDNFGFSMLTV | : | 285 |
| 1.1XP_Cf | : | GSGRPCTINGSECRGGWFGPNHGITHFDNFGFSMLTV | : | 285 |
| 1.1XP_Md | : | GSGRPCTINGSECRGGWFGPNNGITKFDNFGFAMLTV | : | 286 |
| Cav1.3_Hs | : | GNGRQCTANGTECRSGWVGPNGGITNFDNFAFAMLTV | : | 357 |
| Cav1.3_Ms | : | GNGRQCTANGTECRSGWVGPNGGITNFDNFAFAMLTV | : | 357 |
| Cav1.3_Gg | : | GNGRQCVMNTECKGGWVGPNGGITNFDNFAFAMLTV | : | 352 |
| Cav1.3_Rn | : | GNGRQCAANGTECRSGWVGPNGGITNFDNFAFAMLTV | : | 357 |
| Cav1.3_Ma | : | GNGRQCAVNGTECRSGWVGPNGGITNFDNFAFAMLTV | : | 356 |
| 1.3XP_Bt | : | GNGRQCTANGTECRSGWAGPNGGITNFDNFAFAMLTV | : | 357 |
| 1.3XP_Cp | : | GNGRQCTANGTECRSGWVGPNGGITNFDNFAFAMLTV | : | 358 |
| 1.3XP_Cf | : | GNGRQCAANGTECRSGWVGPNGGITNFDNFAFAMLTV | : | 357 |
| 1.3AAA_HS | : | GNGRQCTANGTECRSGWVGPNGGITNFDNFAFAMLTV | : | 357 |
| 1.3B0FYA3 | : | GNGRQCTANGTECRSGWVGPNGGITNFDNFAFAMLTV | : | 357 |
| 1.3Q91W25 | : | GNGRQCAVNGTECRSGWVGPNGGITNFDNFAFAMLTV | : | 348 |
| 1.3Q8JFR0 | : | GHGRQCPINGTECREGWHGPNNGITNFDNFLFAMLTV | : | 360 |
| Cav1.4_Hs | : | GSGRACTLNQTECRGRWFGPNGGITNFDNFFFAMLTV | : | 323 |
| 1.4NP_HS g | : | GSGRACTLNQTECRGRWFGPNGGITNFDNFFFAMLTV | : | 323 |
| 1.4XP_Mm g | : | GSGRACTLNQTECRGRWFGPNGGITNFDNFFFAMLTV | : | 323 |
| 1.4XP_pre | : | GSGRACTLNQTECRGRWAGPNGGITNFDNFFFAMLTV | : | 323 |
| 1.4XP_Cf g | : | GLGRACTLNQTECRGRWAGPNGGITNFDNFFFAMLTV | : | 289 |
| 1.4NP_Ms g | : | GSGRSCTLNHTTECRGRWFGPNGGITNFDNFFFAMLTV | : | 323 |
| 1.4CAM_Ms | : | GSGRSCTLNHTTECRGRWFGPNGGITNFDNFFFAMLTV | : | 323 |
| 1.4Q7TNI3 | : | GSGRSCTLNHTTECRGRWFGPNGGITNFDNFFFAMLTV | : | 323 |
| Cav1.4_Ms | : | GSGRSCTLNHTTECRGRWFGPNGGITNFDNFFFAMLTV | : | 323 |
| 1.4ABD_Rn | : | GSGRSCTLNQTECRGRWFGPNGGITNFDNFFFAMLTV | : | 323 |
| 1.4NP_Rn N | : | GSGRSCTLNQTECRGRWFGPNGGITNFDNFFFAMLTV | : | 323 |
| 1.4NP_Oc N | : | TGHGRQCQNGTVCKPGWDGPKHGITNFDNFAFAMLTV | : | 386 |

| | | | | |
|------------|---|---------------------------------------|---|-----|
| Cav1.2 Oc | : | FQCITMEGWTDVLYWMQDAMGYELPWVYFVSLVIFGS | : | 423 |
| Cav1.2_Hs | : | FQCITMEGWTDVLYWVNDVGRDWPWIYFVTLIIIGS | : | 393 |
| Cav1.2_Ms | : | FQCITMEGWTDVLYWMQDAMGYELPWVYFVSLVIFGS | : | 393 |
| Cav1.2_Rn | : | FQCITMEGWTDVLYWMQDAMGYELPWVYFVSLVIFGS | : | 423 |
| 1.2XP_Gg | : | FQCITMEGWTDVLYWVNDVGRDWPWIYFVTLIIIGS | : | 402 |
| 1.2XP_Cf | : | FQCITMEGWTDVLYWMQDAMGYELPWVYFVSLVIFGS | : | 367 |
| 1.2NP_Hs | : | FQCITMEGWTDVLYWVNDVGRDWPWIYFVTLIIIGS | : | 393 |
| 1.2NP_Ms | : | FQCITMEGWTDVLYWMQDAMGYELPWVYFVSLVIFGS | : | 393 |
| 1.2NP_Oc | : | FQCITMEGWTDVLYWMQDAMGYELPWVYFVSLVIFGS | : | 423 |
| 1.2A0SLC4 | : | FQCITMEGWTDVLYWVNDVGRDWPWIYFVTLIIIGS | : | 393 |
| 1.2EMD_Rn | : | FQCITMEGWTDVLYWMQDAMGYELPWVYFVSLVIFGS | : | 393 |
| Cav1.1_Hs | : | YQCITMEGWTDVLYWVNDVGRDWPWIYFVTLIIIGS | : | 322 |
| Cav1.1_Oc | : | YQCITMEGWTDVLYWVNDVGRDWPWIYFVTLIIIGS | : | 322 |
| Cav1.1_Ms | : | YQCISMEGWTDVLYWVNDVGRDWPWIYFVTLIIIGS | : | 322 |
| Cav1.1_Rc | : | YQCITMEGWTEVLYWVNDVGRDWPWIYFVSLIIIGS | : | 320 |
| 1.1NP_Oc | : | YQCITMEGWTDVLYWVNDVGRDWPWIYFVTLIIIGS | : | 322 |
| 1.1NP_HS | : | YQCITMEGWTDVLYWVNDVGRDWPWIYFVTLIIIGS | : | 322 |
| 1.1XP_Cp | : | YQCITMEGWTDVLYWVNDVGRDWPWIYFVTLIIIGS | : | 322 |
| 1.1XP_Cf | : | YQCITMEGWTDVLYWVNDVGRDWPWIYFVTLIIIGS | : | 322 |
| 1.1XP_Md | : | YQCITMEGWTDVLYWVNDVGRDWPWIYFVSLIIIGS | : | 323 |
| Cav1.3_Hs | : | FQCITMEGWTDVLYWMNDAMGFELPWVYFVSLVIFGS | : | 394 |
| Cav1.3_Ms | : | FQCITMEGWTDVLYWVNDVGRDWPWIYFVSLIIIGS | : | 394 |
| Cav1.3_Gg | : | FQCITMEGWTDVLYWVNDVGRDWPWIYFVSLIIIGS | : | 389 |
| Cav1.3_Rn | : | FQCITMEGWTDVLYWVNDVGRDWPWIYFVSLIIIGS | : | 394 |
| Cav1.3_Ma | : | FQCITMEGWTDVLYWMNDAMGFELPWVYFVSLVIFGS | : | 393 |
| 1.3XP_Bt | : | FQCITMEGWTDVLYWMNDAMGFELPWVYFVSLVIFGS | : | 394 |
| 1.3XP_Cp | : | FQCITMEGWTDVLYWVNDVGRDWPWIYFVSLIIIGS | : | 395 |
| 1.3XP_Cf | : | FQCITMEGWTDVLYWVNDVGRDWPWIYFVSLIIIGS | : | 394 |
| 1.3AAA_HS | : | FQCITMEGWTDVLYWMNDAMGFELPWVYFVSLVIFGS | : | 394 |
| 1.3B0FYA3 | : | FQCITMEGWTDVLYWMNDAMGFELPWVYFVSLVIFGS | : | 394 |
| 1.3Q91W25 | : | FQCITMEGWTDVLYWMNDAMGFELPWVYFVSLVIFGS | : | 385 |
| 1.3Q8JFR0 | : | FQCITMEGWTDVLYWVNDVGRDWPWIYFVSLIIIGS | : | 397 |
| Cav1.4_Hs | : | FQCVTMEGWTDVLYWMQDAMGYELPWVYFVSLVIFGS | : | 360 |
| 1.4NP_HS g | : | FQCVTMEGWTDVLYWMQDAMGYELPWVYFVSLVIFGS | : | 360 |
| 1.4XP_Mm g | : | FQCVTMEGWTDVLYWMQDAMGYELPWVYFVSLVIFGS | : | 360 |
| 1.4XP_pre | : | FQCITMEGWTDVLYWMQDAMGYELPWVYFVSLVIFGS | : | 360 |
| 1.4XP_Cf g | : | FQCVTMEGWTDVLYWMQDAMGYELPWVYFVSLVIFGS | : | 326 |
| 1.4NP_Ms g | : | FQCITMEGWTDVLYWMQDAMGYELPWVYFVSLVIFGS | : | 360 |
| 1.4CAM_Ms | : | FQCITMEGWTDVLYWMQDAMGYELPWVYFVSLVIFGS | : | 360 |
| 1.4Q7TNI3 | : | FQCITMEGWTDVLYWMQDAMGYELPWVYFVSLVIFGS | : | 360 |
| Cav1.4_Ms | : | FQCITMEGWTDVLYWMQDAMGYELPWVYFVSLVIFGS | : | 360 |
| 1.4ABD_Rn | : | FQCITMEGWTDVLYWMQDAMGYELPWVYFVSLVIFGS | : | 360 |
| 1.4NP_Rn N | : | FQCITMEGWTDVLYWMQDAMGYELPWVYFVSLVIFGS | : | 360 |
| 1.4NP_Oc N | : | FQCITMEGWTDVLYWMQDAMGYELPWVYFVSLVIFGS | : | 423 |

|——DI-S6——|

| | | | | |
|------------|---|--|---|-----|
| Cav1.2 Oc | : | FQCITMEGWTDVLYWMQDAMGYELPWVYFVSLVIFGS | : | 423 |
| Cav1.2_Hs | : | FQCITMEGWTDVLYWVNDAVGRDWPWIYFVTLIIIGS | : | 393 |
| Cav1.2_Ms | : | FQCITMEGWTDVLYWMQDAMGYELPWVYFVSLVIFGS | : | 393 |
| Cav1.2_Rn | : | FQCITMEGWTDVLYWMQDAMGYELPWVYFVSLVIFGS | : | 423 |
| 1.2XP_Gg | : | FQCITMEGWTDVLYWVNDAIGRDWPWIYFVTLIIIGS | : | 402 |
| 1.2XP_Cf | : | FQCITMEGWTDVLYWMQDAMGYELPWVYFVSLVIFGS | : | 367 |
| 1.2NP_Hs | : | FQCITMEGWTDVLYWVNDAVGRDWPWIYFVTLIIIGS | : | 393 |
| 1.2NP_Ms | : | FQCITMEGWTDVLYWMQDAMGYELPWVYFVSLVIFGS | : | 393 |
| 1.2NP_Oc | : | FQCITMEGWTDVLYWMQDAMGYELPWVYFVSLVIFGS | : | 423 |
| 1.2A0SLC4_ | : | FQCITMEGWTDVLYWVNDAVGRDWPWIYFVTLIIIGS | : | 393 |
| 1.2EMD_Rn | : | FQCITMEGWTDVLYWMQDAMGYELPWVYFVSLVIFGS | : | 393 |
| Cav1.1_Hs | : | YQCITMEGWTDVLYWVNDAIGNEWPWIIYFVTLILLGS | : | 322 |
| Cav1.1_Oc | : | YQCITMEGWTDVLYWVNDAIGNEWPWIIYFVTLILLGS | : | 322 |
| Cav1.1_Ms | : | YQCISMEGWTDVLYWVNDAIGNEWPWIIYFVTLILLGS | : | 322 |
| Cav1.1_Rc | : | YQCITMEGWTEVLYWVNDAIGNEWPWIIYFVSLILLGS | : | 320 |
| 1.1NP_Oc | : | YQCITMEGWTDVLYWVNDAIGNEWPWIIYFVTLILLGS | : | 322 |
| 1.1NP_HS | : | YQCITMEGWTDVLYWVNDAIGNEWPWIIYFVTLILLGS | : | 322 |
| 1.1XP_Cp | : | YQCITMEGWTDVLYWVNDAIGNEWPWIIYFVTLILLGS | : | 322 |
| 1.1XP_Cf | : | YQCITMEGWTDVLYWVNDAIGNEWPWIIYFVTLILLGS | : | 322 |
| 1.1XP_Md | : | YQCITMEGWTDVLYWVNDAIGNEWPWIIYFVSLILLGS | : | 323 |
| Cav1.3_Hs | : | FQCITMEGWTDVLYWMNDAMGFELPWVYFVSLVIFGS | : | 394 |
| Cav1.3_Ms | : | FQCITMEGWTDVLYWVNDAIGWEWPWVYFVSLIILGS | : | 394 |
| Cav1.3_Gg | : | FQCITMEGWTDVLYWVNDAIGCEWPWIIYFVSLIILGS | : | 389 |
| Cav1.3_Rn | : | FQCITMEGWTDVLYWVNDAIGWEWPWVYFVSLIILGS | : | 394 |
| Cav1.3_Ma | : | FQCITMEGWTDVLYWMNDAMGFELPWVYFVSLVIFGS | : | 393 |
| 1.3XP_Bt | : | FQCITMEGWTDVLYWMNDAMGFELPWVYFVSLVIFGS | : | 394 |
| 1.3XP_Cp | : | FQCITMEGWTDVLYWVNDAIGWEWPWVYFVSLIILGS | : | 395 |
| 1.3XP_Cf | : | FQCITMEGWTDVLYWVNDAIGWEWPWVYFVSLIILGS | : | 394 |
| 1.3AAA_HS | : | FQCITMEGWTDVLYWMNDAMGFELPWVYFVSLVIFGS | : | 394 |
| 1.3B0FYA3_ | : | FQCITMEGWTDVLYWMNDAMGFELPWVYFVSLVIFGS | : | 394 |
| 1.3Q91W25_ | : | FQCITMEGWTDVLYWMNDAMGFELPWVYFVSLVIFGS | : | 385 |
| 1.3Q8JFR0_ | : | FQCITMEGWTDVLYWVNDAIGFGTPAIYFVSLIILGS | : | 397 |
| Cav1.4_Hs | : | FQCVTMEGWTDVLYWMQDAMGYELPWVYFVSLVIFGS | : | 360 |
| 1.4NP_HS g | : | FQCVTMEGWTDVLYWMQDAMGYELPWVYFVSLVIFGS | : | 360 |
| 1.4XP_Mm g | : | FQCVTMEGWTDVLYWMQDAMGYELPWVYFVSLVIFGS | : | 360 |
| 1.4XP_pre_ | : | FQCITMEGWTDVLYWMQDAMGYELPWVYFVSLVIFGS | : | 360 |
| 1.4XP_Cf g | : | FQCVTMEGWTDVLYWMQDAMGYELPWVYFVSLVIFGS | : | 326 |
| 1.4NP_Ms g | : | FQCITMEGWTDVLYWMQDAMGYELPWVYFVSLVIFGS | : | 360 |
| 1.4CAM_Ms | : | FQCITMEGWTDVLYWMQDAMGYELPWVYFVSLVIFGS | : | 360 |
| 1.4Q7TNI3_ | : | FQCITMEGWTDVLYWMQDAMGYELPWVYFVSLVIFGS | : | 360 |
| Cav1.4_Ms | : | FQCITMEGWTDVLYWMQDAMGYELPWVYFVSLVIFGS | : | 360 |
| 1.4ABD_Rn | : | FQCITMEGWTDVLYWMQDAMGYELPWVYFVSLVIFGS | : | 360 |
| 1.4NP_Rn N | : | FQCITMEGWTDVLYWMQDAMGYELPWVYFVSLVIFGS | : | 360 |
| 1.4NP_Oc N | : | FQCITMEGWTDVLYWMQDAMGYELPWVYFVSLVIFGS | : | 423 |

| | | |
|------------|---|---|
| <hr/> | | |
| Cav1.2_Oc | : | FFVLNLVLGVLSGEFSKEREKAKARGDFQKLREKQOL : 460 |
| Cav1.2_Hs | : | FFVLNLVLGVLSGEFSKEREKAKARGDFQKLREKQOL : 430 |
| Cav1.2_Ms | : | FFVLNLVLGVLSGEFSKEREKAKARGDFQKLREKQOL : 430 |
| Cav1.2_Rn | : | FFVLNLVLGVLSGEFSKEREKAKARGDFQKLREKQOL : 460 |
| 1.2XP_Gg | : | FFVLNLVLGVLSGEFSKEREKAKARGDFQKLREKQOL : 439 |
| 1.2XP_Cf | : | FFVLNLVLGVLSGEFSKEREKAKARGDFQKLREKQOL : 404 |
| 1.2NP_Hs | : | FFVLNLVLGVLSGEFSKEREKAKARGDFQKLREKQOL : 430 |
| 1.2NP_Ms | : | FFVLNLVLGVLSGEFSKEREKAKARGDFQKLREKQOL : 430 |
| 1.2NP_Oc | : | FFVLNLVLGVLSGEFSKEREKAKARGDFQKLREKQOL : 460 |
| 1.2A0SLC4_ | : | FFVLNLVLGVLSGEFSKEREKAKARGDFQKLREKQOL : 430 |
| 1.2EMD_Rn | : | FFVLNLVLGVLSGEFSKEREKAKARGDFQKLREKQOL : 430 |
| Cav1.1_Hs | : | FFILNLVLGVLSGEFTKEREKAKSRGTFQKLREKQOL : 359 |
| Cav1.1_Oc | : | FFILNLVLGVLSGEFTKEREKAKSRGTFQKLREKQOL : 359 |
| Cav1.1_Ms | : | FFILNLVLGVLSGEFTKEREKAKSRGTFQKLREKQOL : 359 |
| Cav1.1_Rc | : | FFVLNLVLGVLSGEFTKEREKAKSRGAFQMLREQQAM : 357 |
| 1.1NP_Oc | : | FFILNLVLGVLSGEFTKEREKAKSRGTFQKLREKQOL : 359 |
| 1.1NP_HS | : | FFILNLVLGVLSGEFTKEREKAKSRGTFQKLREKQOL : 359 |
| 1.1XP_Cp | : | FFILNLVLGVLSGEFTKEREKAKSRGTFQKLREKQOL : 359 |
| 1.1XP_Cf | : | FFILNLVLGVLSGEFTKEREKAKSRGTFQKLREKQOL : 359 |
| 1.1XP_Md | : | FFILNLVLGVLSGEFTKEREKAKSRGTFQKLREKQOL : 360 |
| Cav1.3_Hs | : | FFVLNLVLGVLSGEFSKEREKAKARGDFQKLREKQOL : 431 |
| Cav1.3_Ms | : | FFVLNLVLGVLSGEFSKEREKAKARGDFQKLREKQOL : 431 |
| Cav1.3_Gg | : | FFVLNLVLGVLSGEFSKEREKAKARGDFQKLREKQOL : 426 |
| Cav1.3_Rn | : | FFVLNLVLGVLSGEFSKEREKAKARGDFQKLREKQOL : 431 |
| Cav1.3_Ma | : | FFVLNLVLGVLSGEFSKEREKAKARGDFQKLRENEOL : 430 |
| 1.3XP_Bt | : | FFVLNLVLGVLSGEFSKEREKAKARGDFQKLREKQOL : 431 |
| 1.3XP_Cp | : | FFVLNLVLGVLSGEFSKEREKAKARGDFQKLREKQOL : 432 |
| 1.3XP_Cf | : | FFVLNLVLGVLSGEFSKEREKAKARGDFQKLREKQOL : 431 |
| 1.3AAA_HS | : | FFVLNLVLGVLSGEFSKEREKAKARGDFQKLREKQOL : 431 |
| 1.3B0FYA3_ | : | FFVLNLVLGVLSGEFSKEREKAKARGDFQKLREKQOL : 431 |
| 1.3Q91W25_ | : | FFVLNLVLGVLSGEFSKEREKAKARGDFQKLREKQOL : 422 |
| 1.3Q8JFR0 | : | FFVLNLVLGVLSGEFSKEREKAKARGDFQKLREKQOL : 434 |
| Cav1.4_Hs | : | FFVLNLVLGVLSGEFSKEREKAKARGDFQKQREKQOM : 397 |
| 1.4NP_HS g | : | FFVLNLVLGVLSGEFSKEREKAKARGDFQKQREKQOM : 397 |
| 1.4XP_Mm g | : | FFVLNLVLGVLSGEFSKEREKAKARGDFQKQREKQOM : 397 |
| 1.4XP_pre | : | FFVLNLVLGVLSGEFSKEREKAKARGDFQKLREKQOL : 397 |
| 1.4XP_Cf g | : | FFVLNLVLGVLSGEFSKEREKAKARGDFQKLREKQOL : 363 |
| 1.4NP_Ms g | : | FFVLNLVLGVLSGEFSKEREKAKARGDFQKLREKQOM : 397 |
| 1.4CAM_Ms | : | FFVLNLVLGVLSGEFSKEREKAKARGDFQKLREKQOM : 397 |
| 1.4Q7TNI3_ | : | FFVLNLVLGVLSGEFSKEREKAKARGDFQKLREKQOM : 397 |
| Cav1.4_Ms | : | FFVLNLVLGVLSGEFSKEREKAKARGDFQKLREKQOM : 397 |
| 1.4ABD_Rn | : | FFVLNLVLGVLSGEFSKEREKAKARGDFQKLREKQOM : 397 |
| 1.4NP_Rn N | : | FFVLNLVLGVLSGEFSKEREKAKARGDFQKLREKQOM : 397 |
| 1.4NP_Oc N | : | FFVLNLVLGVLSGEFSKEREKAKARGDFQKLREKQOL : 460 |
| ***** | | |

-DII-L45-

```

Cav1.2_Oc : VETKVMSPLGISVLRVRLRLRIFKITRYWNSLSNLVA : 672
Cav1.2_Hs : VETKIMSPLGISVLRVRLRLRIFKITRYWNSLSNLVA : 642
Cav1.2_Ms : VETKIMSPLGISVLRVRLRLRIFKITRYWNSLSNLVA : 642
Cav1.2_Rn : VETKIMSPLGISCWRCVRLRLRIFKITRYWNSLSNLVA : 672
1.2XP_Gg : VETKIMSPLGISVLRVRLRLRIFKITRYWNSLSNLVA : 651
1.2XP_Cf : VETKIMSPLGISVLRVRLRLRIFKITRYWNSLSNLVA : 616
1.2NP_Hs : VETKIMSPLGISVLRVRLRLRIFKITRYWNSLSNLVA : 642
1.2NP_Ms : VETKIMSPLGISVLRVRLRLRIFKITRYWNSLSNLVA : 642
1.2NP_Oc : VETKVMSPLGISVLRVRLRLRIFKITRYWNSLSNLVA : 672
1.2A0SLC4_ : VETKIMSPLGISVLRVRLRLRIFKITRYWNSLSNLVA : 667
1.2EMD_Rn : VETKIMSPLGISVLRVRLRLRIFKITRYWNSLSNLVA : 642
Cav1.1_Hs : VESGAMTPLGISVLR CIRLLRIFKITKYWTSLSNLVA : 550
Cav1.1_Oc : VESGAMTPLGISVLR CIRLLRLFKITKYWTSLSNLVA : 550
Cav1.1_Ms : VESGAMSPLGISVLR CIRLLRLFKITKYWTSLSNLVA : 550
Cav1.1_Rc : VASDIMSPLGISVLR CIRLLRIFKITRYWTSLSNLVA : 549
1.1NP_Oc : VESGAMTPLGISVLR CIRLLRLFKITKYWTSLSNLVA : 550
1.1NP_HS : VESGAMTPLGISVLR CIRLLRIFKITKYWTSLSNLVA : 550
1.1XP_Cp : VESGAMTPLGISVLR CIRLLRIFKITKYWTSLSNLVA : 550
1.1XP_Cf : VESGAMSPLGISVLR CIRLLRIFKITKYWTSLSNLVA : 550
1.1XP_Md : VESGIMTPLGISVLR CIRLLRLFKITKYWTSLSNLVA : 551
Cav1.3_Hs : VELEIMSPLGISVFR CVRLRLRIFKVTRHWTSLNLVA : 641
Cav1.3_Ms : VELEIMSPLGVSVFR CVRLRLRIFKVTRHWTSLNLVA : 661
Cav1.3_Gg : VELEIMSPLGISVFR CVRLRLRIFKVTRHWASLSNLVA : 662
Cav1.3_Rn : VELEIMSPLGVSVFR CVRLRLRIFKVTRHWTSLNLVA : 700
Cav1.3_Ma : VELEIMSPLGVSVFR CVRLRLRIFKVTRHWTSLNLVA : 640
1.3XP_Bt : VELEIMSPLGISVFR CVRLRLRIFKVTRHWTSLNLVA : 641
1.3XP_Cp : VELEIMSPLGISVFR CVRLRLRIFKVTRHWTSLNLVA : 662
1.3XP_Cf : VELEIMSPLGISVFR CVRLRLRIFKVTRHWTSLNLVA : 641
1.3AAA_HS : VELEIMSPLGISVFR CVRLRLRIFKVTRHWTSLNLVA : 641
1.3B0FYA3_ : VELEIMSPLGISVFR CVRLRLRIFKVTRHWTSLNLVA : 641
1.3Q91W25_ : VELEIMSPLGVSVFR CVRLRLRIFKVTRHWTSLNLVA : 632
1.3Q8JFR0 : VELAIMSPLGISVFR CVRLRLRIFKVTRHWQSLNLVA : 662
Cav1.4_Hs : VEVGAMQPLGISVLR CVRLRLRIFKVTRHWASLSNLVA : 647
1.4NP_HS|g : VEVGAMQPLGISVLR CVRLRLRIFKVTRHWASLSNLVA : 647
1.4XP_Mm|g : -----LYKCQLLLLFIIISRHASLSNLVA : 577
1.4XP_pre_ : VEVGAMQPLGISVLR CVRLRLRIFKVTRHWASLSNLVA : 644
1.4XP_Cf|g : VEVGAMQPLGISVLR CVRLRLRIFKVTRHWASLSNLVA : 552
1.4NP_Ms|g : VEVGAMQPLGISVLR CVRLRLRIFKVTRHWASLSNLVA : 647
1.4CAM_Ms| : VEVGAMQPLGISVLR CVRLRLRIFKVTRHWASLSNLVA : 647
1.4Q7TNI3_ : VEVGAMQPLGISVLR CVRLRLRIFKVTRHWASLSNLVA : 647
Cav1.4_Ms : VEVGAMQPLGISVLR CVRLRLRIFKVTRHWASLSNLVA : 647
1.4ABD_Rn| : VEVGAMQPLGISVLR CVRLRLRIFKVTRHWASLSNLVA : 647
1.4NP_Rn|N : VEVGAMQPLGISVLR CVRLRLRIFKVTRHWASLSNLVA : 647
1.4NP_Oc|N : VETKVMSPLGISVLRVRLRLRIFKITRYWNSLSNLVA : 672
*****

```

DII-S5

| | | | | | |
|------------|---|--------------------------|-----------------|---|-----|
| Cav1.2 Oc | : | SLLNSVRSIASLLLLLFLFIIIFS | SLLGMQLFGGKFNF | : | 709 |
| Cav1.2_Hs | : | SLLNSVRSIASLLLLLFLFIIIFS | SLLGMQLFGGKFNF | : | 679 |
| Cav1.2_Ms | : | SLLNSVRSIASLLLLLFLFIIIFS | SLLGMQLFGGKFNF | : | 679 |
| Cav1.2_Rn | : | SLLNSLRSIASLLLLLFLFIIIFS | SLLGMQLFGGKFNF | : | 709 |
| 1.2XP_Gg | : | SLLNSVRSIASLLLLLFLFIIIFS | SLLGMQLFGGKFNF | : | 688 |
| 1.2XP_Cf | : | SLLNSVRSIASLLLLLFLFIIIFS | SLLGMQLFGGKFNF | : | 653 |
| 1.2NP_Hs | : | SLLNSVRSIASLLLLLFLFIIIFS | SLLGMQLFGGKFNF | : | 679 |
| 1.2NP_Ms | : | SLLNSVRSIASLLLLLFLFIIIFS | SLLGMQLFGGKFNF | : | 679 |
| 1.2NP_Oc | : | SLLNSVRSIASLLLLLFLFIIIFS | SLLGMQLFGGKFNF | : | 709 |
| 1.2A0SLC4_ | : | SLLNSVRSIASLLLLLFLFIIIFS | SLLGMQLFGGKFNF | : | 704 |
| 1.2EMD_Rn | : | SLLNSVRSIASLLLLLFLFIIIFS | SLLGMQLFGGKFNF | : | 679 |
| Cav1.1_Hs | : | SLLNSIRSIASLLLLLFLFIVIF | ALLGMQLFGGRYDF | : | 587 |
| Cav1.1_Oc | : | SLLNSIRSIASLLLLLFLFIIIF | ALLGMQLFGGRYDF | : | 587 |
| Cav1.1_Ms | : | SLLNSIRSIASLLLLLFLFIIIF | ALLGMQLFGGRYDF | : | 587 |
| Cav1.1_Rc | : | SLLNSVRSIASLLLLLFLFMIIF | ALLGMQMFGGKFDF | : | 586 |
| 1.1NP_Oc | : | SLLNSIRSIASLLLLLFLFIIIF | ALLGMQLFGGRYDF | : | 587 |
| 1.1NP_HS | : | SLLNSIRSIASLLLLLFLFIVIF | ALLGMQLFGGRYDF | : | 587 |
| 1.1XP_Cp | : | SLLNSIRSIASLLLLLFLFIVIF | ALLGMQLFGGRYDF | : | 587 |
| 1.1XP_Cf | : | SLLNSIRSIASLLLLLFLFIIIF | IDLLGMQLFGGRYDF | : | 587 |
| 1.1XP_Md | : | SLLNSIRSIASLLLLLFLFIIIF | ALLGMQLFGGKYDF | : | 588 |
| Cav1.3_Hs | : | SLLNSMKSIASLLLLLFLFIIIFS | SLLGMQLFGGKFNF | : | 678 |
| Cav1.3_Ms | : | SLLNSMKSIASLLLLLFLFIIIFS | SLLGMQLFGGKFNF | : | 698 |
| Cav1.3_Gg | : | SLLNSMKSIASLLLLLFLFIIIFS | SLLGMQLFGGKFNF | : | 699 |
| Cav1.3_Rn | : | SLLNSMKSIASLLLLLFLFIIIFS | SLLGMQLFGGKFNF | : | 737 |
| Cav1.3_Ma | : | SLLNSMKSIASLLLLLFLFIIIFS | SLLGMQLFGGKFNF | : | 677 |
| 1.3XP_Bt | : | SLLNSMKSIASLLLLLFLFIIIFS | SLLGMQLFGGKFNF | : | 678 |
| 1.3XP_Cp | : | SLLNSMKSIASLLLLLFLFIIIFS | SLLGMQLFGGKFNF | : | 699 |
| 1.3XP_Cf | : | SLLNSMKSIASLLLLLFLFIIIFS | SLLGMQLFGGKFNF | : | 678 |
| 1.3AAA_HS | : | SLLNSMKSSASLLLLLFLFIIIFS | SLLGMQLFGGKFNF | : | 678 |
| 1.3B0FYA3_ | : | SLLNSMKSIASLLLLLFLFIIIFS | SLLGMQLFGGKFNF | : | 678 |
| 1.3Q91W25_ | : | SLLNSMKSIASLLLLLFLFIIIFS | SLLGMQLFGGKFNF | : | 669 |
| 1.3Q8JFR0_ | : | SLLNSMKSIASLLLLLFLFIIIFS | SLLGMQVFGGKFNF | : | 699 |
| Cav1.4_Hs | : | SLLNSMKSIASLLLLLFLFIIIFS | SLLGMQLFGGKFNF | : | 684 |
| 1.4NP_HS g | : | SLLNSMKSIASLLLLLFLFIIIFS | SLLGMQLFGGKFNF | : | 684 |
| 1.4XP_Mm g | : | SLLNSMKSIASLLLLLFLFIIIFS | SLLGMQLFGGKFNF | : | 614 |
| 1.4XP_pre_ | : | SLLNSMKSIASLLLLLFLFIIIFS | SLLGMQLFGGKFNF | : | 681 |
| 1.4XP_Cf g | : | SLLNSMKSIASLLLLLFLFIIIFS | SLLGMQLFGGKFNF | : | 589 |
| 1.4NP_Ms g | : | SLLNSMKSIASLLLLLFLFIIIFS | SLLGMQLFGGKFNF | : | 684 |
| 1.4CAM_Ms | : | SLLNSMKSIASLLLLLFLFIIIFS | SLLGMQLFGGKFNF | : | 684 |
| 1.4Q7TNI3_ | : | SLLNSMKSIASLLLLLFLFIIIFS | SLLGMQLFGGKFNF | : | 684 |
| Cav1.4_Ms | : | SLLNSMKSIASLLLLLFLFIIIFS | SLLGMQLFGGKFNF | : | 684 |
| 1.4ABD_Rn | : | SLLNSMKSIASLLLLLFLFIIIFS | SLLGMQLFGGKFNF | : | 684 |
| 1.4NP_Rn N | : | SLLNSMKSIASLLLLLFLFIIIFS | SLLGMQLFGGKFNF | : | 684 |
| 1.4NP_Oc N | : | SLLNSVRSIASLLLLLFLFIIIFS | SLLGMQLFGGKFNF | : | 709 |

| | | DII-P | | |
|------------|---|---------------------------------------|---|-----|
| Cav1.2_Oc | : | DEMOTRRSTFDNFPQSLLTVFQILTGEDWNSVMYDGI | : | 746 |
| Cav1.2_Hs | : | DEMOTRRSTFDNFPQSLLTVFQILTGEDWNSVMYDGI | : | 716 |
| Cav1.2_Ms | : | DEMOTRRSTFDNFPQSLLTVFQILTGEDWNSVMYDGI | : | 716 |
| Cav1.2_Rn | : | DEMOTRRSTFDNFPQSLLTVFQILTGEDWNSVMYDGI | : | 746 |
| 1.2XP_Gg | : | DEMOTRRSTFDNFPQSLLTVFQILTGEDWNSVMYDGI | : | 725 |
| 1.2XP_Cf | : | DEMOTRRSTFDNFPQSLLTVFQILTGEDWNSVMYDGI | : | 690 |
| 1.2NP_Hs | : | DEMOTRRSTFDNFPQSLLTVFQILTGEDWNSVMYDGI | : | 716 |
| 1.2NP_Ms | : | DEMOTRRSTFDNFPQSLLTVFQILTGEDWNSVMYDGI | : | 716 |
| 1.2NP_Oc | : | DEMOTRRSTFDNFPQSLLTVFQILTGEDWNSVMYDGI | : | 746 |
| 1.2A0SLC4 | : | DEMOTRRSTFDNFPQSLLTVFQILTGEDWNSVMYDGI | : | 741 |
| 1.2EMD_Rn | : | DEMOTRRSTFDNFPQSLLTVFQILTGEDWNSVMYDGI | : | 716 |
| Cav1.1_Hs | : | EDTEVRRSNFDNFPQALISVFQVLTGEDWTSMMYNGI | : | 624 |
| Cav1.1_Oc | : | EDTEVRRSNFDNFPQALISVFQVLTGEDWTSMMYNGI | : | 624 |
| Cav1.1_Ms | : | EDTEVRRSNFDNFPQALISVFQVLTGEDWTSMMYNGI | : | 624 |
| Cav1.1_Rc | : | EDLEVRRSTFDTFPQALITVFQILTGEDWTAVMYNGI | : | 623 |
| 1.1NP_Oc | : | EDTEVRRSNFDNFPQALISVFQVLTGEDWTSMMYNGI | : | 624 |
| 1.1NP_HS | : | EDTEVRRSNFDNFPQALISVFQVLTGEDWTSMMYNGI | : | 624 |
| 1.1XP_Cp | : | EDTEVRRSNFDNFPQALISVFQVLTGEDWTSMMYNGI | : | 624 |
| 1.1XP_Cf | : | EDTEVRRSNFDNFPQALISVFQVLTGEDWTSMMYSGI | : | 624 |
| 1.1XP_Md | : | EDTEVRRSTFDNFPQALISVFQILTGEDWNSIMYNGI | : | 625 |
| Cav1.3_Hs | : | DETQTKRSTFDNFPQALLTVFQILTGEDWNAVMYDGI | : | 715 |
| Cav1.3_Ms | : | DETQTKRSTFDNFPQALLTVFQILTGEDWNAVMYDGI | : | 735 |
| Cav1.3_Gg | : | DETQTKRSTFDNFPQALLTVFQILTGEDWNAVMYDGI | : | 736 |
| Cav1.3_Rn | : | DETQTKRSTFDNFPQALLTVFQILTGEDWNAVMYDGI | : | 774 |
| Cav1.3_Ma | : | DETQTKRSTFDNFPQALLTVFQILTGEDWNAVMYDGI | : | 714 |
| 1.3XP_Bt | : | DETQTKRSTFDNFPQALLTVFQILTGEDWNAVMYDGI | : | 715 |
| 1.3XP_Cp | : | DETQTKRSTFDNFPQALLTVFQILTGEDWNAVMYDGI | : | 736 |
| 1.3XP_Cf | : | DETQTKRSTFDNFPQALLTVFQILTGEDWNAVMYDGI | : | 715 |
| 1.3AAA_HS | : | DETQTKRSTFDNFPQALLTVFQILTGEDWNAVMYDGI | : | 715 |
| 1.3B0FYA3 | : | DETQTKRSTFDNFPQALLTVFQILTGEDWNAVMYDGI | : | 715 |
| 1.3Q91W25 | : | DETQTKRSTFDNFPQALLTVFQILTGEDWNAVMYDGI | : | 706 |
| 1.3Q8JFR0 | : | DETQTKRSTFDNFPQALLTVFQILTGEDWNAVMYDGI | : | 736 |
| Cav1.4_Hs | : | DQTHTKRSTFDTFPQALLTVFQILTGEDWNVVMYDGI | : | 721 |
| 1.4NP_HS g | : | DQTHTKRSTFDTFPQALLTVFQILTGEDWNVVMYDGI | : | 721 |
| 1.4XP_Mm g | : | DQTHTKRSTFDTFPQALLTVFQILTGEDWNVVMYDGI | : | 651 |
| 1.4XP_pre | : | DQTHTKRSTFDTFPQALLTVFQILTGEDWNVVMYDGI | : | 718 |
| 1.4XP_Cf g | : | DQTHTKRSTFDTFPQALLTVFQILTGEDWNVGMYDGI | : | 626 |
| 1.4NP_Ms g | : | DQTHTKRSTFDTFPQALLTVFQILTGEDWNVVMYDGI | : | 721 |
| 1.4CAM_Ms | : | DQTHTKRSTFDTFPQALLTVFQILTGEDWNVVMYDGI | : | 721 |
| 1.4Q7TNI3 | : | DQTHTKRSTFDTFPQALLTVFQILTGEDWNVVMYDGI | : | 721 |
| Cav1.4_Ms | : | DQTHTKRSTFDTFPQALLTVFQILTGEDWNVVMYDGI | : | 721 |
| 1.4ABD_Rn | : | DQTHTKRSTFDTFPQALLTVFQILTGEDWNVVMYDGI | : | 721 |
| 1.4NP_Rn N | : | DQTHTKRSTFDTFPQALLTVFQILTGEDWNVVMYDGI | : | 721 |
| 1.4NP_Oc N | : | DEMOTRRSTFDNFPQSLLTVFQILTGEDWNSVMYDGI | : | 746 |

| | | DII-S6 | | | |
|------------|---|---------------------------------------|-----------|---|-----|
| Cav1.2 Oc | : | MAYGGPSFPGMLVCIYFIILFICGN--- | YILLNVF-L | : | 779 |
| Cav1.2_Hs | : | MAYGGPSFPGMLVCIYFIILFICGN--- | YILLNVF-L | : | 749 |
| Cav1.2_Ms | : | MAYGGPSFPGMLVCIYFIILFICGN--- | YILLNVF-L | : | 749 |
| Cav1.2_Rn | : | MAYGGPSFPGMLVCIYFIILFISPN--- | YILLNLF-L | : | 779 |
| 1.2XP_Gg | : | MAYGGPSFPGMLVCIYFIILFICGN--- | YILLNVF-L | : | 758 |
| 1.2XP_Cf | : | MAYGGPSFPGMLVCIYFIILFICGN--- | YILLNVF-L | : | 723 |
| 1.2NP_Hs | : | MAYGGPSFPGMLVCIYFIILFICGN--- | YILLNVF-L | : | 749 |
| 1.2NP_Ms | : | MAYGGPSFPGMLVCIYFIILFICGN--- | YILLNVF-L | : | 749 |
| 1.2NP_Oc | : | MAYGGPSFPGMLVCIYFIILFICGN--- | YILLNVF-L | : | 779 |
| 1.2A0SLC4 | : | MAYGGPSFPGMLVCIYFIILFICGN--- | YILLNVF-L | : | 774 |
| 1.2EMD_Rn | : | MAYGGPSFPGMLVCIYFIILFICGN--- | YILLNVF-L | : | 749 |
| Cav1.1_Hs | : | MAYGGPSYPGMLVCIYFIILFVCGN--- | YILLNVF-L | : | 657 |
| Cav1.1_Oc | : | MAYGGPSYPGVLVCIYFIILFVCGN--- | YILLNVF-L | : | 657 |
| Cav1.1_Ms | : | MAYGGPTYPGVLVCIYFIILFVCGN--- | YILLNVF-L | : | 657 |
| Cav1.1_Rc | : | MAYGGPTYSGMSVCIYFIILFVCGN--- | YILLNVF-L | : | 656 |
| 1.1NP_Oc | : | MAYGGPSYPGVLVCIYFIILFVCGN--- | YILLNVF-L | : | 657 |
| 1.1NP_HS | : | MAYGGPSYPGMLVCIYFIILFVCGN--- | YILLNVF-L | : | 657 |
| 1.1XP_Cp | : | MAYGGPSYPGMLVCIYFIILFVCGN--- | YILLNVF-L | : | 657 |
| 1.1XP_Cf | : | MAYGGPSYPGVLVCIYFIILFVCGNSPPKIRIKVF-W | | : | 660 |
| 1.1XP_Md | : | MAYGGPSYPGVLVCIYFIILFICGN--- | YILLNVF-L | : | 658 |
| Cav1.3_Hs | : | MAYGGPSSSGMIVCIYFIILFICGN--- | YILLNVF-L | : | 748 |
| Cav1.3_Ms | : | MAYGGPSSSGMIVCIYFIILFICGN--- | YILLNVF-L | : | 768 |
| Cav1.3_Gg | : | MAYGGPSSSGMIVCIYFIILFICGN--- | YILLNVF-L | : | 769 |
| Cav1.3_Rn | : | MAYGGPSSSGMIVCIYFIILFICGN--- | YILLKLF-L | : | 807 |
| Cav1.3_Ma | : | MAYGGPSSSGMIVCIYFIILFICGN--- | YILLNVF-L | : | 747 |
| 1.3XP_Bt | : | MAYGGPSSSGMIVCIYFIILFICGN--- | YILLNVF-L | : | 748 |
| 1.3XP_Cp | : | MAYGGPSSSGMIVCIYFIILFICGN--- | YILLNVF-L | : | 769 |
| 1.3XP_Cf | : | MAYGGPSSSGMIVCIYFIILFICGN--- | YILLNVF-L | : | 748 |
| 1.3AAA_HS | : | MAYGGPSSSGMIVCIYFIILFICGN--- | YILLNVF-L | : | 748 |
| 1.3B0FYA3 | : | MAYGGPSSSGMIVCIYFIILFICGN--- | YILLNVF-L | : | 748 |
| 1.3Q91W25 | : | MAYGGPSSSGMIVCIYFIILFICGN--- | YILLNVF-L | : | 739 |
| 1.3Q8JFR0 | : | MAYGGPSSSGMIVSFYFIILFICGN--- | YILLNVF-L | : | 770 |
| Cav1.4_Hs | : | MAYGGPFFPGMLVCIYFIILFICGN--- | YILLNVF-L | : | 754 |
| 1.4NP_HS g | : | MAYGGPFFPGMLVCIYFIILFICGN--- | YILLNVF-L | : | 754 |
| 1.4XP_Mm g | : | MAYGGPFFPGMLVCIYFIILFICGN--- | YILLNVF-L | : | 684 |
| 1.4XP_pre | : | MAYGGPFFPGMLVCVYFIILFICGN--- | YILLNVF-L | : | 751 |
| 1.4XP_Cf g | : | MAYGGPFFPGMLVCVYFIILFICGN--- | CILG---- | : | 655 |
| 1.4NP_Ms g | : | MAYGGPFFPGMLVCVYFIILFICGN--- | YILLNVF-L | : | 754 |
| 1.4CAM_Ms | : | MAYGGPFFPGMLVCVYFIILFICGN--- | YILLNVF-L | : | 754 |
| 1.4Q7TNI3 | : | MAYGGPFFPGMLVCVYFIILFICGN--- | YILLNVF-L | : | 754 |
| Cav1.4_Ms | : | MAYGGPFFPGMLVCVYFIILFICGN--- | YILLNVF-L | : | 754 |
| 1.4ABD_Rn | : | MAYGGPFFPGMLVCVYFIILFICGN--- | YILLNVF-L | : | 754 |
| 1.4NP_Rn N | : | MAYGGPFFPGMLVCVYFIILFICGN--- | YILLNVF-L | : | 754 |
| 1.4NP_Oc N | : | MAYGGPSFPGMLVCIYFIILFICGN--- | YILLNVF-L | : | 779 |

| | | |
|---|---|-------|
| <hr style="width: 100px; margin-left: 0;"/> | | |
| Cav1.2_Oc | : AIAVDNLADAESLTSAQKEEEEEKERKKLARTASPEK | : 816 |
| Cav1.2_Hs | : AIAVDNLADAESLTSAQKEEEEEKERKKLARTASPEK | : 786 |
| Cav1.2_Ms | : AIAVDNLADAESLTSAQKEEEEEKERKKLARTASPEK | : 786 |
| Cav1.2_Rn | : AIAVDNLADAESLTSAQKEEEEEKERKKLARTASPEK | : 816 |
| 1.2XP_Gg | : AIAVDNLADAESLTSAQKEEEEEKERKKLARTASPEK | : 795 |
| 1.2XP_Cf | : AIAVDNLADAESLTSAQKEEEEEKERKKLARTASPEK | : 760 |
| 1.2NP_Hs | : AIAVDNLADAESLTSAQKEEEEEKERKKLARTASPEK | : 786 |
| 1.2NP_Ms | : AIAVDNLADAESLTSAQKEEEEEKERKKLARTASPEK | : 786 |
| 1.2NP_Oc | : AIAVDNLADAESLTSAQKEEEEEKERKKLARTASPEK | : 816 |
| 1.2A0SLC4 | : AIAVDNLADAESLTSAQKEEEEEKERKKLARTASPEK | : 811 |
| 1.2EMD_Rn | : AIAVDNLADAESLTSAQKEEEEEKERKKLARTASPEK | : 786 |
| Cav1.1_Hs | : AIAVDNLAEAESLTSAQKAKAEKKRRKMSKGLPDKS | : 694 |
| Cav1.1_Oc | : AIAVDNLAEAESLTSAQKAKAEKKRRKMSRGLPDKT | : 694 |
| Cav1.1_Ms | : AIAVDNLAEAESLTSAQKAKAEKKRRKMSKGLPDKS | : 694 |
| Cav1.1_Rc | : AIAVDNLAEAENLTSAQKAKAEKKRRKMLARANPDKT | : 693 |
| 1.1NP_Oc | : AIAVDNLAEAESLTSAQKAKAEKKRRKMSRGLPDKT | : 694 |
| 1.1NP_HS | : AIAVDNLAEAESLTSAQKAKAEKKRRKMSKGLPDKS | : 694 |
| 1.1XP_Cp | : AIAVDNLAEAESLTSAQKAKAEKKRRKMSKGLPDKS | : 694 |
| 1.1XP_Cf | : GIVWKNRGKEKSLLFPPKANPVVRKRRKMSKGLPDKS | : 697 |
| 1.1XP_Md | : AIAVDNLAEAESLTSAQKAKAEKKRRKMSKGLPDKS | : 695 |
| Cav1.3_Hs | : AIAVDNLADAESLNTAQKEEAEEKERKKIAR----- | : 779 |
| Cav1.3_Ms | : AIAVDNLADAESLNTAQKEEAEEKERKKIAR----- | : 799 |
| Cav1.3_Gg | : AIAVDNLADAESLNTAQKEEAEEKERKKIAR----- | : 800 |
| Cav1.3_Rn | : AIAVDNLADAESLNTAQKEEAEEKERKKIAR----- | : 838 |
| Cav1.3_Ma | : AIAVDNLADAESLNTAQKEEAEEKERKKIAR----- | : 778 |
| 1.3XP_Bt | : AIAVDNLADAESLNTAQKEEAEEKERKKIAR----- | : 779 |
| 1.3XP_Cp | : AIAVDNLADAESLNTAQKEEAEEKERKKIAR----- | : 800 |
| 1.3XP_Cf | : AIAVDNLADAESLNTAQKEEAEEKERKKIAR----- | : 779 |
| 1.3AAA_HS | : AIAVDNLADAESLNTAQKEEAEEKERKKIAR----- | : 779 |
| 1.3B0FYA3 | : AIAVDNLADAESLNTAQKEEAEEKERKKIAR----- | : 779 |
| 1.3Q91W25 | : AIAVDNLADAESLNTAQKEEAEEKERKKIAR----- | : 770 |
| 1.3Q8JFR0 | : AIAVDNLGDAESLNAPRDKKEEKKE----- | : 795 |
| Cav1.4_Hs | : AIAVDNLASGDAGTAKDKGGEKSNEKDLPQE----- | : 785 |
| 1.4NP_HS g | : AIAVDNLASGDAGTAKDKGGEKSNEKDLPQE----- | : 785 |
| 1.4XP_Mm g | : AIAVDNLASGDAGTAKDKGGEKSSEKDLPPE----- | : 715 |
| 1.4XP_pre | : AIAVDNLASGDAGTDKDKGREK-ITEETPQE----- | : 781 |
| 1.4XP_Cf g | : ----- | : - |
| 1.4NP_Ms g | : AIAVDNLASGDAGTAKDKGREKSSEGNPPKE----- | : 785 |
| 1.4CAM_Ms | : AIAVDNLASGDAGTAKDKGREKSSEGNPPKE----- | : 785 |
| 1.4Q7TNI3 | : AIAVDNLASGDAGTAKDKGREKSSEGNPPKE----- | : 785 |
| Cav1.4_Ms | : AIAVDNLASGDAGTAKDKGREKSSEGNPPKE----- | : 785 |
| 1.4ABD_Rn | : AIAVDNLASGDAGAAKDKGREKSSEGNPPQE----- | : 785 |
| 1.4NP_Rn N | : AIAVDNLASGDAGAAKDKGREKSSEGNPPQE----- | : 785 |
| 1.4NP_Oc N | : AIAVDNLADAESLTSAQKEEEEEKERKKLARTASPEK | : 816 |
| ***** | | |

Appendix III - Multiply sequence alignment of pore domain III to IV

-DIII-L45-


```

Cav1.2_Oc      : FGIQSSAINVVKILRVLRLPLRAINRAKGLKHVVQ : 1050
Cav1.2_Hs      : FGIQSSAINVVKILRVLRLPLRAINRAKGLKHVVQ : 1040
Cav1.2_Ms      : FGIQSSAINVVKILRVLRLPLRAINRAKGLKHVVQ : 1020
Cav1.2_Rn      : FGIQSSAINVVKILRVLRLPLRLIN-RAKGLKHVVQ : 1049
1.2XP_Gg       : FGIQSSAINVVKILRVLRLPLRAINRAKGLKHVVQ : 1029
1.2XP_Cf       : FGIQSSAINVVKILRVLRLPLRAINRAKGLKHVVQ : 994
1.2NP_Hs       : FGIQSSAINVVKILRVLRLPLRAINRAKGLKHVVQ : 104
1.2NP_Ms       : FGIQSSAINVVKILRVLRLPLRAINRAKGLKHVVQ : 1020
1.2NP_Oc       : FGIQSSAINVVKILRVLRLPLRAINRAKGLKHVVQ : 1050
1.2A0SLC4_     : FGIQSSAINVVKILRVLRLPLRAINRAKGLKHVVQ : 1045
1.2EMD_Rn      : FGIQSSAINVVKILRVLRLPLRAINRAKGLKHVVQ : 1020
Cav1.1_Hs      : MGLESSAISVVKILRVLRLPLRAINRAKGLKHVVQ : 919
Cav1.1_Oc      : MGLESSTISVVKILRVLRLPLRAINRAKGLKHVVQ : 919
Cav1.1_Ms      : MGLESSAISVVKILRVLRLPLRAINRAKGLKHVVQ : 919
Cav1.1_Rc      : MGISSAISVVKILRVLRLPLRAINRAKGLKHVVQ : 917
1.1NP_Oc       : MGLESSTISVVKILRVLRLPLRAINRAKGLKHVVQ : 919
1.1NP_HS       : MGLESSAISVVKILRVLRLPLRAINRAKGLKHVVQ : 919
1.1XP_Cp       : MGLESSTISVVKILRVLRLPLRAINRAKGLKHVVQ : 919
1.1XP_Cf       : MGLESSTISVVKILRVLRLPLRAINRAKGLKHVVQ : 922
1.1XP_Md       : TGISSAISVVKILRVLRLPLRAINRAKGLKHVVQ : 920
Cav1.3_Hs      : FGIQSSAISVVKILRVLRLPLRAINRAKGLKHVVQ : 1006
Cav1.3_Ms      : FGIQSSAISVVKILRVLRLPLRAINRAKGLKHVVQ : 1026
Cav1.3_Gg      : FGIQSSAISVVKILRVLRLPLRAINRAKGLKHVVQ : 1027
Cav1.3_Rn      : FGIQSSAISVVKILRVLRLPLRAINRAKGLKHVVQ : 1065
Cav1.3_Ma      : FGIQSSAISVVKILRVLRLPLRAINRAKGLKHVVQ : 1004
1.3XP_Bt       : FGIQSSAISVVKILRVLRLPLRAINRAKGLKHVVQ : 1006
1.3XP_Cp       : FGIQSSAISVVKILRVLRLPLRAINRAKGLKHVVQ : 1027
1.3XP_Cf       : FGIQSSAISVVKILRVLRLPLRAINRAKGLKHVVQ : 1006
1.3AAA_HS      : FGIQSSAISVVKILRVLRLPLRAINRAKGLKHVVQ : 1006
1.3B0FYA3_     : FGIQSSAISVVKILRVLRLPLRAINRAKGLKHVVQ : 1006
1.3Q91W25_     : FGIQSSAISVVKILRVLRLPLRAINRAKGLKHVVQ : 996
1.3Q8JFR0_     : FGIQSSAISVVKILRVLRLPLRAINRAKGLKHVIQ : 983
Cav1.4_Hs      : FGIHSSAISVVKILRVLRLPLRAINRAKGLKHVVQ : 991
1.4NP_HS|g     : FGIHSSAISVVKILRVLRLPLRAINRAKGLKHVVQ : 991
1.4XP_Mm|g     : FGIHSSAISVVKILRVLRLPLRAINRAKGLKHVVQ : 917
1.4XP_pre_     : FGIHSSAISVVKILRVLRLPLRAINRAKGLKHVVQ : 987
1.4XP_Cf|g     : FGIHSSAISVVKILRVLRLPLRAINRAKGLKHVVQ : 840
1.4NP_Ms|g     : FGIHSSAISVVKILRVLRLPLRAINRAKGLKHVVQ : 994
1.4CAM_Ms|     : FGIHSSAISVVKILRVLRLPLRAINRAKGLKHVVQ : 994
1.4Q7TNI3_     : FGIHSSAISVVKILRVLRLPLRAINRAKGLKHVVQ : 994
Cav1.4_Ms      : FGIHSSAISVVKILRVLRLPLRAINRAKGLKHVVQ : 996
1.4ABD_Rn|     : FGIHSSAISVVKILRVLRLPLRAINRAKGLKHVVQ : 990
1.4NP_Rn|N     : FGIHSSAISVVKILRVLRLPLRAINRAKGLKHVVQ : 990
1.4NP_Oc|N     : FGIQSSAINVVKILRVLRLPLRAINRAKGLKHVVQ : 1050

```

|-----DIII-S5-----|

| | | | | |
|------------|---|---------------------------------------|---|------|
| Cav1.2_Oc | : | CVFVAIRTIGNIVIVTTLQFMFACIGVQLFKGKLYT | : | 1087 |
| Cav1.2_Hs | : | CVFVAIRTIGNIVIVTTLQFMFACIGVQLFKGKLYT | : | 1077 |
| Cav1.2_Ms | : | CVFVAIRTIGNIVIVTTLQFMFACIGVQLFKGKLYT | : | 1057 |
| Cav1.2_Rn | : | CVFVAIRTIGNIVIVTTLQFMFACIGVQLFKGKLYT | : | 1086 |
| 1.2XP_Gg | : | CVFVAIRTIGNIVIVTTLQFMFACIGVQLFKGKLYS | : | 1066 |
| 1.2XP_Cf | : | CVFVAIRTIGNIVIVTTLQFMFACIGVQLFKGKLYT | : | 1031 |
| 1.2NP_Hs | : | CVFVAIRTIGNIVIVTTLQFMFACIGVQLFKGKLYT | : | 1077 |
| 1.2NP_Ms | : | CVFVAIRTIGNIVIVTTLQFMFACIGVQLFKGKLYT | : | 1057 |
| 1.2NP_Oc | : | CVFVAIRTIGNIVIVTTLQFMFACIGVQLFKGKLYT | : | 1087 |
| 1.2A0SLC4_ | : | CVFVAIRTIGNIVIVTTLQFMFACIGVQLFKGKLYT | : | 1082 |
| 1.2EMD_Rn | : | CVFVAIRTIGNIVIVTTLQFMFACIGVQLFKGKLYT | : | 1057 |
| Cav1.1_Hs | : | CMFVAISTIGNIVLVTTLLQFMFACIGVQLFKGKFFR | : | 956 |
| Cav1.1_Oc | : | CVFVAIRTIGNIVLVTTLLQFMFACIGVQLFKGKFFS | : | 956 |
| Cav1.1_Ms | : | CVFVAIRTIGNIVLVTTLLQFMFACIGVQLFKGKFYS | : | 956 |
| Cav1.1_Rc | : | CLFVAIKTIGNIVLVTTLLQFMFSCIGVQLFKGKFYS | : | 954 |
| 1.1NP_Oc | : | CVFVAIRTIGNIVLVTTLLQFMFACIGVQLFKGKFFS | : | 956 |
| 1.1NP_HS | : | CMFVAISTIGNIVLVTTLLQFMFACIGVQLFKGKFFR | : | 956 |
| 1.1XP_Cp | : | CMFVAISTIGNIVLVTTLLQFMFACIGVQLFKVNVFE | : | 956 |
| 1.1XP_Cf | : | CVFVAIRTIGNIVLVTTLLQFMFACIGVQLFKGKFFS | : | 959 |
| 1.1XP_Md | : | CVFVAIRTIGNIVLVTTLLQFMFACIGVQLFKGKFYS | : | 957 |
| Cav1.3_Hs | : | CVFVAIRTIGNIMIVTTLQFMFACIGVQLFKGKFYR | : | 1043 |
| Cav1.3_Ms | : | CVFVAIRTIGNIMIVTTLQFMFACIGVQLFKGKFYR | : | 1063 |
| Cav1.3_Gg | : | CVFVAIRTIGNIMIVTTLQFMFACIGVQLFKGKFYK | : | 1064 |
| Cav1.3_Rn | : | CVFVAIRTIGNIMIVTTLQFMFACIGVQLFKGKFYR | : | 1102 |
| Cav1.3_Ma | : | CVFVAIRTIGNIMIVTTLQFMFACIGVQLFKGKFYR | : | 1041 |
| 1.3XP_Bt | : | CVFVAIRTIGNIMIVTTLQFMFACIGVQLFKGKFYR | : | 1043 |
| 1.3XP_Cp | : | CVFVAIRTIGNIMIVTTLQFMFACIGVQLFKGKFYR | : | 1064 |
| 1.3XP_Cf | : | CVFVAIRTIGNIMIVTTLQFMFACIGVQLFKGKFYR | : | 1043 |
| 1.3AAA_HS | : | CVFVAIRTIGNIMIVTTLQFMFACIGVQLFKGKFYR | : | 1043 |
| 1.3B0FYA3_ | : | CVFVAIRTIGNIMIVTTLQFMFACIGVQLFKGKFYR | : | 1043 |
| 1.3Q91W25_ | : | CVFVAIRTIGNIMIVTTLQFMFACIGVQLFKGKFYR | : | 1033 |
| 1.3Q8JFR0 | : | CVVGAIRTIGNIMIVTTLQFMFACIGVQLFKGKFYR | : | 1020 |
| Cav1.4_Hs | : | CVFVAIRTIGNIMIVTTLQFMFACIGVQLFKGKFYT | : | 1028 |
| 1.4NP_HS g | : | CVFVAIRTIGNIMIVTTLQFMFACIGVQLFKGKFYT | : | 1028 |
| 1.4XP_Mm g | : | CVFVAIRTIGNIMIVTTLQFMFACIGVQLFKGKFYT | : | 954 |
| 1.4XP_pre_ | : | CVFVAIRTIGNIMIVTTLQFMFACIGVQLFKGKFYS | : | 1024 |
| 1.4XP_Cf g | : | CVFVAIRTIGNIMIVTTLQFMFACIGVQLFKGKFYS | : | 877 |
| 1.4NP_Ms g | : | CVFVAIRTIGNIMIVTTLQFMFACIGVQLFKGKFYS | : | 1031 |
| 1.4CAM_Ms | : | CVFVAIRTIGNIMIVTTLQFMFACIGVQLFKGKFYS | : | 1031 |
| 1.4Q7TNI3_ | : | CVFVAIRTIGNIMIVTTLQFMFACIGVQLFKGKFYS | : | 1031 |
| Cav1.4_Ms | : | CVFVAIRTIGNIMIVTTLQFMFACIGVQLFKGKFYS | : | 1033 |
| 1.4ABD_Rn | : | CVFVAIRTIGNIMIVTTLQFMFACIGVQLFKGKFYS | : | 1027 |
| 1.4NP_Rn N | : | CVFVAIRTIGNIMIVTTLQFMFACIGVQLFKGKFYS | : | 1027 |
| 1.4NP_Oc N | : | CVFVAIRTIGNIVIVTTLQFMFACIGVQLFKGKLYT | : | 1087 |



| | | | | |
|------------|---|---|---|------|
| Cav1.2 Oc | : | SKFDFDNVLAAMMALFTVSTFEGWPPELLLYRSIDSHTE | : | 1160 |
| Cav1.2_Hs | : | SKFDFDNVLAAMMALFTVSTFEGWPPELLLYRSIDSHTE | : | 1150 |
| Cav1.2_Ms | : | SKFDFDNVLAAMMALFTVSTFEGWPPELLLYRSIDSHTE | : | 1130 |
| Cav1.2_Rn | : | SKFDFDNVLAAMMALFTVSTFEGWPPELLLYRSIDSHTE | : | 1159 |
| 1.2XP_Gg | : | SKFDFDNVLAAMMALFTVSTFEGWPPELLLYRSIDSHME | : | 1139 |
| 1.2XP_Cf | : | SKFDFDNVLAAMMALFTVSTFEGWPPELLLYRSIDSHTE | : | 1104 |
| 1.2NP_Hs | : | SKFDFDNVLAAMMALFTVSTFEGWPPELLLYRSIDSHTE | : | 1150 |
| 1.2NP_Ms | : | SKFDFDNVLAAMMALFTVSTFEGWPPELLLYRSIDSHTE | : | 1130 |
| 1.2NP_Oc | : | SKFDFDNVLAAMMALFTVSTFEGWPPELLLYRSIDSHTE | : | 1160 |
| 1.2A0SLC4_ | : | SKFDFDNVLAAMMALFTVSTFEGWPPELLLYRSIDSHTE | : | 1155 |
| 1.2EMD_Rn | : | SKFDFDNVLAAMMALFTVSTFEGWPPELLLYRSIDSHTE | : | 1130 |
| Cav1.1_Hs | : | SDFHFDNVLSAMMSLFTVSTFEGWPQLLYKAIDSNAE | : | 1029 |
| Cav1.1_Oc | : | NDFHFDNVLSAMMSLFTVSTFEGWPQLLYKAIDSNEE | : | 1029 |
| Cav1.1_Ms | : | NDFHFDNVLSAMMSLFTVSTFEGWPQLLYKAIDSNEE | : | 1029 |
| Cav1.1_Rc | : | SDFHFDNVLSGMMSLFTISTFEGWPQLLYKAIDSHAE | : | 1027 |
| 1.1NP_Oc | : | NDFHFDNVLSAMMSLFTVSTFEGWPQLLYKAIDSNEE | : | 1029 |
| 1.1NP_HS | : | SDFHFDNVLSAMMSLFTVSTFEGWPQLLYKAIDSNAE | : | 1029 |
| 1.1XP_Cp | : | SDFHFDNVLSAMMSLFTVSTFEGWPQLLYKAIDSNEE | : | 1030 |
| 1.1XP_Cf | : | SDFHFDNVLSAMMSLFTVSTFEGWPQLLYQAIDSYKE | : | 1032 |
| 1.1XP_Md | : | NDFNFDNVLSAMLALFTVSTFEGWPQLLYKAIDTHAE | : | 1030 |
| Cav1.3_Hs | : | SDFNFDNVLSAMMALFTVSTFEGWPALLYKAIDSNGE | : | 1116 |
| Cav1.3_Ms | : | SDFNFDNVLSAMMALFTVSTFEGWPALLYKAIDSNGE | : | 1136 |
| Cav1.3_Gg | : | SDFNFDNVLSAMMALFTVSTFEGWPALLYKAIDSNGE | : | 1137 |
| Cav1.3_Rn | : | SDFNFDNVLSAMMALFTVSTFEGWPALLYKAIDSNGE | : | 1175 |
| Cav1.3_Ma | : | SDFNFDNVLSAMMALFTVSTFEGWPALLYKAIDSNGE | : | 1114 |
| 1.3XP_Bt | : | SDFNFDNVLSAMMALFTVSTFEGWPALLYKAIDSNGE | : | 1116 |
| 1.3XP_Cp | : | SDFNFDNVLSAMMALFTVSTFEGWPALLYKAIDSNGE | : | 1137 |
| 1.3XP_Cf | : | SDFNFDNVLSAMMALFTVSTFEGWPALLYKAIDSNGE | : | 1116 |
| 1.3AAA_HS | : | SDFNFDNVLSAMMALFTVSTFEGWPALLYKAIDSNGE | : | 1116 |
| 1.3B0FYA3_ | : | SDFNFDNVLSAMMALFTVSTFEGWPALLYKAIDSNGE | : | 1116 |
| 1.3Q91W25_ | : | SDFNFDNVLSAMMALFTVSTFEGWPALLYKAIDSNGE | : | 1106 |
| 1.3Q8JFR0 | : | SEFNFDNVLMAMMALFTVSTFEGWPALLYKAIDSNRE | : | 1093 |
| Cav1.4_Hs | : | SDFNFDNVLSAMMALFTVSTFEGWPALLYKAIDAYAE | : | 1101 |
| 1.4NP_HS g | : | SDFNFDNVLSAMMALFTVSTFEGWPALLYKAIDAYAE | : | 1101 |
| 1.4XP_Mm g | : | SDFNFDNVLSAMMALFTVSTFEGWPALLYKAIDAYAE | : | 1027 |
| 1.4XP_pre_ | : | SDFNFDNVLSAMMALFTVSTFEGWPALLYKAIDANAE | : | 1097 |
| 1.4XP_Cf g | : | SDFNFDNVLSAMDGLVPVSTFEGWPALLYKAIDANAE | : | 950 |
| 1.4NP_Ms g | : | SDFNFDNVLSAMMALFTVSTFEGWPALLYKAIDANAE | : | 1104 |
| 1.4CAM_Ms | : | SDFNFDNVLSAMMALFTVSTFEGWPALLYKAIDANAE | : | 1104 |
| 1.4Q7TNI3_ | : | SDFNFDNVLSAMMALFTVSTFEGWPALLYKAIDANAE | : | 1104 |
| Cav1.4_Ms | : | SDFNFDNVLSAMMALFTVSTFEGWPALLYKAIDANAE | : | 1106 |
| 1.4ABD_Rn | : | SDFNFDNVLSAMMALFTVSTFEGWPALLYKAIDAHAE | : | 1100 |
| 1.4NP_Rn N | : | SDFNFDNVLSAMMALFTVSTFEGWPALLYKAIDAHAE | : | 1100 |
| 1.4NP_Oc N | : | SKFDFDNVLAAMMALFTVSTFEGWPPELLLYRSIDSHTE | : | 1160 |

|-----DIII-S6-----|

| | | | | |
|------------|---|---------------------------------------|---|------|
| Cav1.2_Oc | : | DKGPIYNYRVEISIFFIIYIIIIAFFMMNIFVGFVIV | : | 1197 |
| Cav1.2_Hs | : | DKGPIYNYRVEISIFFIIYIIIIAFFMMNIFVGFVIV | : | 1187 |
| Cav1.2_Ms | : | DKGPIYNYRVEISIFFIIYIIIIAFFMMNIFVGFVIV | : | 1167 |
| Cav1.2_Rn | : | DKGPIYNYRVEISIFFIIYIIIIAFFMMNIFVGFVIV | : | 1196 |
| 1.2XP_Gg | : | DVGPIYNHRVEISIFFIIYIIIIAFFMMNIFVGFVIV | : | 1176 |
| 1.2XP_Cf | : | DKGPIYNYRVEISIFFIIYIIIIAFFMMNIFVGFVIV | : | 1141 |
| 1.2NP_Hs | : | DKGPIYNYRVEISIFFIIYIIIIAFFMMNIFVGFVIV | : | 1187 |
| 1.2NP_Ms | : | DKGPIYNYRVEISIFFIIYIIIIAFFMMNIFVGFVIV | : | 1167 |
| 1.2NP_Oc | : | DKGPIYNYRVEISIFFIIYIIIIAFFMMNIFVGFVIV | : | 1197 |
| 1.2A0SLC4 | : | DKGPIYNYRVEISIFFIIYIIIIAFFMMNIFVGFVIV | : | 1192 |
| 1.2EMD_Rn | : | DKGPIYNYRVEISIFFIIYIIIIAFFMMNIFVGFVIV | : | 1167 |
| Cav1.1_Hs | : | DVGPIYNNRVEMAIFFFIYIILIAFFMMNIFVGFVIV | : | 1066 |
| Cav1.1_Oc | : | DMGPVYNNRVEMAIFFFIYIILIAFFMMNIFVGFVIV | : | 1066 |
| Cav1.1_Ms | : | DTGPVYNNRVEMAIFFFIYIILIAFFMMNIFVGFVIV | : | 1066 |
| Cav1.1_Rc | : | DMGPIYNYRIEIAVFFIVYIILIAFFMMNIFVGFVIV | : | 1064 |
| 1.1NP_Oc | : | DMGPVYNNRVEMAIFFFIYIILIAFFMMNIFVGFVIV | : | 1066 |
| 1.1NP_HS | : | DVGPIYNNRVEMAIFFFIYIILIAFFMMNIFVGFVIV | : | 1066 |
| 1.1XP_Cp | : | DVGPIYNNRVEMAIFFFIYIILIAFFMMNIFVGFVIV | : | 1067 |
| 1.1XP_Cf | : | DMGPVYNNRVEMAIFFFIYIILIAFFMMNIFVGFVIV | : | 1069 |
| 1.1XP_Md | : | DMGPIYNNRVEMAIFFFIVYIILIAFFMMNIFVGFIV | : | 1067 |
| Cav1.3_Hs | : | NIGPIYNHRVEISIFFIIYIIIVAFFMMNIFVGFVIV | : | 1153 |
| Cav1.3_Ms | : | NVGPVYNYRVEISIFFIIYIIIVAFFMMNIFVGFVIV | : | 1173 |
| Cav1.3_Gg | : | NVGPVYNYRVEISIFFIIYIIIVAFFMMNIFVGFVIV | : | 1174 |
| Cav1.3_Rn | : | NVGPVYNYRVEISIFFIIYIIIVAFFMMNIFVGFVIV | : | 1212 |
| Cav1.3_Ma | : | NAGPVYNHRVEISIFFIIYIIIVAFFMMNIFVGFVIV | : | 1151 |
| 1.3XP_Bt | : | NVGPIYNYRVEISIFFIIYIIIVAFFMMNIFVGFVIV | : | 1153 |
| 1.3XP_Cp | : | NIGPIYNHRVEISIFFIIYIIIVAFFMMNIFVGFVIV | : | 1174 |
| 1.3XP_Cf | : | NVGPVYNYRVEISIFFIIYIIIVAFFMMNIFVGFVIV | : | 1153 |
| 1.3AAA_HS | : | NIGPIYNHRVEISIFFIIYIIIVAFFMMNIFVGFVIV | : | 1153 |
| 1.3B0FYA3 | : | NIGPIYNHRVEISIFFIIYIIIVAFFMMNIFVGFVIV | : | 1153 |
| 1.3Q91W25 | : | NAGPVYNHRVEISIFFIIYIIIVAFFMMNIFVGFVIV | : | 1143 |
| 1.3Q8JFR0 | : | NLGPIYNYRIEISIFFIIYIIIIAFFMMNIFVGFVIV | : | 1130 |
| Cav1.4_Hs | : | DHGPIYNYRVEISVFFIVYIIIIAFFMMNIFVGFVII | : | 1138 |
| 1.4NP_HS g | : | DHGPIYNYRVEISVFFIVYIIIIAFFMMNIFVGFVII | : | 1138 |
| 1.4XP_Mm g | : | DHGPIYNYRVEISVFFIVYIIIIAFFMMNIFVGFVII | : | 1064 |
| 1.4XP_pre | : | DKGPIYNYHVEISVFFIVYIIIIAFFMMNIFVGFVII | : | 1134 |
| 1.4XP_Cf g | : | DKGPIYNYHVEISVFFIVYIIIIAFFMMNIFVGFVII | : | 987 |
| 1.4NP_Ms g | : | DEGPIYNYHVEISVFFIVYIIIIAFFMMNIFVGFVII | : | 1141 |
| 1.4CAM_Ms | : | DEGPIYNYHVEISVFFIVYIIIIAFFMMNIFVGFVII | : | 1141 |
| 1.4Q7TNI3 | : | DEGPIYNYHVEISVFFIVYIIIIAFFMMNIFVGFVII | : | 1141 |
| Cav1.4_Ms | : | DEGPIYNYHVEISVFFIVYIIIIAFFMMNIFVGFVII | : | 1143 |
| 1.4ABD_Rn | : | DEGPIYNYHVEISVFFIVYIIIIAFFMMNIFVGFVII | : | 1137 |
| 1.4NP_Rn N | : | DEGPIYNYHVEISVFFIVYIIIIAFFMMNIFVGFVII | : | 1137 |
| 1.4NP_Oc N | : | DKGPIYNYRVEISIFFIIYIIIIAFFMMNIFVGFVIV | : | 1197 |

```

Cav1.2_Oc : TFQEQGEQGEYKNCELDKNQRCVEYALKARPLRRYIP : 1234
Cav1.2_Hs : TFQEQGEQGEYKNCELDKNQRCVEYALKARPLRRYIP : 1224
Cav1.2_Ms : TFQEQGEQGEYKNCELDKNQRCVEYALKARPLRRYIP : 1204
Cav1.2_Rn : TFQEQGEQGEYKNCELDKNQRCVEYALKARPLRRYIP : 1233
1.2XP_Gg : TFQEQGEQGEYKNCELDKNQRCVEYALKARPLRRYIP : 1213
1.2XP_Cf : TFQEQGEQGEYKNCELDKNQRCVEYALKARPLRRYIP : 1178
1.2NP_Hs : TFQEQGEQGEYKNCELDKNQRCVEYALKARPLRRYIP : 1224
1.2NP_Ms : TFQEQGEQGEYKNCELDKNQRCVEYALKARPLRRYIP : 1204
1.2NP_Oc : TFQEQGEQGEYKNCELDKNQRCVEYALKARPLRRYIP : 1234
1.2A0SLC4 : TFQEQGEQGEYKNCELDKNQRCVEYALKARPLRRYIP : 1229
1.2EMD_Rn : TFQEQGEQGEYKNCELDKNQRCVEYALKARPLRRYIP : 1204
Cav1.1_Hs : TFQEQGETEYKNCELDKNQRCVQYALKARPLRCYIP : 1103
Cav1.1_Oc : TFQEQGETEYKNCELDKNQRCVQYALKARPLRCYIP : 1103
Cav1.1_Ms : TFQEQGETEYKNCELDKNQRCVQYALKARPLRCYIP : 1103
Cav1.1_Rc : TFQEQGEQGEYKNCELDKNQRCVQYALKARPLRRYIP : 1101
1.1NP_Oc : TFQEQGETEYKNCELDKNQRCVQYALKARPLRCYIP : 1103
1.1NP_HS : TFQEQGETEYKNCELDKNQRCVQYALKARPLRCYIP : 1103
1.1XP_Cp : TFQEQGETEYKNCELDKNQRCVQYALKARPLRCYIP : 1104
1.1XP_Cf : TFQEQGETEYKNCELDKNQRCVQYALKARPLRCYIP : 1106
1.1XP_Md : TFQEQGETEYKNCELDKNQRCVQYALKARPLRCYIP : 1104
Cav1.3_Hs : TFQEQGEKEYKNCELDKNQRCVEYALKARPLRRYIP : 1190
Cav1.3_Ms : TFQEQGEKEYKNCELDKNQRCVEYALKARPLRRYIP : 1210
Cav1.3_Gg : TFQEQGEQGEYKNCELDKNQRCVEYALKARPLRRYIP : 1211
Cav1.3_Rn : TFQEQGEKEYKNCELDKNQRCVEYALKARPLRRYIP : 1249
Cav1.3_Ma : TFQEQGEKEYKNCELDKNQRCVEYALKARPLRRYIP : 1188
1.3XP_Bt : TFQEQGEKEYKNCELDKNQRCVEYALKARPLRRYIP : 1190
1.3XP_Cp : TFQEQGEKEYKNCELDKNQRCVEYALKARPLRRYIP : 1211
1.3XP_Cf : TFQEQGEKEYKNCELDKNQRCVEYALKARPLRRYIP : 1190
1.3AAA_HS : TFQEQGEKEYKNCELDKNQRCVEYALKARPLRRYIP : 1190
1.3B0FYA3 : TFQEQGEKEYKNCELDKNQRCVEYALKARPLRRYIP : 1190
1.3Q91W25 : TFQEQGEKEYKNCELDKNQRCVEYALKARPLRRYIP : 1180
1.3Q8JFR0 : NFQEQGEKEYKNCELDKNQRCVEYALKARPLRRYIP : 1167
Cav1.4_Hs : TFRAQGEQGEYQNCCELDKNQRCVEYALKACPLRRYIP : 1175
1.4NP_HS|g : TFRAQGEQGEYQNCCELDKNQRCVEYALKACPLRRYIP : 1175
1.4XP_Mm|g : TFRAQGEQGEYQNCCELDKNQRCVEYALKACPLRRYIP : 1101
1.4XP_pre : TFRAQGEQGEYQDCELDKNQRCVEYALKACPLRRYIP : 1171
1.4XP_Cf|g : TFRAQGEQGEYQNCCELDKNQRCVEYALKACPLRRYIP : 1024
1.4NP_Ms|g : TFRAQGEQGEYQNCCELDKNQRCVEYALKACPLRRYIP : 1178
1.4CAM_Ms| : TFRAQGEQGEYQNCCELDKNQRCVEYALKACPLRRYIP : 1178
1.4Q7TNI3 : TFRAQGEQGEYQNCCELDKNQRCVEYALKACPLRRYIP : 1178
Cav1.4_Ms : TFRAQGEQGEYQNCCELDKNQRCVEYALKACPLRRYIP : 1180
1.4ABD_Rn| : TFRAQGEQGEYQNCCELDKNQRCVEYALKACPLRRYIP : 1174
1.4NP_Rn|N : TFRAQGEQGEYQNCCELDKNQRCVEYALKACPLRRYIP : 1174
1.4NP_Oc|N : TFQEQGEQGEYKNCELDKNQRCVEYALKARPLRRYIP : 1234
*****

```


| | —DIV-L45— | —DIV-S5— | |
|------------|---|----------|------|
| Cav1.2_Oc | : MRLVKLLSRGEGIRTLLWTFIKSFQALPYVALLIVML | : | 1400 |
| Cav1.2_Hs | : MRLVKLLSRGEGIRTLLWTFIKSFQALPYVALLIVML | : | 1418 |
| Cav1.2_Ms | : MRLVKLLSRGEGIRTLLWTFIKSFQALPYVALLIVML | : | 1370 |
| Cav1.2_Rn | : MRLVKLLSRGEGIRTLLWTFIKSFQALPYVALLIVML | : | 1399 |
| 1.2XP_Gg | : MRLVKLLSRGEGIRTLLWTFIKSFQALPYVALLIVML | : | 1379 |
| 1.2XP_Cf | : MRLVKLLSRGEGIRTLLWTFIKSFQALPYVALLIVML | : | 1344 |
| 1.2NP_Hs | : MRLVKLLSRGEGIRTLLWTFIKSFQALPYVALLIVML | : | 1418 |
| 1.2NP_Ms | : MRLVKLLSRGEGIRTLLWTFIKSFQALPYVALLIVML | : | 1368 |
| 1.2NP_Oc | : MRLVKLLSRGEGIRTLLWTFIKSFQALPYVALLIVML | : | 1400 |
| 1.2A0SLC4_ | : MRLVKLLSRGEGIRTLLWTFIKSFQALPYVALLIVML | : | 1395 |
| 1.2EMD_Rn | : MRLVKLLSRGEGIRTLLWTFIKSFQALPYVALLIVML | : | 1370 |
| Cav1.1_Hs | : MRLIKLLSRAEGVRTLLWTFIKSFQALPYVALLIVML | : | 1277 |
| Cav1.1_Oc | : MRLIKLLSRAEGVRTLLWTFIKSFQALPYVALLIVML | : | 1277 |
| Cav1.1_Ms | : MRLVKLLNRAEGVRTLLWTFIKSFQALPYVALLIVML | : | 1277 |
| Cav1.1_Rc | : LRLVKLLSRGEGVRTLLWTFIKSFQALPYVALLIVML | : | 1264 |
| 1.1NP_Oc | : MRLIKLLSRAEGVRTLLWTFIKSFQALPYVALLIVML | : | 1277 |
| 1.1NP_HS | : MRLIKLLSRAEGVRTLLWTFIKSFQALPYVALLIVML | : | 1277 |
| 1.1XP_Cp | : MRLIKLLSRAEGVRTLLWTFIKSFQALPYVALLIVML | : | 1278 |
| 1.1XP_Cf | : MRLIKLLSRAEGVRTLLWTFIKSFQALPYVALLIVML | : | 1280 |
| 1.1XP_Md | : MRLIKLLSRGEGVRTLLWTFIKSFQALPYVALLIVML | : | 1278 |
| Cav1.3_Hs | : MRLVKLLSRGEGIRTLLWTFIKSFQALPYVALLIAML | : | 1360 |
| Cav1.3_Ms | : MRLVKLLSRGEGIRTLLWTFIKSFQALPYVALLIAML | : | 1380 |
| Cav1.3_Gg | : MRLVKLLSRGEGIRTLLWTFIKSFQALPYVALLIAML | : | 1389 |
| Cav1.3_Rn | : MRLVKLLSRGEGIRTLLWTFIKSFQALPYVALLIAML | : | 1404 |
| Cav1.3_Ma | : MRLVKLLSRGEGIRTLLWTFIKSFQALPYVALLIAML | : | 1358 |
| 1.3XP_Bt | : MRLVKLLSRGEGIRTLLWTFIKSFQALPYVALLIAML | : | 1360 |
| 1.3XP_Cp | : MRLVKLLSRGEGIRTLLWTFIKSFQALPYVALLIAML | : | 1381 |
| 1.3XP_Cf | : MRLVKLLSRGEGIRTLLWTFIKSFQALPYVALLIAML | : | 1345 |
| 1.3AAA_HS | : MRLVKLLSRGEGIRTLLWTFIKSFQALPYVALLIAML | : | 1360 |
| 1.3B0FYA3_ | : MRLVKLLSRGEGIRTLLWTFIKSFQALPYVALLIAML | : | 1345 |
| 1.3Q91W25_ | : MRLVKLLSRGEGIRTLLWTFIKSFQALPYVALLIAML | : | 1350 |
| 1.3Q8JFR0 | : MRLVKLLSRGEGIRTLLWTFIKSFQALPYVALLIAML | : | 1354 |
| Cav1.4_Hs | : MRLVKLLSKGEGIRTLLWTFIKSFQALPYVALLIAMI | : | 1337 |
| 1.4NP_HS g | : MRLVKLLSKGEGIRTLLWTFIKSFQALPYVALLIAMI | : | 1337 |
| 1.4XP_Mm g | : MRLVKLLSKGEGIRTLLWTFIKSFQALPYVALLIAMI | : | 1263 |
| 1.4XP_pre_ | : MRLVKLLSKGEGIRTLLWTFIKSFQALPYVALLIAMI | : | 1333 |
| 1.4XP_Cf g | : MRLVKLLSKGEGIRTLLWTFIKSFQALPYVALLIAMI | : | 1179 |
| 1.4NP_Ms g | : MRLVKLLSKGEGIRTLLWTFIKSFQALPYVALLIAMI | : | 1340 |
| 1.4CAM_Ms | : MRLVKLLSKGEGIRTLLWTFIKSFQALPYVALLIAMI | : | 1333 |
| 1.4Q7TNI3_ | : MRLVKLLSKGEGIRTLLWTFIKSFQALPYVALLIAMI | : | 1340 |
| Cav1.4_Ms | : MRLVKLLSKGEGIRTLLWTFIKSFQALPYVALLIAMI | : | 1342 |
| 1.4ABD_Rn | : MRLVKLLSKGEGIRTLLWTFIKSFQALPYVALLIAMI | : | 1336 |
| 1.4NP_Rn N | : MRLVKLLSKGEGIRTLLWTFIKSFQALPYVALLIAMI | : | 1336 |
| 1.4NP_Oc N | : MRLVKLLSRGEGIRTLLWTFIKSFQALPYVALLIVML | : | 1400 |

|—DIV-P—|

| | | | | |
|------------|---|---------------------------------------|---|------|
| Cav1.2 Oc | : | FFIYAVIGMQVFGKIALNDTTEINRNNNFQTFPQAVL | : | 1437 |
| Cav1.2_Hs | : | FFIYAVIGMQVFGKIALNDTTEINRNNNFQTFPQAVL | : | 1455 |
| Cav1.2_Ms | : | FFIYAVIGMQVFGKIALNDTTEINRNNNFQTFPQAVL | : | 1407 |
| Cav1.2_Rn | : | FFIYAVIGMQVFGKIALNDTTEINRNNNFQTFPQAVL | : | 1436 |
| 1.2XP_Gg | : | FFIYAVIGMQVFGKIALNDTTEINRNNNFQTFPQAVL | : | 1416 |
| 1.2XP_Cf | : | FFIYAVIGMQVFGKIALNDTTEINRNNNFQTFPQAVL | : | 1381 |
| 1.2NP_Hs | : | FFIYAVIGMQVFGKIALNDTTEINRNNNFQTFPQAVL | : | 1455 |
| 1.2NP_Ms | : | FFIYAVIGMQVFGKIALNDTTEINRNNNFQTFPQAVL | : | 1405 |
| 1.2NP_Oc | : | FFIYAVIGMQVFGKIALNDTTEINRNNNFQTFPQAVL | : | 1437 |
| 1.2A0SLC4_ | : | FFIYAVIGMQVFGKIALNDTTEINRNNNFQTFPQAVL | : | 1432 |
| 1.2EMD_Rn | : | FFIYAVIGMQVFGKIALNDTTEINRNNNFQTFPQAVL | : | 1407 |
| Cav1.1_Hs | : | FFIYAVIGMQMFGKIALVDGTOINRNNNFQTFPQAVL | : | 1314 |
| Cav1.1_Oc | : | FFIYAVIGMQMFGKIALVDGTOINRNNNFQTFPQAVL | : | 1314 |
| Cav1.1_Ms | : | FFIYAVIGMQMFGKIAMVDGTOINRNNNFQTFPQAVL | : | 1314 |
| Cav1.1_Rc | : | FFIYAVIGMQVFGKIALVDGTHINRNSNFQTFPQAVL | : | 1301 |
| 1.1NP_Oc | : | FFIYAVIGMQMFGKIALVDGTOINRNNNFQTFPQAVL | : | 1314 |
| 1.1NP_HS | : | FFIYAVIGMQMFGKIALVDGTOINRNNNFQTFPQAVL | : | 1314 |
| 1.1XP_Cp | : | FFIYAVIGMQMFGKIALVDGTOINRNNNFQTFPQAVL | : | 1315 |
| 1.1XP_Cf | : | FFIYAVIGMQMFGKIAMVDGTOINRNNNFQTFPQAVL | : | 1317 |
| 1.1XP_Md | : | FFIYAVIGMQMFGKIAMVDGTOINRNNNFQTFPQAVL | : | 1315 |
| Cav1.3_Hs | : | FFIYAVIGMQMFGKVAMRDNNOINRNNNFQTFPQAVL | : | 1397 |
| Cav1.3_Ms | : | FFIYAVIGMQMFGKVAMRDNNOINRNNNFQTFPQAVL | : | 1417 |
| Cav1.3_Gg | : | FFIYAVIGMQVFGKVAMRDNNOINRNNNFQTFPQAVL | : | 1426 |
| Cav1.3_Rn | : | FFIYAVIGMQMFGKVAMRDNNOINRNNNFQTFPQAVL | : | 1441 |
| Cav1.3_Ma | : | FFIYAVIGMQMFGKVAMRDNNOINRNNNFQTFPQAVL | : | 1395 |
| 1.3XP_Bt | : | FFIYAVIGMQMFGKVAMRDNNOINRNNNFQTFPQAVL | : | 1397 |
| 1.3XP_Cp | : | FFIYAVIGMQMFGKVAMRDNNOINRNNNFQTFPQAVL | : | 1418 |
| 1.3XP_Cf | : | FFIYAVIGMQMFGKVAMRDNNOINRNNNFQTFPQAVL | : | 1382 |
| 1.3AAA_HS | : | FFIYAVIGMQMFGKVAMRDNNOINRNNNFQTFPQAVL | : | 1397 |
| 1.3B0FYA3_ | : | FFIYAVIGMQMFGKVAMRDNNOINRNNNFQTFPQAVL | : | 1382 |
| 1.3Q91W25_ | : | FFIYAVIGMQMFGKVAMRDNNOINRNNNFQTFPQAVL | : | 1387 |
| 1.3Q8JFR0_ | : | FFIYAVIGMQVFGKVAMVDGTHINRNNNFQTFPQAVL | : | 1391 |
| Cav1.4_Hs | : | FFIYAVIGMQMFGKVALQDGTQINRNNNFQTFPQAVL | : | 1374 |
| 1.4NP_HS g | : | FFIYAVIGMQMFGKVALQDGTQINRNNNFQTFPQAVL | : | 1374 |
| 1.4XP_Mm g | : | FFIYAVIGMQMFGKVALQDGTQINRNNNFQTFPQAVL | : | 1300 |
| 1.4XP_pre_ | : | FFIYAVIGMQMFGKVALQDGTQINRNNNFQTFPQAVL | : | 1370 |
| 1.4XP_Cf g | : | FFIYAVIGMQMFGKVALQDGTQINRNNNFQTFPQAVL | : | 1216 |
| 1.4NP_Ms g | : | FFIYAVIGMQMFGKVALQDGTQINRNNNFQTFPQAVL | : | 1377 |
| 1.4CAM_Ms | : | FFIYAVIGMQMFGKVALQDGTQINRNNNFQTFPQAVL | : | 1370 |
| 1.4Q7TNI3_ | : | FFIYAVIGMQMFGKVALQDGTQINRNNNFQTFPQAVL | : | 1377 |
| Cav1.4_Ms | : | FFIYAVIGMQMFGKVALQDGTQINRNNNFQTFPQAVL | : | 1379 |
| 1.4ABD_Rn | : | FFIYAVIGMQMFGKVALQDGTQINRNNNFQTFPQAVL | : | 1373 |
| 1.4NP_Rn N | : | FFIYAVIGMQMFGKVALQDGTQINRNNNFQTFPQAVL | : | 1373 |
| 1.4NP_Oc N | : | FFIYAVIGMQVFGKIALNDTTEINRNNNFQTFPQAVL | : | 1437 |

| | | | | | | | | | | |
|------------|---|---------------|------|----|------|-----|------|---------|-----|--------|
| Cav1.2 Oc | : | LLFRCATGEAWQD | IMLA | CM | PGKK | CAP | EPHN | STEGE | : | 1474 |
| Cav1.2_Hs | : | LLFRCATGEAWQD | IMLA | CM | PGKK | CAP | EP | SNSTEGE | : | 1492 |
| Cav1.2_Ms | : | LLFRCATGEAWQD | IMLA | CM | PGKK | CAP | EP | SNSTEGE | : | 1444 |
| Cav1.2_Rn | : | LLFRCATGEAWQD | IMLA | CM | PGKK | CAP | EP | SNSTEGE | : | 1473 |
| 1.2XP_Gg | : | LLFRCATGEAWQE | IMLA | CL | PD | KK | CD | PDSE | PAN | STEAD |
| 1.2XP_Cf | : | LLFRCATGEAWQD | IMLA | CM | PGKK | CAP | EP | SNSTEGE | : | 1418 |
| 1.2NP_Hs | : | LLFRCATGEAWQD | IMLA | CM | PGKK | CAP | EP | SNSTEGE | : | 1492 |
| 1.2NP_Ms | : | LLFRCATGEAWQD | IMLA | CM | PGKK | CAP | EP | SNSTEGE | : | 1442 |
| 1.2NP_Oc | : | LLFRCATGEAWQD | IMLA | CM | PGKK | CAP | EP | SNSTEGE | : | 1474 |
| 1.2A0SLC4 | : | LLFRCATGEAWQD | IMLA | CM | PGKK | CAP | EP | SNSTEGE | : | 1469 |
| 1.2EMD_Rn | : | LLFRCATGEAWQD | IMLA | CM | PGKK | CAP | EP | SNSTEGE | : | 1444 |
| Cav1.1_Hs | : | LLFRCATGEAWQE | ILL | AC | SY | GKL | CD | PESD | -- | YAPGEE |
| Cav1.1_Oc | : | LLFRCATGEAWQE | ILL | AC | SY | GKL | CD | PESD | -- | YAPGEE |
| Cav1.1_Ms | : | LLFRCATGEAWQE | ILL | AC | SY | GKL | CD | PESD | -- | YAPGEE |
| Cav1.1_Rc | : | LLFRCATGEAWQE | ILL | AC | SY | GKL | CD | PMSD | -- | FQPGEE |
| 1.1NP_Oc | : | LLFRCATGEAWQE | ILL | AC | SY | GKL | CD | PESD | -- | YAPGEE |
| 1.1NP_HS | : | LLFRCATGEAWQE | ILL | AC | SY | GKL | CD | PESD | -- | YAPGEE |
| 1.1XP_Cp | : | LLFRCATGEAWQE | ILL | AC | SY | GKL | CD | PESD | -- | YAPGEE |
| 1.1XP_Cf | : | LLFRCATGEAWQE | ILL | AC | SY | GKL | CD | PESD | -- | YAPGEE |
| 1.1XP_Md | : | LLFRCATGEAWQE | ILL | AC | SY | GKL | CD | PKSD | -- | ASVGEE |
| Cav1.3_Hs | : | LLFRCATGEAWQE | IMLA | CL | PG | KL | CD | PESD | -- | YNPGEE |
| Cav1.3_Ms | : | LLFRCATGEAWQE | IMLA | CL | PG | KL | CD | PDSD | -- | YNPGEE |
| Cav1.3_Gg | : | LLFRCATGEAWQE | IMLA | CL | PG | KR | CD | PESD | -- | YNPGEE |
| Cav1.3_Rn | : | LLFRCATGEAWQE | IMLA | CL | PG | KL | CD | PDSD | -- | YNPGEE |
| Cav1.3_Ma | : | LLFRCATGEAWQE | IMLA | CL | PG | KL | CD | PDSD | -- | YNPGEE |
| 1.3XP_Bt | : | LLFRCATGEAWQE | IMLA | CL | PG | KQ | CD | PDSD | -- | YNPGEE |
| 1.3XP_Cp | : | LLFRCATGEAWQE | IMLA | CL | PG | KL | CD | PESD | -- | YNPGEE |
| 1.3XP_Cf | : | LLFRCATGEAWQE | IMLA | CL | PG | KL | CD | PESD | -- | YNPGEE |
| 1.3AAA_HS | : | LLFRCATGEAWQE | IMLA | CL | PG | KL | CD | PESD | -- | YNPGEE |
| 1.3B0FYA3 | : | LLFRCATGEAWQE | IMLA | CL | PG | KL | CD | PESD | -- | YNPGEE |
| 1.3Q91W25 | : | LLFRCATGEAWQE | IMLA | CL | PG | KL | CD | PDSD | -- | YNPGEE |
| 1.3Q8JFR0 | : | LLFRCATGEAWQE | IMLA | CV | SG | KL | CD | PESD | -- | YNPGEE |
| Cav1.4_Hs | : | LLFRCATGEAWQE | IMLA | SL | PG | NR | CD | PESD | -- | FGPGEE |
| 1.4NP_HS g | : | LLFRCATGEAWQE | IMLA | SL | PG | NR | CD | PESD | -- | FGPGEE |
| 1.4XP_Mm g | : | LLFRCATGEAWQE | IMLA | SL | PG | NR | CD | PESD | -- | FGPGEE |
| 1.4XP_pre | : | LLFRCATGEAWQE | IMLA | SL | PG | SR | CD | PESD | -- | FGPGEE |
| 1.4XP_Cf g | : | LLFRCATGEAWQE | IMLA | SL | PG | SR | CD | PESD | -- | VSPGEE |
| 1.4NP_Ms g | : | LLFRCATGEAWQE | IMLA | SL | PG | NR | CD | PESD | -- | FGPGEE |
| 1.4CAM_Ms | : | LLFRCATGEAWQE | IMLA | SL | PG | NR | CD | PESD | -- | FGPGEE |
| 1.4Q7TNI3 | : | LLFRCATGEAWQE | IMLA | SL | PG | NR | CD | PESD | -- | FGPGEE |
| Cav1.4_Ms | : | LLFRCATGEAWQE | IMLA | SL | PG | NR | CD | PESD | -- | FGPGEE |
| 1.4ABD_Rn | : | LLFRCATGEAWQE | IMLA | SL | PG | NR | CD | PESD | -- | FGPGEE |
| 1.4NP_Rn N | : | LLFRCATGEAWQE | IMLA | SL | PG | NR | CD | PESD | -- | FGPGEE |
| 1.4NP_Oc N | : | LLFRCATGEAWQD | IMLA | CM | PGKK | CAP | EP | SNSTEGE | : | 1474 |

|-----DIV-S6-----|

```

Cav1.2_Oc : TPCGSSFAVFYFISFYMLCAFLIINLFVAVIMDNFDY : 1511
Cav1.2_Hs : TPCGSSFAVFYFISFYMLCAFLIINLFVAVIMDNFDY : 1529
Cav1.2_Ms : TPCGSSFAVFYFISFYMLCAFLIINLFVAVIMDNFDY : 1481
Cav1.2_Rn : TPCGSSFAVFYFISFYMLCAFLIINLFVAVIMDNFDY : 1510
1.2XP_Gg : HSCGSSFAVFYFISFYMLCAFLIINLFVAVIMDNFDY : 1490
1.2XP_Cf : TPCGSSFAVFYFISFYMLCAFLIINLFVAVIMDNFDY : 1455
1.2NP_Hs : TPCGSSFAVFYFISFYMLCAFLIINLFVAVIMDNFDY : 1529
1.2NP_Ms : TPCGSSFAVFYFISFYMLCAFLIINLFVAVIMDNFDY : 1479
1.2NP_Oc : TPCGSSFAVFYFISFYMLCAFLIINLFVAVIMDNFDY : 1511
1.2A0SLC4_ : TPCGSSFAVFYFISFYMLCAFLIINLFVAVIMDNFDY : 1506
1.2EMD_Rn : TPCGSSFAVFYFISFYMLCAFLIINLFVAVIMDNFDY : 1481
Cav1.1_Hs : YTCGTNFAYYYFISFYMLCAFLVINLFVAVIMDNFDY : 1386
Cav1.1_Oc : YTCGTNFAYYYFISFYMLCAFLIINLFVAVIMDNFDY : 1386
Cav1.1_Ms : HTCGTNFAYYYFISFYMLCAFLIINLFVAVIMDNFDY : 1386
Cav1.1_Rc : YTCGTSFAYFYFISFYMLCAFLIINLFVAVIMDNFDY : 1373
1.1NP_Oc : YTCGTNFAYYYFISFYMLCAFLIINLFVAVIMDNFDY : 1386
1.1NP_HS : YTCGTNFAYYYFISFYMLCAFLVINLFVAVIMDNFDY : 1386
1.1XP_Cp : YTCGTNFAYYYFISFYMLCAFLVINLFVAVIMDNFDY : 1387
1.1XP_Cf : YTCGTNFAYYYFISFYMLCAFLIINLFVAVIMDNFDY : 1389
1.1XP_Md : YTCGTGFAYFYFISFYMLCAFLIINLFVAVIMDNFDY : 1387
Cav1.3_Hs : YTCGSNFAIVYFISFYMLCAFLIINLFVAVIMDNFDY : 1469
Cav1.3_Ms : YTCGSNFAIVYFISFYMLCAFLIINLFVAVIMDNFDY : 1489
Cav1.3_Gg : YTCGSNFAIYYFISFYMLCAFLIINLFVAVIMDNFDY : 1498
Cav1.3_Rn : YTCGSNFAIVYFISFYMLCAFLIINLFVAVIMDNFDY : 1513
Cav1.3_Ma : YTCGSNFAIVYFISFYMLCAFLIINLFVAVIMDNFDY : 1467
1.3XP_Bt : YTCGSNFAIVYFISFYMLCAFLIINLFVAVIMDNFDY : 1469
1.3XP_Cp : YTCGSNFAIVYFISFYMLCAFLIINLFVAVIMDNFDY : 1490
1.3XP_Cf : YTCGSNFAIVYFISFYMLCAFLIINLFVAVIMDNFDY : 1454
1.3AAA_HS : HTCGSNFAIVYFISFYMLCAFLIINLFVAVIMDNFDY : 1469
1.3B0FYA3_ : YTCGSNFAIVYFISFYMLCAFLIINLFVAVIMDNFDY : 1454
1.3Q91W25_ : YTCGSNFAIVYFISFYMLCAFLIINLFVAVIMDNFDY : 1459
1.3Q8JFR0 : MTCGASFAYIYFISFYMLCAFLIINLFVAVIMDNFDY : 1463
Cav1.4_Hs : FTCGSNFAIAYFISFFMLCAFLIINLFVAVIMDNFDY : 1446
1.4NP_HS|g : FTCGSNFAIAYFISFFMLCAFLIINLFVAVIMDNFDY : 1446
1.4XP_Mm|g : FTCGSNFAIAYFISFFMLCAFLIINLFVAVIMDNFDY : 1372
1.4XP_pre_ : FSCGSNFAIAYFISFFMLCAFLIINLFVAVIMDNFDY : 1442
1.4XP_Cf|g : FTCGSNFAIAYFISFFMLCAFLIINLFVAVIMDNFDY : 1288
1.4NP_Ms|g : FTCGSSFAIVYFISFFMLCAFLIINLFVAVIMDNFDY : 1449
1.4CAM_Ms| : FTCGSSFAIVYFISFFMLCAFLIINLFVAVIMDNFDY : 1442
1.4Q7TNI3_ : FTCGSSFAIVYFISFFMLCAFLIINLFVAVIMDNFDY : 1449
Cav1.4_Ms : FTCGSSFAIVYFISFFMLCAFLIINLFVAVIMDNFDY : 1451
1.4ABD_Rn| : FTCGSNFAIVYFISFFMLCAFLIINLFVAVIMDNFDY : 1445
1.4NP_Rn|N : FTCGSNFAIVYFISFFMLCAFLIINLFVAVIMDNFDY : 1445
1.4NP_Oc|N : TPCGSSFAVFYFISFYMLCAFLIINLFVAVIMDNFDY : 1511
*****

```

Curriculum Vitae

CHONTICHA SUWATTANASOPHON

chonticha.suwattanasophon@univie.ac.at

Personal data

Nationality: Thai

Gender: Female

Date of Birth: 1 November 1979

Education

2007 - present **UNIVERSITY OF VIENNA** Vienna, Austria

Ph.D Candidate , Physics

- Interaction determinants between pore regions and voltage sensors in calcium channels

2001-2004 **MAHIDOL UNIVERSITY** Bangkok, Thailand

Master of Science, Physics

- Master thesis: Molecular Dynamics of *Bacillus Thuringiensis* Cry4Ba Toxin

1997-2001 **King Mongkut's University of Technology Thonburi** Bangkok, Thailand

Bachelor of Science, Physics

- Senior project: Study the second harmonic of Nd-YAG laser

Professional experience

| | | |
|-----------|--|------------------------|
| 2004-2006 | Pibulsongkharm Rajabhat University <i>Lecturer</i> | Phitsanuloke, Thailand |
| 2001-2002 | MAHIDOL UNIVERSITY <i>Teacher Assistance</i> | Bangkok, Thailand |

Academic awards

| | |
|----------------------|---|
| April 2010-June 2010 | Short Term Grant Abroad of University of Vienna. (Department of Chemical Engineering and Materials Science, University of California Davis – 3 months) |
| 2007-2010 | Initiative Groups at University of Vienna Scholarship. (Molecular Drug Target - Department of Pharmacology and Toxicology, University of Vienna) |
| 2002-2004 | The Shell Centenary Scholarship Fund |

Presentation

- Chonticha Suwattanasophon, Roland Faller, Peter Wolschann , Anna Stry-Weinzinger. Molecular Dynamics Simulations on the Function of the Transmembrane Cav1.2 Channel in Dependence of the Content of Cholesterol in the Membrane, 8 th European Biophysics Congress, Budapest, Hungary, 23-27 August 2011.
- Chonticha Suwattanasophon, Anna Stry and Peter Wolschann. Homology Modelling of Cav1.2 Calcium Channel, Drug Design and Discovery for Developing Countries, ICS-UNIDO, Trieste, Italy, 30 June-5 July 2008.
- Chonticha Suwattanasophon, Anna Stry, Peter Wolschann and Gerhard Buchbauer. Homology Modelling of Odorant Receptors, Österreichische Chemietage, Klagenfurt, Austria 2007.

Publications

- A. Sary, C. Suwattanasophon, P. Wolschann and G. Buchbauer. 2007. Difference in (-) citronellal binding to various odorant receptors. *J. Biochem. Biophys. Res. Commun* 4: 941-945.
- M. Karmazinova, S. Beyl, A. Sary, C. Suwattanasophon, N. Klugbauer, S. Hering, L. Lacinova. 2010. Cysteines in the loop between IS5 and the pore helix of CaV3.1 are essential for channel gating, *Pflügers Archiv-European Journal of Physiology* 6: 1015-1028.
- C. Suwattanasophon, R. Faller, P. Wolschann and A. Sary. Molecular Dynamics Simulation on the Function of the Transmembrane Cav1.2 Channel in Dependence of the Content of Cholesterol in the Membrane. *European Biophysics Journal with Biophysics Letters*. 40: p. 118-118.